

Copyright Warning & Restrictions

The copyright law of the United States (Title 17, United States Code) governs the making of photocopies or other reproductions of copyrighted material.

Under certain conditions specified in the law, libraries and archives are authorized to furnish a photocopy or other reproduction. One of these specified conditions is that the photocopy or reproduction is not to be “used for any purpose other than private study, scholarship, or research.” If a user makes a request for, or later uses, a photocopy or reproduction for purposes in excess of “fair use” that user may be liable for copyright infringement,

This institution reserves the right to refuse to accept a copying order if, in its judgment, fulfillment of the order would involve violation of copyright law.

Please Note: The author retains the copyright while the New Jersey Institute of Technology reserves the right to distribute this thesis or dissertation

Printing note: If you do not wish to print this page, then select “Pages from: first page # to: last page #” on the print dialog screen

The Van Houten library has removed some of the personal information and all signatures from the approval page and biographical sketches of theses and dissertations in order to protect the identity of NJIT graduates and faculty.

ABSTRACT

NOVEL APPLICATIONS OF MASS SPECTROMETRY FOR QUANTITATION AND REACTION MECHANISM ELUCIDATION

**by
Pengyi Zhao**

Mass spectrometry (MS) has been growing as one of the most widely used tools in the field of analytical chemistry. Various applications have been developed to harness the high sensitivity and specificity of mass spectrometric analysis. In this dissertation, two major challenges are addressed. By developing mass spectrometric-based methods, absolute quantitation of proteins/peptides have been achieved. Elucidation of various reaction mechanisms are also enabled. These are the focuses of this dissertation.

In Chapters 2 to 4, a novel quantitation method is developed, titled as coulometric mass spectrometry (CMS). The strength of this method is that no reference standard or isotope-labeled compound is required for absolute quantitation. The method relies on electrochemical oxidation of an electrochemically active target compound to determine the amount of the oxidized compound using Faraday's Law. On the other hand, the oxidation reaction yield can be determined based on the MS signal change following electrolysis. Therefore, the absolute amount of the analyte can be calculated. In the project for quantifying the mixture of dopamine and serotonin, this method is optimized and proved to quantify the compounds in a mixture after the chromatographic separation. Gradient elution is used for separation and each compound can be quantified using the electrochemical mass spectrometry method. Furthermore, the tyrosine-containing peptides are targeted and electrochemically oxidized to generate electric current for successful quantitation by CMS method. In addition, the CMS method is further applied to absolute

quantitation of proteins, as proteins can be digested into peptides. The results for surrogate peptide quantity measured by our method and by traditional isotope dilution method are in excellent agreement, with the discrepancy of 0.3-3%, validating our CMS method for absolute protein quantitation. Due to the high specificity and sensitivity of MS and no need to use isotope-labeled peptide standards, the CMS method would be of high value for the absolute proteomic quantification.

In Chapter 5, elucidation of ion dissociation patterns for structural analysis is presented by using an atmospheric pressure thermal dissociation mass spectrometry (APTD-MS) technique. By using this technique, neutral CO resulting from amino acid and peptide ion dissociation is detected. In the future, more meaningful analytes can be investigated by APTD-MS to study dissociation mechanisms at the ambient environment.

In Chapter 6, a gold-catalyzed oxidative coupling reaction is reported via electrochemical approach. Oxidation of Au(I) to Au(III) can be achieved through anode oxidation, which facilitates facile access to conjugated diynes via homo-coupling or cross-coupling. Besides, transient reaction intermediates are detected and confirmed by mass spectrometry which provides evidence to mechanistic studies.

In Chapter 7, a novel and rapid method is developed for antibody characterization. By which, multiple reactions (e.g., reduction, digestion and deglycosylation) can take place on antibodies in microseconds in the microdroplets. The resulting antibody fragments can be either collected or online analyzed by mass spectrometry. It suggests that microdroplet environment is a powerful reactor for both exploring large molecule reactions and speeding their analysis.

**NOVEL APPLICATIONS OF MASS SPECTROMETRY FOR QUANTITATION
AND REACTION MECHANISM ELUCIDATION**

**by
Pengyi Zhao**

**A Dissertation
Submitted to the Faculty of
New Jersey Institute of Technology
in Partial Fulfillment of the Requirements for the Degree of
Doctor of Philosophy in Chemistry**

Department of Chemistry and Environmental Science

December 2020

Copyright © 2020 by Pengyi Zhao

ALL RIGHTS RESERVED

APPROVAL PAGE

**NOVEL APPLICATIONS OF MASS SPECTROMETRY FOR QUANTITATION
AND REACTION MECHANISM ELUCIDATION**

Pengyi Zhao

Dr. Hao Chen, Dissertation Advisor Date
Professor of Chemistry and Environmental Science, NJIT

Dr. Kevin D. Belfield, Committee Member Date
Professor of Chemistry and Environmental Science, and Dean of CSLA, NJIT

Dr. Edgardo T. Farinas, Committee Member Date
Associate Professor of Chemistry and Environmental Science, NJIT

Dr. Mengyan Li, Committee Member Date
Associate Professor of Chemistry and Environmental Science, NJIT

Dr. Vivek A. Kumar, Committee Member Date
Assistant Professor of Biomedical Engineering NJIT

BIOGRAPHICAL SKETCH

Author: Pengyi Zhao
Degree: Doctor of Philosophy
Date: December 2020

Undergraduate and Graduate Education:

- Doctor of Philosophy in Chemistry, New Jersey Institute of Technology, Newark, NJ, 2020
- Master of Science in Food Science, Illinois Institute of Technology, Chicago, IL, 2015
- Bachelor of Science in Pharmaceutical Science, China Pharmaceutical University, Nanjing, P. R. China, 2012

Major: Chemistry

Presentations and Publications:

Wang, Q.; Bhattarai, M.; Zhao, P.; Alnsour, T.; Held, M.; Faik, A.; Chen, H. Fast and Sensitive Detection of Oligosaccharides Using Desalting Paper Spray Mass Spectrometry (DPS-MS). *J. Am. Soc. Mass Spectrom.* 2020, 31 (10), 2226–2235.

Zhao, P.; Wang, Q.; Kaur, M.; Kim, Y.-I.; Dewald, H. D.; Mozziconacci, O.; Liu, Y.; Chen, H. Absolute Quantitation of Proteins by Coulometric Mass Spectrometry. *Anal. Chem.* 2020, 92 (11), 7877-7883.

Yuan, T.; Ye, X.; Zhao, P.; Teng, S.; Yi, Y.; Wang, J.; Shan, C.; Wojtas, L.; Jean, J.; Chen, H.; Shi, X. Regioselective Crossed Aldol Reactions under Mild Conditions via Synergistic Gold-Iron Catalysis. *Chem* 2020, 6 (6), P1420-1431.

Wang, J.; Wei, C.; Li, X.; Zhao, P.; Shan, C.; Wojtas, L.; Chen, H.; Shi, X. Gold Redox Catalysis with a Selenium Cation as Mild Oxidant. *Chem. – A Eur. J.* 2020, 26 (27), 5946–5950.

Ye, X.; Zhao, P.; Zhang, S.; Zhang, Y.; Wang, Q.; Shan, C.; Wojtas, L.; Guo, H.; Chen, H.; Shi, X. Facilitating Gold Redox Catalysis with Electrochemistry: An Efficient Chemical-Oxidant-Free Approach. *Angew. Chemie Int. Ed.* 2019, 58 (48), 17226–17230.

- Zhao, P.; Zare, R. N.; Chen, H. Absolute Quantitation of Oxidizable Peptides by Coulometric Mass Spectrometry. *J. Am. Soc. Mass Spectrom.* **2019**, 30 (11), 2398–2407.
- Zhao, P.; Guo, Y.; Dewald, H. D.; Chen, H. Improvements for Absolute Quantitation Using Electrochemical Mass Spectrometry. *Int. J. Mass Spectrom.* **2019**, 443, 41–45.
- Xu, C.; Zheng, Q.; Zhao, P.; Paterson, J.; Chen, H. A New Quantification Method Using Electrochemical Mass Spectrometry. *J. Am. Soc. Mass Spectrom.* **2019**, 30 (4), 685–693.
- Zhao, P.; White, T.; Graham Cooks, R.; Chen, Q.; Liu, Y.; Chen, H. Detection of Neutral CO Lost During Ionic Dissociation Using Atmospheric Pressure Thermal Dissociation Mass Spectrometry (APTD-MS). *J. Am. Soc. Mass Spectrom.* **2018**, 29 (12), 2317–2326.
- Lu, M.; Su, Y.; Zhao, P.; Ye, X.; Cai, Y.; Shi, X.; Masson, E.; Li, F.; Campbell, J. L.; Chen, H. Direct Evidence for the Origin of Bis-Gold Intermediates: Probing Gold Catalysis with Mass Spectrometry. *Chem. - A Eur. J.* **2018**, 24 (9), 2144–2150.
- Liu, P.; Zhao, P.; Cooks, R. G.; Chen, H. Atmospheric Pressure Neutral Reionization Mass Spectrometry for Structural Analysis. *Chem. Sci.* **2017**, 8 (9), 6499–6507.

*I dedicate this dissertation to my parents: Mr. Ming Zhao and Mrs. Qifen Song,
family, and friends.*

ACKNOWLEDGMENT

I wish to give my special thanks to Dr. Hao Chen, my dissertation advisor, for his countless hours of reflecting, reading, mentoring, encouraging, and most of all patience throughout the entire process. I also thank Dr. Kevin Belfield, Dr. Edgardo Farinas, Dr. Mengyan Li, and Dr. Vivek Kumar for agreeing to serve on my committee.

I would like to acknowledge the National Science Foundation (grant # CHE-1915878, CHE-1709075, CHE-1455554, to Dr. Hao Chen), and the Department of Chemistry and Environmental Science for their financial support.

I would like to acknowledge to all my collaborators, Dr. Xiaodong Shi and Dr. Xiaohan Ye (University of South Florida); Dr. Richard N. Zare (Stanford University); Dr. R. Graham Cooks (Purdue University); Dr. Yong Liu and Dr. Mozziconacci (Merck Research Laboratories); and Dr. Howard D. Dewald (Ohio University) and Dr. Harsha P. Gunawardena (Janssen Research & Development) for their generous guidance and help.

I would like to acknowledge to all former and current members in Dr. Hao Chen's group, Dr. Pengyuan Liu, Dr. Mei Lu, Dr. Qiuling Zheng, Chang Xu, Qi Wang, Yongling Ai, Teng Yuan, Dr. Jin Wang, Dr. Yuejie Zhao and Dr. Mengxuan Jia for their support and assistance.

Finally, I would like to acknowledge and thank my department for allowing me to conduct my research and providing any assistance requested. Special thanks go to Genti M. Price, Leslie M. Williams, and Dr. Kathleen Gilbert for their continuous support.

TABLE OF CONTENTS

Chapter	Page
1 INTRODUCTION.....	1
1.1 Mass Spectrometry	1
1.2 Mass Spectrometer.....	1
1.3 Ionization Methods.....	2
1.4 Mass Analyzers.....	7
1.5 Electrochemical Mass Spectrometry.....	11
2 IMPROVEMENTS FOR ABSOLUTE QUANTITATION USING ELECTROCHEMICAL MASS SPECTROMETRY	15
2.1 Introduction	15
2.2 Experiments.....	17
2.2.1 Chemicals.....	17
2.2.2 Instrumentation.....	17
2.3 Results and Discussion.....	19
2.4 Conclusions.....	28
3 ABSOLUTE QUANTITATION OF OXIDIZABLE PEPTIDES BY COULOMETRIC MASS SPECTROMETRY.....	29
3.1 Introduction.....	29
3.2 Experiments.....	32
3.2.1 Chemicals.....	32
3.2.2 Instrumentation.....	33
3.3 Results and Discussion.....	35

TABLE OF CONTENTS
(Continued)

Chapter	Page
3.4 Conclusions.....	53
4 ABSOLUTE QUANTITATION OF PROTEINS BY COULOMETRIC MASS SPECTROMETRY.....	55
4.1 Introduction	55
4.2 Experiments.....	58
4.2.1 Chemicals.....	58
4.2.2 Protein Expression and Purification.....	59
4.2.3 Proteolytic Digestion.....	59
4.2.4 Instrumentation.....	61
4.3 Results and Discussion.....	63
4.4 Conclusions.....	81
5 STRUCTURAL ELUCIDATION USING ATMOSPHERIC PRESSURE THERMAL DISSOCIATION MASS SPECTROMETRY.....	82
5.1 Introduction	82
5.2 Experiments.....	86
5.2.1 Chemicals	86
5.2.2 Instrumentation.....	86
5.2.3 Synthesis of Binuclear Rhodium Complex cis- [Rh ₂ (C ₆ H ₄ PPH ₂) ₂ (O ₂ CCH ₃) ₂](HOAc) ₂	87
5.2.4 MS Analysis of Carbon Monoxide Trapped by Binuclear Rhodium Complex Solution.....	87
5.2.5 UV-Vis Analysis of Carbon Monoxide Trapped by Binuclear Rhodium Complex Solution.....	88

TABLE OF CONTENTS
(Continued)

Chapter	Page
5.3 Results and Discussion.....	88
5.4 Conclusions.....	106
6 ELECTROSYNTHESIS AND DETECTION OF TRANSIENT INTERMEDIATES IN GOLD-CATALYZED REACTIONS BY MASS SPECTROMETRY.....	108
6.1 Introduction.....	108
6.2 Experiments.....	110
6.2.1 Chemicals.....	110
6.2.2 General Procedure for Homo-diyne Coupling.....	111
6.2.3 General Procedure for Hetero-diyne Coupling.....	111
6.2.4 General Procedure for Phenylacetylene Oxidative Coupling.....	112
6.3 Results and Discussion.....	113
6.4 Conclusion.....	116
7 MICRODROPLET ULTRAFAST REACTIONS SPEEDS ANTIBODY CHARACTERIZATION.....	118
7.1 Introduction.....	118
7.2 Experiments.....	120
7.2.1 Chemicals.....	120
7.2.2 Microdroplet Generation.....	120
7.2.3 Microdroplet Digestion with nESI-MS Analysis.....	121
7.2.4 Microdroplet Digestion with Online EESI-MS Analysis.....	123
7.2.5 Glycated IgG1 Characterization.....	124

TABLE OF CONTENTS
(Continued)

Chapter	Page
7.2.6 Deglycosylation of IgG1 by PNGase F.....	124
7.3 Results and Discussion.....	124
7.4 Conclusion.....	139
8 SUMMARY AND FUTURE WORK.....	141
REFERENCES	145

LIST OF TABLES

Table	Page
2.1 Electric Current and MS Data for DA and NE	24
2.2 Electric Current and MS Data for 5-HT and DA	27
2.3 Communication System.....	34
3.1 Relationship Between the Peptide Quantity and the Peptide EIC Peak Area.....	31
3.2 Amino Acids Known to Be Oxidizable.....	35
3.3 List of Peptides Quantified by CMS.....	37
3.4 Electric Current and MS Data for GGYR.....	40
3.5 Electric Current and MS Data for DRVY.....	43
3.6 Electric Current and MS Data for Oxytocin.....	45
3.7 Electric Current and MS Data for [Arg ⁸]-Vasotocin.....	46
3.8 MS Data for TDP at Different Sample Injection Flow Rates (0.1-0.3 mL/min)...	47
3.9 Electric Current and MS Data for TDP.....	49
3.10 Electric Current and MS Data for Phosphopeptide UOM9.....	52
3.11 Electric Current and MS Data for Sensitivity Evaluation of CMS Using DRVY..	53
4.1 Electric Current and MS Data for A Peptide Mixture (GGYR, DRVY, and Arg8-Vasocotin)	66
4.2 Sequence Information of the Proteins Tested in the Experiments (the Chosen Surrogate Peptides for Quantitation are Highlighted in Bold)	68
4.3 Electric Current and MS Data for Digested B-Casein (the Selected Surrogate Peptide: AVPYYPQR)	70

LIST OF TABLES
(Continued)

Table	Page
4.4 Electric Current and MS Data for Digested Apomyoglobin (the Selected Surrogate Peptide: YKELGFQG)	73
4.5 Electric Current and MS Data for Digested KaiB (the Selected Surrogate Peptide: VLIGLDLLYGELQDSDDF)	76
4.6 Electric Current and MS Data for Digested KaiB (the Selected Surrogate Peptides are NILEVEFQGVYALK and VLIGLDLLYGELQDSDDF)	78
4.7 Electric Current and MS Data for Digested IgG2 (the Selected Surrogate Peptide: LLIYDASNLETGVPSR)	81
5.1 Measurements of Carbon Monoxide Produced from APTD of 1) ACN/H ₂ O/HOAc (50:50:0.1) Blank Solvent, 2) 5 mM Peptide GHG in ACN/H ₂ O/HOAc (50:50:0.1), 3) 5 mM Peptide GWG in ACN/H ₂ O/HOAc (50:50:0.1). The Peptide Sample Solution was Sprayed for APTD from An ESSI Source at the Flow Rate of 10 μL/min with the Assistance of + 5 kV Voltage and 170 psi Nebulizing N ₂ gas. A Potential of 90 V was Applied to the Heating Tape and the APTD Tube was Heated up to 300 °C. All of Measurements were Made in Triplicate as Shown.....	106
7.1 Comparison Between Measured Mass for Igg1 Fragments in Figure 7.2c by Microdroplet Digestion and Previously Published Data.....	125

LIST OF FIGURES

Figure	Page
1.1 Basic configuration of a mass spectrometer.....	2
1.2 The EI ion source.....	3
1.3 Schematic of the electrospray ionization process.....	4
1.4 Schematic of ESSI source.....	5
1.5 Schematic of typical DESI setup.....	6
1.6 Diagram showing a quadrupole MS.	8
1.7 Schematic diagram of a TOF-MS.....	9
1.8 Schematic diagram of a two-dimensional linear ion trap	10
1.9 Schematic drawing of an Orbitrap mass analyzer.....	11
1.10 Scheme of an HPLC-EC-MS setup.....	13
2.1 A schematic showing of the first 7.5 min of the injection sequence, where 0-2 min was a blank solvent injection for cleaning purpose; 2-4 min was an analyte injection in the “cell-off” mode. The electrochemical cell was turned on at 4 min, and a charging current was generated as the potential was applied. Another injection for the analyte solution was injected in the “cell-on” mode, 1.5 min after the cell was turned on. The time period of 0-7.5 min could be considered as a cycle, and the second consecutive cycle started at 7.5 min (see Figure 2.2)...	20
2.2 Electrochemical currents of DA and NE compounds in a no-column injection sequence.....	21
2.3 ESI-MS spectra of dopamine when the applied potential was a) 0 V and b) +1.05 V. The peak of the oxidized product of dopamine (DQ) was seen at m/z 152 (+1 charged) in b). Electric current responses were shown c) from the blank solvent and d) the oxidation of dopamine.....	23

LIST OF FIGURES
(Continued)

Figure	Page
2.4 ESI-MS spectra of norepinephrine when the applied potential was a) 0 V and b) +1.05 V. The peak of the oxidized product of norepinephrine (NQ) was seen at m/z 168 (+1 charged) in b). Electric current responses were shown c) from the blank solvent and d) the oxidation of norepinephrine.....	24
2.5 ESI-MS spectra of 5-HT when the applied potential was a) 0 V and b) +1.05 V. The peak of the oxidized product of 5-HT was seen at m/z 190 (+1 ion) in b). ESI-MS spectra of DA when the applied potential was c) 0 V and b) +1.05 V. The peak of the oxidized product of DA was seen at m/z 152 (+1 ion) in d). Electric current responses were shown e) from the blank solvent and f) the oxidation of 5-HT and DA.....	27
3.1 EIC peaks of ion m/z 452 for a) 60 pmol of GGYR and b) 30 pmol of GGYR....	31
3.2 Electric current responses of a) blank solvent, b) GHG, c) bradykinin (RPPGFSPFR), d) MG, e) KRTLRR, f) RGD, g) SLIGKV-amide, h) RKRSRAE-amide, i) SFLLRN-amide, and j) FLFQPQRF-amide, and k) RRLIEDAEpYAARG. No electric current peak was detected, even under the oxidation potential of +1.1 V.....	38
3.3 ESI-MS spectra of GGYR when the applied potential was a) 0 V and b) +1.0 V. The peak of the oxidized product GGY'R was clearly seen at m/z 450 in b). EIC of GGYR was recorded when the applied potential was c) 0 V and d) +1.0 V. Electric current responses were shown due to the oxidation of e) a blank solvent and f) GGYR peptide.....	40
3.4 CID MS/MS spectra of a) the oxidized peptide ion [GGY'R+H] ⁺ (m/z 450) and b) the intact peptide ion [GGYR+H] ⁺ (m/z 452). Fragment ion of m/z 344 in a) resulted from the loss of the oxidized tyrosine side chain from m/z 450.....	41

LIST OF FIGURES
(Continued)

Figure	Page
3.5 ESI-MS spectra of DRVY when the applied potential was a) 0 V and b) +1.0 V. The peak of the oxidation product of DRVY was seen at m/z 550. EIC of DRVY was recorded when the applied potential was c) 0 V and d) +1.0 V. Electric current responses were e) due to the blank solvent and f) the oxidation of DRVY sample. Note that there is a small peak of m/z 550 in a, which might be caused by in-source oxidation of DRVY.....	43
3.6 ESI-MS spectra of oxytocin when the applied potential was a) 0 V and b) +1.0 V. The peak of the oxidized product of oxytocin was seen at m/z 503 (+2 charged) in b. EIC of the +2 charged oxytocin ion was recorded when the applied potential was c) 0 V and d) +1.0 V. Electric current responses were shown e) from the blank solvent and f) the oxidation of oxytocin peptide.....	45
3.7 ESI-MS spectra of [Arg ⁸]-vasotocin when the applied potential was a) 0 V and b) +1.0 V. The peak of the oxidized product of [Arg ⁸]-vasotocin was seen at m/z 524 (+2 charged) in b. EIC of the +2 ion of [Arg ⁸]-vasotocin was recorded when the applied potential was c) 0 V and d) +1.0 V. Electric current responses were shown e) due to the blank solvent and f) the oxidation of [Arg ⁸]-vasotocin peptide.....	46
3.8 ESI-MS spectra of TDP when the applied potential was a) 0 V and b) +1.05 V. The major peak of the oxidized product of TDP was seen at m/z 439.98 (+4 charged) in b. EIC of the +4 charged TDP ion was recorded when the applied potential was c) 0 V and d) +1.05 V. Electric current responses were shown e) due to the blank solvent and f) the oxidation of TDP peptide.....	49
3.9 ESI-MS spectra of phosphorylated UOM9 when the applied potential was a) 0 V and b) +1.05 V (vs. Ag/AgCl). The peak of the oxidized peptide product was seen at m/z 284.94 (+5 ion) in b. EIC of the +5 ion of phosphorylated UOM9 was recorded when the applied potential was c) 0 V and d) +1.05 V. Electric current responses were shown e) from the blank solvent and f) the oxidation of the phosphorylated UOM9 peptide.....	52
4.1 Extracted ion chromatograms of a) GGYR, b) DRVY, and c) Arg ⁸ -vasotocin. Electric oxidation current diagrams are shown due to the oxidation of d) a solvent blank and e) the peptide mixture. ESI-MS spectra of GGYR was recorded f) when the cell was turned off and g) when the cell was turned on (applied potential: +0.95 V). The +2 ion of the oxidized GGYR product was observed at m/z 225.6 in g).....	65

LIST OF FIGURES
(Continued)

Figure	Page
4.2 EIC spectra of GGYR, DRVY, and Arg ⁸ -vasotocin were recorded when the applied potential was 0 V in a), c), e), and +0.95 V in b), d), f).....	66
4.3 MS spectra of AVPYRQR from the β-casein tryptic digest a) when the cell was off and b) when the cell was turned on (applied potential: +0.95 V). The oxidation product of AVPYRQR was detected at <i>m/z</i> 414.7. EICs of AVPYRQR were acquired c) when the cell was off and d) when the cell was turned on (applied potential: +0.95 V). Electric current diagrams were collected from e) blank solvent and f) the oxidation of AVPYRQR.....	70
4.4 Calibration curve using isotope-labelled peptide AVPYRQR [^] as an internal standard.....	71
4.5 ESI-MS spectra of YKELGFQG from the apomyoglobin tryptic digest when the applied potential was a) 0 V and b) +1.05 V. The peak of the oxidation product of YKELGFQG was seen at <i>m/z</i> 470.2 in b). EIC of YKELGFQG was recorded when the applied potential was c) 0 V and d) +1.05 V. Electric current responses were due to the oxidation of e) blank solvent and f) YKELGFQG. Note that there is a small peak of <i>m/z</i> 470.2 in a), which might be caused by in-source oxidation of YKELGFQG.....	73
4.6 MS spectra of VLIGLDLLYGELQDSDDF from the KaiB tryptic digest a) when the cell was off and b) when the cell was turned on (applied potential: +0.95 V). The oxidized product peak was detected at <i>m/z</i> 1012.0 (+2 ion) in b). Electric current response curves are shown, due to oxidation of c) solvent blank and d) VLIGLDLLYGELQDSDDF.....	76
4.7 Calibration curve using isotope-labelled peptide VL [^] IGLDLLYGELQDSDDF as an internal standard.....	77
4.8 ESI-MS spectra of LLIYDASNLETGVPSR from the IgG2 tryptic digest when the applied potential was a) 0 V and b) +1.05 V. The peak of the oxidation product was seen at <i>m/z</i> 873.46 in b). EIC of LLIYDASNLETGVPSR was recorded when the applied potential was c) 0 V and d) +1.05 V. Electric current responses were due to the oxidation of e) the blank solvent and f) LLIYDASNLETGVPSR.....	80
5.1 APTD–MS spectra for phenylalanine at a) 45 °C, b) 180 °C, and c) 300 °C. Phenylalanine solution in ACN/H ₂ O/HOAc (0.25 mM; 50:50:0.1 by volume) was sprayed by ESSI (spray voltage: +5 kV) into a hot coiled tube at a flow rate of 10 μL/min.....	89

LIST OF FIGURES
(Continued)

Figure	Page
5.2 APTD–MS spectra for ¹³ C-phenylalanine at a) 45 °C, b) 180 °C, c) 300 °C. 0.25 mM ¹³ C-phenylalanine solution in ACN/H ₂ O/HOAc (50:50:0.1) was sprayed into the APTD tube by ESSI (spray voltage +5 kV) at a flow rate of 10 μL/min..	90
5.3 Measurements of carbon monoxide produced from APTD of 1) ACN/H ₂ O/HOAc (50:50:0.1) blank solvent, 2) 25 mM phenethylamine in ACN/H ₂ O/HOAc (50:50:0.1), 3) 25 mM phenylalanine in ACN/H ₂ O/HOAc (50:50:0.1). All of measurements were made in triplicate as shown.....	91
5.4 UV-Vis spectra of a) 1 mM dinuclear rhodium complex 1 ·(HOAc) ₂ in chloroform (black line a), b) 1 mM dinuclear rhodium complex 1 ·(HOAc) ₂ in chloroform after trapping gaseous species flowing out of the APTD when a blank solvent ACN/H ₂ O/HOAc (50:50:0.1) was sprayed into the APTD tube at 300 °C (red line b), c) 1 mM dinuclear rhodium complex 1 ·(HOAc) ₂ in chloroform after trapping species flowing out of the APTD when 25 mM phenethylamine in ACN/H ₂ O/HOAc (50:50:0.1) was sprayed into the APTD tube at 300 °C (blue line c), and d) 1 mM dinuclear rhodium complex 1 ·(HOAc) ₂ in chloroform after trapping species flowing out of the APTD when 25 mM phenylalanine in ACN/H ₂ O/HOAc (50:50:0.1) was sprayed into the APTD tube at 300 °C (orange line d).....	93
5.5 ESI-MS spectra of a) 3 mM dinuclear rhodium complex 1 ·(HOAc) ₂ in chloroform, b) 3 mM dinuclear rhodium complex 1 ·(HOAc) ₂ in chloroform after trapping gaseous species flowing out of the APTD tube when a blank solvent of ACN/H ₂ O/HOAc (50:50:0.1) was sprayed into the APTD tube at 300 °C , c) 3 mM dinuclear rhodium complex 1 ·(HOAc) ₂ in chloroform after trapping gaseous species flowing out of the APTD tube when 25 mM phenethylamine in ACN/H ₂ O/HOAc (50:50:0.1) was sprayed into the APTD tube at 300 °C , d) 3 mM dinuclear rhodium complex 1 ·(HOAc) ₂ in chloroform after trapping gaseous species flowing out of the APTD tube when 25 mM phenylalanine in ACN/H ₂ O/HOAc (50:50:0.1) was sprayed into the APTD tube at 300 °C , e) 3 mM dinuclear rhodium complex 1 ·(HOAc) ₂ in chloroform after trapping standard carbon monoxide gas (purity 99.99%) for 3 min.....	96
5.6 CID MS/MS spectra of a) [1 -OAc+CO] ⁺ (<i>m/z</i> 814.99) and b) [1 -OAc+ ¹³ CO] ⁺ (<i>m/z</i> 815.99). The HCD energy used for dissociation was 20 eV.....	97
5.7 ESI-MS spectrum of 3 mM dinuclear rhodium complex 1 ·(HOAc) ₂ in chloroform after trapping gaseous species from the APTD tube when 25 mM ¹³ C-phenylalanine in ACN/H ₂ O/HOAc (50:50:0.1) was sprayed into the tube for APTD at 300 °C.....	98

LIST OF FIGURES
(Continued)

Figure	Page
5.8 APTD-MS spectrum of 0.25 mM phenylalanine in ACN/H ₂ O/HOAc (50:50:0.1) solution. The sample injection flow rate for ESSI was 10 μL/min, and + 5 kV voltage was used for ESSI. The temperature of APTD tube was 300 °C.....	99
5.9 APNR-MS spectra for detecting HCOOH from APTD of phenylalanine in the negative ion mode, when a) only solvent ACN/H ₂ O/HOAc (50:50:0.1) was sprayed into the APTD tube at 300 °C and b) 0.25 mM phenylalanine solution was sprayed into the APTD tube at 300 °C. ACN/H ₂ O/NH ₃ ·H ₂ O (50:50:0.1) was sprayed to ionize neutral species flowing out of the APTD tube. The absolute abundances of <i>m/z</i> 45 (referred to formate ion) in a) and in b) were 5.09×10 ³ and 5.29×10 ³ , respectively. No obvious increase in the <i>m/z</i> 45 signal was observed after phenylalanine was added into the spray sample.....	100
5.10 ESI-MS spectrum of 3 mM dinuclear rhodium complex 1 ·(HOAc) ₂ in chloroform after trapping neutral species flowing out of the APTD tube when 25 mM HCOOH in ACN/H ₂ O/HOAc (50:50:0.1) was sprayed into the tube for APTD at 300 °C.....	101
5.11 APTD-MS spectra of a) leucine, b) histidine, and c) tryptophan. Loss of 46 Da from the protonated amino acid was observed in all cases.....	102
5.12 ESI-MS spectra of into 3 mM dinuclear rhodium complex 1 ·(HOAc) ₂ in chloroform after trapping neutral species flowing out of the APTD tube when a) 25 mM leucine, b) 25 mM histidine, and c) 25 mM tryptophan in ACN/H ₂ O/HOAc (50:50:0.1) was sprayed into the tube for APTD at 300 °C.....	103
5.13 APTD-MS spectra of a) 5 mM GHG in ACN/H ₂ O/HOAc (50:50:0.1); b) 5 mM GWG in ACN/H ₂ O/HOAc (50:50:0.1). The temperature of the APTD tube was 300 °C.....	104
5.14 ESI-MS spectra of 3 mM dinuclear rhodium complex 1 ·(HOAc) ₂ solution after trapping neutral species flowing out of the APTD tube when a) ACN/H ₂ O/HOAc (50:50:0.1), b) 5 mM GHG in ACN/H ₂ O/HOAc (50:50:0.1) and c) 5 mM GWG in ACN/H ₂ O/HOAc (50:50:0.1) was sprayed into the tube for APTD at 300 °C.....	105
6.1 Exploring gold-catalyzed alkyne oxidation coupling.....	114
6.2 MS monitoring of gold-catalyzed phenylacetylene oxidative coupling.....	115
6.3 The observed Au(III) intermediate peaks compared with simulated results.....	116

LIST OF FIGURES
(Continued)

Figure	Page
6.4 The collision-induced dissociation spectrum of Au(III) intermediate (m/z 672)...	116
7.1 Microdroplet digestion of IgG1 (the NIST IgG1 monoclonal antibody reference material 8671) by IdeS enzyme: (a) Schematic drawing of intact IgG1 and IdeS-cleaved IgG1 fragments; The light chain, heavy chain, and hinge region are highlighted in green, blue, and grey, respectively. Black solid lines indicate disulfide bonds connecting heavy and light chains. The IdeS cleavage site is indicated with scissors and dash line. (b) Workflow of microdroplet digestion of IgG1 by IdeS; nESI-MS spectra of (c) antibody fragments obtained from microdroplet digestion of IgG1 by IdeS at room temperature and (d) In-solution digested IgG1 by IdeS for 5 min at 37°C.....	124
7.2 Simultaneous microdroplet digestion and reduction of IgG1. (a) Schematic representation of intact IgG1 and fragment structures of IgG1 after IdeS digestion and TCEP reduction. (b) Schematic drawing of the microdroplet digestion and reduction workflow. (c) The expanded MS spectrum with LC, Fd' and glycosylated scFc fragments detected and annotated. (d) The corresponding deconvoluted MS spectrum of (c). (e) Schematic drawing of simultaneous microdroplet digestion and reduction coupled with online EESI-MS detection. (f) Deconvoluted MS spectrum of digested and reduced IgG1 from online EESI-MS detection.....	128
7.3 Stepwise microdroplet digestion and reduction of IgG1 in 5 mM NH_4HCO_3 buffer (pH 8). In this approach, IgG1 was first cleaved by IdeS into $\text{F}(\text{ab}')_2$ and scFc fragments, then TCEP was added to reduce $\text{F}(\text{ab}')_2$ into LC and Fd'. a) The expanded view of MS spectrum; b) The corresponding deconvoluted MS spectrum; c) 2D spectrum with m/z along the x-axis and charge number along the y-axis; and d) 2D spectrum with mass served along the x-axis and charge number along the y-axis.....	129
7.4 Stepwise microdroplet digestion and reduction of IgG1 in 5 mM phosphate buffer (pH 8). In this approach, IgG1 was first cleaved by IdeS into $\text{F}(\text{ab}')_2$ and scFc fragments, then TCEP was added to reduce $\text{F}(\text{ab}')_2$ into LC and Fd'. a) The expanded view of MS spectrum; b) The corresponding deconvoluted MS spectrum; c) 2D spectrum with m/z along the x-axis and charge number along the y-axis; and d) 2D spectrum with mass served along the x-axis and charge number along the y-axis.....	130

LIST OF FIGURES
(Continued)

Figure	Page
<p>7.5 Stepwise microdroplet reduction and digestion of IgG1 in 5 mM NH₄HCO₃ buffer (pH 8). In this approach, IgG1 was first reduced into LC and HC fragments by TCEP, then IdeS was added to cleave HC into Fd' and scFc. a) The expanded view of MS spectrum; b) The corresponding deconvoluted MS spectrum; c) 2D spectrum with <i>m/z</i> along the x-axis and charge number along the y-axis; and d) 2D spectrum with mass served along the x-axis and charge number along the y-axis.....</p>	131
<p>7.6 Microdroplet digestion of glycosylated IgG1. In this approach, glycosylated IgG1, IdeS and TCEP were mixed and reacted together in one-pot. The subunits of LC (and glycosylated-LC), Fd' (and glycosylated- Fd') and scFc fragments were produced simultaneously. (a) The expanded view of MS spectrum of non-glycosylated IgG1 (at day 0); (b) The MS spectrum of glycosylated IgG1 (incubated 2 days); (c) The MS spectrum of glycosylated IgG1 (incubated 5 days); (d) The deconvoluted MS spectrum of glycosylated IgG1 after 5 days incubation; and (e) 2D spectrum of glycosylated IgG1 after 5 days incubation with <i>m/z</i> along the x-axis and charge number along the y-axis.....</p>	134
<p>7.7 “One-pot” microdroplet reactions with IgG1, PNGase F, IdeS, and TCEP. (a) Schematic illustrating the PNGase F deglycosylation; (b) The expanded MS spectrum with LC, Fd' and scFc (both deglycosylated and glycosylated) fragments detected and annotated; (c) The deconvoluted MS spectrum of (b).....</p>	136
<p>7.8 a) Schematic of microdroplet deglycosylation workflow; b) Deconvoluted MS spectrum of deglycosylated IgG1 by microdroplet reaction; c) MS spectrum of deglycosylated IgG1 by PNGase F in microdroplets at room temperature; d) MS spectrum of intact IgG1 as a comparison.....</p>	137

LIST OF SCHEMES

Scheme	Page
2.1 Schematic showing the LC/EC/MS apparatus used for absolute quantitation	18
3.1 Our approach for quantitation of tyrosine-containing peptides. Note that, if other oxidizable residues co-exists, the oxidation could be more complicated.....	30
3.2 Schematic showing our LC/EC/MS apparatus for peptide quantitation.....	34
3.3 Equation showing electrochemical oxidation of a peptide tyrosine residue. Note that, if other oxidizable residues co-exists, the oxidation could be more complicated.....	36
4.1 Schematic showing our approach for absolute quantitation of protein.....	56
4.2 Schematic drawing of the LC/EC/MS setup for absolute quantitation of proteins.....	62
5.1 Three proposed amino acid fragmentation pathways toward the formation of iminium ion (illustrated using phenylalanine as an example): a) losses of CO and H ₂ O molecules, b) loss of dihydroxycarbene C(OH) ₂ , and c) loss of formic acid HCOOH.....	83
5.2 Schematic drawing of the APTD apparatus and processes: 1) direct detection of ionic fragments from the APTD coiled tube by MS, 2) use of CO sensor to directly detect carbon monoxide emerging from the APTD coiled tube and 3) use a binuclear rhodium complex solution to trap CO molecules followed with offline characterization by MS and/or UV/Vis.....	83
5.3 Scheme showing dissociation from peptide <i>b</i> ion to <i>a</i> ion by the loss of neutral CO. Note that <i>a</i> and <i>b</i> ions are drawn in the way shown in their original definitions; their true structures may well be cyclic.....	86
5.4 Selective binding of CO by the binuclear rhodium complex 1 ·(HOAc) ₂ . The complex product 1 ·(CO, HOAc) forms after CO binding.....	92
5.5 Schematic showing the process and apparatus used for APNR-MS.....	100
6.1 Electrochemical approach for gold-redox catalysis.....	109
6.2 General procedures for the ElectraSyn Setup.....	112
7.1 Schematic showing two microdroplet digestion workflows.....	127

CHAPTER 1

INTRODUCTION

1.1 Mass Spectrometry

Mass spectrometry (MS) has been growing as one of the most sensitive and powerful analytical techniques to identify chemicals by measuring the mass-to-charge ratio (m/z).¹ Tremendous remarkable developments have been achieved in a variety of applications during the past several decades. In addition, tandem mass spectrometry (MS/MS) has been used to dissociate the ions of interest into fragment ions to facilitate the structure elucidation of target analytes.² Various hyphenated techniques and applications have also been established, which couples other analytical separation techniques such as liquid chromatography (LC), gas chromatography (GC), capillary electrophoresis (CE), etc., to assist the analysis of more complicated mixtures. These features and applications make MS widely used to analyze various analytes covering from small organic molecules to large biological samples.³ Therefore, MS has now become an indispensable tool and has been extensively applied in broad research areas including pharmaceutical, clinical, proteomics, metabolomics, and environmental science.⁴

1.2 Mass Spectrometer

The mass spectrometer usually consists of a sample inlet, ion source, mass analyzer, ion detector, and data analysis system (see Figure 1.1). The analyte for MS analysis can be introduced to the inlet via a direct injection pump, LC, GC, etc. The ion source ionizes analyte molecules into gas-phase ions and then accelerates them into the mass analyzer. In

the mass analyzer, the ions are selected and filtered according to their mass-to-charge ratios (m/z). After ions are separated, the selected ions would be collected and detected in the ion detector, where the signal is amplified and recorded as a mass spectrum showing the relative abundance of ions as a function of m/z .

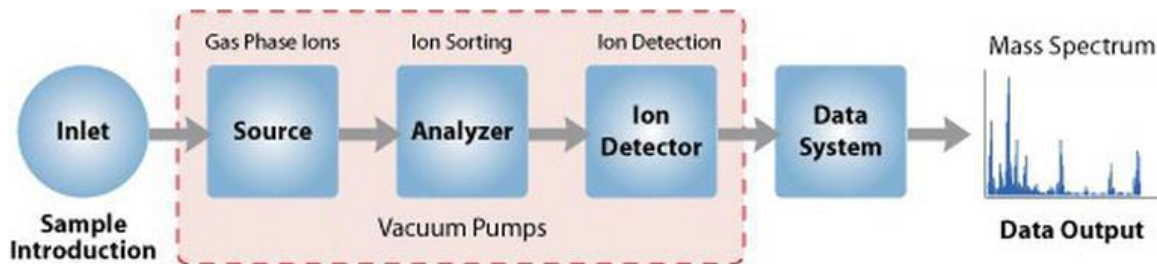


Figure 1.1 Basic configuration of a mass spectrometer.⁵

Source: Baghel, U. S.; Singh, A.; Singh, D.; Sinha, M. *Application of Mass Spectroscopy in Pharmaceutical and Biomedical Analysis. In Spectroscopic Analyses - Developments and Applications; InTech, 2017.*

1.3 Ionization Methods

Nowadays, numerous ionization methods have been developed by scientists in order to serve further MS analysis. The selection of varying ionization methods depends on the physical and chemical properties of target analytes.

Electron ionization (EI, see Figure 1.2) is an ionization method in which energetic electrons interact with solid or gas phase atoms or molecules to produce ions.⁶ Though EI was one of the first ionization techniques developed for mass spectrometry,⁷ this method is still widely used. EI is considered a “hard” ionization method because high-energy electrons have been used to produce ions, which leads to extensive fragmentation and can be helpful for the structure determination of unknown compounds. EI is one of the most powerful tools for organic compounds which have a molecular weight below 600 Da. Also,

several other thermally stable and volatile compounds in solid, liquid and gas states can be detected using this technique when coupled with various separation methods.⁸

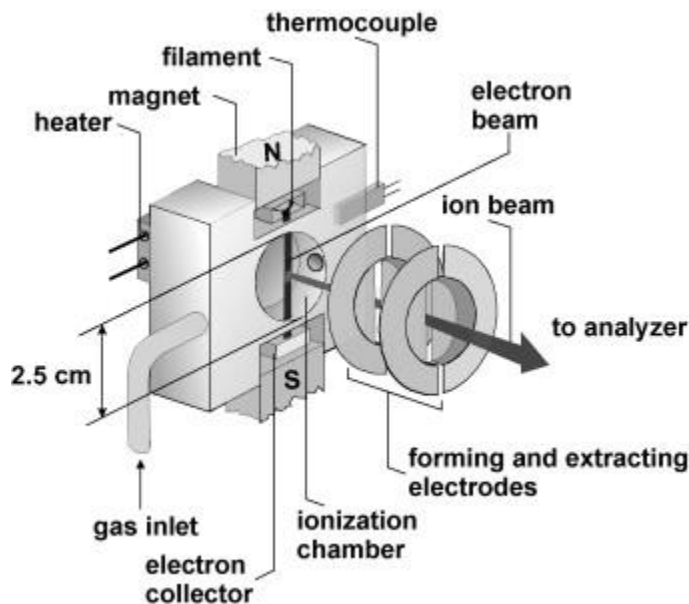


Figure 1.2 The diagram of EI ion source.⁹

Source: Gluch, K.; Cytawa, J.; Michalak, L. *Electron Impact Ionization of Acrylonitrile. Int. J. Mass Spectrom.* 2008, 278 (1), 10–14.

The electrospray ionization (ESI) was first reported by John Fenn and Masamichi Yamashita in 1984¹⁰ and later awarded the Nobel Prize in 2002 for this discovery. In the last two decades, ESI has become one of the most dominant ionization methods in the field of MS analysis. The ESI serves as an essential tool to analyze large molecules such as proteins, antibodies, etc., which could not be ionized with traditional methods like electron ionization (EI) and chemical ionization (CI).^{11,12} It works under atmospheric pressure and is considered as a soft ionization technique.

In ESI (see Figure 1.3), a solution of analyte is introduced through a capillary. A high voltage (2-5 kV) is applied to the capillary where the Taylor cone is formed at the

capillary tip under an electric field in ambient conditions to emit droplets. The resulting ions are transferred into the MS for analysis. There are two proposed mechanisms to explain ESI. One is the charge residue model (CRM), which developed by Dole *et al.* and claimed that a droplet containing a single residual analyte ion remains caused by successive cycles of solvent evaporation and Coulombic fissions at the Raleigh limit, followed by a complete evaporation of the solvent comprising this droplet, finally to yield a naked and charged analyte ion.¹³ The other mechanism is the ion evaporation model (IEM) proposed by Iribarne and Thomson.¹⁴ It is based on transition-state, and it supposes that the desolvation process of a droplet is in priority. Then the sufficient strong repulsion force between the charged analyte ions and the other charges in the droplet overcomes solvation forces. The analyte ion is ejected from the droplet surface into the gas phase.¹⁵

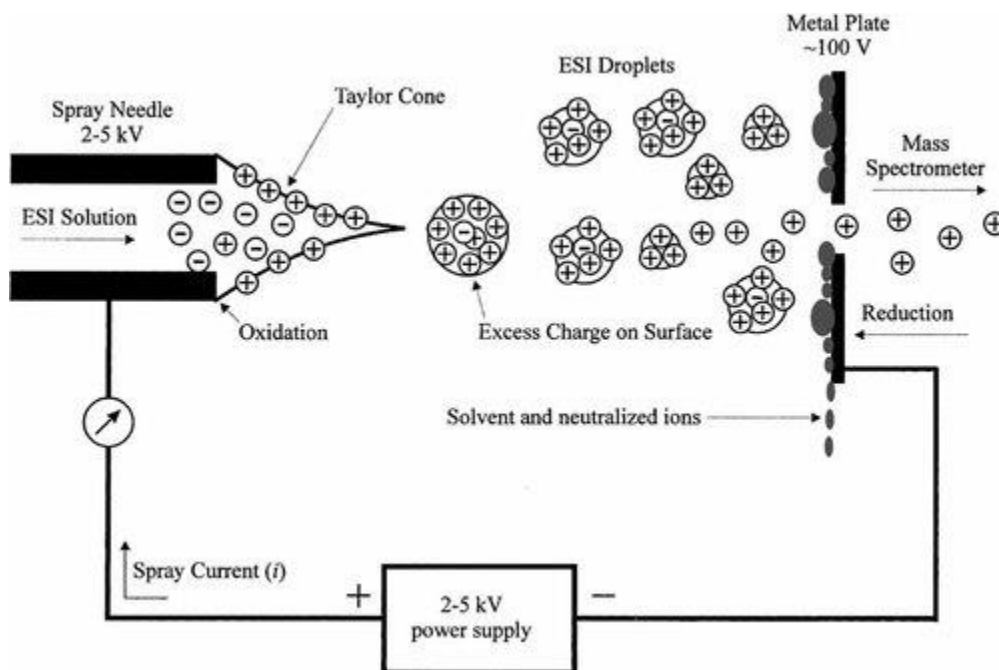


Figure 1.3 Schematic of the electrospray ionization process.¹⁶

Source: Cech, N. B.; Enke, C. G. *Practical Implications of Some Recent Studies in Electrospray Ionization Fundamentals. Mass Spectrom. Rev.* 2001, 20 (6), 362–387.

Nano-electrospray ionization (nESI or Nano-ESI) is generally recognized as a variant form of ESI with a low sample flow rate and improved ionization efficiency.¹⁷ With reduced sample flow rate (nL/min) or little sample loading amount (nL to μL), sample spray and ions can be effectively generated by a high voltage (1-2 kV) without sheath gas provided. Therefore, it is advantageous for limited amount of samples. Also, the sample signal can last for a long time with nESI, during which more MS scans and data could be collected for better sample characterization.

Cooks and coworkers first reported electrosonic spray ionization (ESSI, see Figure 1.4), another variant of ESI in 2004.¹⁸ Compared to conventional ESI, the ESSI uses much higher nebulization gas flow which could generate supersonic flow, affording ESSI more flexibility including flow rate, high voltage and geometry.¹⁹ It has been claimed that narrower peaks could be received when using the ESSI for multiply charged protein ions. Also, noncovalent complexes were reported to be observed by using the ESSI technique.¹⁸

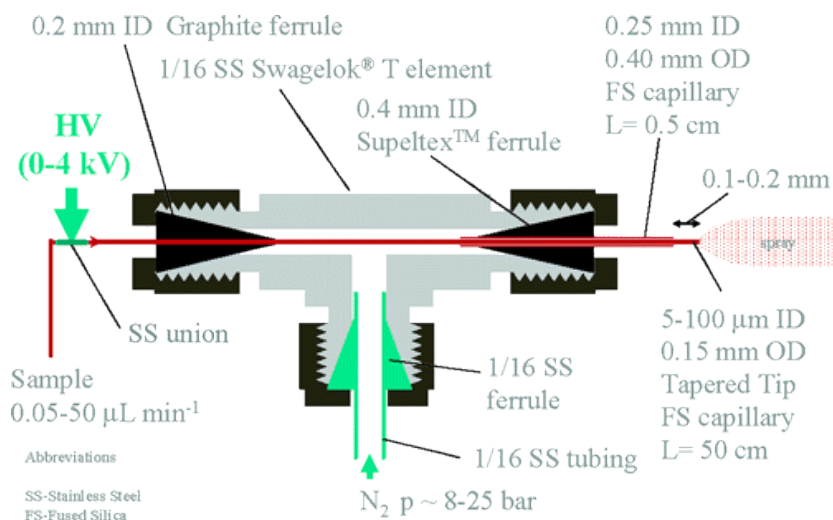


Figure 1.4 Schematic of ESSI source.¹⁸

Source: Takáts, Z.; Wiseman, J. M.; Gologan, B.; Cooks, R. G. *Electrosonic Spray Ionization. A Gentle Technique for Generating Folded Proteins and Protein Complexes in the Gas Phase and for Studying Ion-Molecule Reactions at Atmospheric Pressure.* *Anal. Chem.* 2004, 76 (14), 4050–4058.

Unlike ESI, ambient mass spectrometry has established a recent advance which directly ionizes analytes with little or no sample preparation. Two most widely used ambient techniques are desorption electrospray ionization (DESI)²⁰ developed by Cooks and paper spray (PS)²¹ developed by Ouyang. As shown in Figure 1.5, the DESI setup consists of a DESI sprayer, a sample deposition surface, and a mass spectrometer. The DESI sprayer is used to generate charged solvent droplets by the high voltage and nebulization gas. The charged solvent droplets spray directly onto the analyte deposited on the surface, to desorb and ionize the analyte molecules. The desorbed ions travel through the atmospheric inlet into the mass spectrometer.²² The advantages of DESI-MS include minimal sample preparation, in-situ detection, applicable to both small and large molecules, high-throughput analysis, and label-free imaging.^{23–25}

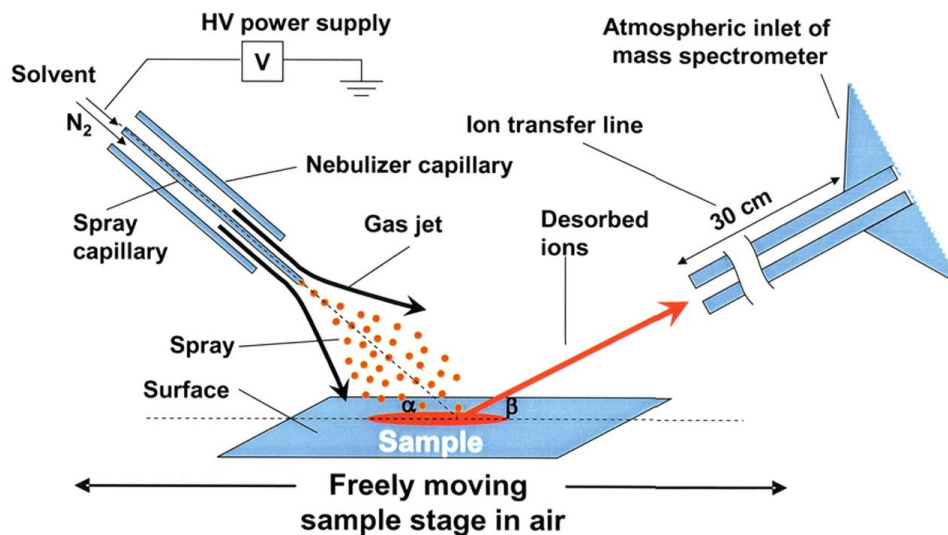


Figure 1.5 Schematic of typical DESI setup.²⁰

Source: Takáts, Z.; Wiseman, J. M.; Gologan, B.; Cooks, R. G. *Mass Spectrometry Sampling under Ambient Conditions with Desorption Electrospray Ionization*. *Science* (80). 2004, 306 (5695), 471–473.

1.4 Mass Analyzers

A mass analyzer is the mass spectrometer component that takes ionized masses and separates them based on charge to mass ratios and outputs them to the detector where they are detected and later converted to a digital output. Different mass analyzers have their specific characteristics.

Quadrupole mass analyzer (see Figure 1.6) consists of four parallel cylindrical metal rods inside a vacuum chamber and each opposing rod pair is connected electrically. Both a direct current (DC) and high radio frequency (RF) are applied to the quadrupole to manipulate ions with the target m/z successfully pass through and transmit to the detector. By changing DC and RF in time, ions with different m/z can be delivered to the detector. The quadrupole mass analyzer is simple to manufacture and use, affordable, and robust for routine target compounds analysis, widely used in pharmaceutical and biological analysis.²⁶ The limitations include relatively low resolution (< 3000), poor mass accuracy (> 100 ppm), and limited mass range (typically ≤ 3000 Da).²⁷ Quadrupoles can be considered as the most frequently used analyzers are commonly coupled to GC-MS and LC-MS instruments.

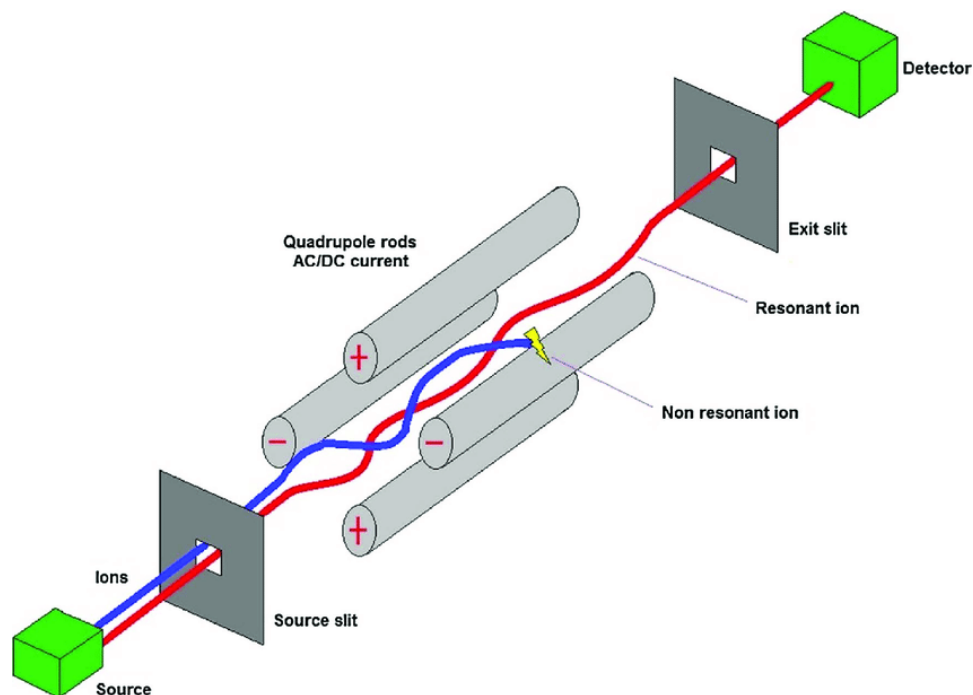


Figure 1.6 Diagram showing a quadrupole MS.²⁸

Source: Santoiemma, G. *Recent Methodologies for Studying the Soil Organic Matter*. *Appl. Soil Ecol.* 2018, 123, 546–550.

A time-of-flight (TOF, see Figure 1.7) analyzer consists of a pulsed ion source, an accelerating grid, a field-free flight tube, and a detector. The ion travel time has been measured by TOF MS to separate and detect ions of different m/z . First, ions generated in an ionization source can be accumulated and introduced into a flight tube, where these ions are accelerated by applying a high acceleration voltage between the electrodes. The corresponding kinetic energy is described in Equation (1.1). With a constant acceleration voltage as well as kinetic energy, each ion flies at its unique velocity inside the flight tube to reach the ion detector. As shown in Equation (1.2), time of flight (T) is proportional to the square root of m/z , in a fixed flight distance (L). Ions with smaller m/z reach the detector sooner than those with larger m/z . Therefore, the time of flight (T) can be converted directly

to m/z . Since there is no limit to the time of flight in TOF MS, it can theoretically measure an unlimited mass range.

$$KE_{\text{ion}} = \frac{1}{2}mv^2 = zeV \quad (1.1)$$

$$T = \frac{\text{distance}}{\text{velocity}} = \sqrt{\frac{m}{z}} \times \frac{L}{\sqrt{2eV}} \quad (1.2)$$

Where T is time of flight, m is mass of the ion, v is velocity of the ion, z is charge of the ion, e is elementary charge, V is accelerating voltage applied, L is flight distance.

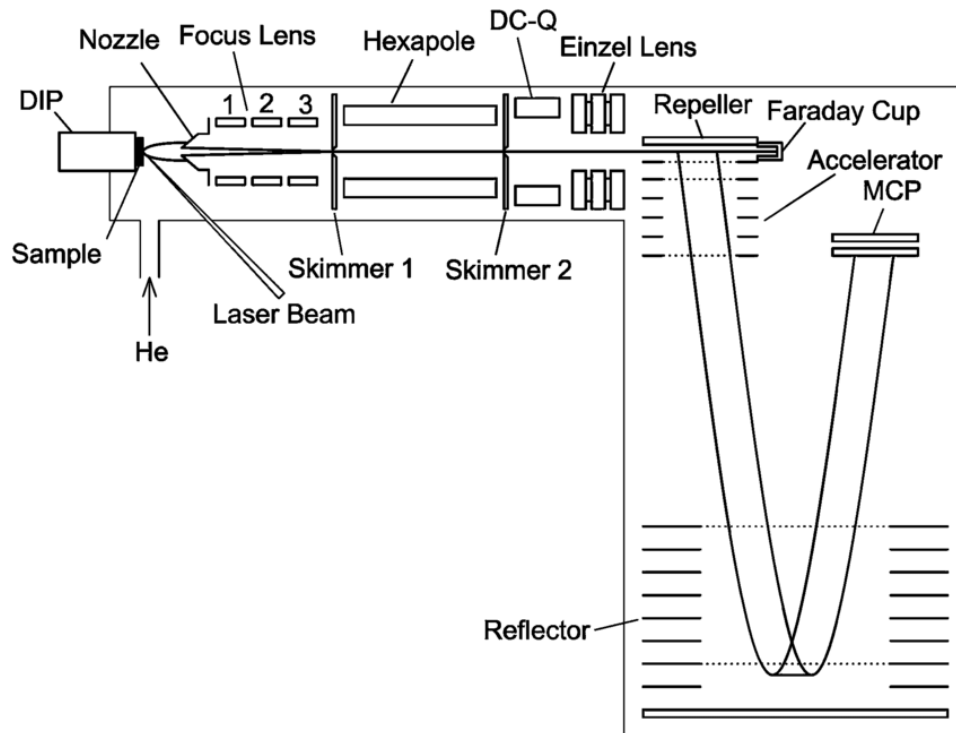


Figure 1.7 Schematic diagram of a TOF-MS.²⁹

Source: Tong, Q.; Yu, Q.; Jin, X.; He, J.; Hang, W.; Huang, B. *Semi-Quantitative Analysis of Geological Samples Using Laser Plasma Time-of-Flight Mass Spectrometry*. *J. Anal. At. Spectrom.* 2009, 24 (2), 228–231.

An ion trap mass analyzer uses an oscillating electric field to store ions. There are several types of ion trap MS, linear ion trap (LIT) and Orbitrap will be discussed in this dissertation. The linear ion trap (LIT) serves as a potential well for the ions. As shown in Figure 1.8, a set of quadrupole rods is used to confine ions radially and axially by a two-dimensional radio frequency (RF) field and a static electrical potential, respectively. Ions will maintain their positions within the center of the ion trap. The RF voltage is adjusted and multi-frequency resonance ejection waveforms are applied to the trap to eliminate all but the desired ions in preparation for subsequent fragmentation and mass analysis.³⁰

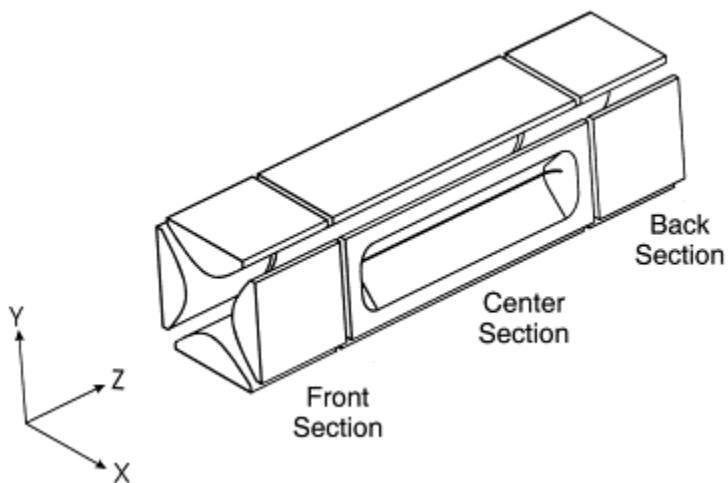


Figure 1.8 Schematic diagram of a two-dimensional linear ion trap.³¹

Source: Schwartz, J. C.; Senko, M. W.; Syka, J. E. P. *A Two-Dimensional Quadrupole Ion Trap Mass Spectrometer*. *J. Am. Soc. Mass Spectrom.* 2002, 13 (6), 659–669.

Orbitrap (see Figure 1.9) is the newest addition to the family of high-resolution mass analyzer. In orbitrap, moving ions are trapped in an electrostatic field. The electrostatic attraction towards the central electrode is compensated by a centrifugal force that arises from ions' initial tangential velocity. The electrostatic field which ions experience inside the orbitrap forces them to move in intricate spiral patterns. The axial

component of these oscillations is independent of initial energy, angles and positions. It can be detected as an image current on the two halves of an electrode encapsulating the orbitrap. A Fourier transform is employed to obtain oscillation frequencies for ions with different masses, resulting in an accurate reading of their m/z .³²

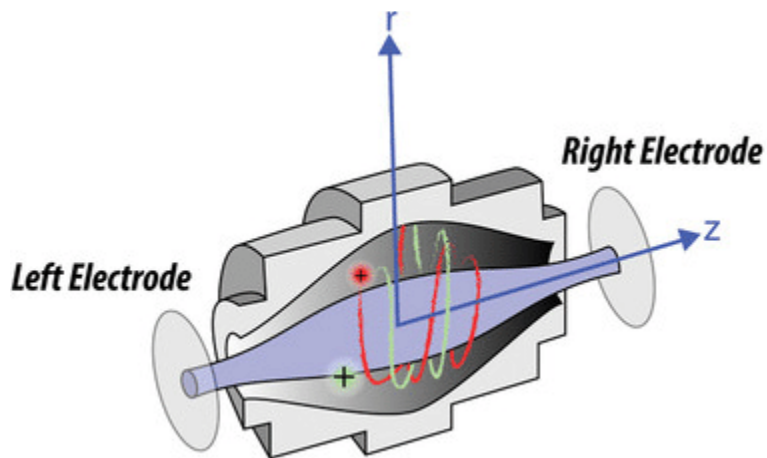


Figure 1.9 Schematic drawing of an Orbitrap mass analyzer.³³

Source: Savaryn, J. P.; Toby, T. K.; Kelleher, N. L. *A Researcher's Guide to Mass Spectrometry-Based Proteomics*. *Proteomics* 2016, 16 (18), 2435–2443.

1.5 Electrochemical Mass Spectrometry

Electrochemical mass spectrometry brings up the online combination of electrochemistry (EC) and mass spectrometry (MS). EC is the study of chemical processes that cause electrons to move. The electricity, which is the movement of electrons, can be generated from one element to another in a reaction known as oxidation-reduction (“redox”) reaction.³⁴ By measuring the electric current and potential, analytes’ concentration or chemical reactivity can be determined.³⁵ However, only measuring electric signals for analyte identification is limited and not direct in complex redox reactions generating complicated products or intermediates. This triggers EC to couple with other analytical

techniques (e.g., electron microscopy³⁶, UV³⁷, FTIR³⁸, etc.) to achieve better analyte characterization performance. Notably, the coupling of EC and MS has received growing attentions in the past years. The advantage of hyphenating MS with EC is that MS can offer analyte molecular weight information with high sensitivity and low limit of detection. Moreover, tandem MS (MS/MS) can further provide analyte structural information by dissociation. Therefore, EC/MS serves as a powerful tool in identifying electrochemical reaction products or intermediates to elucidate reaction mechanisms and play a valuable role in quantitative analysis of electroactive analytes. Extensive applications have been demonstrated in the field of bioanalysis and mechanic studies.³⁹⁻⁴⁸

ESI is one of the most commonly used ionization methods for MS analysis. In ESI-MS, A high voltage is applied to ionize sample analytes, while a small potential is used in the electrochemical cell. A grounding point is needed and often introduced between the ESI source and the electrochemical cell to overcome the potential difference. Van Berkel, Bond, and Dupont are the pioneers to apply EC/ESI-MS approach in various research investigations.⁴⁹⁻⁵⁴ One of the advantages of coupling EC with ESI-MS is that ESI can ionize polar, nonvolatile, and thermally labile compounds (e.g., biomolecules).¹⁰ Van Berkel and Zhou also first demonstrated applications that using different types of electrochemical flow cells (i.e., thin-layer electrode, tubular electrode, and porous electrode flow cells) coupled with ESI-MS analysis.⁵⁵

The separation techniques such as high-performance liquid chromatography (HPLC), ultra-high performance liquid chromatography (UPLC) and capillary electrophoresis (CE) can be applied to support online EC-MS studies. By using the combinational system of LC, EC and MS, additional retention behavior and polarity

information of analyte can be obtained. The first attempt to conduct an online electrochemical reaction after LC separation (see Figure 1.10) was carried out by Karst and coworkers to detect different ferrocenecarboxylic acid esters.⁵⁶ By using the hyphenation of EC/ESI-MS with chromatographic separation methods, recent online studies can identify organic substance speciation and quantify inorganic constituents of oxidative roxarsone⁵⁷; monitor main phase I metabolites of insecticide chlorpyrifos and fungicide fluopyram^{58,59}; electrochemically digest proteins⁶⁰; and absolute quantify various biomolecules without addition of internal standards⁶¹. A wide variety of rising complexity applications are reported, in most of which redox behavior of analytes is often investigated and optimized by EC. At the same time, LC-MS is applied to characterize retention behavior and mass of products.

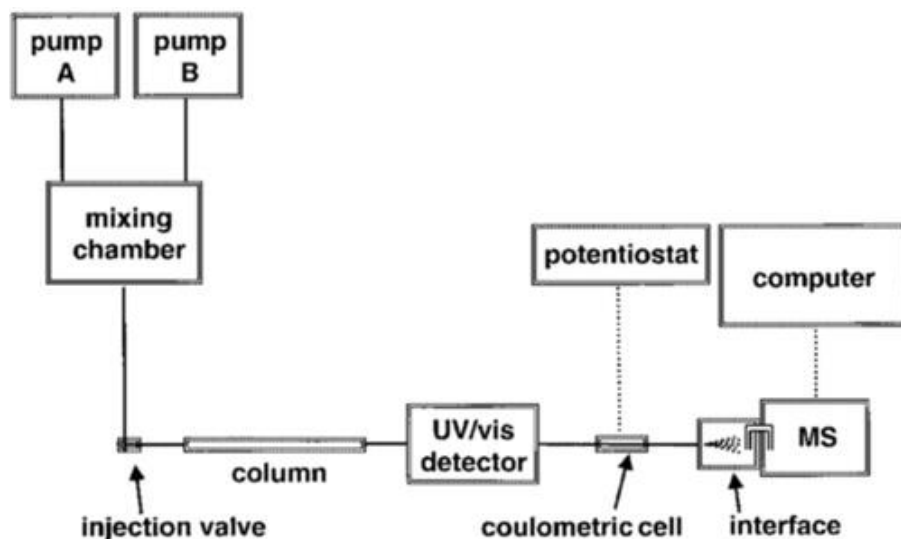


Figure 1.10 Scheme of an HPLC-EC-MS setup.⁵⁶

Source: Diehl, G.; Liesener, A.; Karst, U. *Liquid Chromatography with Post-Column Electrochemical Treatment and Mass Spectrometric Detection of Non-Polar Compounds*. *Analyst* 2001, 126 (3), 288–290.

CHAPTER 2

IMPROVEMENTS FOR ABSOLUTE QUANTITATION USING ELECTROCHEMICAL MASS SPECTROMETRY

Adapted from Zhao, P.; Guo, Y.; Dewald, H. D.; Chen, H. *Int. J. Mass Spectrom.* **2019**, 443, 41–45. Copyright 2019, Elsevier.

2.1 Introduction

Mass Spectrometry (MS) has become a powerful tool commonly used for identification of a variety of chemical species due to its high sensitivity and capability of providing structural information^{62–66}. Nevertheless, accurate quantitation by MS is still challenging due to fluctuation of the MS signals; and the signal intensity in a MS spectrum does not always correlate well with the amount of analytes^{67–69}. Therefore, accurate MS quantitation often has to use reference standards for calibration or isotope-labeled compounds as a reference^{70,71}. To date, many quantitative MS methods have been developed with great successes, such as isotope-coded affinity tags (ICAT)^{72–78}, stable isotope labeling with amino acids in cell culture (SILAC)^{76,79–82}, isobaric tags for relative and absolute quantification (iTRAQ)^{83–86}, metal element chelated tags (MECT)⁸⁷ and isotope-coded protein labeling (ICPL)⁸⁸ *etc.*. However, the reference standards or isotope-labeled compounds that are required for quantification might not be readily available, and sometimes cost prohibitive and time-consuming^{89–92}.

To overcome this issue, we recently developed an electrochemistry (EC)-assisted absolute quantitation method using MS without the need for the reference standards or isotope-labeled compounds⁶¹. In our method, a target analyte, if electrochemically oxidizable, is first introduced to an electrochemical cell for oxidation and followed by MS

detection. The integration of the resulting electrochemical current peak over time provides information about the amount of the oxidized compound, based on the Faraday's Law:

$$n = \frac{Q}{zF\Delta i} \quad (2.1)$$

where n is the moles of the oxidized analyte, Q is the total charge involved in the oxidation reaction, z is the number of electrons transferred per molecule during oxidation, F is the Faraday constant (9.65×10^4 C/mol), and Δi is the redox conversion yield. Meanwhile, this electrochemically active analyte shows a reduced intensity in the acquired MS spectra from electrochemical oxidation. The relative MS intensity change can be used to determine the redox conversion yield (Δi). Thus, the amount of the oxidized analyte can be calculated using Eq. (2.1). Using this approach, various analytes such as dopamine, norepinephrine, and rutin as well as peptide glutathione in low quantity were successfully quantified. However, only pure compounds or a single species in a biological matrix (e.g., uric acid in urine) was quantified in this prototype experiment⁶¹.

In this study, we further show that our method can be applied to absolute quantitation of individual compounds in a mixture following chromatographic separation. As a demonstration, dopamine and serotonin (5-HT) were separated using a hydrophilic interaction liquid chromatography (HILIC) column with gradient elution, followed by electrochemical oxidation and MS detection for quantitation.

On the other hand, for absolute quantitation of samples that are already purified, LC column can be removed (i.e., flow-through analysis) so that analysis time for each injected sample can be greatly reduced, from 10 min in our previous study⁹³ to 2 min. By

using an auto-sampler, consecutive injections can be made sequentially, allowing fast analysis of multiple samples. These improvements would help to expand the application of our method for quantitative analysis.

2.2 Experiments

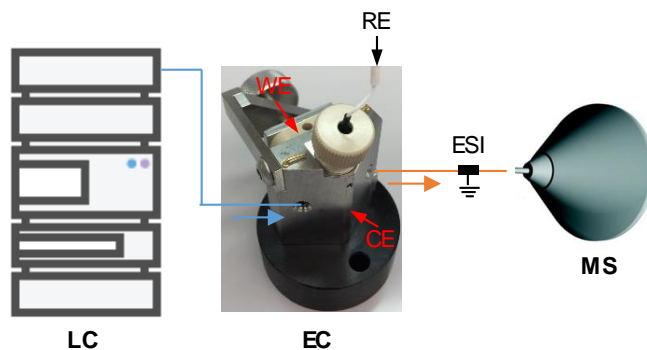
2.2.1 Chemicals

Dopamine (DA) hydrochloride, (-)-norepinephrine (NE), and serotonin (5-HT) hydrochloride were purchased from Sigma Aldrich (St. Louis, MO). Formic acid and acetonitrile were obtained from Fisher Chemical (Fair Lawn, NJ), and deionized water used for sample preparation was obtained using a Millipore Direct-Q5 purification system (Burlington, MA).

2.2.2 Instrumentation

For the experimental setup (illustrated in Scheme 2.1), a Waters Ultra-Performance Liquid Chromatography (UPLC, Milford, MA) was coupled with a BASi electrochemical thin-layer flow cell (West Lafayette, IN). The electrochemical cell was equipped with a glassy carbon disc electrode (*i.d.*, 6 mm) as the working electrode (WE). A Ag/AgCl (3M NaCl) electrode was used as the reference electrode (RE) and stainless steel cell body served as a counter electrode (CE). A positive potential of +1.05 V (vs. Ag/AgCl) was applied to the WE electrode for analyte oxidation. The oxidation current response was monitored and recorded by a ROXYTM potentiostat (Antec BV, Netherland). The electric current peak area was integrated by importing the current data to OriginPro 2018b to calculate the total electric charge (Q) involved in the oxidation reaction. The eluate flowing out of the cell was subsequently analyzed using online electrospray ionization mass spectrometry (ESI-

MS). MS data were collected using a high-resolution Q-Exactive Orbitrap mass spectrometer (Thermo Scientific, San Jose, CA). The sheath gas flow rate was 10 L/h. The spray voltage was +4 kV and the inlet capillary temperature was kept at 250 °C. Extracted ion chromatograms (EIC) of the analytes were acquired by Thermo Xcalibur (3.0.63).



Scheme 2.1 Schematic showing the LC/EC/MS apparatus used for absolute quantitation.

For flow-through analysis of the pure compounds, the LC column was removed. The mobile phase flow rate was kept at 100 $\mu\text{L}/\text{min}$. An auto-sampler was used to inject samples with the injection volume of 6 μL . As illustrated in Figure 2.1, an injection sequence consisted of three steps: 1) a blank solvent (ACN/H₂O/FA, 50:50:0.1 by volume) injection to check if there was any sample leftover, 2) an analyte solution injection when the electrochemical cell was turned off (i.e., the “cell-off “mode), 3) an analyte solution injection when the electrochemical cell was turned on (i.e., the “cell-on “mode). The running time for each injected sample was 2 min, except that the electrochemical cell was turned on 1.5 min step 3), so that the charging current could fade away and not interfere with the analyte oxidation current. DA and NE were chosen as two test samples and their injected concentrations were 50 μM .

For the mixture analysis, A Waters XBridge™ Amide column (2.1 mm × 150 mm, 3.5 μm) was selected for HILIC separation. A mixed solution containing DA and 5-HT was tested as a demonstration. The mobile phase flow rate was 200 μL/min. The mobile phase A was 10 mM of NH₄OAc dissolved in ACN/H₂O (90:10) solution, and mobile phase B was 10 mM of NH₄OAc in H₂O. The mobile phase B started from 5% and increased to 15% in 10 min, and then climbed to 35% from 10 min to 20 min. After that the mobile phase B was kept at 35% for 5 min, and then went back to 5% in 1 min. The concentrations of DA and 5-HT were both 50 μM in the mixture solution, and the injection volume was 3 μL.

2.3 Results and Discussion

To speed up the LC/EC/MS workflow, we reasoned that it is unnecessary to have LC column used when pure compounds are aimed to be quantified in our approach. In this case, the LC column was removed and flow-through analysis was conducted. In our quantitation experiment, the MS spectra of the analyte were collected to determine the conversion yield before and after the electrode was turned on. Each compound was measured in triplicates. As shown in the first step of the sample injection sequence (Figure 2.1), a solvent blank was injected for cleaning purpose to prevent carryover and cross-contamination, followed by an injection of the analyte in the “cell-off” mode. After that, the cell was turned on and a charging current showed up immediately. The charging current faded away and went back to baseline in around 1.5 min. Then another injection of the analyte was made in the “cell-on” mode and a faradaic current from the oxidation of the target analyte was recorded. Each injection analysis was 2 min, which is only 1/5 of the

time in our previous study where a LC column was installed in the LC/EC/MS system ⁶¹. After the first cycle, a second injection sequence could be performed, as illustrated in Figure 2.2. In this experiment, DA and NE were chosen as two analyte samples and each of them was run in triplicates (Figure 2.2). In this way, 12 injections of both DA and NE samples and 6 injections of blank solvent were done in a total 45 min sequence, whereas 120 min would be needed for 10 min per injection using the previous protocol that we reported ⁶¹, excluding extra time needed for LC column equilibration and cleaning. The analysis results of DA and NE from the triplicate measurements are discussed below.

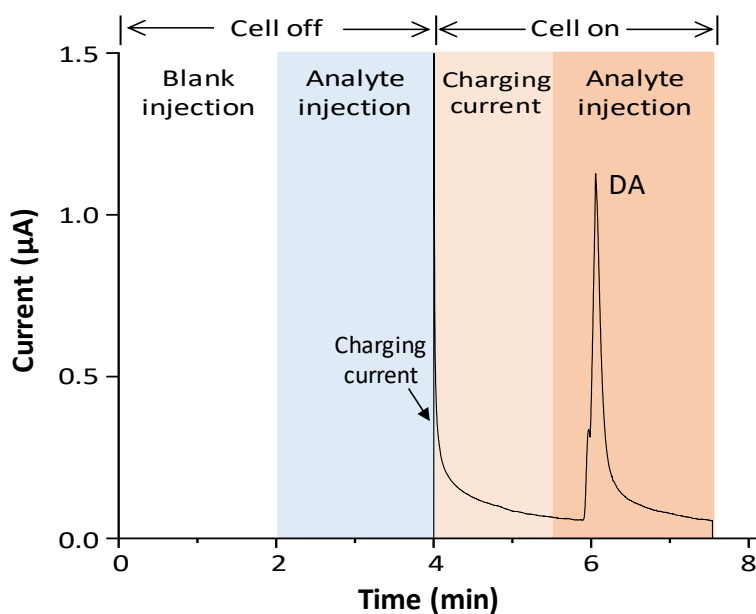


Figure 2.1 A schematic showing of the first 7.5 min of the injection sequence, where 0-2 min was a blank solvent injection for cleaning purpose; 2-4 min was an analyte injection in the “cell-off” mode. The electrochemical cell was turned on at 4 min, and a charging current was generated as the potential was applied. Another injection for the analyte solution was injected in the “cell-on” mode, 1.5 min after the cell was turned on. The time period of 0-7.5 min could be considered as a cycle, and the second consecutive cycle started at 7.5 min (see Figure 2.2).

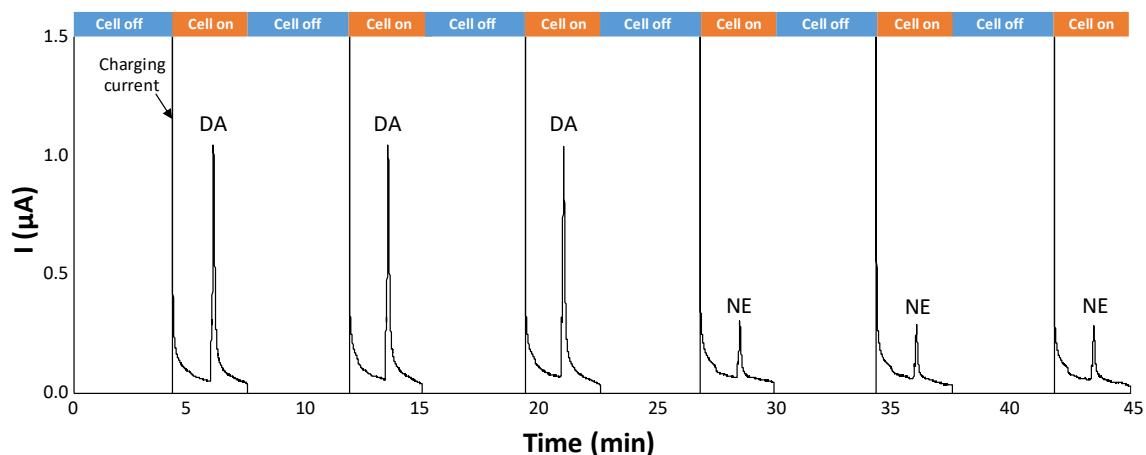
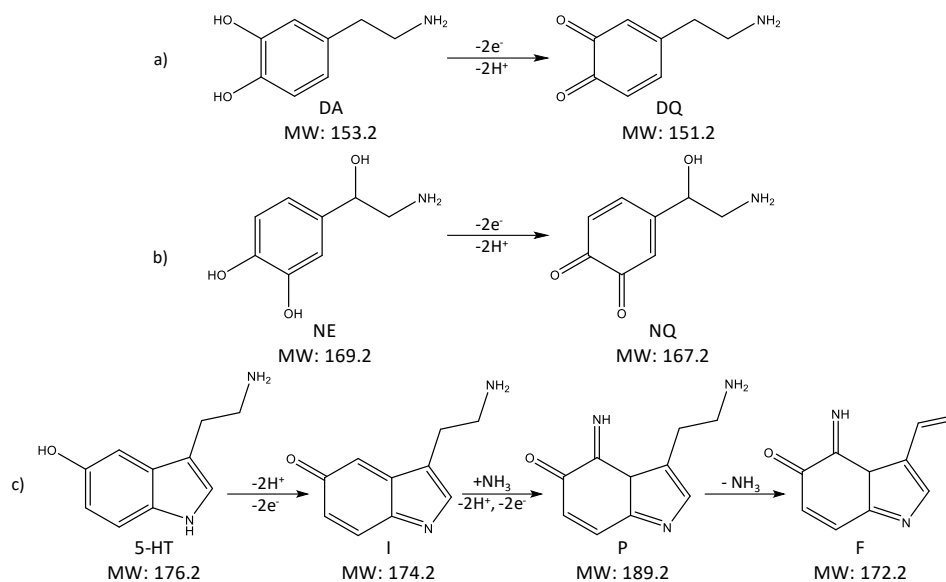


Figure 2.2 Electrochemical currents of DA and NE compounds in a no-column injection sequence.

DA, a known neurotransmitter, undergoes electrochemical oxidation via a two-electron transfer reaction to produce dopamine *o*-quinone (DQ, Scheme 2.2-a). Before electrolysis (Figure 2.3), the protonated DA was detected at m/z 154. After electrolysis (Figure 2.3-b), a peak at m/z 152 was observed, corresponding to +1 ion of the oxidized DA product. The integrated area for the MS peak was reduced by 8.1% on average upon electrolysis, indicating that the oxidation yield for DA was 8.1% (see data in Table 2.1). In the cell-on mode, the DA oxidation current peak was detected, as shown in Figure 2.3-d (Figure 2.3-c shows the background current diagram for blank solvent sample under the same + 1.05 V potential as a contrast). Based on the integration of the current peak area, the amount of the oxidized DA was calculated to be 25.5 pmol on average. Therefore, our measured amount of DA was 314 pmol, which was close to the injected amount of 300 pmol with a measurement error of 4.8% (Table 2.1).



Scheme 2.2 Equations showing the electrochemical oxidation of a) DA, b) NE, and c) 5-HT.

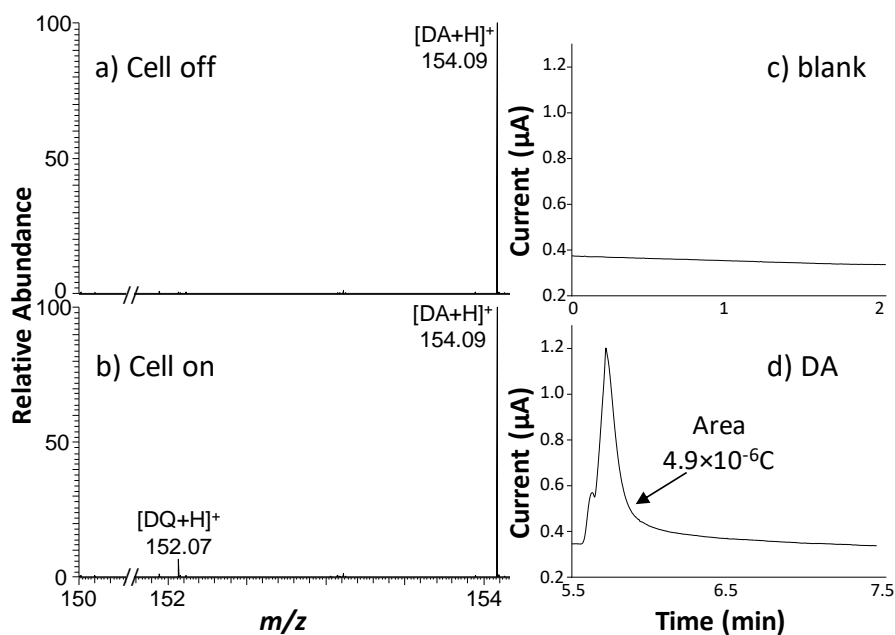


Figure 2.3 ESI-MS spectra of dopamine when the applied potential was a) 0 V and b) +1.05 V. The peak of the oxidized product of dopamine (DQ) was seen at m/z 152 (+1 charged) in b). Electric current responses were shown c) from the blank solvent and d) the oxidation of dopamine.

Norepinephrine (NE), another neurotransmitter compound, is known to undergo electrochemical oxidation via a two-electron transfer reaction to form norepinephrine *o*-quinone (NQ, Scheme 2.2-b). The mean oxidation yield was measured to be 2.4% by MS analysis of the NE compound before and after electrolysis (Table 2.1). Figure 2.4-d displays the electric current diagram showing a sharp peak resulting from the NE oxidation. Integration of the oxidation peak showed the amount of oxidized NE to be 6.8 pmol (Table 2.1). Therefore, the measured amount of NE was 288 pmol. In comparison to the injection amount of 300 pmol (6 μ L of 50 μ M of NE was injected for analysis), our quantitation measurement error was -4.0%. Good quantitation accuracy was obtained, using such an automated analysis sequence with reduced analysis time.

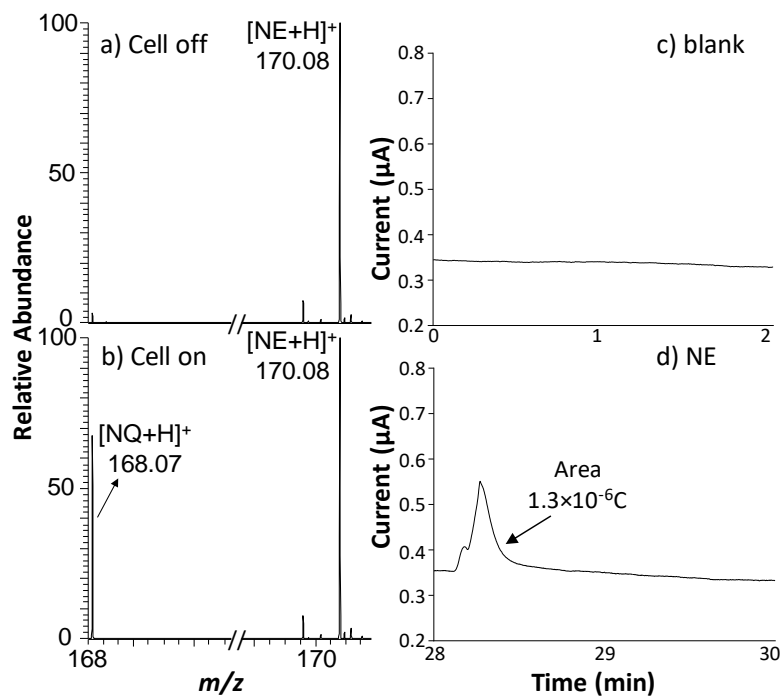


Figure 2.4 ESI-MS spectra of norepinephrine when the applied potential was a) 0 V and b) +1.05 V. The peak of the oxidized product of norepinephrine (NQ) was seen at m/z 168 (+1 charged) in b). Electric current responses were shown c) from the blank solvent and d) the oxidation of norepinephrine.

Table 2.1 Electric Current and MS Data for DA and NE

	Q ($\mu\text{A}\cdot\text{min}$)	Q (C)	Amount of the oxidized analyte (pmol)	Averaged oxidized amount (pmol)	Oxidation yield	Measured amount (pmol)	Theoretical amount (pmol)	Measurement error
DA	0.08223	4.93E-06	25.56					
	0.08297	4.98E-06	25.79	25.52	8.12%	314.29	300	4.76%
	0.08105	4.86E-06	25.20					
NE	0.02208	1.32E-06	6.86					
	0.02259	1.35E-06	7.02	6.80	2.36%	288.14	300	-3.95%
	0.02123	1.27E-06	6.60					
			EIC peak area of m/z 154 before electrolysis	EIC peak area of m/z 154 after electrolysis	% Change	Averaged % change upon electrolysis		
DA			510550789	469016876	8.14%	8.12%		
			458117903	414847377	9.45%			
			445404888	415231857	6.77%			
			EIC peak area of m/z 170 before electrolysis	EIC peak area of m/z 170 after electrolysis	% Change	Averaged % change upon electrolysis		
NE			25743844	25108446	2.47%	2.36%		
			25438928	24878913	2.20%			
			25873838	25246286	2.43%			

This quantitation approach can also be applied to chromatographic separation. As a simple demonstration, we tested a mixture of DA and 5-HT by first separating them on a LC column and then electrochemically oxidized each eluting compound. Due to the high polarity of both DA and 5-HT, a HILIC column was adopted for separation⁹⁴. The mobile phase used was ACN/H₂O with additives of NH₄OAc, which was found to be compatible with the subsequent electrolysis and ESI-MS detection. By using a HILIC column, 5-HT and DA were separated with the retention time at 6.6 min and 9.4 min, respectively. Before electrolysis (Figure 2.5-a), the +1 charged 5-HT ion was detected at m/z 177. After electrolysis (Figure 2.5-b), a peak at m/z 190 was observed, corresponding to +1 ion of the oxidized 5-HT product [$\text{P}+\text{H}$]⁺ (see the proposed reaction mechanism in Scheme 2.2-c). Note that the appearance of peaks at m/z 177 and 190 seen in Figure 2.5-a was probably due to in-source oxidation. During the electrochemical oxidation, 5-HT could first lose two

electrons and two protons to become an intermediate structure **I** (MW 174.2 Da). Then addition of ammonia (probably from the mobile phase NH_4OAc) occurred, followed by further oxidation via losses of two electrons and two protons to produce the final product ion $[\text{P}+\text{H}]^+$ (theoretical mass 190.09749, observed mass 190.09757, mass error: 0.42 ppm). A similar mechanism for electrochemical oxidation of 5-HT was proposed in literature⁹⁵. A fragment **F** ($[\text{P}+\text{H}-\text{NH}_3]^+$) was observed at 173 (theoretical mass 173.07094, observed mass 173.07111, mass error: 0.98 ppm), presumably from the precursor ion of 190 by loss of NH_3 due to in-source ion dissociation. The integrated area for the 5-HT peak at m/z 177 was reduced by 15.7% upon electrolysis (see data in Table 2.2). In the cell-on mode, the 5-HT oxidation current peak was detected as shown in Figure 2.5-f (Figure 2.5-e shows the background current diagram for blank solvent sample under the same + 1.05 V potential as a contrast). Based on the integration of the current peak area, the amount of the oxidized 5-HT was calculated to be 24.3 pmol on average ($z=4$ in this case). Therefore, our measured amount of 5-HT was 155 pmol, which was close to the injection amount of 150 pmol with the measurement error of 3.2%.

In addition, like the flow-through analysis of pure DA mentioned above, the +1 ion of DA in the mixture was detected at m/z 154 following HILIC separation (Figure 2.5-a). After electrolysis (Figure 2.5-b), a peak at m/z 152 was observed, corresponding to +1 ion of the oxidized DA product. The integrated area for the DA peak was reduced by 17.8% upon electrolysis (Table 2.2). The higher oxidation yield in this case than that in the flow-through analysis (8.1%) is probably due to that fact that it is easier to oxidize DA in a neutral media than in an acidic mobile phase. The DA oxidation current peak was also detected, as shown in Figure 2.5-f. Based on the integration of the current peak area, the

amount of the oxidized DA on average was calculated to be 25.6 pmol. Therefore, our measured amount of DA was 144 pmol, which was close to the injection amount of 150 pmol with the measurement error being -3.9%.

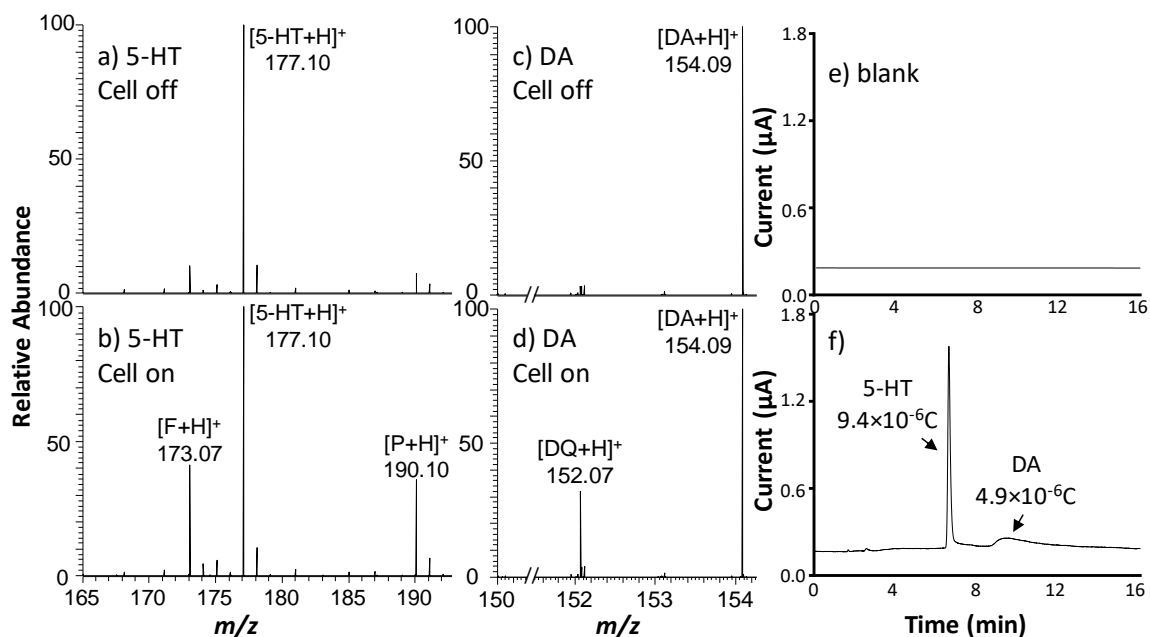


Figure 2.5 ESI-MS spectra of 5-HT when the applied potential was a) 0 V and b) +1.05 V. The peak of the oxidized product of 5-HT was seen at m/z 190 (+1 ion) in b). ESI-MS spectra of DA when the applied potential was c) 0 V and b) +1.05 V. The peak of the oxidized product of DA was seen at m/z 152 (+1 ion) in d). Electric current responses were shown e) from the blank solvent and f) the oxidation of 5-HT and DA.

Table 2.2 Electric Current and MS Data for 5-HT and DA

	Q ($\mu\text{A}\cdot\text{min}$)	Q (C)	Amount of the oxidized analyte (pmol)	Average oxidized amount (pmol)	Oxidation yield	Measured amount (pmol)	Theoretical amount (pmol)	Measurement error
5-HT	0.19231	1.15E-05	29.89	24.30	15.70%	154.78	150	3.19%
	0.15142	9.09E-06	23.54					
	0.12524	7.51E-06	19.47					
DA	0.10390	6.23E-06	32.30	25.63	17.77%	144.23	150	-3.85%
	0.08015	4.81E-06	24.92					
	0.06332	3.80E-06	19.68					
			EIC peak area of m/z 177 before electrolysis	EIC peak area of m/z 177 after electrolysis	% Change	Averaged % change upon electrolysis		
5-HT			357271906	291097753	18.52%	15.70%		
			368535793	310394981	15.78%			
			345836867	301546456	12.81%			
			EIC peak area of m/z 154 before electrolysis	EIC peak area of m/z 154 after electrolysis	% Change	Averaged % change upon electrolysis		
DA			132308839	109243311	17.43%	17.77%		
			135153342	110955734	17.90%			
			131939105	108228742	17.97%			

2.4 Conclusions

In this study, absolute quantitation of electrochemically oxidizable compounds using electrochemical mass spectrometry without using reference standards or calibration curves were demonstrated again with improvements in two aspects. For pure compounds, a flow-through analysis sequence was developed using a LC auto-sampler and resulted in a significant decrease in the sample analysis time. This would be of value for high throughput quantitation analysis. This approach could be applied to fast screen and quantify electroactive compounds in the pharmaceutical ingredients. Furthermore, we also demonstrated the feasibility of applying the EC/MS detection to quantitate individual components in a mixture of 5-HT and DA following HILIC separation. It could be extended and applied to quantify electro-oxidizable compounds or peptides in more complicated

biological samples. These improvements would facilitate the implementation of the electrochemical mass spectrometry method for real-world applications.

CHAPTER 3

ABSOLUTE QUANTITATION OF OXIDIZABLE PEPTIDES BY COULOMETRIC MASS SPECTROMETRY

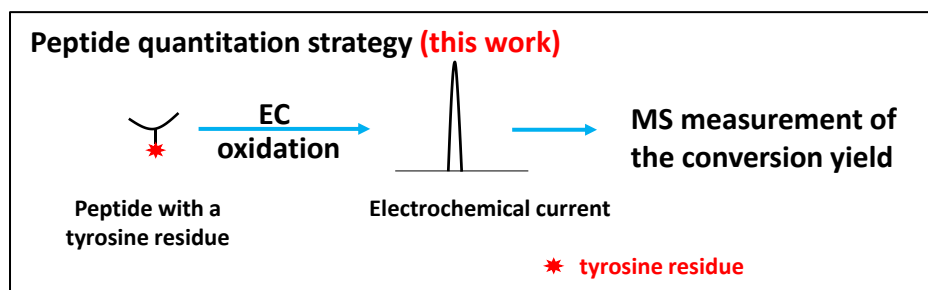
Adapted from Zhao, P.; Zare, R. N.; Chen, H. *J. Am. Soc. Mass Spectrom.* **2019**, 30 (11), 2398–2407. Copyright 2019, American Chemistry Society.

3.1 Introduction

With rapid advances in instrumentation and technologies, quantitation methods based on mass spectrometry (MS) have gained increasing popularity in proteomics research.^{96–105} Relative and absolute quantitation strategies are two categories that all the approaches fall into and protein quantitation is performed, based on the quantification of peptides resulting from protein digestion.¹⁰⁶

Relative quantitation strategies compare the levels of each peptide in a sample to the same peptide in an identical but modified sample. One label-free approach is to analyze samples and compare their MS spectra by determining peptide abundance in one sample relative to another.^{107,108} More commonly, relative quantitation methods use isotopes to label peptides from two samples with heavy and light isotopic atoms. The peak intensities of heavy- and light-labeled peptides are then compared to determine the change in abundance of one sample relative to the other. Methods using this approach include isotope-coded affinity tags (ICAT),^{72,75,109,110} stable isotope labeling by amino acids in cell culture (SILAC),^{79,80,111–113} isobaric tags for relative and absolute quantitation (iTRAQ),^{86,114–116} metal element chelated tags (MECT),⁸⁷ isotope-coded protein labeling (ICPL)¹¹⁷, and *N, N*-dimethyl leucine (DiLeu) isobaric tag methods.^{118–121} In absolute proteomic quantitation approaches, a known amount of isotope-labeled target peptides is

spiked into an experimental sample and then LC-MS or LC-MS/MS analysis is performed.¹²² Unlike relative quantitation, the abundance of the target peptide in the experimental sample is compared to the corresponding labeled peptide and then selected reaction monitoring (SRM) method can be used to construct a standard curve to yield absolute quantitation of the target peptide.¹²³ It appears that absolute quantitation should be a more advantageous method compared to relative quantitation because absolute amounts of target peptides from different samples can be determined. However, standard or isotope-labeled peptides that are needed for absolute quantitation might not be available at hand and their synthesis can be costly and time-consuming.^{92,124} It would be ideal to have a label-free, standards-free absolute quantitation method available to quantify peptides and proteins for proteomics research.



Scheme 3.1 Our approach for quantitation of tyrosine-containing peptides. Note that, if other oxidizable residues co-exists, the oxidation could be more complicated.

Herein, we present an electrochemistry (EC)-assisted absolute quantitation method for peptides by MS without the use of standards or isotope-labeled peptides. In our method (illustrated in Scheme 3.1), a target peptide, if it contains a tyrosine (an electrochemically oxidizable amino acid with an oxidation potential of 0.93 V vs. NHE),¹²⁵ is first introduced to an electrochemical cell for electrochemical oxidation and followed by MS detection.

Electrochemical oxidation reaction results in an electric current response. The integration of the current peak over time provides information about the amount of the oxidized compound, using the Faraday's Law. According to the Faraday's Law, the total electric charge (Q) involved in the oxidation reaction, which can be measured from the integration of Faradaic current over time, is proportional to quantity of the oxidized peptide: $Q = nzF$, where n is the moles of the oxidized peptide, z is the number of electrons transferred per molecule during the redox reaction, and F is the Faraday constant (9.65×10^4 C/mol). Therefore, the moles of the oxidized peptide can be calculated as $n = Q/zF$. Meanwhile, the electrochemically active peptide shows a reduced intensity in the acquired MS spectra from electrochemical oxidation, and the relative MS intensity change upon oxidation, Δi , reflects the redox conversion yield. In a case where the peptide is introduced to the electrochemical cell by liquid chromatography (LC), Δi can be calculated by comparing the integrated peak area of the target peptide ion in the extracted ion chromatogram (EIC) before and after electrolysis. Indeed, in a separate experiment, we confirmed that the EIC peak area is proportional to the peptide quantity (see Figure 3.1 and Table 3.1).

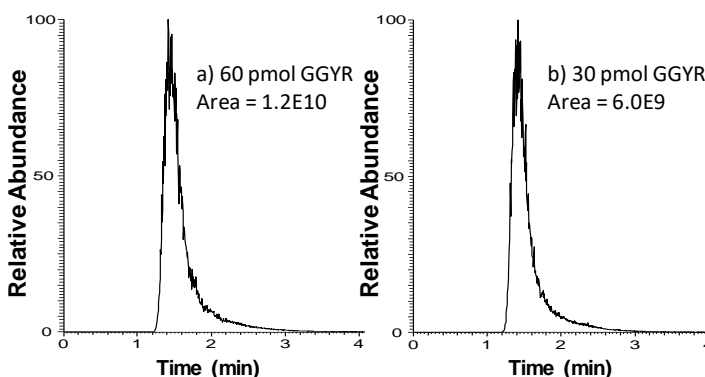


Figure 3.1 EIC peaks of ion m/z 452 for a) 60 pmol of GGYR and b) 30 pmol of GGYR.

Table 3.1 Relationship Between the Peptide Quantity and the Peptide EIC Peak Area

	30 pmol GGYR	60 pmol GGYR	Ratio
EIC Peak Area	6073443032	12289332040	
	5994790305	11892106849	
Average	6034116669	12090719445	2.003726495

Thus, the moles of the oxidized peptide, in combination with the conversion yield, can be used to calculate the total amount of the peptide analyte. In other words,

$$\begin{aligned} & \text{Total amount of the peptide} \\ & = (\text{amount of the oxidized peptide})/(\text{the oxidation yield}) \quad (3.1) \\ & = (Q/zF)/\Delta i \\ & = Q/(zF\Delta i) \end{aligned}$$

Previously we have shown that this strategy can be used for accurately quantifying organic molecules such as neurotransmitters (e.g., dopamine and norepinephrine), flavonoid (e.g., rutin), and urea.⁶¹ Peptide glutathione can be also measured by this method, based on the cysteine oxidation to form a disulfide bond. In this work, the method is extended to the quantitation of peptides containing tyrosine, which is more abundant in proteins than the cysteine residue.¹²⁶ It was reported that the occurrence frequencies per residue in proteins for tyrosine and cysteine are 2.86% and 1.16%, respectively (Table 1).¹²⁶

3.2 Experiments

3.2.1 Chemicals

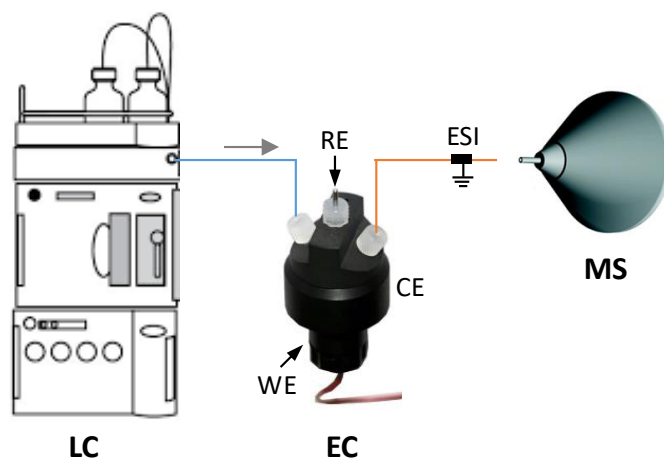
Gly-Gly-Tyr-Arg (GGYR, HPLC grade), Met-Gly (MG, HPLC grade), Lys-Arg-Thr-Leu-Arg-Arg (KRTLRR, HPLC grade), Arg-Gly-Asp (RGD, HPLC grade), Ser-Leu-Ile-Gly-Lys-Val-amide (SLIGKV-amide, HPLC grade), Arg-Lys-Arg-Ser-Arg-Ala-Glu

(RKRSRAE, HPLC grade), Ser-Phe-Leu-Leu-Arg-Asn-amide (SFLLRN-amide, HPLC grade), Phe-Leu-Phe-Gln-Pro-Gln-Arg-Phe-amide (FLFQPQRF-amide, HPLC grade), oxytocin (CYIQNCPLG, disulfide bridge 1-6, HPLC grade), alkaline phosphatase and bradykinin acetate salt (RPPGFSPFR, HPLC grade) were purchased from Sigma Aldrich (St. Louis, MO). Asp-Arg-Val-Tyr (DRVY, HPLC grade) and [Arg8]-vasotocin (CYIQNCPRG, disulfide bridge 1-6) were purchased from American Peptide (Sunnyvale, CA). Gly-His-Gly (GHG) was obtained from MP Biomedicals (Santa Ana, CA). Tyrosine phosphopeptide (RRLIEDAEpYAARG, HPLC grade) was purchased from EMD Millipore (Temecula, CA). Phosphorylated UOM9 (KRPpSQRHGSKY, HPLC grade) was purchased from AnaSpec (Fremont, CA).

2.2.2 Instrumentation

For the setup (illustrated in Scheme 3.2), a Waters ultra-performance liquid chromatography setup (UPLC, Milford, MA) was coupled with an Antec electrochemical thin-layer flow cell (Antec BV, The Netherlands) or a BASi electrochemical flow cell (West Lafayette, IN). The Antec electrochemical cell was equipped with a Magic Diamond (boron-doped diamond) disc electrode (*i.d.*, 8 mm) as the working electrode (WE) used for peptide oxidation. A HyREFTM electrode was used as the reference electrode (RF) and carbon-loaded PTFE was used as a counter electrode (CE). The BASi electrochemical cell was equipped with a 6-mm *i.d.* glassy carbon WE and a Ag/AgCl RE. A BEH C18 reversed phase column (2.1 mm × 50 mm, 1.7 μm) was installed for the UPLC separation. A positive potential of +1.0-1.1 V was applied to the WE electrode for oxidation of LC-separated peptides. The oxidation current response was monitored and recorded by using a ROXYTM potentiostat (Antec BV, The Netherlands). The electric current peak area was integrated by

importing the current data point to software OriginPro 2018b to calculate the total electric charge Q involved in the oxidation reaction. The eluate flowing out of the cell was subsequently analyzed using online electrospray ionization mass spectrometry (ESI-MS). MS data were collected using a high-resolution Q-Exactive Orbitrap mass spectrometer (Thermo Scientific, San Jose, CA). The sheath gas flow rate was 10 L/h. The spray voltage was +4 kV and the capillary temperature was kept at 250 °C. Extracted ion chromatograms (EIC) of peptides were acquired by Thermo Xcalibur (3.0.63).



Scheme 3.2 Schematic showing our LC/EC/MS apparatus for peptide quantitation.

Peptides that contain one tyrosine residue, including GGYR, DRVY, oxytocin, [Arg⁸]-vasotocin, and phosphorylated UOM9 were analyzed using the online LC/EC/MS apparatus, and the mobile phase flow rate was set as 0.1 mL/min. An isocratic elution program using 80% A (mobile phase A: water with 0.1% acetic acid and mobile phase B: acetonitrile with 0.1% acetic acid) for 5 min was used for all of compounds. The peptide concentration used was 50 μ M and the injection volume was 3-6 μ L.

Peptides containing no tyrosine residue such as GHG, MG, KRTLRR, RGD, SLIGKV-amide, RKRSRAE-amide, SFLLRN-amide, FLFQPQRF-amide, and bradykinin were also analyzed using LC/EC/MS apparatus as controls. An isocratic elution program was used with 80% A for 10 min with the mobile phase flow rate of 0.1 mL/min. The peptide injection concentration and volume were 50 μ M and 6 μ L, respectively. The potential applied for oxidation was + 1.1 V.

Angiotensinogen 1-14 (also called tetradecapeptide TDP), containing two tyrosine residues, was also tested. The mobile phase flow rate was set as 0.3 mL/min. An isocratic elution program using 80% A (mobile phase A: water with 0.1% acetic acid and mobile phase B: acetonitrile with 0.1% acetic acid) for 5 min was used. The concentration used was 50 μ M and the injection volume was 6 μ L.

Electrodes after use can be cleaned using alternating positive and negative potentials.

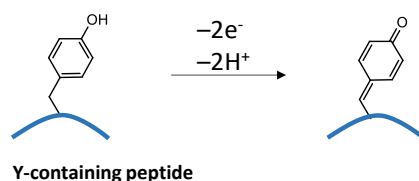
2.3 Results and Discussion

Among the 20 naturally occurring amino acids, four are oxidizable: cysteine (C), tyrosine (Y), tryptophan (W), and methionine (M), given in the order of increasing oxidation potential. Table 3.1 lists values for their respective oxidation potentials and occurrence frequencies per residue in proteins. Tyrosine has a relatively low oxidation potential and relatively high abundance in proteins.

Table 3.2 Amino Acids Known to be Oxidizable

Electroactive Amino Acids	Tyrosine (Y)	Tryptophan (W)	Cysteine (C)	Methionine (M)
Oxidation potential (vs. NHE)	0.93 V ¹²⁵	1.01 V ¹²⁵	0.23 V ¹²⁷	1.51 V ¹²⁸
Occurrence frequency per residue in proteins ¹²⁶	2.86%	1.50%	1.16%	2.86%

The combination of MS and EC^{129–138} has been our research interest, and previously we have shown that the combined EC/MS technique can be used to detect transient electrochemical reaction intermediates^{139–142} and to assist protein sequencing and protein conformational structure elucidation by using fast electrochemical reduction of disulfides.^{143–149} In consideration of the fact that tyrosine is electroactive, our goal in this study was to develop a direct quantitation method for peptides based on tyrosine residue oxidation, without using any standards or isotope-labeled peptides. Under an appropriate oxidation potential, the phenol side chain of a peptide tyrosine residue can be oxidized into a semi-quinone by loss of two electrons and two protons (Scheme 3.3), in which a mass shift of 2 Da occurs, which can be readily monitored by MS analysis. It has been reported that peptides and proteins carrying tyrosine (or tryptophan) can be electrochemically oxidized and analyzed by MS.^{150–152} However, peptide quantitation based on tyrosine oxidation appears not to have been explored. Several peptides were tested and quantified in this work, based on the electrochemical oxidation of their tyrosine residues (See summarized results in Table 3.2).



Scheme 3.3 Equation showing electrochemical oxidation of a peptide tyrosine residue. Note that, if other oxidizable residues co-exists, the oxidation could be more complicated.

Table 3.3 List of Peptides Quantified by CMS

#	Name	Peptide Sequence	Molecular Weight (Da)	Electric Current from Oxidation (Y/N)	# of Y Residues (Oxidative Residues)	Quantitation Measurement Error
1	Gly-His-Gly	GHG	269.3	N	0	-
2	Met-Gly	MG	206.3	N	0	-
3	Lys-Arg-Thr-Leu-Arg-Arg	KRTLRR	829.0	N	0	-
4	Arg-Gly-Asp	RGD	346.3	N	0	-
5	Ser-Leu-Ile-Gly-Lys-Val-amide	SLIGKV-NH ₂	614.8	N	0	-
6	Arg-Lys-Arg-Ser-Arg-Glu-amide	RKRSRAE-NH ₂	901.0	N	0	-
7	Ser-Phe-Leu-Leu-Arg-Asn-amide	SFLLRN-NH ₂	747.9	N	0	-
8	Phe-Leu-Phe-Gln-Pro-Gln-Arg-Phe-amide	FLFQPQRF-NH ₂	1081.3	N	0	-
9	bradykinin	RPPGFSPFR	1060.2	N	0	-
10	Tyrosine phosphopeptide	RRLIEDAEpYAA RG	1598.7	N	0	-
11	Gly-Gly-Tyr-Arg	GGYR	451.5	Y	1	-5.0%
12	Asp-Arg-Val-Tyr	DRVY	551.6	Y	1	-7.5%
13	oxytocin	CYIQNC PLG, disulfide bond 1-6	1007.2	Y	1	2.4%
14	[Arg ⁸]- vasotocin	CYIQNC PRG, disulfide bond 1-6	1050.2	Y	1	0.8%
15	Angiotensinogen (1-14)	DRVYIH PFHLLV YS	1760.1	Y	2	-5.5%
16	Phosphorylated UOM9	KRPpSQ RHGSKY	1422.5	Y	1	-5.8%

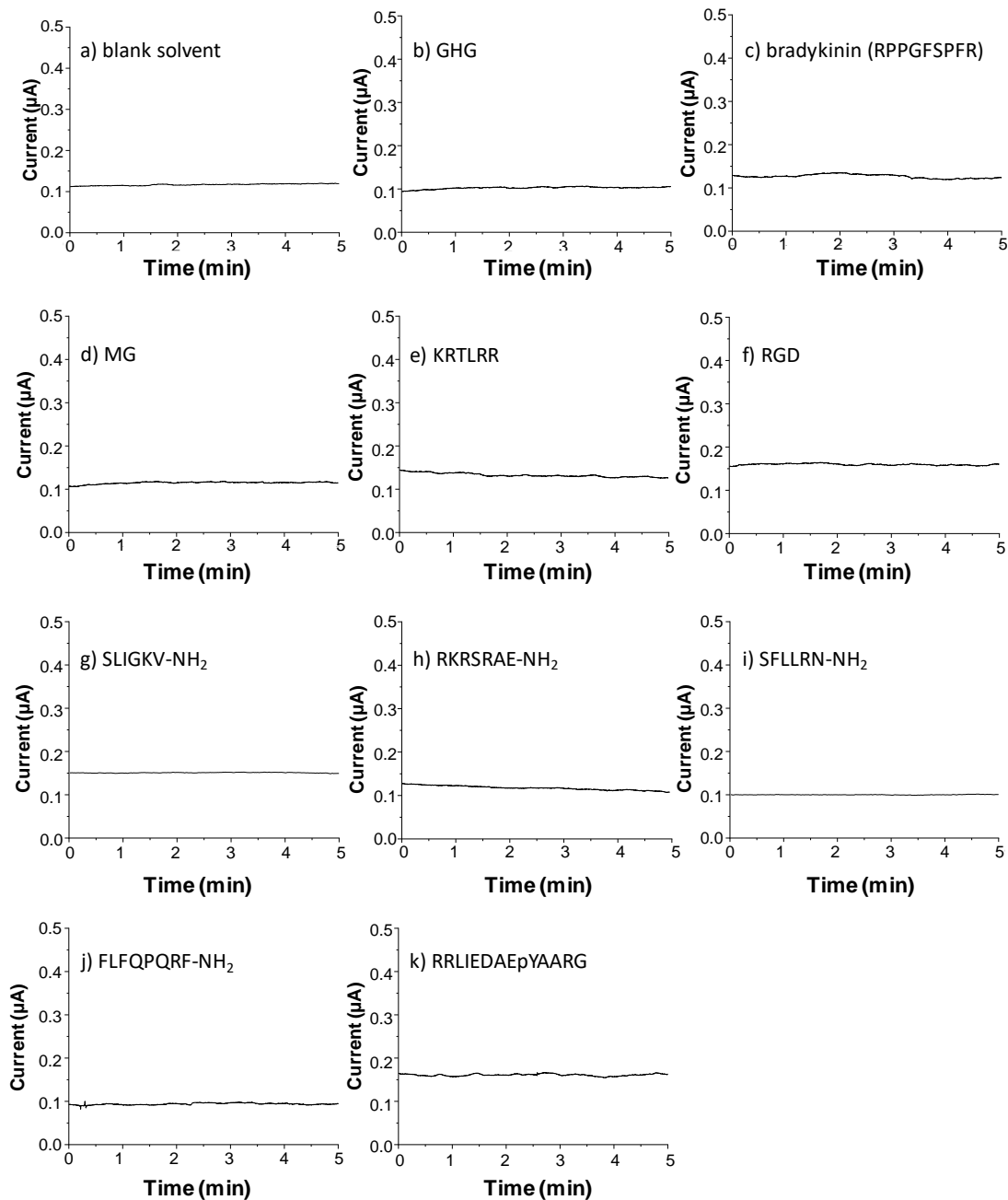


Figure 3.2. Electric current responses of a) blank solvent, b) GHG, c) bradykinin (RPPGFSPFR), d) MG, e) KRTLRR, f) RGD, g) SLIGKV-amide, h) RKRSRAE-amide, i) SFLLRN-amide, and j) FLFQPQRF-amide, and k) RRLIEDAEpYAARG. No electric current peak was detected, even under the oxidation potential of +1.1 V.

GGYR was first chosen as a test example. GGYR is a Tyr-containing peptide and it can be oxidized by losing two electrons. Indeed, before electrolysis (Figure 3.3-a), the

protonated GGYR was detected at m/z 452. After electrolysis (Figure 3.3-b), a peak at m/z 450 was observed, corresponding to +1 ion of the oxidized GGYR product, GGY'R (Y' represents the oxidized tyrosine residue). Figure 3.3-c and 1d showed the EIC (m/z 452, the protonated GGYR) of 50 μ M GGYR with an injection volume of 6 μ L (injected amount: 300 pmol) with the applied potential of 0 V and +1.0 V, respectively. The integrated area for the peak shown in Figure 3.3-d was smaller by 5.2%, in comparison with that of the peak shown in Figure 3.3-c, indicating that the oxidation yield for GGYR was 5.2% (averaged value from a triplicate measurement). On the other hand, a sharp GGYR oxidation current peak was detected, as shown in Figure 3.3-f. Figure 3.3-e shows the background current diagram from a blank solvent injection under the same oxidation condition as a control. In contrast, no electric current peak was observed for the solvent, suggesting that the electric current detected in Figure 3.3-f is caused by the oxidation of GGRY. In addition, a series of peptides containing no tyrosine residues such as GHG, MG, bradykinin (RPPGFSPFR), KRTLRR, RGD, SLIGKV-amide, RKRSRAE-amide, SFLLRN-amide, and FLFQPQRF-amide were tested as control experiments and no oxidation electric current was recorded (Figure 3.2), indicating that the oxidation might occur to the tyrosine residue in the case of GGRY. Based on the integration of the current peak area (Figure 3.3-f), the amount of the oxidized GGYR on average was calculated to be 14.9 pmol. Therefore, our measured amount of GGYR was 285 pmol, which was close to the injection amount of 300 pmol with the measurement error of -5.0% (see data in Table 3.3). In this study, we call our method coulometric mass spectrometry (CMS) due to the use of Faraday's Law, although the oxidation yield is not 100%.

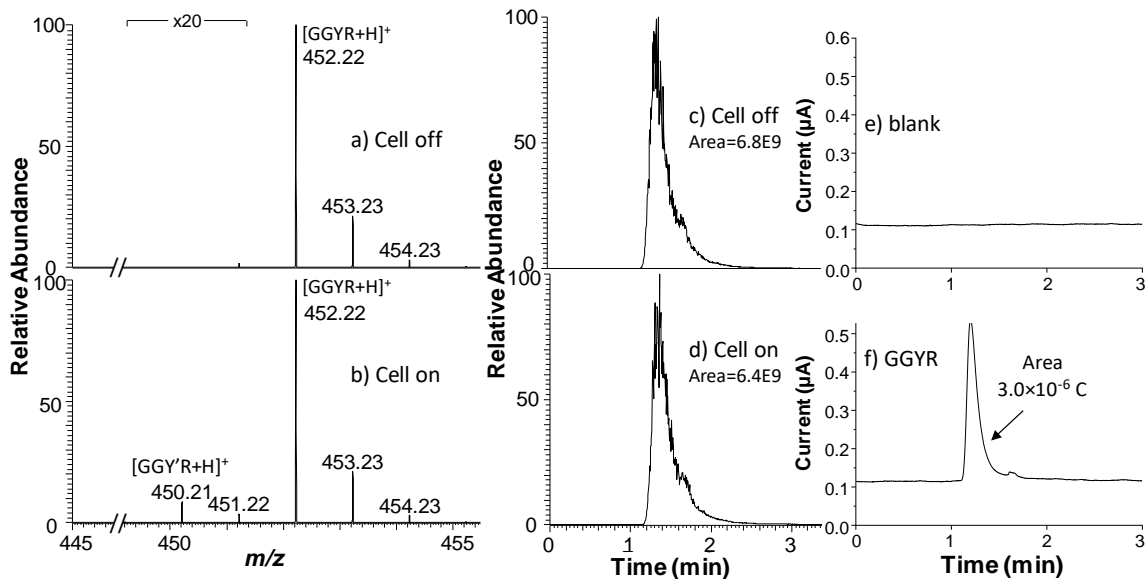


Figure 3.3 ESI-MS spectra of GGYR when the applied potential was a) 0 V and b) +1.0 V. The peak of the oxidized product GGY'R was clearly seen at m/z 450 in b). EIC of GGYR was recorded when the applied potential was c) 0 V and d) +1.0 V. Electric current responses were shown due to the oxidation of e) a blank solvent and f) GGYR peptide.

Table 3.4 Electric Current and MS Data for GGYR

	Q ($\mu\text{A}\cdot\text{min}$)	Q (C)	Amount of the oxidized analyte (pmol)	Average oxidized amount (pmol)	Oxidation yield	Measured amount (pmol)	Theoretical amount (pmol)	Measurement error
GGYR	0.05071	3.04E-06	15.76					
	0.06216	3.73E-06	19.32	14.92	5.23%	285.09	300.00	-4.97%
	0.03109	1.87E-06	9.67					
	EIC peak area of m/z 452 before electrolysis		EIC peak area of m/z 452 after electrolysis		% Change	Averaged % change upon electrolysis		
GGYR	6801706173		6430677412		5.45%	5.23%		
	6199039201		5785961899		6.66%			
	7004425591		6753685704		3.58%			

To confirm that the oxidized product (m/z 450) was truly produced from electrochemical oxidation of tyrosine in the GGYR, MS/MS analysis of m/z 450 was performed. In this experiment, the GGYR sample was injected into the electrochemical cell by a syringe pump for oxidation at +1.0 V potential. The resulted product was collected and re-ionized by nano-electrospray ionization (nESI), in which the oxidation product

GGY'R (Y' represents the oxidized tyrosine) was observed at m/z 450. Collision-induced dissociation (CID) data of m/z 450 was recorded, to compare with that of the intact peptide GGYR ion of m/z 452. As shown in Figure 3.4, upon CID, the oxidized peptide ion (m/z 450) gave rise to fragment ions y_1 (m/z 175) and y_2' (m/z 336) while the intact peptide (m/z 450) produced y_1 (m/z 175) and y_2 (m/z 338), confirming that the oxidation occurrence to the 3rd tyrosine residue of GGYR, in which two hydrogen losses took place, resulting in 2 Da mass shift for the y_2 ion. Furthermore, we observed the fragment ion of m/z 344 resulting from dissociation of m/z 450 by loss of the oxidized tyrosine side chain $O=C_6H_4=CH_2$ as shown in Figure 3.4-a, providing evidence that oxidation indeed occurs to the side chain of tyrosine of this peptide.

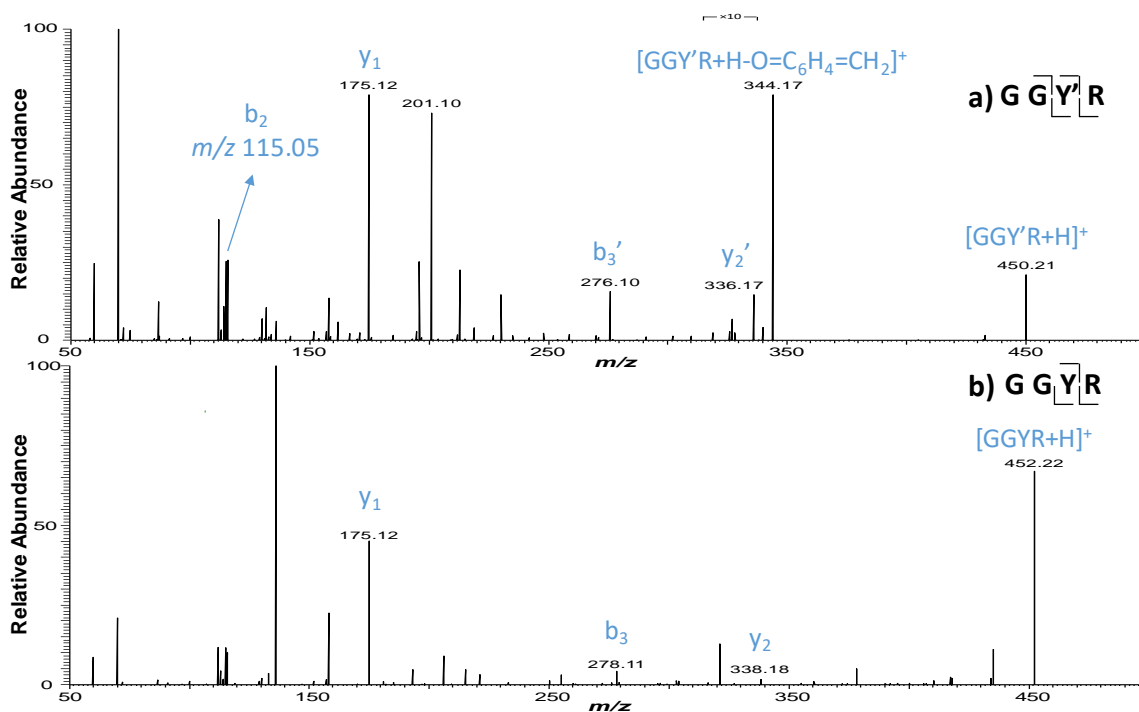


Figure 3.4 CID MS/MS spectra of a) the oxidized peptide ion $[GGY'R+H]^+$ (m/z 450) and b) the intact peptide ion $[GGYR+H]^+$ (m/z 452). Fragment ion of m/z 344 in a) resulted from the loss of the oxidized tyrosine side chain from m/z 450.

In this experiment, it is critical to control both oxidation potential and oxidation time. To ensure that the recorded current is Faradic current from the oxidation of peptide residues, not from solvent, it is important to control the applied oxidation potential to avoid solvent oxidation (e.g., water oxidation). In our study, we found that a low potential like +1.0 V allows for selective oxidation of peptide (see Figure 3.3-e and f). It is also known that peptides with tyrosine (and also tryptophan) could undergo secondary electrochemical oxidation and eventually lead to peptide cleavage upon electrolysis¹⁵⁰⁻¹⁵². This would cause it to be difficult to apply the Faraday's Law for quantitation, as the value of n in eq. 1 is not clear. Our strategy to achieve selective primary oxidation (as shown in Scheme 3) and to avoid these side reactions is to control the electro-oxidation time. When the peptide is introduced by LC into a thin-layer electrochemical cell, the small dead volume of the cell (0.7 μL) and a relatively high mobile phase flow rate (100 $\mu\text{L}/\text{min}$) led to the oxidation of the peptide in less than 0.5 ms. Indeed, we observed no side oxidation reactions including peptide cleavage and secondary oxidation of tyrosine for GGYR under these conditions.

DRVY, another tetrapeptide that contains Tyr, was also analyzed by the same approach. Before electrolysis (Figure 3.5-a), the protonated DRVY was detected at m/z 552. After electrolysis (Figure 3.5-b), a peak at m/z 550 was observed, corresponding to +1 ion of oxidized DRVY product, DRVY⁺. Figure 3.5-c and d showed the EIC (m/z 552, the protonated DRVY) of 50 μM DRVY with an injection volume of 6 μL (injected amount: 300 pmol) with the applied potential of 0 V and +1.0 V, respectively. The integrated area for the peak shown in Figure 3.5-d was smaller by 3.1%, in comparison with that of the peak shown in Figure 3.5-c, indicating that the oxidation yield for DRVY was 3.1% (see data in Table 3.4). On the other hand, the DRVY oxidation current peak was detected, as

shown in Figure 3.5-f (Figure 3.5-e shows the background current diagram for blank solvent sample under the same + 1.0 V potential as a contrast). Based on the integration of the current peak area, the amount of the oxidized DRVY on average was calculated to be 8.5 pmol. Therefore, our measured amount of DRVY was 277 pmol, which was close to the injection amount of 300 pmol with a measurement error of -7.5% (Table 3.4).

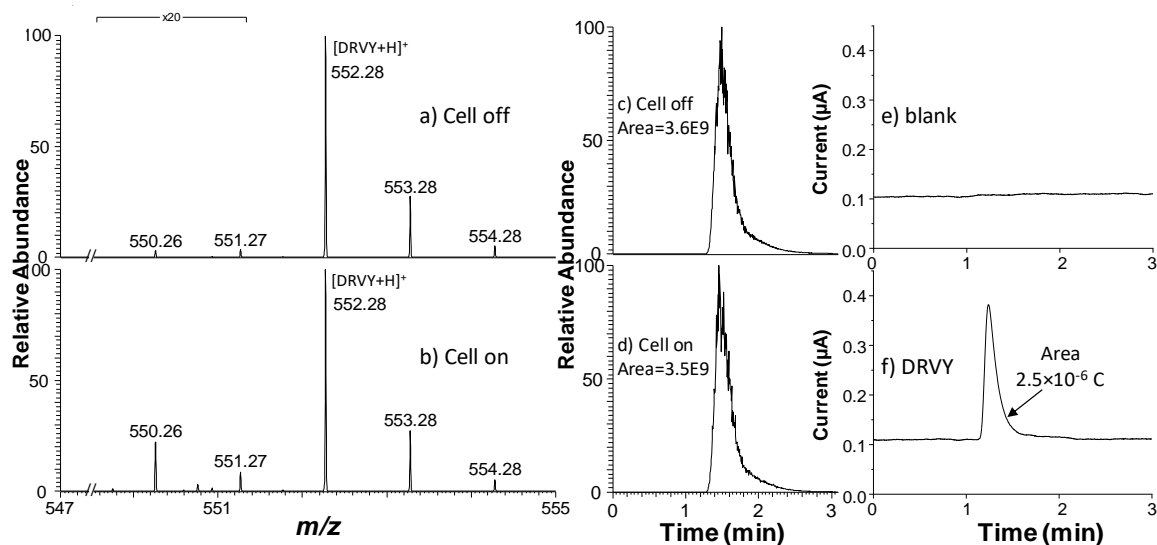


Figure 3.5 ESI-MS spectra of DRVY when the applied potential was a) 0 V and b) +1.0 V. The peak of the oxidation product of DRVY was seen at m/z 550. EIC of DRVY was recorded when the applied potential was c) 0 V and d) +1.0 V. Electric current responses were e) due to the blank solvent and f) the oxidation of DRVY sample. Note that there is a small peak of m/z 550 in a, which might be caused by in-source oxidation of DRVY.

Table 3.5 Electric Current and MS Data for DRVY

	Q ($\mu\text{A}\cdot\text{min}$)	Q (C)	Amount of the oxidized analyte (pmol)	Average oxidized amount (pmol)	Oxidation yield	Measured amount (pmol)	Theoretical amount (pmol)	Measurement error
	0.04225	2.54E-06	13.13					
DRVY	0.02156	1.29E-06	6.70	8.46	3.05%	277.38	300.00	-7.54%
	0.01781	1.07E-06	5.54					
	EIC peak area of m/z 552		EIC peak area of m/z 552		% Change	Averaged % change upon electrolysis		
	before electrolysis		after electrolysis					
	3630388465		3461650795		4.65%			
DRVY	3980301187		3887135911		2.34%	3.05%		
	3752901206		3672338415		2.15%			

We also tested oxytocin (CYIQNCPLG, disulfide bridge 1-6), a larger Tyr-containing peptide than GGYR and DRVY. Before electrolysis (Figure 3.6-a), the +2 charged oxytocin ion was detected at m/z 504. After electrolysis (Figure 3.6-b), a peak at m/z 503 was observed, corresponding to +2 ion of the oxidized oxytocin product (2 Da mass shift corresponding to losses of two hydrogens). Figure 3.6-c and 3.6-d showed the EIC (m/z 504, the +2 charged oxytocin ion) of 50 μ M oxytocin with an injection volume of 6 μ L (injected amount: 300 pmol) with the applied potential of 0 V and +1.0 V, respectively. The integrated area for the peak shown in Figure 3.6-d was smaller by 4.7%, in comparison with that of the peak shown in Figure 3.6-c, indicating that the oxidation yield for oxytocin was 4.7% (see data in Table 3.5). On the other hand, the oxytocin oxidation current peak was detected, as shown in Figure 3.6-f (Figure 3.6-e shows the background current diagram for blank solvent sample under the same + 1.0 V potential as a contrast). Based on the integration of the current peak area, the amount of the oxidized oxytocin on average was calculated to be 14.4 pmol. Therefore, our measured amount of oxytocin was 307 pmol, which was close to the injection amount of 300 pmol with the measurement error being 2.4%. We also successfully quantified another neurohypophyseal peptide, [Arg⁸]-Vasotocin, which shared structural similarity with oxytocin. Using the same approach, the measurement error was found to be 0.8% (see Figure 3.7 and Table 3.6).

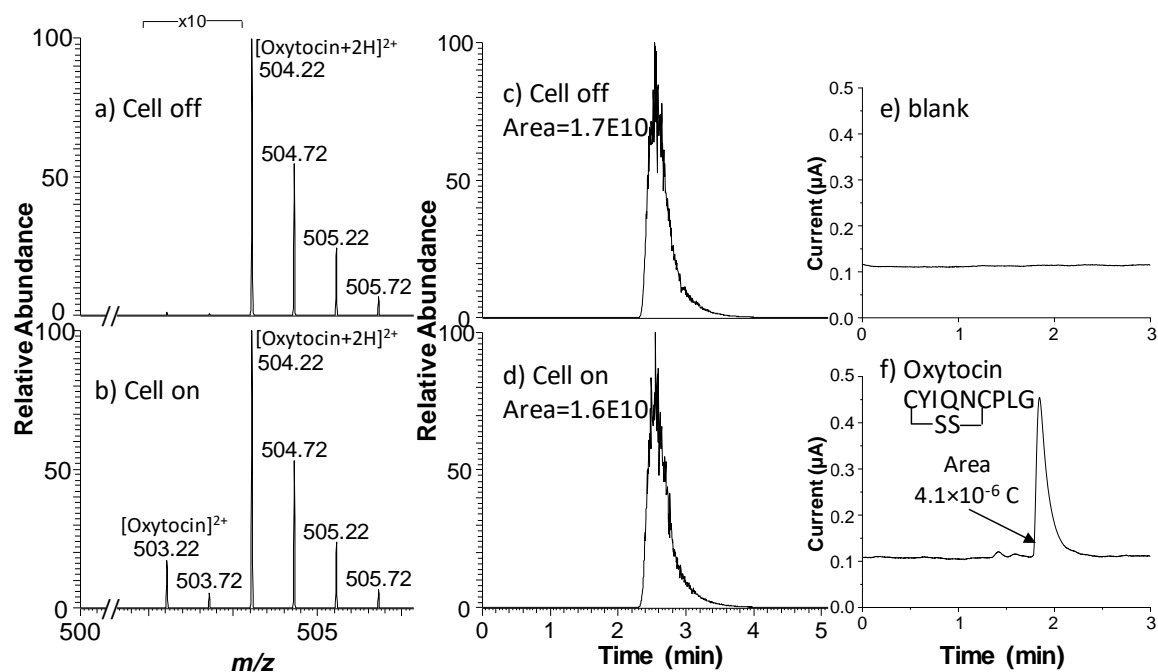


Figure 3.6 ESI-MS spectra of oxytocin when the applied potential was a) 0 V and b) +1.0 V. The peak of the oxidized product of oxytocin was seen at m/z 503 (+2 charged) in b. EIC of the +2 charged oxytocin ion was recorded when the applied potential was c) 0 V and d) +1.0 V. Electric current responses were shown e) from the blank solvent and f) the oxidation of oxytocin peptide.

Table 3.6 Electric Current and MS Data for Oxytocin

	Q ($\mu\text{A}\cdot\text{min}$)	Q (C)	Amount of the oxidized analyte (pmol)	Average oxidized amount (pmol)	Oxidation yield	Measured amount (pmol)	Theoretical amount (pmol)	Measurement error
	0.06867	4.12E-06	21.35					
Oxytocin	0.03519	2.11E-06	10.94	14.37	4.68%	307.27	300.00	2.43%
	0.03480	2.09E-06	10.82					
	EIC peak area of m/z 504		EIC peak area of m/z 504		% Change	Averaged % change upon electrolysis		
	before electrolysis		after electrolysis					
	16969674394		15623386694		7.93%			
Oxytocin	16900400688		16259136897		3.79%	4.68%		
	16440089145		16061818587		2.30%			

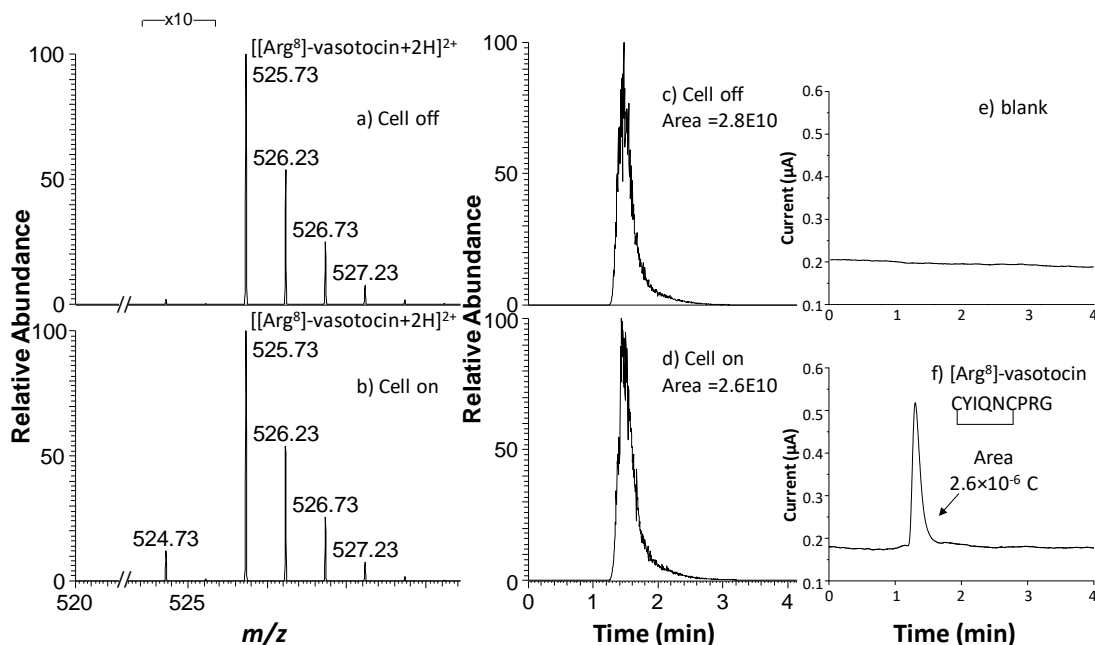


Figure 3.7 ESI-MS spectra of [Arg⁸]-vasotocin when the applied potential was a) 0 V and b) +1.0 V. The peak of the oxidized product of [Arg⁸]-vasotocin was seen at m/z 524 (+2 charged) in b. EIC of the +2 ion of [Arg⁸]-vasotocin was recorded when the applied potential was c) 0 V and d) +1.0 V. Electric current responses were shown e) due to the blank solvent and f) the oxidation of [Arg⁸]-vasotocin peptide.

Table 3.7 Electric Current and MS Data for [Arg⁸]-vasotocin

	Q ($\mu\text{A}\cdot\text{min}$)	Q (C)	Amount of the oxidized analyte (pmol)	Average amount of oxidized analyte (pmol)	Oxidation yield	Measured amount (pmol)	Theoretical amount (pmol)	Measure- ment error
[Arg ⁸]-vasotocin	0.04262	2.56E-06	13.25					
	0.04916	2.95E-06	15.28	14.66	9.69%	151.19	150.00	0.79%
	0.04967	2.98E-06	15.44					
		EIC peak area of m/z 525 before electrolysis	EIC peak area of m/z 525 after electrolysis	% Change	Averaged % change upon electrolysis			
[Arg ⁸]-vasotocin		28203536860	25564046285	0.093587219				
		27903634599	25153790153	0.098547895	9.69%			
		28560399871	25741167956	0.098711220				

So far, we have only considered peptides having one tyrosine residue. But, CMS can also be applied to peptides containing more than one tyrosine residue. One successful strategy is to choose conditions so that we oxidize only one of the tyrosine residues. As an

example, we examined angiotensinogen (1-14), a known tetradecapeptide (TDP) having the sequence DRVYIHPFHELLVYS. This is a peptide precursor of angiotensin I, which is a peptide hormone leading to vasoconstriction and blood pressure increase.¹⁵³ To avoid simultaneous oxidation of two tyrosine residues of TDP, we reasoned that a high sample flow rate (in other words, a short residence time in the electrochemical cell) could help. To confirm this hypothesis, we introduced TDP into the electrochemical cell by LC at different mobile phase flow rates (0.1-0.3 mL/min) for oxidation. Indeed, upon oxidation, two +4 ions of products appeared at m/z 439.98 and 439.48, corresponding to the oxidation products resulting from one tyrosine oxidation and from two tyrosine oxidations, respectively. When the sample introduction flow rate was increased from 0.1 to 0.3 mL/min, the intensity ratio of m/z 439.48 to m/z 439.98 decreased from 39.9 to 4.2% (Table 3.7), supporting our hypothesis that less oxidation time allows oxidation to occur predominantly at only one of the tyrosine residues of the peptide.

Table 3.8 MS Data for TDP at Different Sample Injection Flow Rates (0.1-0.3 mL/min)

	Flow rate (mL/min)	EIC Peak Area for oxidized peptide ions*		% of m/z 439.48 to m/z 439.98
		m/z 439.98	m/z 439.48	
TDP (DRVYIHPFHELLVYS)	0.1	256644901	81407344	39.99%
	0.2	293503987	46687873	13.58%
	0.3	306309288	29546924	4.15%

* background subtracted EIC peak area

To better tolerate a relatively high flow rate of 0.3 mL/min and the pumping pressure, again, we used a BASi stainless electrochemical flow cell (West Lafayette, IN) equipped with a 6-mm *i.d.* glassy carbon WE and a Ag/AgCl RE. Before electrolysis

(Figure 3.8-a), the +4 charged TDP ion was detected at m/z 440.49. After electrolysis (Figure 3.8-b), a peak at m/z 439.98 was observed, corresponding to the +4 ion of oxidized TDP product resulting from oxidation of one of the tyrosines. Another smaller peak at m/z 439.98 resulting from the oxidation of both tyrosines was also seen (Figure 3.8-b) with the intensity ratio of m/z 439.48 to m/z 439.98 being 0.12:1. Figure 3.8-c and 4d showed the EIC of m/z 440.49, the +4 charged TDP ion, from the injection of 6 μ L of 50 μ M TDP (total amount: 300.0 pmol) with the applied potential of 0 V and +1.05 V (vs. Ag/AgCl), respectively. The integrated area for the peak shown in Figure 3.8-d was smaller by 2.6% than that of the peak shown in Figure 3.8-c, indicating that the oxidation yield for TDP was 2.6% (see data in Table 3.8). On the other hand, the TDP oxidation current peak was detected, as shown in Figure 3.8-f (Figure 3.8-e shows the background current diagram for blank solvent sample under the same + 1.05 V potential as a contrast). By integration of the current peak area, the total electric charge Q involved in the TDP oxidation, leading to the formation of m/z 439.98 via one tyrosine oxidation ($2 e^-$ per mole peptide) and the formation of m/z 439.48 via two tyrosine oxidation ($4 e^-$ per mole peptide), could be calculated. In consideration of the intensity ratio of m/z 439.48 to m/z 439.98 of 0.12:1 and the similarity of the two structures of the oxidation products, the molar ratio of the two oxidation products would be approximately 0.12:1. Thus, we calculate the total amount of the oxidized peptide to be 7.2 pmol (an averaged value from triplicate measurements). Considering the oxidation yield of 2.6%, our measured amount of TDP was therefore 283 pmol. In comparison to the injection amount of 300 pmol, we find the quantitation error to be -5.5% (see Table 3.2 and Table 3.8). This result illustrates one approach that is able to successfully quantitate peptides containing more than one tyrosine residue.

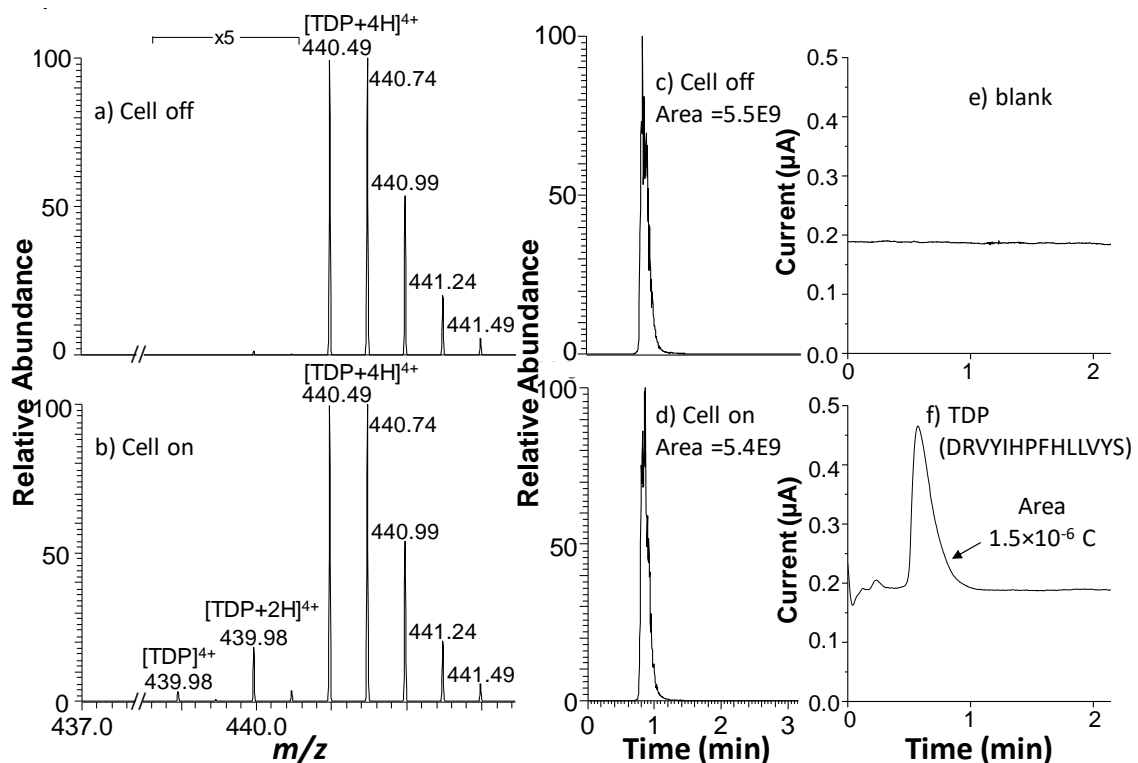


Figure 3.8 ESI-MS spectra of TDP when the applied potential was a) 0 V and b) +1.05 V. The major peak of the oxidized product of TDP was seen at m/z 439.98 (+4 charged) in b. EIC of the +4 charged TDP ion was recorded when the applied potential was c) 0 V and d) +1.05 V. Electric current responses were shown e) due to the blank solvent and f) the oxidation of TDP peptide.

Table 3.9 Electric Current and MS Data for TDP

	Flow rate (mL/min)	EIC Peak Area for oxidized peptide ions*		% of <i>m/z</i> 439.48 to <i>m/z</i> 439.98 (on average)
		<i>m/z</i> 439.98	<i>m/z</i> 439.48	
TDP (DRVYIHPFLLVYS)	0.3	181659931	36733840	12.20%
		184146966	35681381	
		180264335	30369961	

* background subtracted EIC peak area

	EIC peak area of <i>m/z</i> 440.49 before electrolysis	EIC peak area of <i>m/z</i> 440.49 after electrolysis	% Change	Averaged % change upon electrolysis
TDP	5493230265	5348975475	0.026260467	
(DRVYIHPFLLVYS)	5531495790	5387129612	0.026098940	2.55%
	5500755787	5368119852	0.024112311	

	Q (μ A.min)	Q (C)	Amount of the oxidized analyte (pmol)	Averaged amount of oxidized analyte (pmol)	Oxidation yield	Measured amount (pmol)	Theoretical amount (pmol)	Measurement error
TDP (DRVYIHPFLLVYS)	0.02670	1.60E-06	7.40					
	0.02583	1.55E-06	7.16	7.22	2.55%	283.41	300.00	-5.53%
	0.02569	1.54E-06	7.12					

It may not be possible, however, to find suitable conditions in which only one of the tyrosine residues is oxidized. In such cases, we might need to invoke the assumption, based on the similarity of structures, that the intensities of the different mass peaks of the oxidized products represent to good approximation the concentrations of the different oxidized forms, allowing us nevertheless to determine the amount of the original peptide from CMS.

We also tested the phosphopeptide RRLIEDAepYAARG, whose tyrosine residue is phosphorylated. Interestingly, such a peptide does not display an oxidation current upon oxidation (Figure 3.2-k). This result is in agreement with previously reported electrochemical studies of phosphopeptides^{154,155} and provides another way to judge whether or not a peptide tyrosine residue is phosphorylated.^{156,157}

Furthermore, our method can be used to directly quantify phosphopeptides containing a free oxidizable residue such as tyrosine. Absolute quantitation of phosphopeptides typically needs multiple-step synthesis of isotope-labeled phosphopeptide standards.¹⁵⁸ In our approach, phosphorylated UOM9 (sequence: KRPPSQRHGSKY), a kinase substrate peptide originating from myelin basic protein (MBP),¹⁵⁹ was chosen as a test sample. The peptide is phosphorylated in its serine residue and contains one free tyrosine residue. Before electrolysis (Figure 3.9-a), the +5 ion of the peptide was detected at m/z 285.35. After electrolysis (Figure 3.9-b), a peak at m/z 284.94 was observed, corresponding to +5 ion of the oxidized product. Figures 3.9c and d showed the EIC (m/z 285.35) of 50 μ M phosphorylated UOM9 with an injection volume of 6 μ L (injected amount: 300 pmol) with the applied potential of 0 V and +1.05 V (vs. Ag/AgCl), respectively. The integrated area for the peak shown in Figure 3.9-d was smaller by 2.9%, in comparison with that of the peak shown in Figure 3.9-c, indicating that the oxidation yield for this peptide was 2.9% (see data in Table 3.9). On the other hand, the peptide oxidation current peak was detected, as shown in Figure 3.9-f (Figure 3.9-e shows the background current diagram for blank solvent sample under the same + 1.05 V potential as a contrast). Based on the integration of the current peak area, the amount of the oxidized peptide on average was calculated to be 8.1 pmol. Therefore, our measured amount of phosphorylated UOM9 was 283 pmol, which was close to the injection amount of 300 pmol with a measurement error of -5.8% (Table 3.9). To the best of our knowledge, this data represents absolute quantitation of phosphopeptide without using any standards, for the first time.

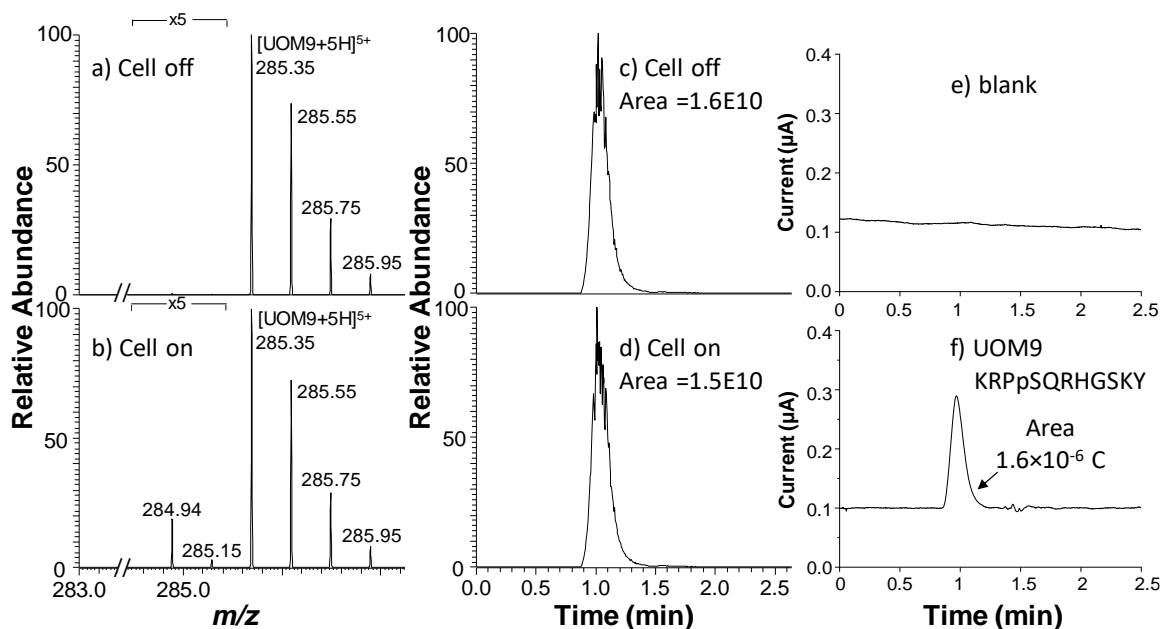


Figure 3.9 ESI-MS spectra of phosphorylated UOM9 when the applied potential was a) 0 V and b) +1.05 V (vs. Ag/AgCl). The peak of the oxidized peptide product was seen at m/z 284.94 (+5 ion) in b). EIC of the +5 ion of phosphorylated UOM9 was recorded when the applied potential was c) 0 V and d) +1.05 V. Electric current responses were shown e) from the blank solvent and f) the oxidation of the phosphorylated UOM9 peptide.

Table 3.10 Electric Current and MS Data for Phosphopeptide UOM9

Q ($\mu\text{A}\cdot\text{min}$)	Q (C)	Amount of the oxidized analyte (pmol)	Average oxidized amount (pmol)	Oxidation yield	Measured amount (pmol)	Theoretical amount (pmol)	Measurement error
0.02483	1.49E-06	7.72					
UOM9	0.02600	1.56E-06	8.08	2.88%	282.51	300.00	-5.83%
	0.02757	1.65E-06	8.57				
		EIC peak area of m/z 285.35 before electrolysis	EIC peak area of m/z 285.35 after electrolysis	% Change	Averaged % change upon electrolysis		
		15594819650	15165221085	2.75%			
UOM9		15773357129	15316634821	2.89%	2.88%		
		15352655959	14895616290	2.98%			

The sensitivity of the method was also evaluated, using a low quantity of peptide DRVY. In our experiment, a BASi stainless electrochemical flow cell (West Lafayette, IN) equipped with a 6-mm *i.d.* glassy carbon WE and a Ag/AgCl RE was used. 3 μL of 0.1 μM

DRVY (injection amount: 300 fmol) was injected into LC/EC/MS for quantitation and the measured peptide quantity was 319 fmol (6.2% quantitation error, see detailed results in Table 3.10), indicating the reasonably good sensitivity and accuracy of our method. Further improvements in sensitivity are possible if background noise in electric current measurement could be reduced, for example, using a newer potentiostat with a Faraday cage.

Table 3.11 Electric Current and MS Data for Sensitivity Evaluation of CMS Using DRVY

	Q (nA.min)	Q (C)	Amount of the oxidized analyte (fmol)	Average oxidized amount (fmol)	Oxidation yield	Measured amount (fmol)	Theoretical amount (fmol)	Measurement error
DRVY	3.70E-01	2.22E-08	115.03					
	3.10E-01	1.86E-08	96.37	106.74	33.50%	318.62	300.00	6.21%
	3.50E-01	2.10E-08	108.81					
	EIC peak area of <i>m/z</i> 552 before electrolysis		EIC peak area of <i>m/z</i> 552 after electrolysis		% Change	Averaged % change upon electrolysis		
DRVY	37654132		24745981		34.28%	33.50%		
	37093511		25335433		31.70%			
	37345161		24453493		34.52%			

3.4 Conclusions

In this study, several tyrosine-containing peptides including phosphopeptides were successfully quantified using coulometric mass spectrometry. The striking strength of this method is that it requires no standard/isotope-labeled peptides for absolute quantification. In addition, the use of MS provides a means to identify the electrochemical reaction products, which is difficult to achieve by using electrochemical technologies alone. The results demonstrate the validity of this method in which we achieve absolute quantitation of peptides by electrochemical oxidation of tyrosine. It is most likely that this approach can be applicable to quantify peptides containing other oxidizable residues such as tryptophan,

methionine and cysteine. Future work will be focused on the method sensitivity improvement and the application of this method to quantitation of peptides from protein digestion, which may provide a new way to quantify proteins. In addition, this CMS method is also expected to be potentially useful in proteomics including quantitation of hormone, antibacterial, and neurotransmitter peptides.¹⁶⁰⁻¹⁶²

CHAPTER 4

ABSOLUTE QUANTITATION OF PROTEINS BY COULOMETRIC MASS SPECTROMETRY

Adapted from Zhao, P.; Wang, Q.; Kaur, M.; Kim, Y. I.; Dewald, H. D.; Mozziconacci, O.; Liu, Y.; Chen, H. *Anal. Chem.* **2020**, 92 (11), 7877–7883. Copyright 2020, American Chemistry Society.

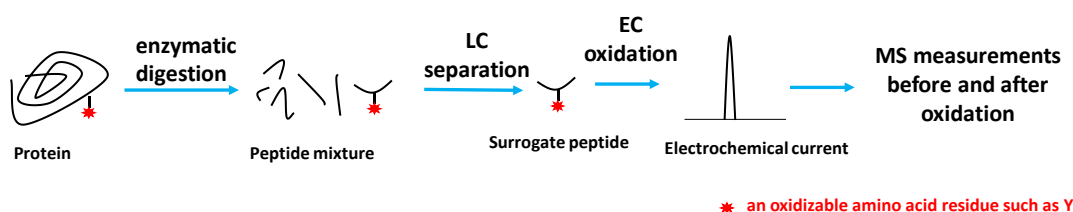
4.1 Introduction

Accurate protein quantitation is a fundamental requirement in a multitude of biological research areas.^{78,97–100,102,163,164} An accurate measurement of absolute protein amount in the sample can be performed by quantitative proteomics approaches such as selected reaction monitoring (SRM) or high-resolution mass spectrometry (HRMS) in combination with isotope-labelled standards.¹⁶⁵ The method requires a known concentration of internal standard, typically doped in the tryptic digest of the target protein, which is labeled with isotopically heavy atoms to mimic native surrogate peptide formed by proteolysis. The sample mixture containing the isotope-labelled peptide standard and the surrogate peptide is then analyzed by LC-MS. Similar to the relative quantitation using isotope-labelled standards, peptides of equal chemistry co-elute and are analyzed by MS simultaneously. Using a pre-determined calibration curve, the ion abundances of the surrogate peptide and the isotope-labeled standard are compared to calculate the absolute quantity of the target surrogate peptide, which represents the target protein content. Thus, absolute quantitation is a targeted quantitative proteomics technique that exhibits robust efficacy and has been increasingly utilized for a wide variety of quantitative proteomics studies.^{158,166–169}

Nevertheless, it has some associated drawbacks. First, isotope-labeled standard peptides are synthesized de novo, which takes time and their syntheses are very costly. The

synthesized peptide standards contain more or less some impurities (typically up to 5% impurity). Second, the ionization efficiencies for the heavy and light isotope-labeled peptides, although very close, are not exactly the same, which may contribute to quantitation error.^{170,171} Third, the heavy isotope-labeled and the light isotope-labeled peptides sometimes cannot have exactly the same chromatographic elution time (e.g., for deuterium labeled peptides), making their precise comparison difficult.¹⁷² Fourth, there is an upper limit for multiplexing analysis using isotope-labeling approach, as simultaneous comparison of too many peptides with different isotope-labelling in one MS spectrum can be difficult.^{173,174} More importantly, any existing background peak that overlaps with the isotope-labeled peptide standard peak would prevent the use of this method. Therefore, new strategies for improved MS-based protein quantitation are still in need.

In this study, we present the development of a conceptually new approach of using electrochemistry (EC)-assisted mass spectrometry for absolute quantitation of proteins. The striking feature of our method is that our method does not need the use of any standard or isotope-labeled peptides or any standard curves, for absolute quantitation.



Scheme 4.1 Schematic showing our approach for absolute quantitation of protein.

As illustrated in Scheme 4.1, in our approach, a target protein is first digested into peptides. By using chromatographic separation, a peptide containing electrochemically

active residue (e.g., tyrosine), can be separated out and chosen as a surrogate signature peptide and then introduced for oxidation in an electrochemical flow cell, followed with MS detection. Electric current is generated and recorded during electrochemical oxidation. Based on the Faraday's Law, Q , the total electricity can be calculated by integrating the Faradaic current over time. Q is related to the moles of the peptide that has been oxidized, as shown in the equation of $Q = nzF$ (n , z and F denote the moles of the oxidized peptide, the number of electrons lost from oxidizing every peptide molecule, the Faraday constant of 9.65×10^4 C/mol, respectively). Thus, n is equal to Q/zF . Upon oxidation, ion intensity of the surrogate peptide decreases. The relative reduction of the peptide ion peak area in the recorded MS data before and after the electrochemical oxidation reflects the oxidation yield (denoted as Δi). Thus, the total amount of the surrogate peptide can be calculated as the quotient of the amount of the oxidized peptide n and the oxidation yield Δi (i.e., $Q/(zF\Delta i)$).

Recently we have shown that this CMS method can be used for accurately quantifying small molecules^{61,175,176} and tyrosine- or cysteine-containing peptides including phosphopeptides.¹⁷⁷ In this study, the method is applied to absolute protein quantitation, for the first time, as protein can be digested into peptides and stoichiometrically one protein molecule typically produces one peptide molecule in theory (antibody can be an exception). By using our approach, we successfully quantified the absolute amounts of β -casein, apomyoglobin, and KaiB proteins expressed from *E. Coli*. The peptide amount measured by CMS is in excellent agreement with traditional isotope dilution method (<3% difference) and also can reflect the amount of the corresponding protein. Our measurement error for quantitation of these proteins, defined as the difference

between the moles of surrogate peptides and the moles of the corresponding proteins (determined from either the known weight or the Bradford Assay), ranges from -11.1% to 12.8%. The negative error indicates there is likely a slight sample loss during the tryptic digestion of proteins to peptides. IgG2 antibody can also be quantified by CMS method. The relatively large quantitation error of -26.4% is likely due to the difficulty in the digesting this large protein.

4.2 Experiments

4.2.1 Chemicals

Apomyoglobin from horse skeletal muscle (protein sequencing grade) and β -casein from bovine milk (bioultra grade) were bought from Sigma Aldrich (St. Louis, MO). The monoclonal antibody drug VectibixTM (panitumumab, IgG2) was purchased from Amgen (Thousand Oaks, CA). Peptides GGYR, DRVY and Arg⁸-vasotocin (sequence: CYIQNCPRG, two cysteines are connected with one disulfide bridge) were obtained from Genscript Biotech (Piscataway, NJ). Stable isotope-labelled peptide standards AVYPYQR[^] (labeled at arginine, ¹³C6, ¹⁵N4, 95% purity) and VL[^]IGLDLLYGELQDSDDF (labeled at leucine, ¹³C6, ¹⁵N, 95% purity) were both purchased from New England Peptide (Gardner, MA). Trypsin (sequencing grade) was purchased from Promega (Madison, WI). Acetonitrile (ACN, HPLC grade) and acetone (ACS grade) were bought from Fisher Scientific (Fair Lawn, NJ). Formic acid (HPLC grade), urea (electrophoresis grade), ammonium bicarbonate (bioultra grade), dithiothreitol (DTT, bioultra grade), Tris(2-carboxyethyl)phosphine hydrochloride (TCEP, bioultra grade) and iodoacetamide (IAA, bioultra grade) were all bought from Sigma Aldrich (St. Louis, MO). A Millipore Direct-

Q5 purification system (Burlington, MA) was used to obtain purified water for sample preparation.

4.2.2 Protein Expression and Purification

The cloning and purification of KaiB were performed as described previously with minor modifications.^{178,179} Basically, the open reading frame of KaiB from *Synechococcus elongatus* was amplified using polymerase chain reaction (PCR) and cloned into the pET-28b expression vector with a small ubiquitin-related modifier (SUMO) using NdeI and HindIII cloning sites. *Escherichia coli* BL21(DE3) was used for the overexpression of KaiB. Transformed *E. coli* culture was grown in 1 L LB at 37°C until A_{600} reaches 0.7. The culture was induced with 1 mM isopropyl β -D-thiogalactopyranoside (Calbiochem, San Diego, CA) to overexpress recombinant KaiB. After 6 hours, the cells were harvested and stored at -80°C overnight. The cell pellets were resuspended in the buffer (500 mM NaCl, 20 mM Tris·HCl, 5 mM imidazole, and pH = 7.0). The cell lysate was clarified by centrifugation at 20,000 g for 60 min at 4°C. The supernatant was filtered with 0.45 μ m vacuum filter to remove small particles. The His-tagged KaiB was purified with Ni column and the anion-exchange chromatography was applied for further purification. Ulp1 protease was added to the eluent to cut the tag out. The His-tag was cleaved from KaiB after incubation at 4 °C overnight. To separate KaiB from His-tag, Ni column was used again, and another anion-exchange column was applied to complete the purification. The purity was checked by SDS/PAGE and dialyzed with the buffer (150 mM NaCl, 20 mM Tris·HCl, pH 8.0). The expressed KaiB protein was concentrated and determined at a concentration of 206 μ M by the Bradford protein assay. The protein sample was then stored at -80 °C, prior to CMS quantitation.

4.2.3 Proteolytic Digestion

200 μg of β -casein from bovine milk was dissolved in 50 mM ammonium bicarbonate (NH_4HCO_3 , pH 7.4), followed by adding 50 μL of 0.2 $\mu\text{g}/\mu\text{L}$ trypsin solution. The protein sample was incubated at 37°C for overnight. The digested β -casein sample was diluted to the final concentration of 30 μM by adding mobile phase A (water with 0.1% formic acid). 100 μg of apomyoglobin from horse skeletal muscle was dissolved in 50 mM ammonium bicarbonate (NH_4HCO_3 , pH 7.4), followed by adding 50 μL of 0.2 $\mu\text{g}/\mu\text{L}$ trypsin solution. The protein sample was incubated at 37°C for overnight. The digested apomyoglobin sample was slightly diluted to the final concentration of 25 μM by adding mobile phase A (water with 0.1% formic acid).

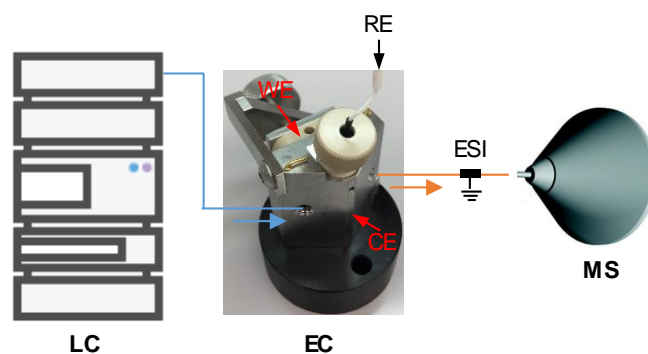
The Vectibix IgG2 antibody was efficiently acetone precipitated and on-pellet digested by a reported procedure^{180,181} with minor modifications. Briefly, the total concentration of the IgG2 was adjusted to 4 mg/mL and 25 μL was precipitated by addition of three aliquots of cold acetone (50 μL each) while vortexing. The sample was incubated overnight at -20°C and then centrifuged at 12000 g for 20 min. The supernatant was carefully removed, and the pellet was air-dried at room temperature. Then a 50 μL of 0.08 $\mu\text{g}/\mu\text{L}$ trypsin (in 50 mM Tris buffer, pH 8) was added to dissolve the pellet. After a brief vortexing, the sample solution was incubated in a water bath at 37°C for 4 h. After that the sample was reduced with 5 mM TCEP at 95°C for 5 min, and then alkylated with 10 mM IAA at 37°C for 30 min in the dark. A second aliquot of trypsin (0.1 $\mu\text{g}/\mu\text{L}$, 40 μL) was added to the sample solution. The sample was incubated at 37°C overnight to achieve complete digestion. The final volume of the digested solution was 100 μL , and the final concentration of digested antibody was 3.4 μM .

100 μg of KaiB protein was precipitated from the expressed protein sample solution using cold acetone at -20°C overnight to remove salts and buffers. The protein pellet was obtained by centrifugation at 13,000 g for 10 min. Then protein pellet was washed by cold acetone once and air-dried at room temperature. After that, the protein pellet was re-dissolved in 100 μL of 8 M urea. The protein was reduced by DTT at 37°C for 30 min and alkylated by IAA at room temperature in the dark for 30 min. DTT was added again to quench extra amount of IAA. The sample was diluted by adding 100 mM NH_4HCO_3 to reduce urea concentration lower than 2 M. 4 μg of trypsin (protease: protein = 1:25, w/w) was added into the protein sample solution and incubated at 37°C for overnight. The digestion process was terminated by adding 1% formic acid (v/v). Peptides were then desalted by using C18 spin columns from G-Biosciences (St. Louis, MO). The desalted peptides were collected and diluted to the final concentration of 28 μM by adding mobile phase A (water with 0.1% formic acid) before LC/EC/MS analysis.

4.2.4 Instrumentation

As shown in Scheme 4.2, the experimental setup consisted of a ultra-performance liquid chromatography (UPLC, Waters, Milford, MA) coupled with an electrochemical thin-layer flow cell (BASi, West Lafayette, IN; cell dead volume: ca. 1 μL) and a high-resolution Orbitrap Q Exactive mass spectrometer (Thermo Scientific, San Jose, CA). The electrochemical cell used a glassy carbon disc (*i.d.*, 6 mm, catalog# MF-1015) as the working electrode (WE). An Ag/AgCl (3M NaCl) working electrode electrode was adopted as the reference electrode (RE, catalog# RE-6) and the cell stainless steel body served as a counter electrode (CE, catalog# MF-1092). A reversed phase column (BEH C18, 2.1 mm \times 50 mm, 1.7 μm) was used for separation. A potential of +0.95 V or +1.05 V (vs.

Ag/AgCl) was applied to WE to trigger the oxidation of LC-separated peptides (the potential used in this study was chosen and optimized for achieving selective oxidation of tyrosine-containing peptides due to the relatively low oxidation potential of tyrosine residue compared to other residues²³). A ROXY™ potentiostat (Antec BV, The Netherlands) was used to monitor and record the oxidation current. OriginPro 2018b was used to import and integrate the electric current peak to calculate the total electric charge of Q. The peptide flowing out of electrochemical cell was online analyzed using the Orbitrap mass spectrometer equipped with a heated electrospray ionization (HESI) source. The flow rate of sheath gas and the applied ionization voltage were 10 L/h and the +4 kV, respectively. The ion transfer inlet capillary temperature was kept at 250 °C. Mass spectra were acquired by Thermo Xcalibur (3.0.63). The working electrode were cleaned by polishing with alumina slurry after use.



Scheme 4.2 Schematic drawing of the LC/EC/MS setup for absolute quantitation of proteins.

For LC/MS analysis of peptide mixtures, the mobile phase flow rate was 200 $\mu\text{L}/\text{min}$. In a gradient elution, the mobile phase B (acetonitrile with 0.1% formic acid) increased from 5% to 8% in 3 min, and reached to 15% in 1 min. Then, mobile phase B

was reduced back to 10% in 1 min and kept at 10% for 4 min before returned to 5%. The concentrations of GGYR, DRVY, and Arg8-vasotocin in the peptide mixture were 20 μM , 20 μM , and 25 μM , respectively. The injection volume was 3 μL per analysis.

For LC/MS setup of digested β -casein, apomyoglobin, and KaiB, the mobile phase flow rate was 200 $\mu\text{L}/\text{min}$. The mobile phase B (acetonitrile with 0.1% formic acid) increased from 5% to 40% in 10 min, and climbed to 70% from 10 min to 15 min. Then, the mobile phase B went back to 5% in 1 min, and then kept at 5% for 4 min. The concentrations of digested β -casein, apomyoglobin, and KaiB were 30 μM , 25 μM , and 28 μM , respectively. The injection volume was 3 μL per analysis.

For LC/MS setup of digested antibody, the mobile phase flow rate was 200 $\mu\text{L}/\text{min}$. The mobile phase B (acetonitrile with 0.1% formic acid) increased from 5% to 20% in 5 min, and reached to 30% from 5 min to 25 min. Then, the mobile phase B climbed to 95% in 1 min and kept at 95% for 5 min. After that the mobile phase B returned to 5% in 1 min and finally isocratic at 5% for 5 min. The concentration of digested IgG2 antibody was 3.4 μM . The injection volume was 3 μL per analysis.

4.3 Results and Discussion

The most commonly used approach for MS quantitation of proteins is surrogate peptide analysis in which a protein analyte is digested into peptides and a peptide is selected and quantified by MS. The measured quantity of the surrogate peptide reflects the amount of its precursor protein analyte. Our CMS method for protein absolute quantitation also adopts the protein digestion step but quantifies the surrogate peptide using MS combined with electrochemistry (EC). To test if CMS is applicable to quantify peptides from a protein

digest, we first examined the feasibility of measuring peptides from a mixture. In our experiment, three tyrosine-containing peptides, GGYR, DRVY, and Arg⁸-vasotocin (sequence: CYIQNCPRG-NH₂, 1-6 disulfide bond) were mixed together to serve as a mixture sample which underwent reversed-phase LC separation under gradient elution conditions, online electrochemical oxidation and subsequent MS detection. Extracted-ion chromatograms (EIC) of +2 ions of the three peptides after UPLC separation are shown in Figures 4.1-a, b, and c, respectively. The injection volume of mixture was 3 μ L (injected amount: 60 pmol GGYR, 60 pmol DRVY, and 75 pmol Arg⁸-vasotocin). At the same time, oxidation current peaks corresponding to different peptides were recorded (Figure 4.1-e). In contrast, no oxidation current peaks were observed in Figure 4.1-d from a blank solvent sample under the same oxidation potential of + 0.95 V, indicating that those peaks observed in Figure 4.1-e are results of electrochemical oxidation of the three peptides. Indeed, the online MS detection following the electrochemical oxidation confirmed that those peaks are from the peptide as labeled in Figure 4.1-e. For instance, before electrolysis (Figure 4.1-f, no potential was applied to the cell), the +2 ion of GGYR was observed at m/z 226.6. When +0.95 V was applied to the cell for oxidation (Figure 4.1-g), a peak at m/z 225.61 arose, corresponding to +2 ion of the oxidized peptide product (one tyrosine residue loses two hydrogens and two electrons ($z=2$) to form semi-quinone upon oxidation; as a result, 2 Da mass shift occurs to the peptide ion¹⁷⁷). The electrochemical oxidation consumed peptide and therefore its intensity dropped after electrolysis. Due to the dependence of ion intensity on concentration, the relative peptide ion intensity change would suggest the relative concentration change (i.e., the oxidation yield of the peptide). As shown in Figure 4.2, the integrated EIC peak area for the GGYR ion (m/z 226.6, the +2 ion) at +0.95 V was

smaller than that at 0 V by 15.6%. This result indicates that the GGYR oxidation yield was 15.6% (Table 4.1). Meanwhile, by applying the Faraday's Law with the integrated current peak area, the amount of GGYR that was oxidized was shown to be 9.9 pmol. Therefore, the total amount of GGYR was measured to 63.5 pmol by CMS. A triplicate measurement gave the average amount of GGYR to be 63.8 ± 0.6 pmol, which turned out to be close to the injection amount (60 pmol) with the measurement error of 6.3%. Following the same procedure, the quantitation errors for the other two peptides, DRVY and Arg⁸-vasotocin, were 2.7% and 1.9% (Table 4.1), respectively.

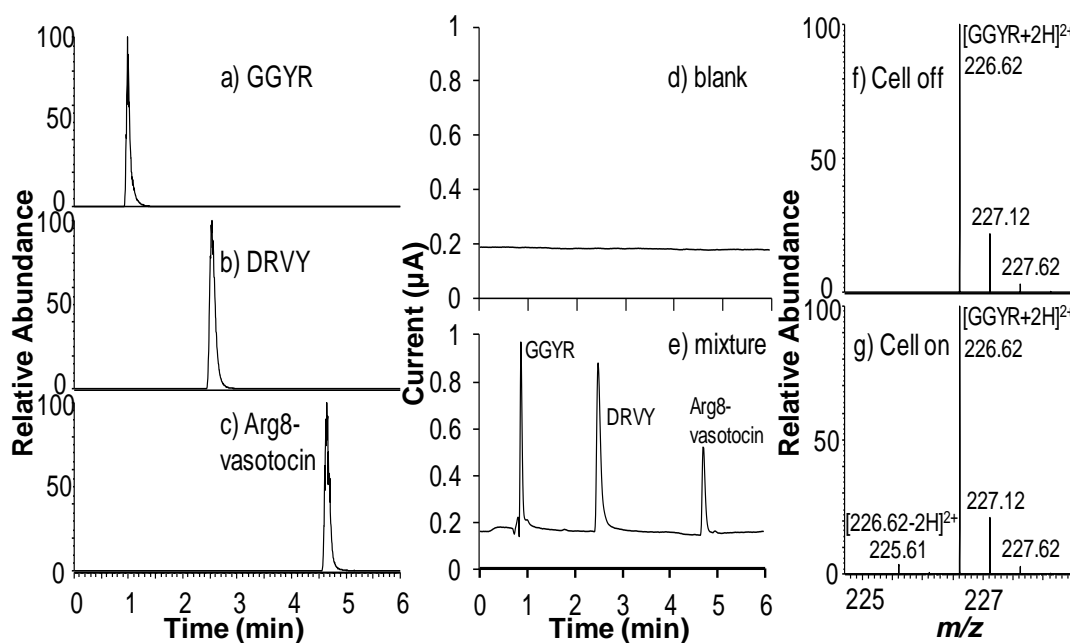


Figure 4.1 Extracted ion chromatograms of a) GGYR, b) DRVY, and c) Arg⁸-vasotocin. Electric oxidation current diagrams are shown due to the oxidation of d) a solvent blank and e) the peptide mixture. ESI-MS spectra of GGYR was recorded f) when the cell was turned off and g) when the cell was turned on (applied potential: +0.95 V). The +2 ion of the oxidized GGYR product was observed at m/z 225.6 in g).

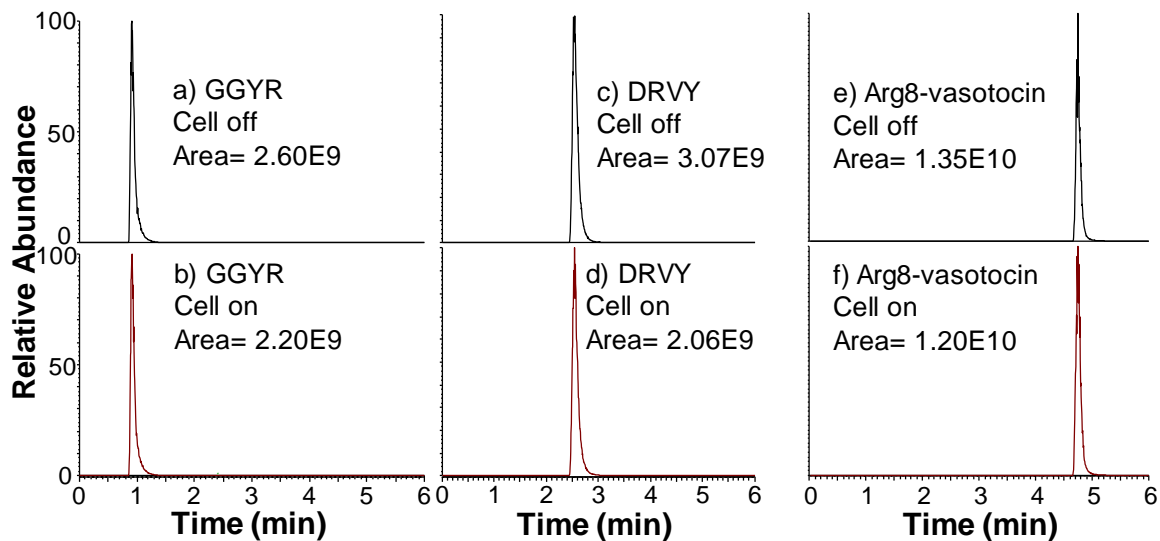


Figure 4.2 EIC spectra of GGYR, DRVY, and Arg8-vasotocin were recorded when the applied potential was 0 V in a), c), e), and +0.95 V in b), d), f).

Table 4.1 Electric Current and MS Data for a Peptide Mixture (GGYR, DRVY, and Arg8-vasotocin)

	Q (μ A.min)	Q (C)	Amount of the oxidized analyte (pmol)	Oxidation yield	Measured amount (pmol)	Averaged amount (pmol)	Theoretical amount (pmol)	Measurement error
GGYR	3.28E-02	1.97E-06	10.18756477	0.16067802	63.40359914	63.8 \pm 0.6	60	6.3%
	3.19E-02	1.91E-06	9.904663212	0.15587608	63.54190593			
	3.20E-02	1.92E-06	9.932642487	0.15403844	64.48158321			
DRVY	6.67E-02	4.00E-06	20.72953368	0.32998131	62.82032664	61.6 \pm 1.4	60	2.7%
	6.54E-02	3.92E-06	20.32849741	0.32804153	61.96927996			
	6.08E-02	3.65E-06	18.91088083	0.31504823	60.02535177			
Arg8-vasotocin	2.72E-02	1.63E-06	8.440414508	0.113258599	74.52338792	76.4 \pm 1.8	75	1.9%
	2.74E-02	1.65E-06	8.521243523	0.109328705	77.94150240			
	2.66E-02	1.60E-06	8.281865285	0.107745151	76.86531791			

	EIC peak area of m/z 226.62 before electrolysis	EIC peak area of m/z 226.62 after electrolysis	Oxidation yield
GGYR	2729641626	2291048213	0.16067802
	2604523292	2198540412	0.15587608
	2626944251	2222293856	0.15403844
	EIC peak area of m/z 276.64 before electrolysis	EIC peak area of m/z 276.64 after electrolysis	Oxidation yield
DRVY	3262116841	2185679243	0.32998131
	3070881323	2063504722	0.32804153
	3038422284	2081172731	0.31504823
	EIC peak area of m/z 525.72 before electrolysis	EIC peak area of m/z 525.72 after electrolysis	Oxidation yield
Arg8-vasotocin	13772412086	12212567994	0.113258599
	13573551414	12089572611	0.109328705
	13476967282	12024889401	0.107745151

With the success in using CMS to quantify peptides in mixture, we started absolute protein quantitation, using the surrogate peptide approach. β -casein, a commonly found phosphoprotein in mammalian milk (224 amino acids, sequence shown in Table 4.2), was tested by CMS. The protein was first tryptic digested and a tyrosine-containing peptide AVPYRQR was separated out by chromatography for electrochemical oxidation and quantified by our method. Without oxidation (Figure 4.3-a), the protonated AVPYRQR was observed at m/z 415.7. As shown in Figure 4.3-b, after electrolysis, a peak

corresponding to +2 ion of the oxidized AVPYYPQR product was observed at m/z 414.7. EICs of the +2 ion of AVPYYPQR (m/z 415.7) from 3 μ L of the 30 μ M β -casein digest (injected amount: 90 pmol) without and with oxidation are shown in Figures 4.3-c and 4.3-d, respectively. The integrated peak area of m/z 414.7 shown in Figure 4.3-d was smaller by 5.9% compared to the same peak in Figure 4.3-c, suggesting that the oxidation yield for AVPYYPQR was 5.9% (see detailed data in Table 4.3). Figure 4.3-f shows the electric current peak from oxidation of AVPYYPQR (as a control, no oxidation current peak was observed in Figure 4.3-e from solvent blank under the same oxidation potential). The amount of oxidized AVPYYPQR was calculated to be 4.8 pmol, based on the integration of the current peak area. Therefore, the measured amount of AVPYYPQR was 80.1 pmol (Table 4.3). In a triplicate measurement, the averaged quantity of this peptide measured by CMS was 79.1 pmol (Table 4.3). For confirmation, an isotope-labelled peptide AVPYYPQR[^] (labeled at arginine, ¹³C6, ¹⁵N4) was purchased and used as an internal standard to quantify AVPYYPQR in the same β -casein digest. By this traditional isotope dilution method, AVPYYPQR in β -casein digest was measured to be 78.9 pmol (Figure 4.3). This value is in excellent agreement with the quantity of 79.1 pmol from our CMS method (only differed by 0.3%), confirming the possibility of CMS for quantitation. In comparison, traditional absolute quantitation based on the use of isotope labeled peptide standards would need 3-5 data points (i.e., 3-5 sample injections) to construct the calibration curve for quantitation. In comparison, our CMS method is faster, as it actually just needs 2 injections for quantifying one sample. Furthermore, the quantity of 79.1 pmol from our CMS measurement is also close to the initial amount of β -casein (90 pmol) that was used to generate the digest. The measurement error of -12.1%, defined as the difference between

the moles of AVPYQR peptide and the moles of β -casein (determined by weight), indicates that there is likely a slight sample loss during the process for tryptic digestion of proteins to peptides.¹⁸²

Table 4.2 Sequence Information of the Proteins Tested in the Experiments (the Chosen Surrogate Peptides for Quantitation are Highlighted in Bold)

Protein Name	Uniprot #	Sequence
β -casein	P02666	MKVLILACLVALALARELEELNVPGEIVESLSSSEESITRINKKIE KFSSEEQQQTEDELQDKIHPFAQTQSLVYPFPGPIPNSLPQNIPPL TQTPVVVPPFLQPEVMGVSKVKEAMAPKHKEMPFPKYPVEPFT ESQSLTLTDVENLHLPLLLQSWMHQPHQLPPTVMFPPQSVLS LSQSKVLPVPQK AVPYQR DMPQAFLLYQEPVLGPVVRGPFPIIV
Apomyoglobin	P68082	MGLSDGEWQQVLNVWGKVEADIAHGQEVLRIRLFTGHPETLE KFDKFKHLKTEAEMKASEDLKKGHTVVLTAALGGILKKKGHHE AELKPLAQSHATKHKIPIKYLEFISDAIHHVLHSHKHPGDFGADAQ GAMTKALELFRNDIAAK YKELGFQG
KaiB	Q79PF5	MSPRKTYILKLYVAGNTPNSVRALKTLKNILEVEFQGVYALKVI DVLKNPQLAEEDKILATPTLAKVLPLPVRRIIGDLSDREK VLIGL DLLYGELQDSDDF
IgG2		> IgG2 heavy chain QVQLQESGPGLVKPSSETLSLTCTVSGGSVSSGDYYWTWIRQSPG KGLEWIGHIYYSGNTNYPNPSLKSRLTISIDTSKTQFSLKLSVTA ADTAIYCVDRDRVTGAFDIWGQTMVTVSSASTKGPSVFPLAP CSRSTSESTAALGCLVKDYFPEPVTVSWNSGALTSQVHTFPAVL QSSGLYSLSSVTVPSNFGTQTYTCNVDHKPSNTKVDKTVR KCCVECPAPPVAGPSVFLFPPKPKDTLMISRTPEVTCVVVD VSHEDPEVQFNWYVDGVEVHNAKTKPREEQFNSTFRVVSFLT VVHQDWLNGKEYCKVSNKGLPAPIEKTISKTKGQPREPQVYTL PPSREEMTKNQVSLTCLVKGFYPSDIAVEWESNGQPENNYKTP PMLDSDGSFFLYSKLTVDKSRWQQGNVFSCSVMHEALHNHYT QKSLSLSPGK > IgG2 light chain DIQMTQSPSSLSASVGDRTITTCQASQDISNYLNWYQQKPGKAP KLLIYDASNLETGVPSRFSGSGSGTDFFTISSLPEDIATYFCQ HFDHLPALAFGGGKVEIKRTVAAPSVFIFPPSDEQLKSGTASVVC LLNMFYPREAKVQWKVDNALQSGNSQESVTEQDSKDSSTYLSL TLTSLKADYEKHKVYACEVTHQGLSSPVTKSFNRGEC

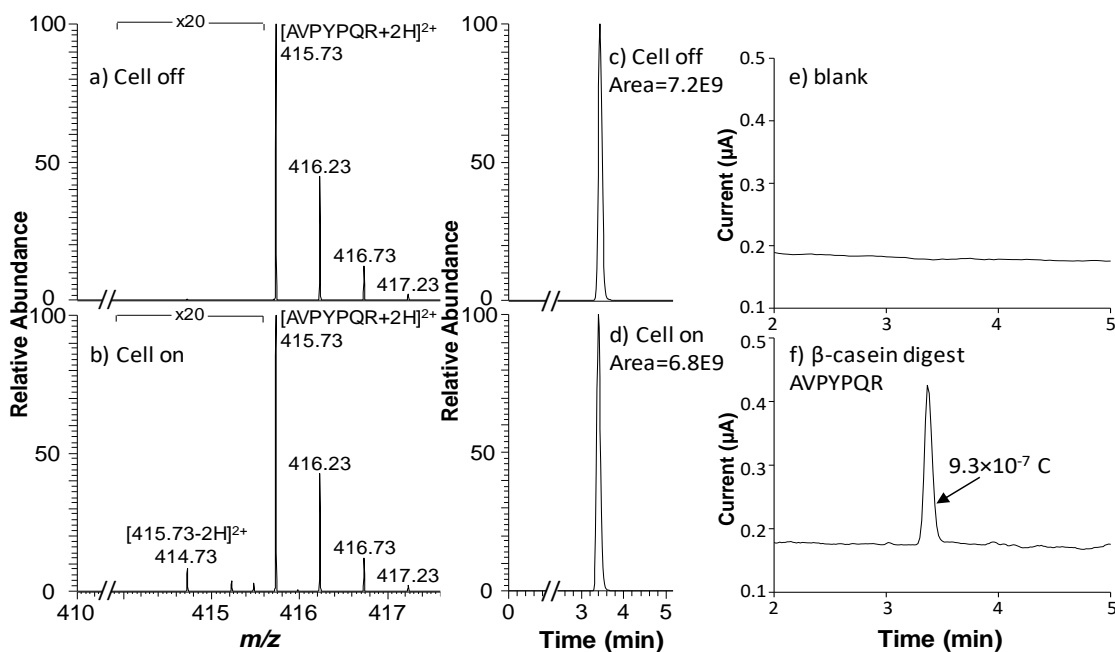


Figure 4.3 MS spectra of AVPYYPQR from the β -casein tryptic digest a) when the cell was off and b) when the cell was turned on (applied potential: +0.95 V). The oxidation product of AVPYYPQR was detected at m/z 414.7. EICs of AVPYYPQR were acquired c) when the cell was off and d) when the cell was turned on (applied potential: +0.95 V). Electric current diagrams were collected from e) blank solvent and f) the oxidation of AVPYYPQR.

Table 4.3 Electric Current and MS Data for Digested β -casein (the Selected Surrogate Peptide: AVPYYPQR)

	Q ($\mu\text{A}\cdot\text{min}$)	Q (C)	Amount of the oxidized analyte (pmol)	Oxidation yield	Measured amount (pmol)	Averaged amount (pmol)	Theoretical amount (pmol)	Measurement error
AVPYYPQR	1.50E-02	8.99E-07	4.660103627	0.058658538	79.44459214			
	1.55E-02	9.31E-07	4.821761658	0.059472399	81.07562061	79.1 \pm 2.1	90	-12.1%
	1.62E-02	9.69E-07	5.020725389	0.065316679	76.86743211			
			EIC peak area of m/z 415.73 before electrolysis	EIC peak area of m/z 415.73 after electrolysis	Oxidation yield			
			7169424228	6748876285	0.058658538			
AVPYYPQR			7233464233	6803272760	0.059472399			
			6981750243	6525725502	0.065316679			

The isotope-labelled peptide AVPYQR^h (labelled at arginine) was spiked into the digested β -casein sample at the final concentrations of 4.8, 7.1, 14.3, 28.5, and 57.0 μM (the 95% purity of isotope-labelled standard was taken into consideration for the sample concentration calculation), respectively. The LC/MS was set at the mobile phase flow rate of 200 $\mu\text{L}/\text{min}$. The mobile phase B started from 5% and increased to 40% in 10 min, and then climbed to 70% from 10 min to 15 min. After that the mobile phase B went back to 5% in 1 min, and then kept at 5% for 4 min. The injection volume was 3 μL per analysis. The ion intensity ratio of $[\text{AVPYQR}^{\text{h}}]/[\text{AVPYQR}]$ plotted against the concentration of the spiked heavy peptide AVPYQR^h is shown below.

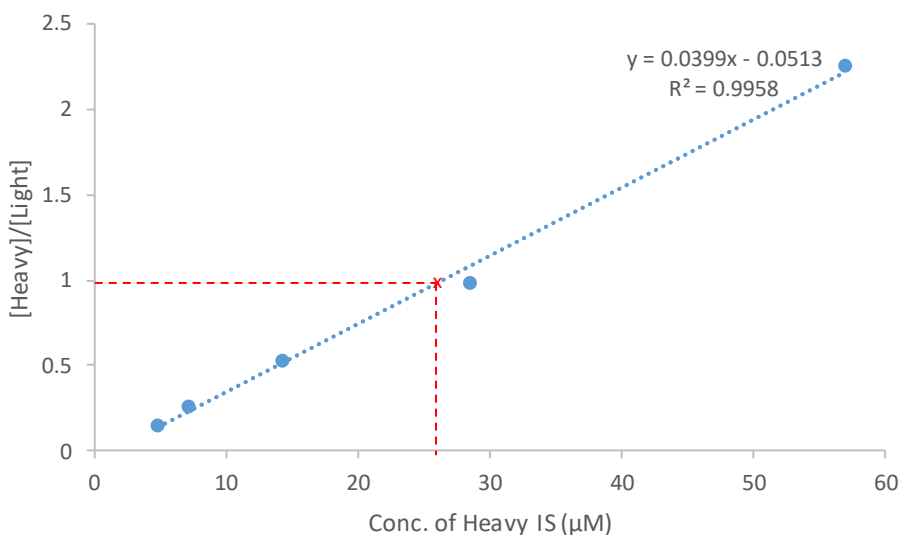


Figure 4.4 Calibration curve using isotope-labelled peptide AVPYQR^h as an internal standard.

From the plot above, one can see that: when $y=1$, $x=26.3 \mu\text{M}$ ($C_{[\text{light}]} = C_{[\text{heavy}]}$). So, the measured concentration of the light peptide AVPYQR from the β -casein digest was

26.3 μM . Considering that the injection volume of 3 μL , the measured quantity for AVYPYQR by this isotope dilution method was 78.9 pmol.

Another protein, apomyoglobin (153 amino acids, sequence is shown Table 4.2), was also analyzed by CMS. After proteolytic digestion, YKELGFQG, a Tyr-containing and electro-oxidizable peptide, was identified and separated by LC/MS analysis, which can be used for quantitation with our method. Without oxidation (Figure 4.5-a), the protonated YKELGFQG was observed at m/z 471.2. As shown in Figure 4.5-b, after electrolysis, a peak corresponding to +2 ion of the oxidized YKELGFQG product was observed at m/z 470.2, due to two hydrogen losses from tyrosine oxidation. EICs the +2 ion of YKELGFQG (m/z 471.2) from 3 μL of 25 μM apomyoglobin digest (injected amount: 75 pmol) without and with oxidation are shown in Figures 4.5-c and 4.5-d, respectively. The peak area of m/z 471.2 decreased by 0.98% upon oxidation (comparing Figures 4.5-c and 4.5-d), showing that the yield of peptide YKELGFQG oxidation was 0.98% (Table 4.4). In addition, the current peak as a result of oxidation of YKELGFQG was detected (Figure 4.5-f). The amount of oxidized YKELGFQG was calculated to be 0.68 pmol, based on the current peak integration. Therefore, the measured amount of YKELGFQG was 68.9 pmol and a triplicate measurement gave an averaged quantity of 66.6 pmol (Table 4.4). Assuming that one molecule of protein apomyoglobin produces one molecule of peptide YKELFQG (note that further cleavage between K and E residues in YKELFQG by trypsin was negligible, probably due to the influence of adjacent acidic residue E which forms a salt bridge with K residue¹⁸³), the measured protein amount is therefore 66.6 pmol. This value is quite close to the amount of protein of 75.0 pmol (11.1% error, Table 4.4) for

generating the 3 μL of the protein digest that was analyzed. This result further confirms the viability of using CMS for protein quantitation.

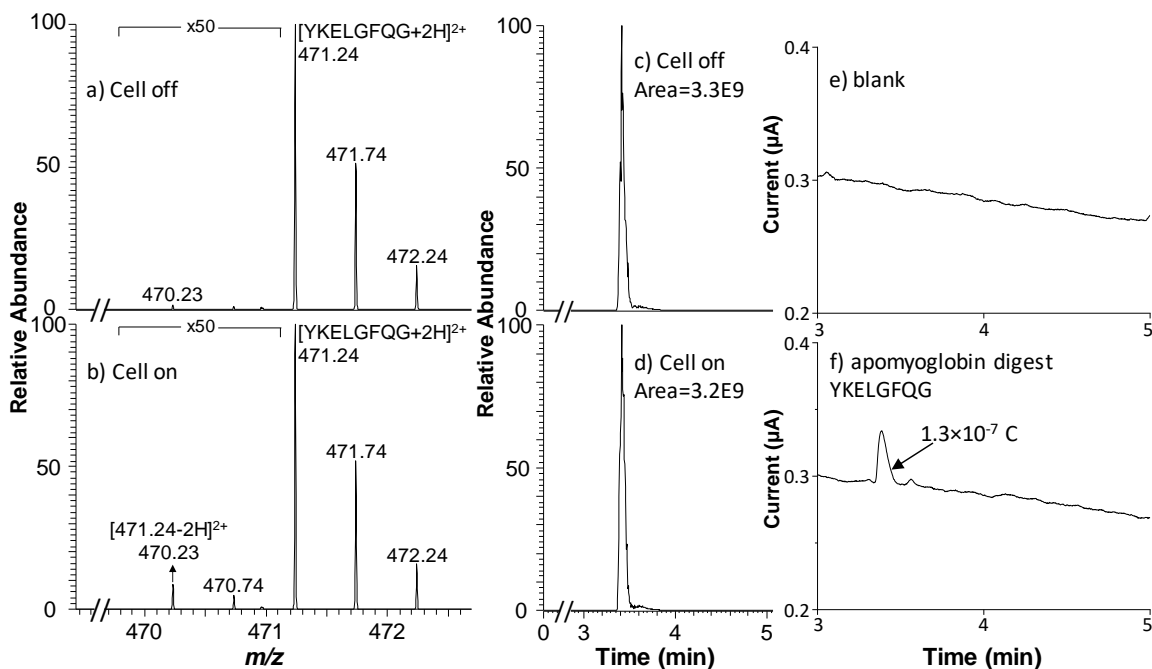


Figure 4.5 ESI-MS spectra of YKELGFQG from the apomyoglobin tryptic digest when the applied potential was a) 0 V and b) +1.05 V. The peak of the oxidation product of YKELGFQG was seen at m/z 470.2 in b). EIC of YKELGFQG was recorded when the applied potential was c) 0 V and d) +1.05 V. Electric current responses were due to the oxidation of e) blank solvent and f) YKELGFQG. Note that there is a small peak of m/z 470.2 in a), which might be caused by in-source oxidation of YKELGFQG.

Table 4.4 Electric Current and MS Data for Digested Apomyoglobin (the Selected Surrogate Peptide: YKELGFQG)

	Q ($\mu\text{A}\cdot\text{min}$)	Q (C)	Amount of the oxidized analyte (pmol)	Oxidation yield	Measured amount (pmol)	Averaged amount (pmol)	Theoretical amount (pmol)	Measurement error
YKELGFQG	2.47E-03	1.48E-07	0.767875648	0.011311603	67.88389303	66.6 \pm 3.2	75	-11.1%
	2.18E-03	1.31E-07	0.677720207	0.009829221	68.94953395			
	1.77E-03	1.06E-07	0.550259067	0.008729073	63.03751464			
			EIC peak area of m/z 471.24 before electrolysis	EIC peak area of m/z 471.24 after electrolysis	Oxidation yield			
			2596956965	2567581219	0.011311603			
YKELGFQG			3266148058	3234044367	0.009829221			
			3071323798	3044513987	0.008729073			

With the success in quantifying standard model proteins, we took a step further to use our CMS method for the quantitation of a biological sample of KaiB protein isolated from *E. Coli* (sequence shown in Table 4.2). KaiB protein is a circadian clock protein in cyanobacteria. The circadian clock is an endogenous timekeeping mechanism that provides many advantages for life in a rhythmically changing environment.¹⁸⁴ The gene expression, metabolism, physiology, and behavior of almost all light-perceiving organisms living on earth are governed by a circadian (~24-hour) clock, which anticipates the daily rhythm of the sunlight and the ambient temperature.^{185,186} Disruption of the circadian clock in humans is correlated with many health issues, such as cancer, heart attacks, obesity, diabetes, fatigue, mood disorders, and most notably jet lag.¹⁸⁷⁻¹⁹¹ The cyanobacterial circadian clock is a simple model system of the human circadian clock. The cyanobacterial circadian clock regulates more than 30% of its gene expression which affects the physiology of the cell.¹⁸⁹ In cyanobacteria, the amounts of the gene expression products oscillate with a 24-hour period. Till now, there is no commercially available protein standard for the KaiB protein quantitation. The quantitation of the transcription products (RNA) has been reported^{192,193} but the quantitation of the translation products of protein KaiB has not been reported yet. Because the proteins are the major determinant of the cell physiology, the timely measurement of the protein amount is significantly important to understand the circadian regulation of the gene expression and its physiology of cyanobacteria.

In our experiment, the cloning and purification of KaiB were performed as described previously with minor modifications^{178,179} and details are shown in the Experimental Section. After digestion of KaiB protein isolated from *E. coli*, a Tyr-

containing peptide VLIGLDLLYGELQDSDDF could be separated out and quantified by CMS. Without oxidation (Figure 4.6-a), the +2 ion of VLIGLDLLYGELQDSDDF was observed at m/z 1013.0. When the electrochemical cell was turned on for oxidation (Figure 4.6-b), +2 ion of the oxidized peptide product arose at m/z 1012.0. The integrated area for the m/z 1013.0 peak after electrochemical oxidation was smaller by 6.5% (note that there is a little contribution to the peak of m/z 1013.0 from the third isotopic peak of m/z 1012.0, which was corrected for the oxidation yield calculation; see details in Table 4.5), compared to the same peak before oxidation, which indicated the oxidation yield was 6.5%. Meanwhile, the electric current as a result of oxidation of VLIGLDLLYGELQDSDDF was observed (shown in Figure 4.6-d). The amount of VLIGLDLLYGELQDSDDF that underwent oxidation was calculated to be 4.6 pmol, based on the integration of the current peak area. Therefore, the amount of peptide measured by CMS was 71.3 pmol (the averaged value from a triplicate measurement: 73.3 pmol, Table 4.5). For comparison, an isotope-labelled peptide VL¹³IGLDLLYGELQDSDDF (labeled at leucine, ¹³C6, ¹⁵N) was purchased and used as an internal standard to quantify the same KaiB protein digest. The measured quantity for VLIGLDLLYGELQDSDDF by this isotope dilution method was 71.1 pmol (see data Figure 4.7). Again, the peptide quantity measured by two different methods are in excellent agreement (differed by 3.0%), providing validation of this CMS quantitative analysis approach. Based on our Bradford assay of the initial KaiB protein sample, the total amount that was used to produce the KaiB digest was estimated to be 84 pmol (28 μ M, 3 μ L). The moles of the surrogate peptide VLIGLDLLYGELQDSDDF measured by our CMS is close to the moles of KaiB protein, with the measurement error of -12.8% (likely due to sample loss during the digestion/desalting processes).

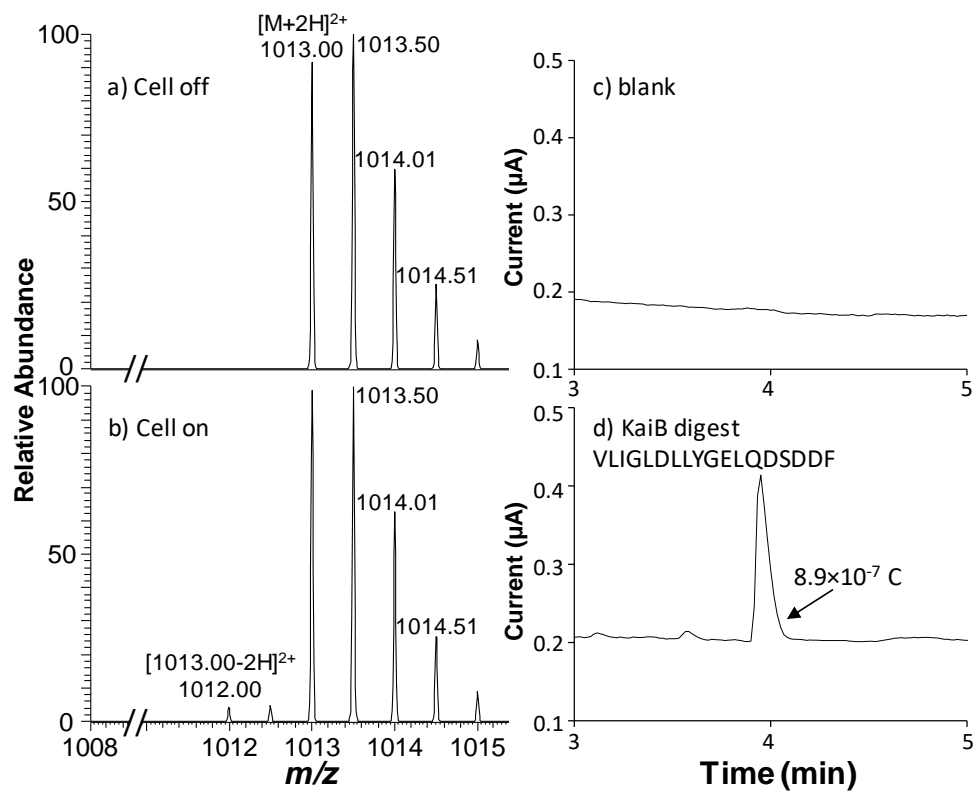


Figure 4.6 MS spectra of VLIGLDLLYGELQDSDDF from the KaiB tryptic digest a) when the cell was off and b) when the cell was turned on (applied potential: +0.95 V). The oxidized product peak was detected at m/z 1012.0 (+2 ion) in b). Electric current response curves are shown, due to oxidation of c) solvent blank and d) VLIGLDLLYGELQDSDDF.

Table 4.5 Electric Current and MS Data for Digested KaiB (the Selected Surrogate Peptide: VLIGLDLLYGELQDSDDF)

	Q ($\mu\text{A}\cdot\text{min}$)	Q (C)	Amount of the oxidized analyte (pmol)	Oxidation yield	Measured amount (pmol)	Averaged amount (pmol)	Theoretical amount (pmol)	Measurement error
VLIGLDLLYGELQDSDDF	9.29E-03	5.57E-07	2.888082902	0.036395796	79.35210160			
	1.48E-02	8.89E-07	4.604145078	0.064535700	71.34260693	73.3 \pm 5.4	84	-12.8%
	1.61E-02	9.64E-07	4.995854922	0.072336493	69.06410188			
			EIC peak area of m/z 1013.00 before electrolysis	EIC peak area of m/z 1013.00 after electrolysis	Corrected EIC peak area of m/z 1013.00	Oxidation yield		
			3963974050	3960770050	3819702058	0.036395796		
			5072494677	4883731893	4745137681	0.064535700		
			4018493894	3794767970	3727810140	0.072336493		

The isotope-labelled peptide VL^{13C6, 15N}IGLDLLYGELQDSDDF (labelled at leucine, ¹³C6, ¹⁵N) was spiked into the digested KaiB sample at the final concentrations of 4.8, 14.3, 28.5, and 52.3 μM (the 95% purity of VL^{13C6, 15N}IGLDLLYGELQDSDDF was taken into account for its concentration calculation), respectively. The LC/MS was set at the mobile phase flow rate of 200 μL/min. The mobile phase B started from 5% and increased to 40% in 10 min, and then climbed to 70% from 10 min to 15 min. After that the mobile phase B went back to 5% in 1 min, and then kept at 5% for 4 min. The injection volume was 3 μL per analysis. The ion intensity ratio of [VL^{13C6, 15N}IGLDLLYGELQDSDDF]/[VLIGLDLLYGELQDSDDF] plotted against the concentration of the spike heavy peptide VL^{13C6, 15N}IGLDLLYGELQDSDDF is shown below.

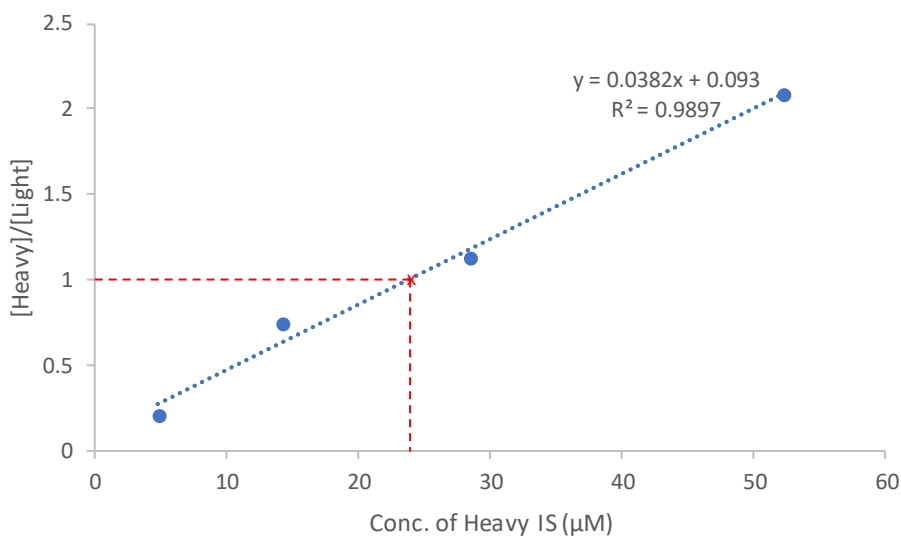


Figure 4.7 Calibration curve using isotope-labelled peptide VL^{13C6, 15N}IGLDLLYGELQDSDDF as an internal standard.

From the plot above, one can see that: when $y=1$, $x=23.7 \mu\text{M}$ ($c[\text{light}] = c[\text{heavy}]$). So, the measured concentration of the light peptide VLIGLDLLYGELQDSDDF from

KaiB digest was 23.7 μM . Considering that the injection volume of 3 μL , the measured quantity for VLIGLDLLYGELQDSDDF by this isotope dilution method was 71.1 pmol. Besides that, an alternative comparison by quantifying two tryptic digested peptide fragments from the same KaiB digestion sample was conducted to further validate this method. Two peptide fragments NILEVEFQGVYALK and VLIGLDLLYGELQDSDDF were selected and quantified from the same injection run in a separate trial (Table 4.6). While VLIGLDLLYGELQDSDDF was determined by CMS to be 17.6 pmol, another peptide NILEVEFQGVYALK was measured to be 18.5 pmol, and their quantities were in good agreement (4.9% difference). Such a redundancy experiment could help to confirm the robustness and reproducibility of the CMS method.

Table 4.6 Electric Current and MS Data for Digested KaiB (the Selected Surrogate Peptides are NILEVEFQGVYALK and VLIGLDLLYGELQDSDDF)

	Q ($\mu\text{A}\cdot\text{min}$)	Q (C)	Amount of the oxidized analyte (pmol)	Oxidation yield	Measured amount (pmol)	Averaged amount (pmol)
NILEVEFQGVYALK	3.16E-3	1.90E-07	0.98238342	0.050724133	19.36717999	18.5 \pm 0.7
	3.45E-3	2.07E-07	1.07253886	0.059629154	17.98681991	
	3.51E-3	2.11E-07	1.09119171	0.059798044	18.24794979	
VLIGLDLLYGELQDSDDF	3.54E-3	2.12E-07	1.100518135	0.059042871	18.63930587	17.6 \pm 0.9
	3.67E-3	2.20E-07	1.140932642	0.067123959	16.99739784	
	3.62E-3	2.17E-07	1.125388601	0.065343615	17.22262542	
			EIC peak area of m/z 811.9 before electrolysis	EIC peak area of m/z 811.9 after electrolysis	Corrected EIC peak area of m/z 811.9	Oxidation yield
NILEVEFQGVYALK			642667065	627095864	610068335	0.050724133
			702442081	684881095	660556054	0.059629154
			711346295	693134219	668809178	0.059798044
			EIC peak area of m/z 1013.0 before electrolysis	EIC peak area of m/z 1013.0 after electrolysis	Corrected EIC peak area of m/z 1013.00	Oxidation yield
VLIGLDLLYGELQDSDDF			222622460	217010542	207029344	0.059042871
			232397926	226217064	214474478	0.067123959
			233467511	227619811	215877225	0.065343615

To further test the capability of the CMS method, Vectibix (panitumumab, approximate molecular weight 147 kDa, sequence shown in Table 4.2), a recombinant human IgG2 kappa monoclonal antibody binding specifically to the human epidermal growth factor receptor (EGFR) was also tested and quantified in the experiment. After antibody was acetone precipitated and on-pellet digested, LLIYDASNLETGVPSR, a Tyr-containing peptide from light chain was identified and separated by LC/MS analysis, which can be used for quantitation by our method. Without oxidation (Figure 4.8-a), peptide LLIYDASNLETGVPSR was observed at m/z 874.5 (+2 ion) and chosen as the surrogate peptide. As shown in Figure 4.8-b, after electrolysis, the oxidized product of LLIYDASNLETGVPSR (+2 ion) was detected at m/z 873.5, due to two hydrogen losses from tyrosine oxidation. Figures 4.8-c and 4.8-d show the EIC the +2 ion of LLIYDASNLETGVPSR (m/z 874.5) from 3 μ L of 3.4 μ M IgG2 antibody digest (10.2 pmol) without and with oxidation, respectively. Note that one IgG2 molecule contains two identical light chains in which the surrogate peptide fragment is located. Therefore the theoretical amount of surrogate peptide was 20.4 pmol per injection by calculation. The oxidation yield for LLIYDASNLETGVPSR was suggested to be 8.2% (Table 4.7), by comparing the peak area of m/z 874.5 before and after oxidation (Figures 4.8-c and 4.8-d). Meanwhile, the amount of the oxidized LLIYDASNLETGVPSR was calculated to be 1.28 pmol, based on the area integration of electric current peak observed from peptide oxidation (Figure 4.8-f). Therefore, the measured amount of LLIYDASNLETGVPSR was 15.7 pmol (triplicate average: 15.0 pmol). Compared to the theoretical amount (20.4 pmol) of this surrogate peptide, the measurement error was -26.4%. The error is relatively bigger as those shown above for other proteins, probably due to the large size of this antibody

which may lead to difficulty in its digestion. Indeed, sample loss up to 32% during antibody digestion was reported before.⁴⁰ Other possible contributing factors affecting the digestion efficiency are the low antibody concentration, multiple preparation and digestion steps, artificial degradations, and rich disulfide bonds structure, *etc.*^{182,194–197} A possible solution to alleviate the sample losses could be the use of combined enzymes such as Lys-C and trypsin to increase digestion efficiency. Nevertheless, the CMS method has demonstrated its capability to absolute quantitation of large biomolecules and potential practical utility in drug development. Although quantitation of mainly pure protein samples were demonstrated in this study, our CMS method is expected to be applicable for quantifying proteins in mixture as it allows selective electrochemical oxidation of tyrosine-containing surrogate peptides.²³ Such an experiment is under way.

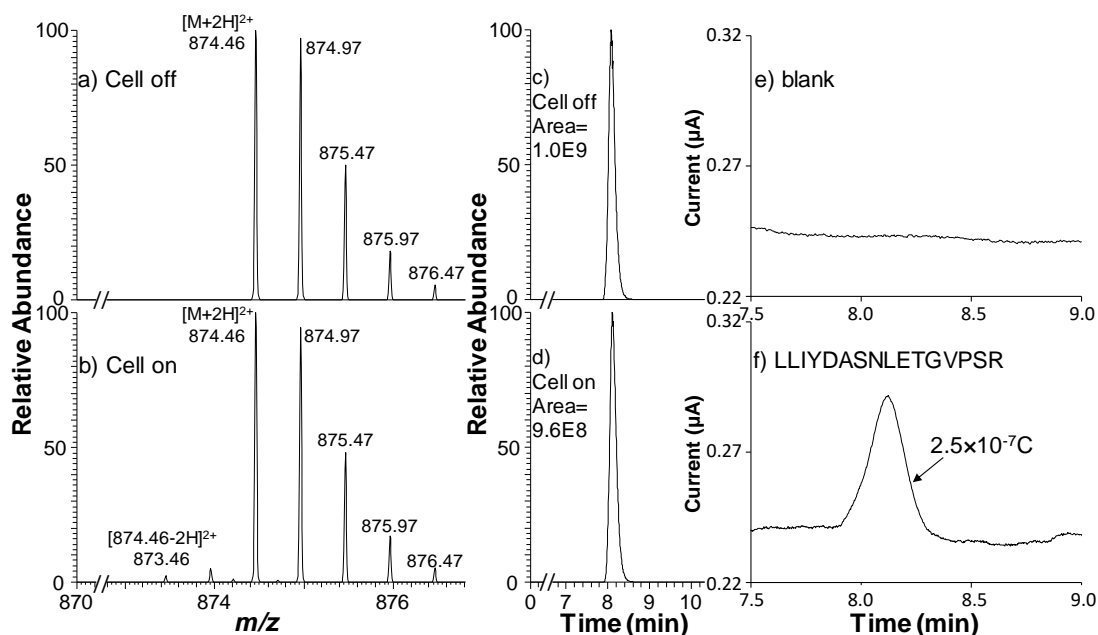


Figure 4.8 ESI-MS spectra of LLIYDASNLETGVPSR from the IgG2 tryptic digest when the applied potential was a) 0 V and b) +1.05 V. The peak of the oxidation product was seen at m/z 873.46 in b). EIC of LLIYDASNLETGVPSR was recorded when the applied potential was c) 0 V and d) +1.05 V. Electric current responses were due to the oxidation of e) the blank solvent and f) LLIYDASNLETGVPSR.

Table 4.7 Electric Current and MS Data for Digested IgG2 (the Selected Surrogate Peptide: LLIYDASNLETGVPSR)

	Q (μ A.min)	Q (C)	Amount of the oxidized analyte (pmol)	Oxidation yield	Measured amount (pmol)	Averaged amount (pmol)	Theoretical amount (pmol)	Measurement error
LLIYDASNLETGVPSR	4.36E-03	2.62E-07	1.355440415	0.092871476	14.59479776	15.0 \pm 0.6	20.4	-26.4%
	4.12E-03	2.47E-07	1.280829016	0.081836381	15.65109544			
	3.99E-03	2.39E-07	1.240414508	0.084028980	14.76174665			
			EIC peak area of m/z 874.46 before electrolysis	EIC peak area of m/z 874.46 after electrolysis	Corrected EIC peak area of m/z 874.46	Oxidation yield		
			1006918882	920117747	913404839	0.092871476		
			1036441991	958336237	951623329	0.081836381		
			1048967089	967536363	960823455	0.084028980		

4.4 Conclusions

In this study, we demonstrated the proof-of-concept of using coulometric mass spectrometry approach to quantify proteolytic surrogate peptides with the aim of quantifying proteins. Several proteins were successfully quantified by using this CMS method, after digestion. The results measured by CMS were very comparable to the results by isotope-labeling method. The advantage of this method is that neither standard peptide nor isotope-labeled peptide is in need for absolute protein quantitation. Our CMS experiment is virtually a typical bottom-up LC/MS proteomics experiment. With only addition of an EC component, quantitative information of proteins can be obtained, showing the power of our CMS method. It is also fast as no standard curve needs to be obtained for quantitation. Redundancy experiment for simultaneous quantifying two peptides from one protein digest is possible. Future work will be focused on applying CMS method for real-world applications in absolute protein quantitation of biological samples.

CHAPTER 5

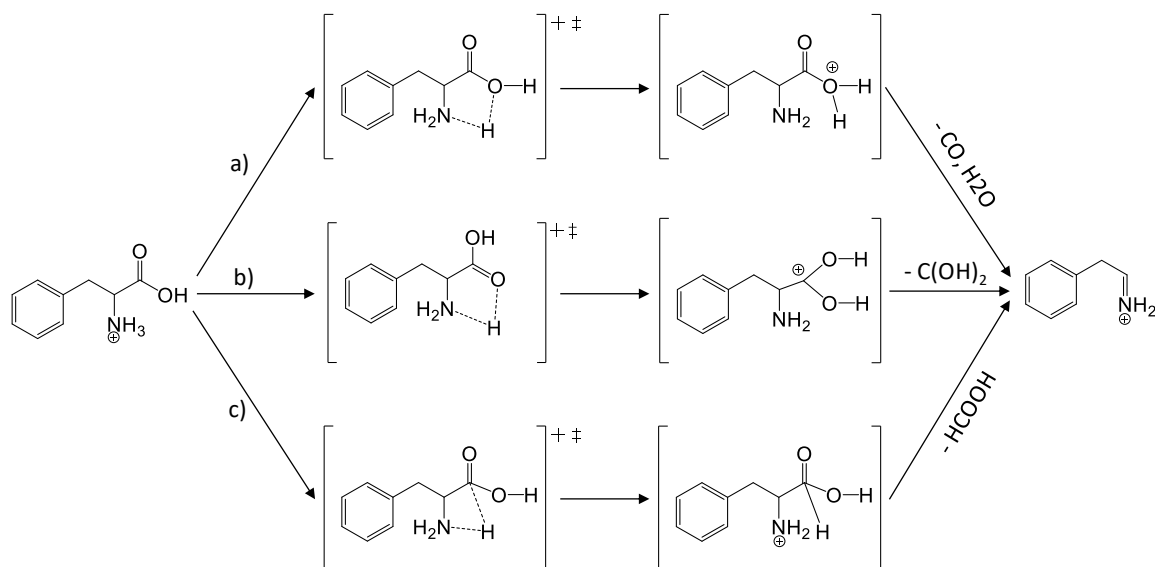
STRUCTURAL ELUCIDATION USING ATMOSPHERIC PRESSURE THERMAL DISSOCIATION MASS SPECTROMETRY

Adapted from Zhao, P.; White, T.; Graham Cooks, R.; Chen, Q.; Liu, Y.; Chen, H. *J. Am. Soc. Mass Spectrom.* **2018**, 29 (12), 2317–2326. Copyright 2018, American Chemistry Society.

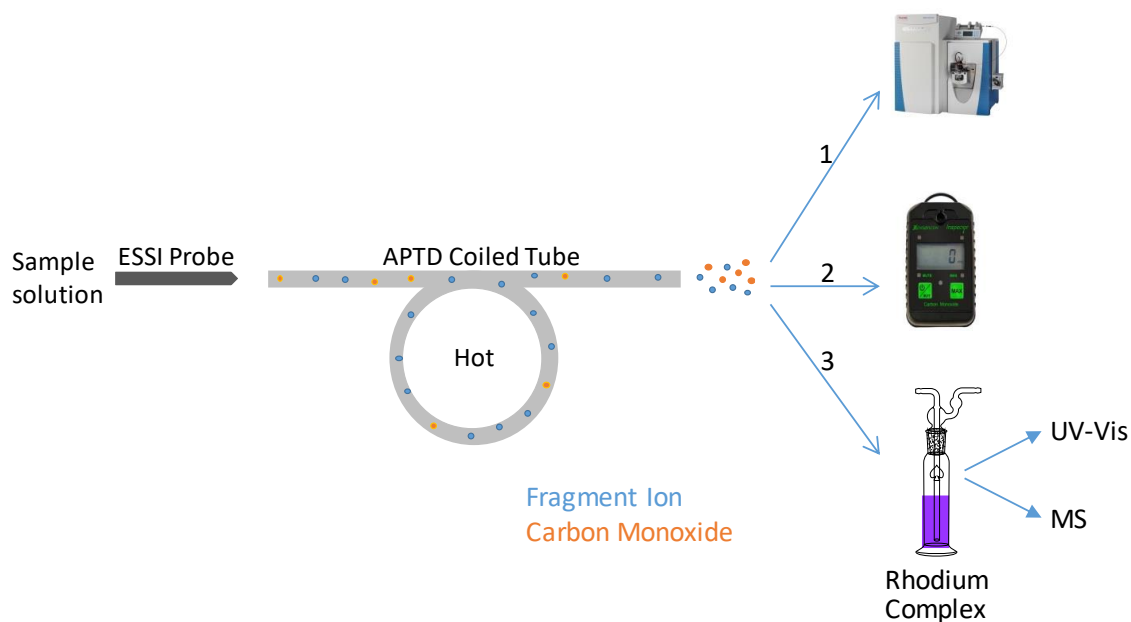
5.1 Introduction

Ionic dissociation is the usual basis for structural analysis by MS.^{198–205} However, a significant limitation is that only charged fragments from ion dissociation events are detected while neutral fragments are simply lost. Researchers began to pay attention to the ‘lost’ neutral fragments several decades ago. Analysis of neutral species by mass spectrometric techniques became possible when neutralization-reionization mass spectrometry (NRMS)^{206–208} and neutral fragment reionization (NfR)²⁰⁹ were introduced, based on reionization of the resulting neutrals by collision with another target (e.g., O₂) via electron transfer or charge stripping. However, although this type of technique is very powerful, it requires specialized instrumentation and it is implemented in vacuum, which limits its utility. Recently we reported our efforts to solve this problem by developing atmospheric pressure neutral reionization mass spectrometry (APNR).^{210–214} In APNR, analyte ions are thermally dissociated using atmospheric pressure thermal dissociation (APTD) followed by online ambient reionization using electrosonic spray ionization (ESSI) or corona discharge. In this study, we report that neutral CO species lost during fragmentation can be characterized by several techniques including online CO sensor and reionization MS monitoring, and offline UV-Vis or MS detection following complexation with a binuclear rhodium complex. Detection of CO is significant as CO was proposed to

be produced from two important ion dissociation pathways: the dissociation of protonated amino acids to form iminium ions (loss of 46 Da) and the conversion from peptide *b* ions to *a* ions (loss of 28 Da).



Scheme 5.1 Three proposed amino acid fragmentation pathways toward the formation of iminium ion (illustrated using phenylalanine as an example): a) losses of CO and H₂O molecules, b) loss of dihydroxycarbene C(OH)₂, and c) loss of formic acid HCOOH.



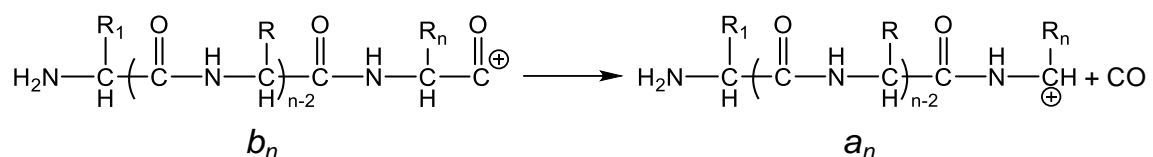
Scheme 5.2 Schematic drawing of the APTD apparatus and processes: 1) direct detection of ionic fragments from the APTD coiled tube by MS, 2) use of CO sensor to directly detect carbon monoxide emerging from the APTD coiled tube and 3) use a binuclear rhodium complex solution to trap CO molecules followed with offline characterization by MS and/or UV/Vis.

Although gas-phase ion dissociation of protonated amino acids has been extensively studied under a variety of ionization conditions and methods,^{215–224} the mechanism for the formation of iminium ion during amino acid or peptide ion dissociation^{225–227} has been the subject of debate. Three main mechanisms have been previously proposed in different studies (see Scheme 5.1): a) losses of H₂O and CO; b) loss of dihydroxycarbene, :C(OH)₂ and c) loss of formic acid, HCOOH.²²⁸ However, none of these studies have given unambiguous experimental evidence regarding the structure of the lost neutrals. In the report by Harrison *et al.*, which proposed pathway **a** (Scheme 5.1), the authors demonstrated that the reaction was analogous to the retro-Koch reaction and required a translocation of the proton from nitrogen to the OH group with a subsequent loss of CO and H₂O.²²⁴ Pathway **b** (Scheme 5.1), proposed to produce C(OH)₂, was

supported by Kulik and coworkers via metastable ion and collisional activation fast atom bombardment (FAB) technique.²²⁹ Unfortunately, the result showed no evidence for an intact C(OH)₂ neutral product. Pathway c (Scheme 5.1) was proposed by Meot-Ner and Field, and formic acid was suggested to be produced. However, this mechanism requiring a four-centered transition state was expected to be thermodynamically unfavorable.²³⁰ Later, O'Hair and coworkers explored this ion dissociation mechanism through a computational study. Based on *ab initio* and density functional theory calculations, the losses of CO and H₂O neutrals were shown to be both thermodynamically and kinetically favored over the alternative HCOOH or :C(OH)₂ fragmentation process.²²⁸ Furthermore, the unimolecular chemistry of protonated amino acids was also explored in detail by Wesdemiotis *et al.*¹⁹⁸ However, direct characterization of CO neutral resulting from amino acid ion dissociation has not previously been achieved and that is the focus of the current study.

In this paper, we applied the APTD technique to dissociate protonated amino acids such as +1 ion of phenylalanine, generated by electrosonic spray ionization (ESSI, a soft ionization method similar to electrospray ionization²³¹), to generate both ionic and neutral fragments at atmospheric pressure. As APTD operates outside the mass spectrometer rather than in vacuum, it should be possible to access the neutrals and characterize them. As shown in Scheme 5.2, an amino acid (e.g., phenylalanine) was sprayed by ESSI into a coiled and heated tube outside the mass spectrometer where it underwent thermal dissociation to produce fragment ions and neutrals. The coiled shape increases gas turbulence, facilitating ion dissociation. Our results showed that neither formic acid (HCOOH) nor dihydroxycarbene C(OH)₂ was detected during APTD of phenylalanine. On

the other hand, CO was successfully detected in the process. This study provides direct evidence to support the production of carbon monoxide in the process for the formation of iminium ion from amino acid ion dissociation. In addition, upon ion activation such as collision-induced dissociation (CID), *b* ions are often produced as a result of peptide amide backbone cleavage. It is also well accepted that *a* ions are generated from *b* ions via further dissociation by loss of CO (Scheme 5.3).^{232–235} However, CO was not characterized previously in this ion dissociation process. This experiment also was attempted to provide evidence for this widely accepted assumption.



Scheme 5.3 Scheme showing dissociation from peptide *b* ion to *a* ion by the loss of neutral CO. Note that *a* and *b* ions are drawn in the way shown in their original definitions; their true structures may well be cyclic.^{236–239}

5.2 Experiments

5.2.1 Chemicals

Phenylalanine, leucine, histidine, tryptophan, ¹³C-labelled phenylalanine, phenylethylamine, and rhodium acetate dimer were purchased from Sigma-Aldrich (St. Louis, MO). Gly-His-Gly and Gly-Trp-Gly peptides were bought from MP Biomedicals, LLC (Solon, OH) and Chem-Impex Int'l Inc., (Wood Dale, IL), respectively. HPLC-grade acetonitrile was purchased from Fisher Scientific (Hampton, NH). Acetic anhydride was purchased from Spectrum Chemical (New Brunswick, NJ). Ammonium hydroxide was purchased from GFS Chemicals (Powell, OH). Deionized water for sample preparation was

obtained from a Nanopure Diamond Barnstead purification system (Barnstead International, Dubuque, IA).

5.2.2 Instrumentation

The APTD device was home-made, as a one-loop stainless steel tube (3.2 mm o.d., 1.6 mm i.d., 20 cm length, and 2.5 cm loop diameter) wrapped by heating tape.²¹⁴ Either a LCQ DECA XP MAX (Thermo Finnigan, San Jose, CA) or a Thermo Fisher Orbitrap QE Plus mass spectrometer (San Jose, CA) was used to analyze the APTD-produced ions. A 90 V voltage was applied to the heating tape and the stainless-steel tube was heated to 300 °C. The temperature of the APTD tube was measured using an infrared thermometer (Tenma, Taiwan). The sample solution (typically, 0.25 mM) was sprayed from an ESSI source operated at the flow rate of 10 μ L/min with the assistance of + 5 kV voltage and 170 psi nebulizing N₂ gas.

5.2.3 Synthesis of Binuclear Rhodium Complex cis-[Rh₂(C₆H₄PPH₂)₂(O₂CCH₃)₂](HOAc)₂

The synthesis followed a reported procedure.²⁴⁰ A 100 mg quantity of rhodium acetate dimer Rh₂(O₂CCH₃)₄, and 150 mg of triphenylphosphine were added into 10 mL of acetic acid in a flask under a nitrogen gas atmosphere. The mixture solution was refluxed for 2 h during which the blue coloration was replaced by red-brown, and then a dark purple color. The solution was concentrated to half of its initial volume and the purple solid deposit was filtered off and washed by ACN. The ¹H-NMR for this compound was δ 1.17 (s, [O₂CCH₃], 6H), 2.15 (s, CH₃COOH, 6H), 6.4-7.7 (m, [(C₆H₅)₂P(C₆H₄)], 28H) (Signal of CH₃COOH was not observed due to proximity to Rh).

5.2.4 MS Analysis of Carbon Monoxide Trapped by Binuclear Rhodium Complex Solution

A 25 mM phenylalanine in ACN/H₂O/HOAc solution was sprayed by an ESSI source and dissociated in the APTD tube and the species flowing out of the tube was then directed into a trap containing 5 mL of 3 mM dinuclear rhodium complex solution in chloroform for 3 min. The amino acid sample injection flow rate was 10 μ L/min and the nebulizing gas pressure used was 100 psi. After trapping, the solution was diluted by ACN with 0.1% HOAc (1:1 dilution), and then subject to ESI-MS analysis. The ESI-MS spectra were collected by using a Thermo Fisher Orbitrap QE Plus mass spectrometer (San Jose, CA) in the positive ion mode.

5.2.5 UV-Vis Analysis of Carbon Monoxide Trapped by Binuclear Rhodium Complex Solution

The dinuclear rhodium complex solution (3 mL, 1 mM) was used to capture the carbon monoxide from the phenylalanine APTD dissociation. The trapping period was 3 min for each sample. The amino acid sample injection flow rate for APTD was 10 μ L/min and the nebulizing gas pressure used was 100 psi. The UV spectra were collected by using an Agilent 8453 UV-visible spectrophotometer (Santa Clara, CA).

5.3 Results and Discussion

The dissociation of the amino acid phenylalanine (Phe) by APTD was first investigated at several different temperatures (Figure 5.1). At relatively low temperature (45 °C, APTD coiled tube temperature), the [Phe+H]⁺ peak (m/z 166) was dominant, which meant that most of [Phe+H]⁺ had not dissociated at this temperature. Only a small peak at m/z 120 was seen, corresponding to the iminium ion [Phe+H-CO₂H₂]⁺ from dissociation of

[Phe+H]⁺ via loss of a neutral(s) with chemical formula CO₂H₂ (total mass 46 Da). When the temperature was increased, the intensity of [Phe+H-CO₂H₂]⁺ peak (*m/z* 120) increased as well. At 300 °C, the [Phe+H-CO₂H₂]⁺ peak (*m/z* 120) was abundant and the [Phe+H]⁺ peak (*m/z* 166) had disappeared from the spectrum. As expected, when phenylalanine was replaced by ¹³C-labeled phenylalanine sample, a major fragment ion [¹³C-Phe+H-¹³CO₂H₂]⁺ (*m/z* 120) was also observed, resulting from dissociation of [¹³C-Phe+H]⁺ via loss of a neutral(s) with chemical formula ¹³CO₂H₂ (total mass 47 Da, Figure 5.2). Indeed, in this ion dissociation experiment, although the fragment ion of *m/z* 120 was observed, the corresponding neutrals were not detected, and they could be either CO+H₂O, HCOOH or carbene :C(OH)₂.

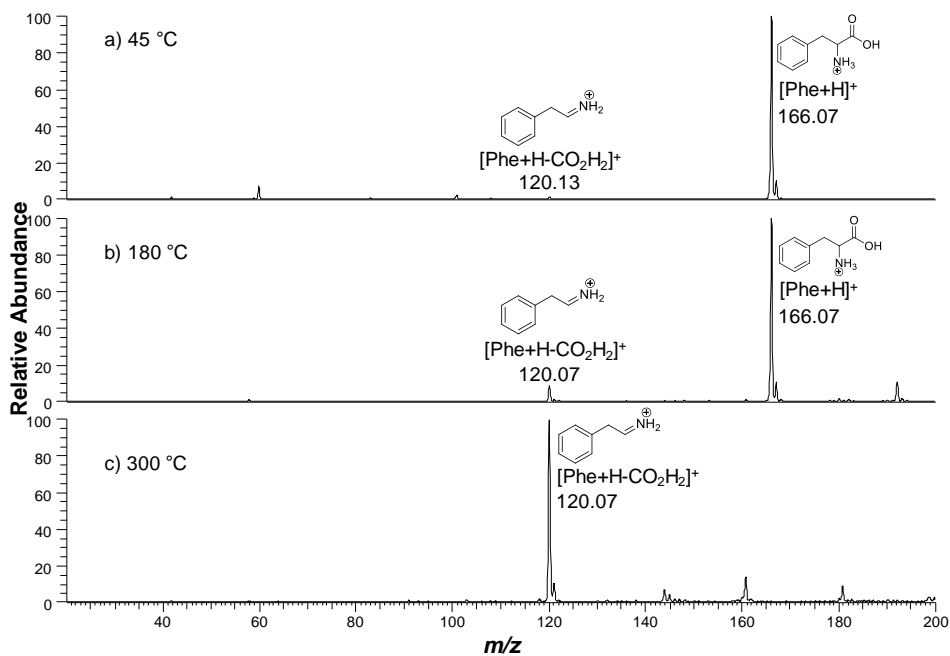


Figure 5.1 APTD–MS spectra for phenylalanine at a) 45 °C, b) 180 °C, and c) 300 °C. Phenylalanine solution in ACN/H₂O/HOAc (0.25 mM; 50:50:0.1 by volume) was sprayed by ESSI (spray voltage: +5 kV) into a hot coiled tube at a flow rate of 10 μL/min.

A ^{13}C -labeled phenylalanine sample was dissociated and monitored via the APTD-MS process. With the increased temperature of the APTD tube, the intensity of m/z 120, corresponding to the fragment ion $[\text{}^{13}\text{C-Phe-}^{13}\text{COOH}]^+$, increased significantly.

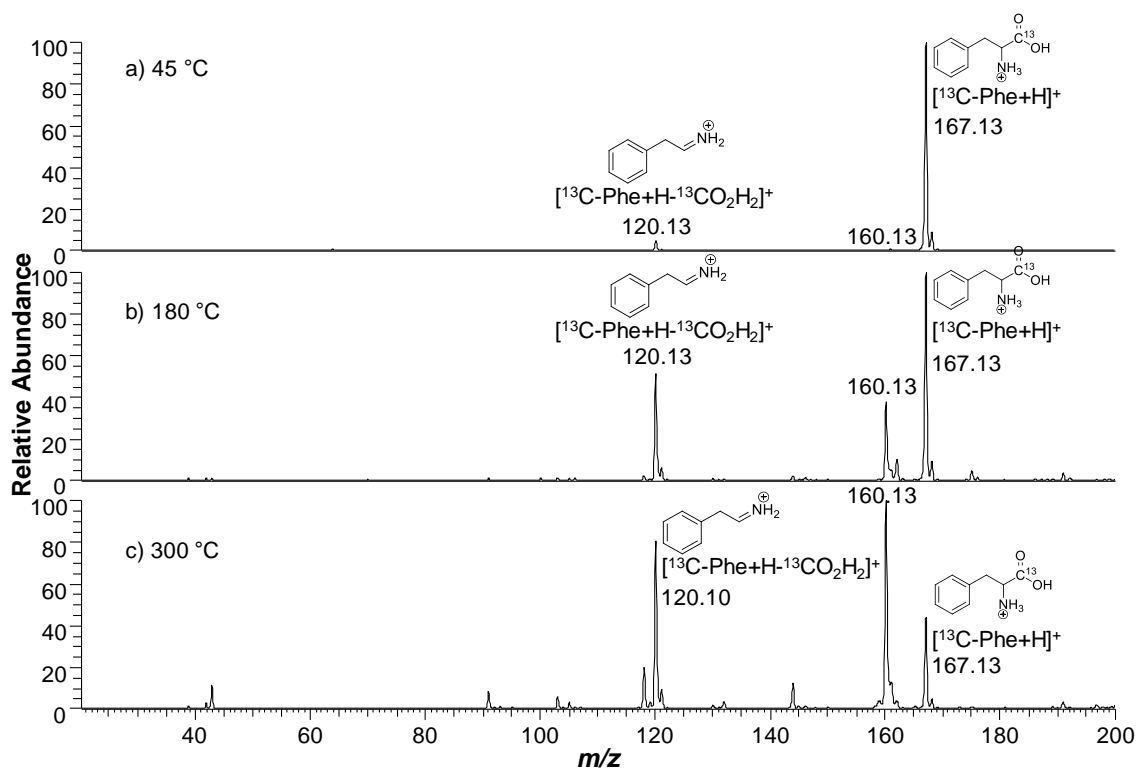


Figure 5.2 APTD–MS spectra for ^{13}C -phenylalanine at a) 45 °C, b) 180 °C, c) 300 °C. 0.25 mM ^{13}C -phenylalanine solution in ACN/H₂O/HOAc (50:50:0.1) was sprayed into the APTD tube by ESSI (spray voltage +5 kV) at a flow rate of 10 $\mu\text{L}/\text{min}$.

Loss of a neutral fragment(s) with mass 46 Da from $[\text{Phe+H}]^+$ (m/z 166) yielded the fragment ion $[\text{Phe+H-CO}_2\text{H}_2]^+$ (m/z 120) upon APTD of phenylalanine at 300 °C. O’Hair *et al.*²²⁸ proposed that protonated aliphatic amino acids could lose neutral H₂O and CO (the combined mass is 46 Da) upon fragmentation in the gas phase, based on computation. Previously established methods for carbon monoxide detection include gas chromatography,²⁴¹ carboxy-myoglobin (Mb-CO) assay,^{242,243} electrochemical

assays,^{244,245} colorimetric CO sensing,^{246,247} and laser infrared absorption methods.²⁴⁸ In this study, a Sensorcon carbon monoxide detector, a household product for monitoring the presence of CO due to safety concerns, was used to detect CO generated in the amino acid APTD process. The detection mechanism of the CO sensor is that CO is oxidized on a platinum working electrode. The current generated from the electrochemical reaction gives a measure of the concentration of CO in the atmosphere.²⁴⁹⁻²⁵¹ In this experiment, the CO detector was held about 1 cm from the outlet of APTD tube. All the blank solvents and samples were measured in triplicates (Figure 5.3). While CO was not detected by the sensor from APTD of the blank solvent (Figure 5.3-1), phenylalanine sample did show a positive reading from CO detector (15 ppm on average, Figure 5.3-3). In addition, phenethylamine, structurally similar to phenylalanine except for the absence of a carboxylic acid group, was also sprayed by ESSI and underwent dissociation in APTD tube. As expected, no CO was detected by the sensor reading (Figure 5.3-2). As phenethylamine and phenylalanine only differ in a terminal carboxylic group, the CO sensor detection result strongly suggested that CO was produced from the loss of the carboxylic group of phenylalanine.


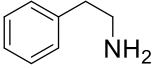

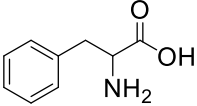

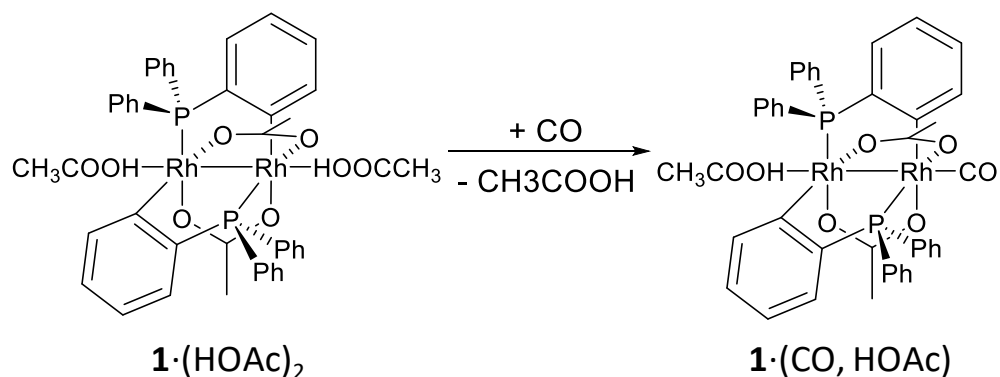
#	Structure	Triplicated Trials	Avg. Readings (ppm)
1	blank solvent		0
2			0
3			15

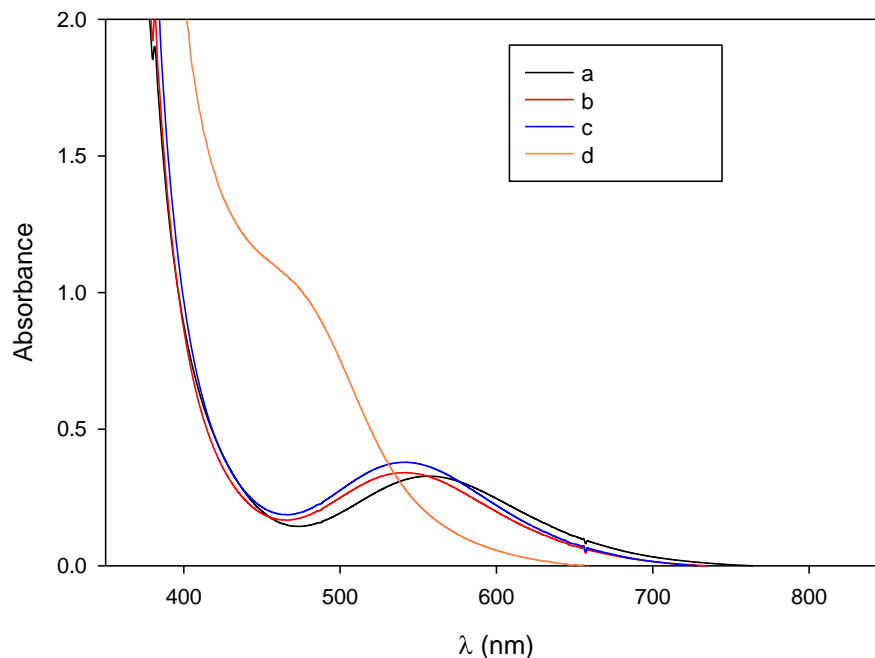
Figure 5.3 Measurements of carbon monoxide produced from APTD of 1) ACN/H₂O/HOAc (50:50:0.1) blank solvent, 2) 25 mM phenethylamine in ACN/H₂O/HOAc (50:50:0.1), 3) 25 mM phenylalanine in ACN/H₂O/HOAc (50:50:0.1). All of measurements were made in triplicate as shown.

In order to more thoroughly examine our hypothesis, a binuclear rhodium complex *cis*-[Rh₂(C₆H₄PPh₂)₂(O₂CCH₃)₂](HOAc)₂, **1**.(HOAc)₂, was chosen to trap the APTD-generated carbon monoxide gas, and the resulting complex **1**.(CO, HOAc) was then analyzed by UV-Vis spectroscopy. This binuclear rhodium complex was first synthesized by Cotton *et al.*,²⁴⁰ and further developed into a colorimetric sensing method by Esteban *et al.*^{246,247} The molecule contains two cyclometalated phosphine ligands and two acetic acid molecules attached to the two rhodium atoms. When this binuclear rhodium complex is exposed to carbon monoxide gas, one acetic acid molecule can be replaced by a CO molecule (Scheme 5.4). Upon CO binding, a characteristic UV-Vis absorption peak at 480 nm can be seen. This complex is highly selective to CO, and does not bind other gases like CO₂, N₂, O₂, or Ar.²⁴⁶



Scheme 5.4 Selective binding of CO by the binuclear rhodium complex $\text{1}\cdot(\text{HOAc})_2$. The complex product $\text{1}\cdot(\text{CO}, \text{HOAc})$ forms after CO binding.

In this experiment, the UV-Vis spectrum of the pure dinuclear rhodium complex $\text{1}\cdot(\text{HOAc})_2$ in chloroform (1 mM) was measured first and the absorption at 480 nm was low (line a, Figure 5.4). When 25 mM phenylalanine in ACN/H₂O/HOAc (50:50:0.1) was sprayed into the coiled tube at 300 °C for APTD and the gaseous species flowing out of the APTD tube was bubbled through the trapping solution of dinuclear rhodium complex $\text{1}\cdot(\text{HOAc})_2$ in chloroform (1 mM), the UV-Vis spectrum of the resulting solution showed a pronounced increase in absorption at 480 nm (line d, Figure 5.4). The duration for the CO collection was 3 min. The result indicates the formation of CO during APTD of phenylalanine. Several control experiments were also conducted. When no phenylalanine was in the spray solvent for APTD, no increase in 480 nm absorption was noted (line b, Figure 5.4). Furthermore, when phenylethylamine solution was sprayed for APTD, no change in 480 nm absorption was detected (line c, Figure 5.4). Similar to the CO sensor measurement result mentioned above, these UV-Vis controls showed that CO is formed from APTD of phenylalanine and originates from the carboxylic acid group of the amino acid.



Sample	Abs (557 nm)	Abs (541 nm)	Abs (480 nm)
a	0.32781	0.31407	0.14806
b	0.32571	0.34058	0.18570
c	0.36231	0.37862	0.20637
d	0.18610	0.28450	0.96927

Figure 5.4 UV-Vis spectra of a) 1 mM dinuclear rhodium complex $1 \cdot (\text{HOAc})_2$ in chloroform (black line a), b) 1 mM dinuclear rhodium complex $1 \cdot (\text{HOAc})_2$ in chloroform after trapping gaseous species flowing out of the APTD when a blank solvent ACN/H₂O/HOAc (50:50:0.1) was sprayed into the APTD tube at 300 °C (red line b), c) 1 mM dinuclear rhodium complex $1 \cdot (\text{HOAc})_2$ in chloroform after trapping species flowing out of the APTD when 25 mM phenethylamine in ACN/H₂O/HOAc (50:50:0.1) was sprayed into the APTD tube at 300 °C (blue line c), and d) 1 mM dinuclear rhodium complex $1 \cdot (\text{HOAc})_2$ in chloroform after trapping species flowing out of the APTD when 25 mM phenylalanine in ACN/H₂O/HOAc (50:50:0.1) was sprayed into the APTD tube at 300 °C (orange line d).

MS should be an accurate, sensitive and reliable tool to detect small molecules like carbon monoxide. However, the mass of CO is smaller than the cutoff mass of our mass spectrometers. Therefore, direct online analysis of CO from APTD was not an option in

this case. We reasoned that CO could be detectable after selective trapping with the binuclear rhodium complex. Figure 5.5-a displays the ESI-MS spectrum of 3 mM dinuclear rhodium complex **1**·(HOAc)₂ in chloroform. The peak of *m/z* 786.99 corresponding to the binuclear rhodium complex cation [**1**-OAc]⁺ (theoretical mass 786.9909, observed mass 786.9882, mass error 3.43 ppm), was detected. Notably, when the gaseous species flowing out of the heated tube after APTD of phenylalanine was trapped by the dinuclear rhodium complex **1**·(HOAc)₂, analysis of the rhodium complex revealed a new peak at *m/z* 814.99 (Figure 5.5-d), corresponding to [**1**-OAc+CO]⁺ (theoretical mass 814.9859, observed mass 814.9852, mass error 0.86 ppm). CID of *m/z* 814.99 gave rise to fragment ions at *m/z* 786.99 and 726.97 (Figure 5.6-a), by consecutive losses of CO and HOAc, consistent with its structural assignment. Furthermore, when standard carbon monoxide gas was bubbled into the dinuclear rhodium complex **1**·(HOAc)₂, the adduct ion [**1**-OAc+CO]⁺ (*m/z* 814.99) was also observed (Figure 5.5-e). These results show that APTD of phenylalanine does produce CO. Meanwhile, when only solvent or the structurally similar compound phenethylamine was sprayed for APTD and subsequent trapping by the rhodium complex, no peak at *m/z* 814.99 was detected (Figure 5.5-b and c).

In addition, a ¹³C-labeled phenylalanine sample (the carboxylic carbon is labeled with ¹³C) was subjected to APTD and the rhodium complex trapping, a peak of *m/z* 815.99, corresponding to [**1**-OAc+¹³CO]⁺ (theoretical mass 815.9879, observed mass 815.9883, mass error 0.49 ppm) was detected, as expected (Figure 5.7). CID of *m/z* 815.99 produced fragment ions at *m/z* 786.99 and 726.97 (Figure 5.6-b), by consecutive losses of ¹³CO and HOAc, consistent with its structural assignment. This result supported the hypothesis that APTD of phenylalanine produces CO and the CO stems from the carboxylic group of the

amino acid.

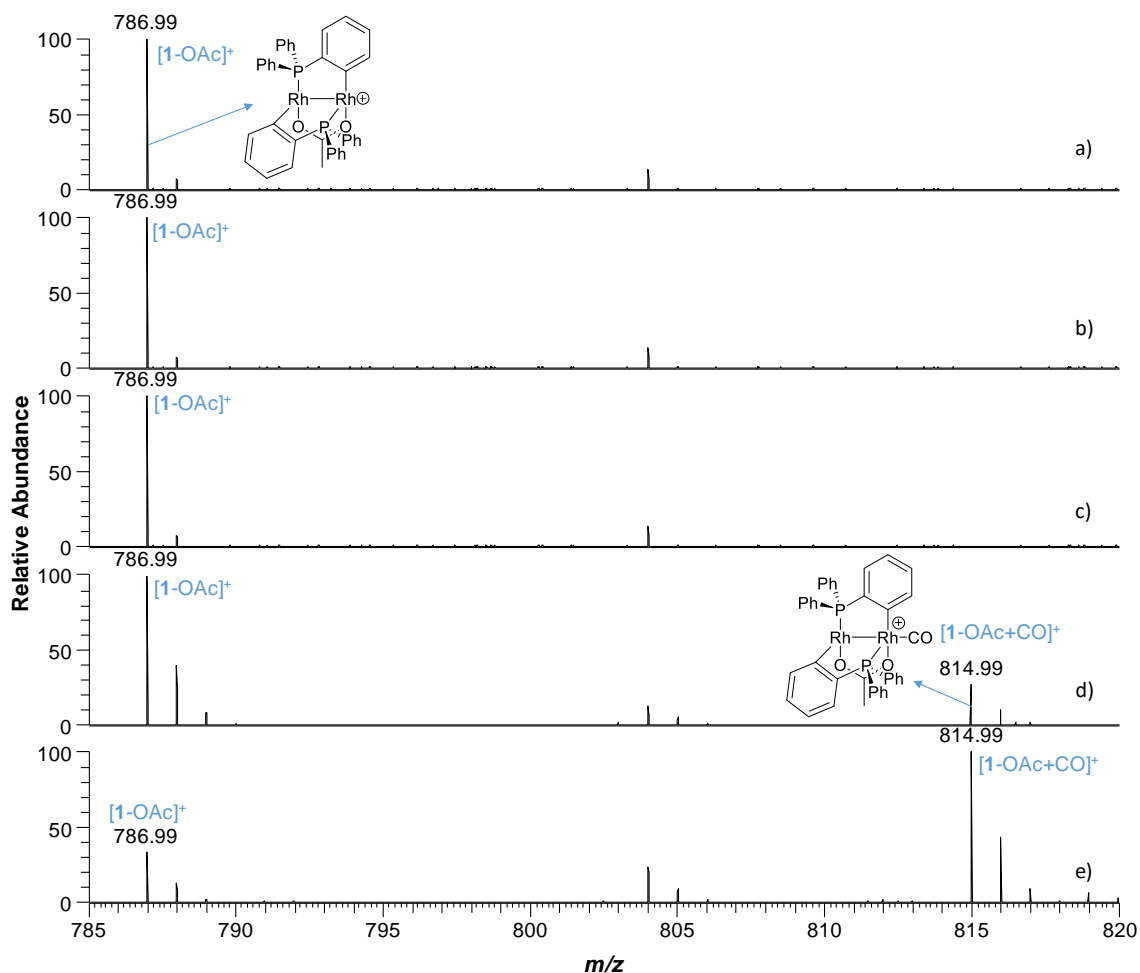


Figure 5.5 ESI-MS spectra of a) 3 mM dinuclear rhodium complex 1·(HOAc)₂ in chloroform, b) 3 mM dinuclear rhodium complex 1·(HOAc)₂ in chloroform after trapping gaseous species flowing out of the APTD tube when a blank solvent of ACN/H₂O/HOAc (50:50:0.1) was sprayed into the APTD tube at 300 °C, c) 3 mM dinuclear rhodium complex 1·(HOAc)₂ in chloroform after trapping gaseous species flowing out of the APTD tube when 25 mM phenethylamine in ACN/H₂O/HOAc (50:50:0.1) was sprayed into the APTD tube at 300 °C, d) 3 mM dinuclear rhodium complex 1·(HOAc)₂ in chloroform after trapping gaseous species flowing out of the APTD tube when 25 mM phenylalanine in ACN/H₂O/HOAc (50:50:0.1) was sprayed into the APTD tube at 300 °C, e) 3 mM dinuclear rhodium complex 1·(HOAc)₂ in chloroform after trapping standard carbon monoxide gas (purity 99.99%) for 3 min.

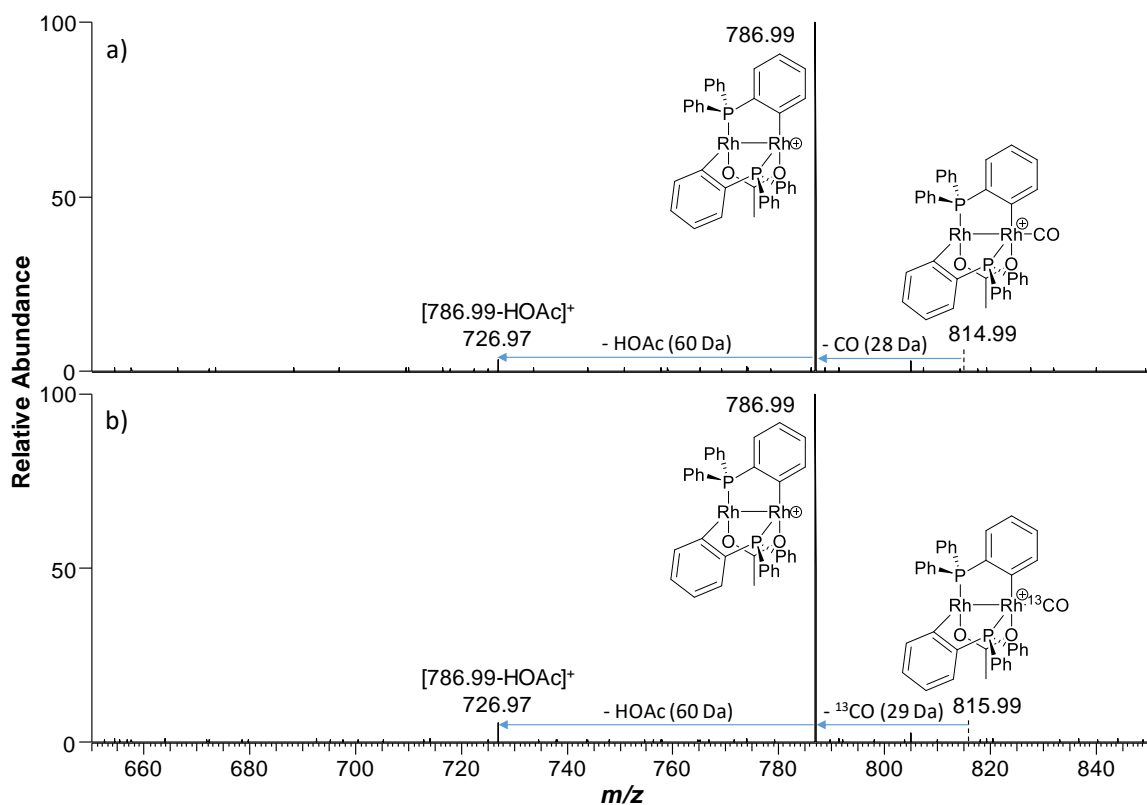


Figure 5.6 CID MS/MS spectra of a) [1-OAc+CO]⁺ (*m/z* 814.99) and b) [1-OAc+¹³C]⁺ (*m/z* 815.99). The HCD energy used for dissociation was 20 eV.

A ¹³C-labeled phenylalanine sample was investigated in this experiment. The peak of [1-OAc+¹³C]⁺ (theoretical mass 815.98790, observed mass 815.98828, mass error 0.46 ppm) was detected, showing loss of CO was from the carboxylic acid group of phenylalanine during the APTD process. Note that there was a small peak of [1-OAc+¹²C]⁺ (*m/z* 814.98) in the spectrum. This might be due to the impurity of the isotopic-labeled phenylalanine.

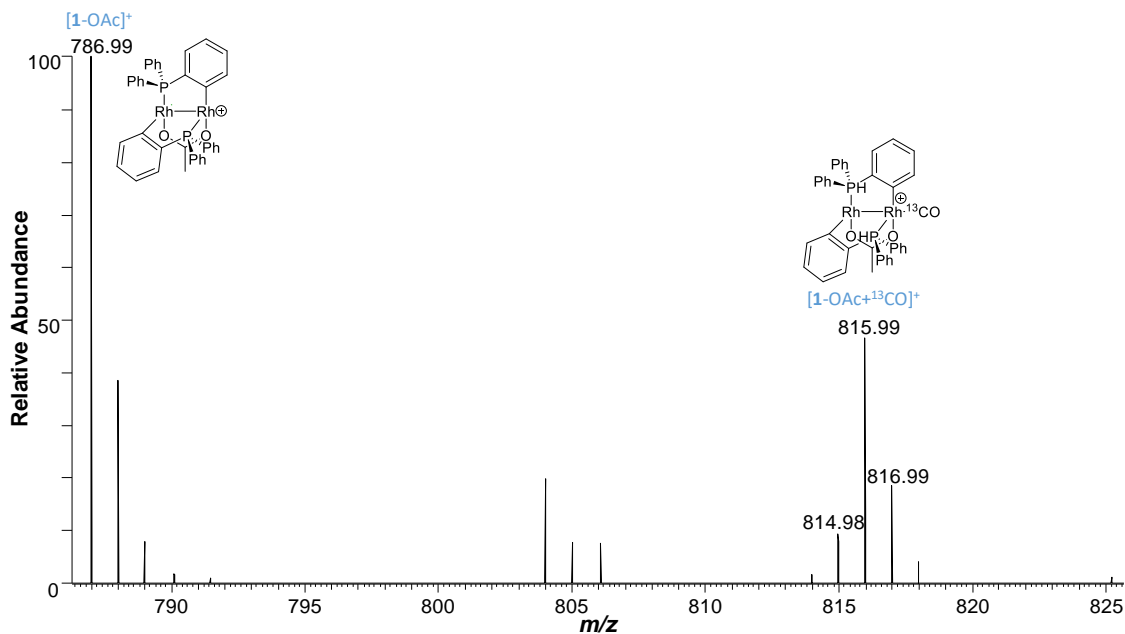


Figure 5.7 ESI-MS spectrum of 3 mM dinuclear rhodium complex **1**·(HOAc)₂ in chloroform after trapping gaseous species from the APTD tube when 25 mM ¹³C-phenylalanine in ACN/H₂O/HOAc (50:50:0.1) was sprayed into the tube for APTD at 300 °C.

At the same time, the possibility of producing dihydroxycarbene :C(OH)₂ (pathway b, Scheme 5.1) was also investigated. Due to the high reactivity of carbene, the dihydroxycarbene would react with water from the spray solvent via insertion into the O-H bond of H₂O,²⁵² and a product peak at *m/z* 65, corresponding to [HC(OH)₃+H]⁺, should be detected by the APTD-MS in the positive ion mode. However, there was no such peak in the acquired MS spectrum, which suggested that dihydroxycarbene was not formed from APTD of phenylalanine (Figure 5.8).

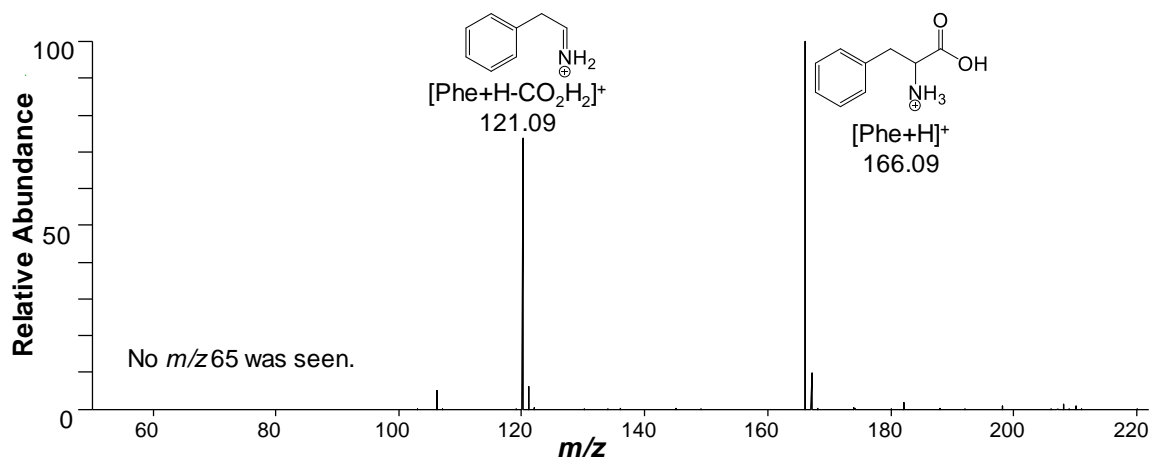
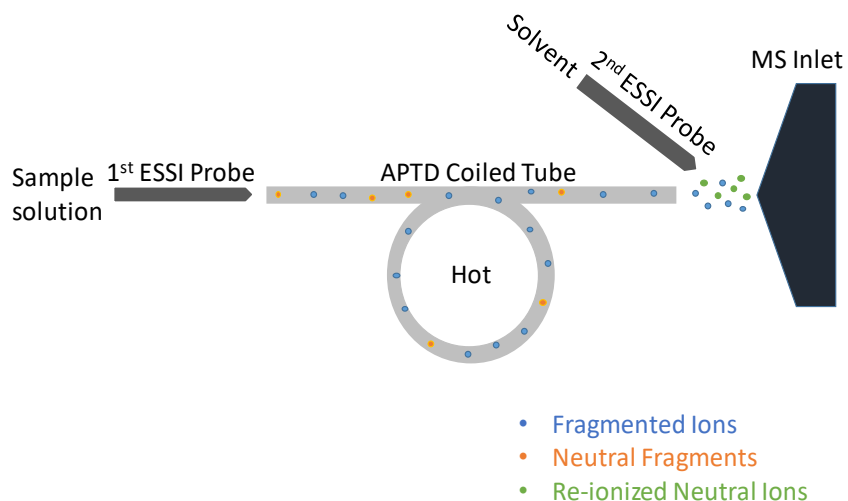


Figure 5.8 APTD-MS spectrum of 0.25 mM phenylalanine in ACN/H₂O/HOAc (50:50:0.1) solution. The sample injection flow rate for ESSI was 10 μ L/min, and + 5 kV voltage was used for ESSI. The temperature of APTD tube was 300 $^{\circ}$ C.

Furthermore, the possibility of producing formic acid (HCOOH) following APTD of the amino acid (pathway c, Scheme 5.1) was also examined. To detect neutral species HCOOH, we reasoned that HCOOH could be re-ionized into formate ion HCOO⁻ (m/z 45) in the negative ion mode, by using the atmospheric pressure neutral re-ionization (APNR) technique.²¹⁴ Thus, in our APTD experiment of phenylalanine, a second ESSI sprayer was added downstream so as to spray solvent ACN/H₂O/ammonia (50:50:0.1). The generated microdroplet could capture neutral species flowing out of the APTD tube and get them ionized. The re-ionized neutrals could be detected by the nearby mass spectrometer (Scheme 5.5). When only solvent ACN/H₂O/HOAc (50:50:0.1) was sprayed into the APTD tube at 300 $^{\circ}$ C, APNR-MS spectrum (Figure 5.9-a) shows a background peak at m/z 45 with intensity of 5.09×10^3 (manufacturer's arbitrary unit of counts). When phenylalanine was added into the solvent for APTD, the peak of m/z 45 did not show a significant increase (peak intensity 5.29×10^3 , Figure 5.9-b). This result suggests that no HCOOH was formed from APTD of phenylalanine.



Scheme 5.5 Schematic showing the process and apparatus used for APNR-MS.

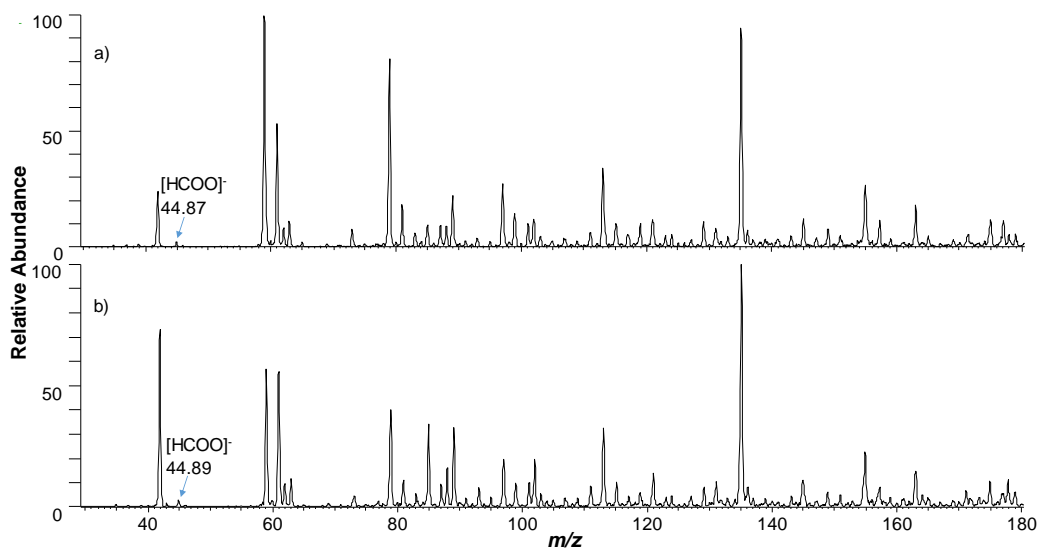


Figure 5.9 APNR-MS spectra for detecting HCOOH from APTD of phenylalanine in the negative ion mode, when a) only solvent ACN/H₂O/HOAc (50:50:0.1) was sprayed into the APTD tube at 300 °C and b) 0.25 mM phenylalanine solution was sprayed into the APTD tube at 300 °C. ACN/H₂O/NH₃·H₂O (50:50:0.1) was sprayed to ionize neutral species flowing out of the APTD tube. The absolute abundances of m/z 45 (referred to formate ion) in a) and in b) were 5.09×10^3 and 5.29×10^3 , respectively. No obvious increase in the m/z 45 signal was observed after phenylalanine was added into the spray sample.

As formic acid HCOOH could decompose into CO and H₂O²⁵³ at elevated temperature, we also performed an experiment to exclude the possibility that the detected CO from APTD of phenylalanine was a HCOOH decomposition product. In a separate experiment, HCOOH was directly sprayed into APTD tube at 300 °C and the gaseous species coming out of the tube was trapped by the dinuclear rhodium complex solution. After trapping and subsequent ESI-MS analysis, no peak was detected at *m/z* 814.99 (Figure 5.10).

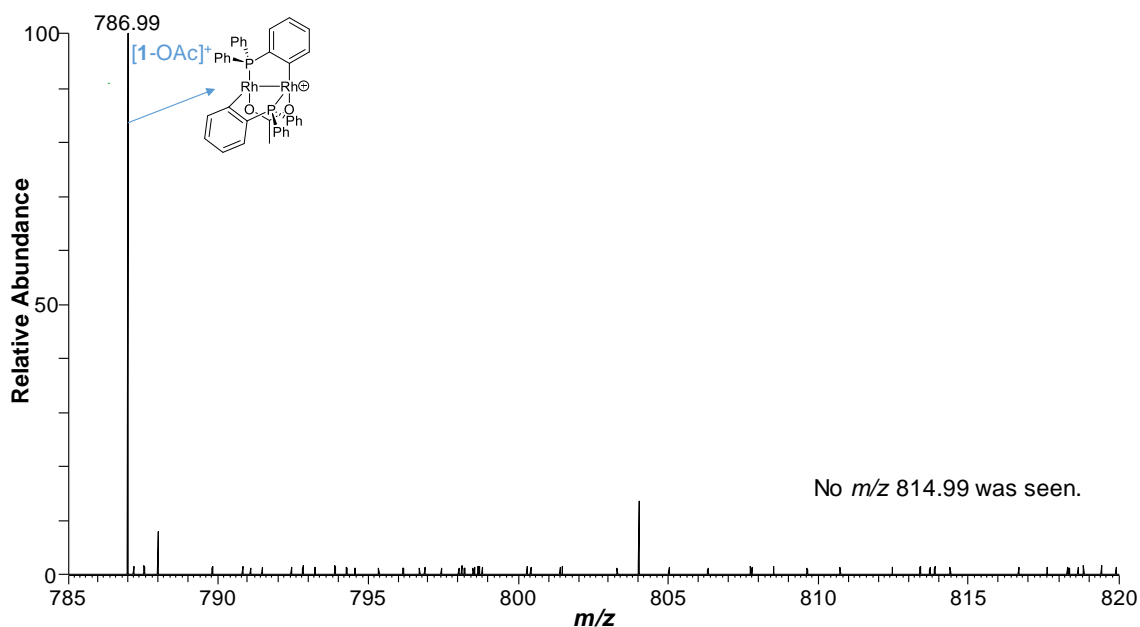


Figure 5.10 ESI-MS spectrum of 3 mM dinuclear rhodium complex **1**·(HOAc)₂ in chloroform after trapping neutral species flowing out of the APTD tube when 25 mM HCOOH in ACN/H₂O/HOAc (50:50:0.1) was sprayed into the tube for APTD at 300 °C.

Other amino acids (leucine, histidine, and tryptophan) were also tested for APTD in our study. The amino acids were dissociated first by APTD and the loss of 46 Da from the protonated amino acid was seen in all cases (Figure 5.11). Then the released neutral CO molecules were trapped by rhodium complex solution and successfully detected by MS

(Figure 5.12). This information further revealed that CO released from the dissociation of protonated amino acid into iminium ion is a quite general pathway.

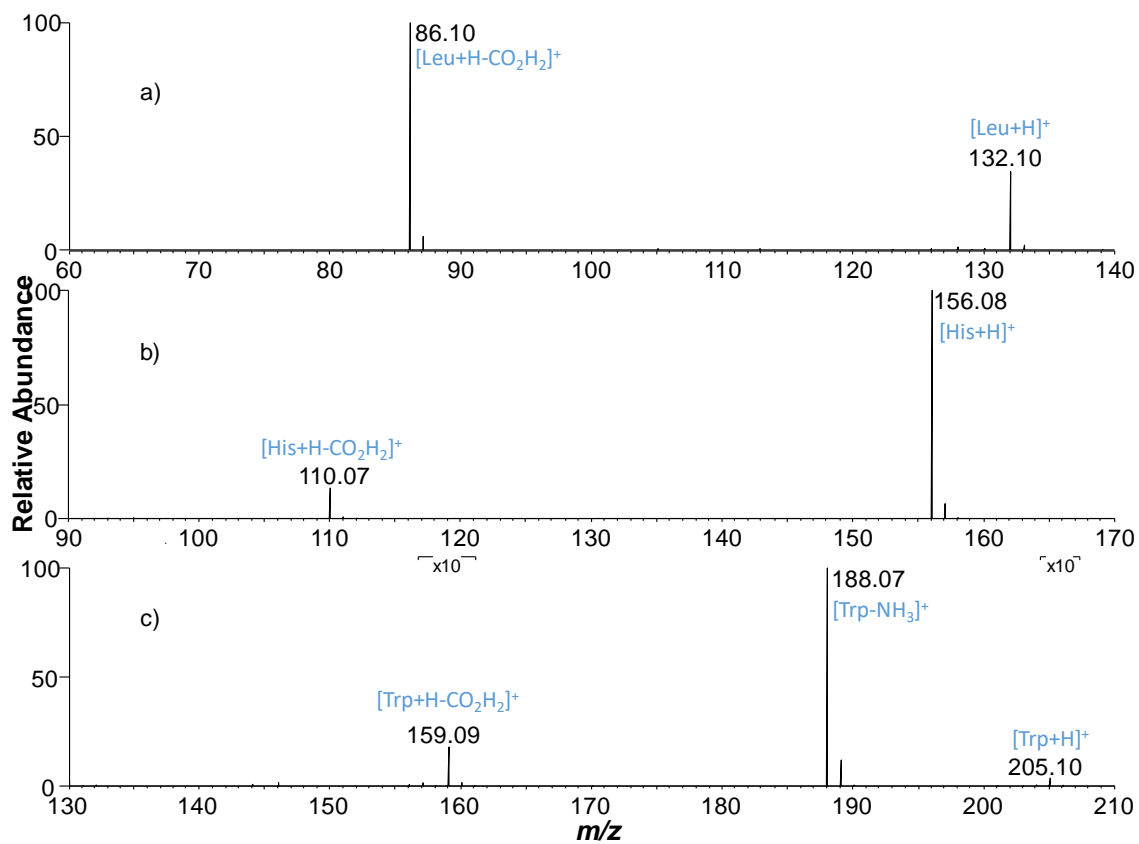


Figure 5.11 APTD-MS spectra of a) leucine, b) histidine, and c) tryptophan. Loss of 46 Da from the protonated amino acid was observed in all cases.

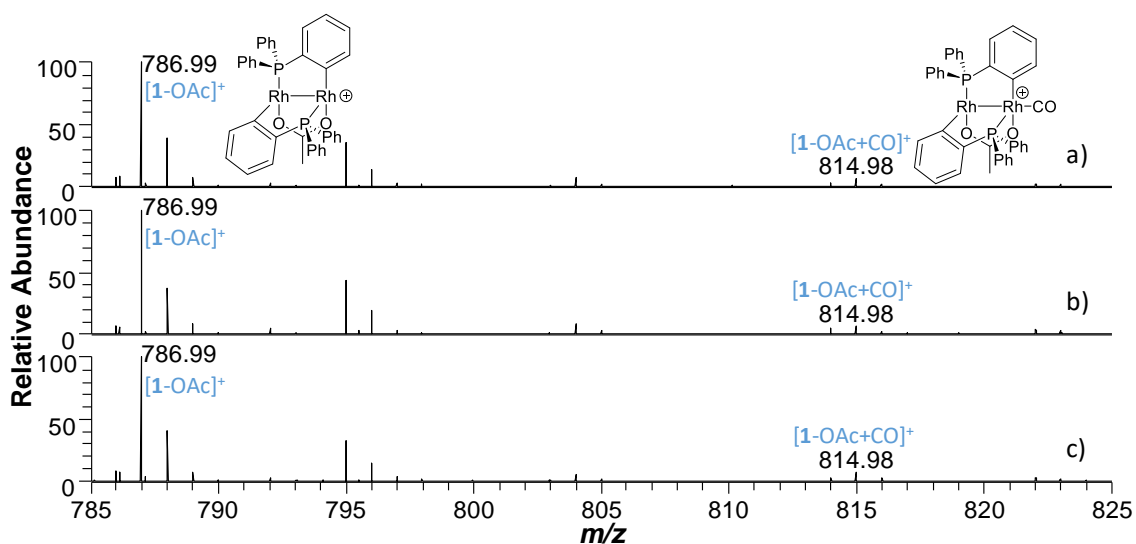


Figure 5.12 ESI-MS spectra of into 3 mM dinuclear rhodium complex **1**·(HOAc)₂ in chloroform after trapping neutral species flowing out of the APTD tube when a) 25 mM leucine, b) 25 mM histidine, and c) 25 mM tryptophan in ACN/H₂O/HOAc (50:50:0.1) was sprayed into the tube for APTD at 300 °C.

The APTD method can also be used to dissociate peptides. Two peptides, Gly-His-Gly (GHG) and Gly-Trp-Gly (GWG), were chosen as test samples in this experiment. Compared to APTD dissociation of amino acids, loss of 46 Da from the two peptide ions was not observed (Figure 5.13). However, both *a* and *b* ions are seen in the two cases. It has been long regarded that *a* ions originate from *b* ion, by facile loss of CO. However, no direct experimental evidence is reported in the literature, to our knowledge. Thus, by simply carrying out trapping of gaseous species from APTD of these two peptides using the dinuclear rhodium complex we were able to detect the characteristic adduct ion [1-OAc+CO]⁺ (*m/z* 814.99, Figure 5.14). This data provides evidence to corroborate the formation of CO during the dissociation of these peptide ions, which is most likely ascribed to the conversion of *b* into *a* ions. Therefore, *a* ions should arise from further dissociation of *b* ions, rather than from direct dissociation of precursor peptide ions, as no CO would

be formed in the latter case. (Note that under some circumstances, direct formation of CO during *a* ion and *y* ion formation is possible,^{254,255} however, this appears not to be the case for the peptides that were examined in this study, as neither [peptide-CO]⁺ or *y*₁ ions was detected during the APTD process (Figure 5.13)).

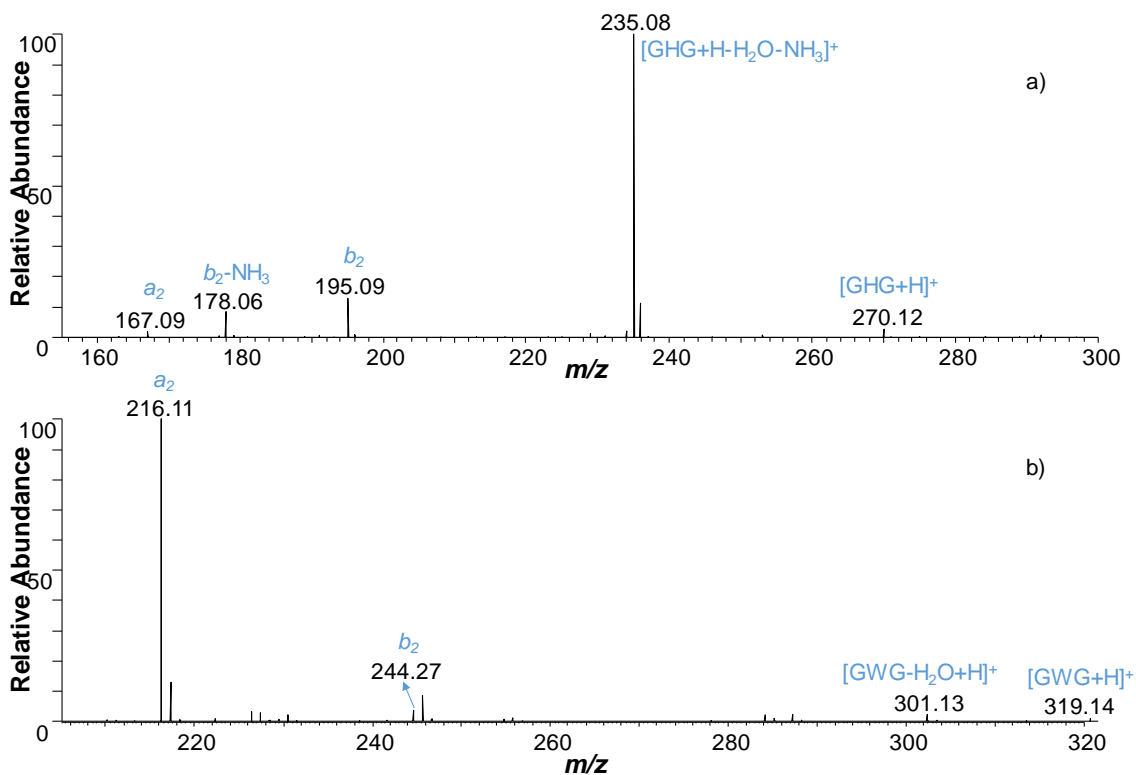


Figure 5.13 APTD-MS spectra of a) 5 mM GHG in ACN/H₂O/HOAc (50:50:0.1); b) 5 mM GWG in ACN/H₂O/HOAc (50:50:0.1). The temperature of the APTD tube was 300 °C.

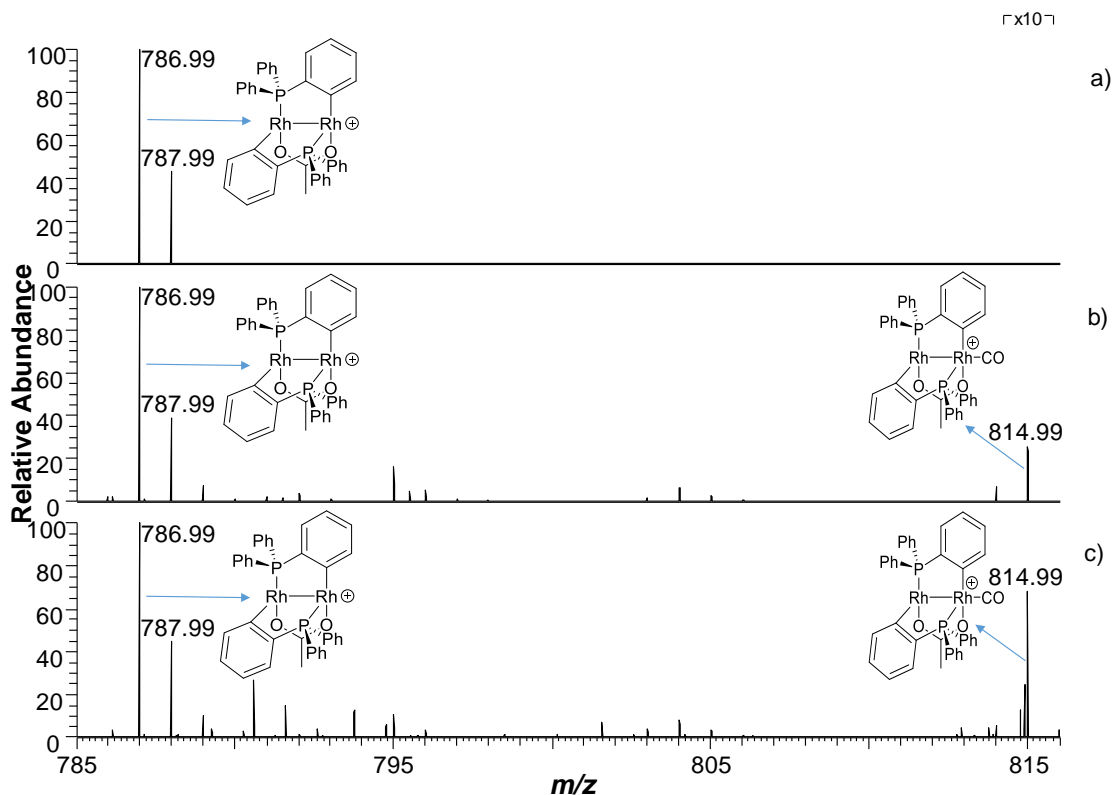





Figure 5.14 ESI-MS spectra of 3 mM dinuclear rhodium complex **1**·(HOAc)₂ solution after trapping neutral species flowing out of the APTD tube when a) ACN/H₂O/HOAc (50:50:0.1), b) 5 mM GHG in ACN/H₂O/HOAc (50:50:0.1) and c) 5 mM GWG in ACN/H₂O/HOAc (50:50:0.1) was sprayed into the tube for APTD at 300 °C.

Furthermore, the approach of CO neutral characterization of this study can be used in a more quantitative manner. A quantitative comparison experiment was run to compare the amount of CO produced from APTD of peptides GHG and GWG. As measured by the CO sensor, the averaged values from APTD of GHG and GWG were 7 ppm and 8.3 ppm, respectively (Table 5.1). The result showed that the dissociation of GWG generated more CO than GHG under the same experimental conditions. Likewise, as shown in the Figures 5.14-b and c, the relative intensity of the adduct ion [**1**-OAc+CO]⁺ at m/z 814.99 (relative to the binuclear rhodium complex cation [**1**-OAc]⁺ at m/z 786.99) was higher in the case

of GWG than that for GHG, which is in line with the CO sensor measurement result. As shown in Figure 5.13, the *a* ion appears to be dominant in the case of GWG upon APTD, therefore, this result also supports the assumption that CO was produced along with generation of the *a* ion for the peptides studied.

Table 5.1 Measurements of Carbon Monoxide Produced from APTD of 1) ACN/H₂O/HOAc (50:50:0.1) Blank Solvent, 2) 5 mM Peptide GHG in ACN/H₂O/HOAc (50:50:0.1), 3) 5 mM Peptide GWG in ACN/H₂O/HOAc (50:50:0.1). The Peptide Sample Solution was Sprayed for APTD from an ESSI Source at the Flow Rate of 10 μ L/min with the Assistance of + 5 kV Voltage and 170 psi Nebulizing N₂ gas. A Potential of 90 V was Applied to the Heating Tape and the APTD Tube was Heated up to 300 °C. All of Measurements were Made in Triplicate as Shown

#	Structure	Triplicated Trials	Avg. Readings (ppm)
1	blank solvent		0
2	GHG		7.0
3	GWG		8.3

5.4 Conclusions

This study demonstrates a new application of APTD in investigating the amino acid and peptide ion dissociation mechanisms, specifically identification of the neutral loss species CO involved in dissociation of protonated amino acid into iminium ion and peptide ion $b \rightarrow a$ conversion. Due to the fact that ion dissociation in APTD occurs at atmospheric

pressure, characterization of neutral species becomes possible, as demonstrated using either online CO sensor or offline spectroscopic/mass spectrometric tools. Our results demonstrate that the fragmentation of protonated amino acids into iminium ions involves losses of CO and H₂O rather than loss of HCOOH or :C(OH)₂. Detection of CO from the tested peptide ions demonstrates that *a* ion is most likely to come from *b* ion dissociation by loss of CO. Our study once again suggests that APTD has utility for structure analysis and elucidation of ion dissociation mechanism. Due to the neutral fragment characterization could provide increased structural information, this method could be used to elucidate complicated ion dissociation mechanisms, such as the investigation of cyclic peptide or glycan ion dissociation behaviors, which could be helpful to cyclic peptide sequencing and glycan structural analysis.

CHAPTER 6

ELECTROSYNTHESIS AND DETECTION OF TRANSIENT INTERMEDIATES IN GOLD-CATALYZED REACTIONS BY MASS SPECTROMETRY

Adapted from Ye, X.; Zhao, P.; Zhang, S.; Zhang, Y.; Wang, Q.; Shan, C.; Wojtas, L.; Guo, H.; Chen, H.; Shi, X. Facilitating Gold Redox Catalysis with Electrochemistry: An Efficient Chemical-Oxidant-Free Approach. *Angew. Chemie Int. Ed.* **2019**, 58 (48), 17226–17230. Copyright 2019 John Wiley & Sons, Inc.

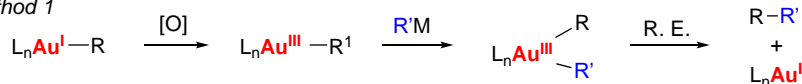
6.1 Introduction

Homogeneous gold catalysis has been flourished during the past two decades.²⁵⁶ As a superior π -acid for C-C multiple bonds activation, Au(I) catalysts have been applied as a powerful tool towards various transformations to build up molecular complexity.²⁵⁷ Gold redox chemistry is also attractive, because it presents an alternative coupling approach.²⁵⁸ However, gold redox chemistry was significantly underexplored, largely due to the high oxidation potential of Au(I)/Au(III) redox couple (+1.40 V).²⁵⁹ More recently, a series of breakthrough discoveries have been reported in this new direction of gold catalysis by applying external oxidants for Au(I)/Au(III) oxidation. Currently, two major strategies in promoting gold redox catalysis are A) strong chemical oxidant, such as hypervalent iodide or Selectfluor, and B) photo/thermo activation of diazonium salts (Scheme 6.1A).^{260,261} Despite these great progresses, there are still severe limitations. First, the involvement of stoichiometric amounts of strong oxidants, which usually are expensive and exhibit poor functional group compatibility, greatly restricts scope of substrates. Second, the photoactivation approach requires the usage of reactive aromatic diazonium salts under strict oxygen-free environment, which presents clear drawbacks to the overall process. Thus, a new efficient strategy to achieve Au(I)/Au(III) redox catalysis is not only highly

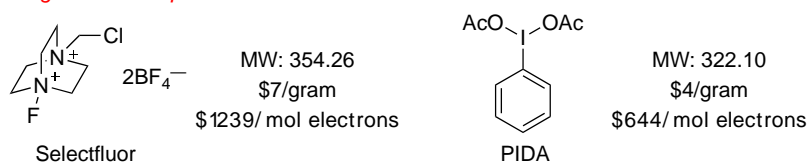
desirable but also crucial for this chemistry to be considered practical for industrial process. Herein, we re-report the first example of electrochemical-promoted gold redox catalysis (Scheme 6.1B). The challenging gold oxidation was facilitated through electrochemical process without requiring any external oxidant, which allowed the overall transformation to occur under mild conditions with high yields and broad scope.

A) Literature reported strategies in promoting gold redox catalysis

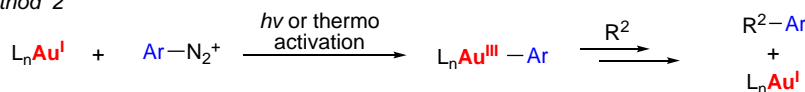
Method 1



Strong oxidants required:

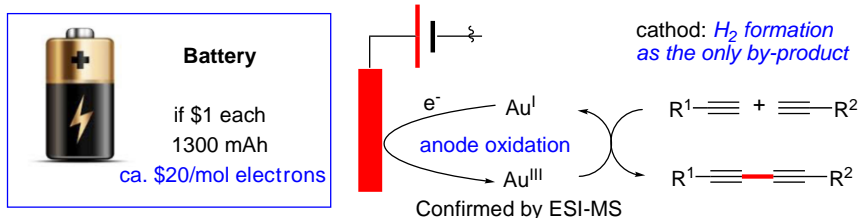


Method 2



Oxidant as part of reaction substrates; Limited reaction scope.

B) This work: Electrochemistry as a *new stratage* in gold redox chemistry



Scheme 6.1 Electrochemical approach for gold-redox catalysis.

Synthetic organic electrochemistry has received tremendous attention over the past several years.²⁶² Compared to traditional redox chemistry, facile oxidation (anode) and/or reduction (cathode) can be achieved under mild conditions without requiring external oxidants/reductants. In particular, electrochemical anodic oxidation is more attractive to the community, since it serves as an environmentally friendly and sustainable alternative

oxidation strategy.²⁶³ Recent works have demonstrated its capability to promote the challenging oxidation of transition metal cations to their higher oxidative states, such as Pd(II)/(IV), Co(II)/(III) oxidation.²⁶⁴ Another advantage of electrochemical oxidation is the feasibility in accessing controllable cell potential (E_{cell}), which allows fine-tuning of transition metal re-dox process for optimal reactivity. Considering these advantages, we set out to explore the possibility of achieving gold redox catalysis under electrochemical conditions in order to overcome the high oxidation potential between Au(I) and Au(III). Notably, until now no success example has been reported using electro-chemical strategy in homogenous gold catalysis. This is likely due to several challenges associated with the process including: 1) reduction of Au(I) catalyst on the cathode as a decomposition pathway; 2) potential side reactions when HOX type solvent (water or alcohol) is involved, such as O-alkenylation and Telly hydration.

6.2 Experiments

6.2.1 Chemicals

Lithium perchlorate (LiClO₄), phenylacetylene, tetrabutylammonium acetate were purchased from Sigma (St. Louis, MO). The reticulated vitreous carbon (RVC) material was obtained from ERG Materials and Aerospace Corp (Oakland, CA). Acetonitrile, methanol, formic acid, and acetic acid were purchased from Fisher Scientific (HPLC grade, Fair Lawn, NJ).

6.2.2 General Procedure for Homo-diyne Coupling

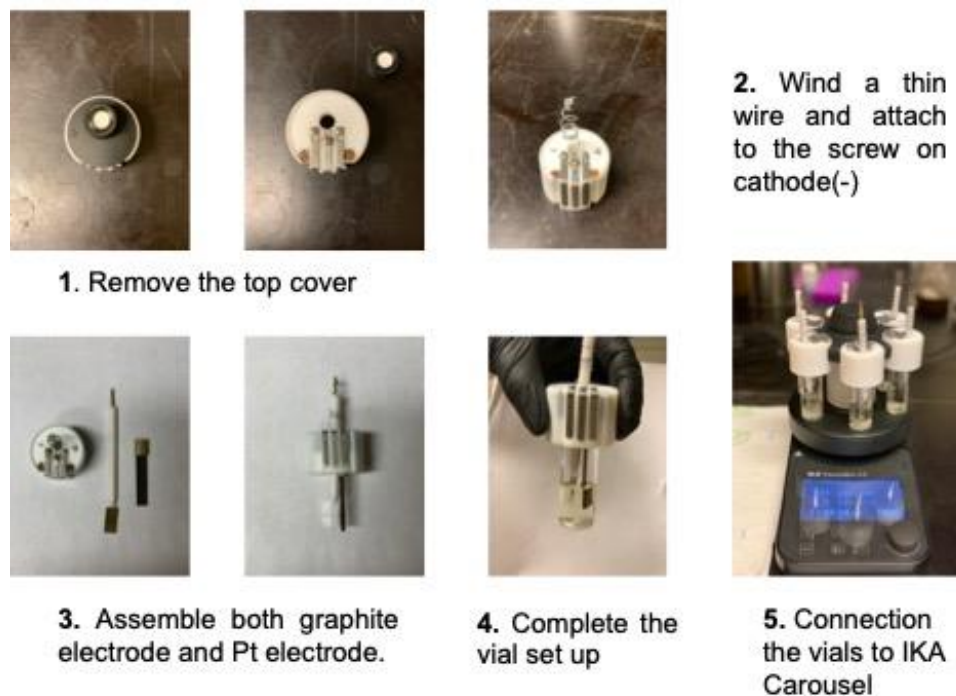
To a 10 mL ElectraSyn screwed vial with 0.5 M nBu₄NOAc (2.5 mmol, purchased from TCI, catalog# T2694) in MeCN : HOAc = 4:1 (5mL), alkyne (0.5 mmol, 1.0 equiv.), TAAu

(0.019 mmol, 7.5 mol%), and Phen (0.1 mmol, 40 mol %) was added (see Scheme 6.2). The vial was placed on IKA Carousel and run under constant current at 5mA. The reaction is monitor by TLC for the completion. After the reaction was completed, the solvent was removed under reduced pressure and the residue was purified by flash chromatography on silica gel to give desired diyne product.

6.2.3 General Procedure for Hetero-diyne Coupling

To a 10 mL ElectraSyn screwed vial with 0.5 M nBu₄NOAc (2.5 mmol) in MeCN : HOAc = 1:1 (5mL), aromatic alkyne (0.25 mmol, 1.0 equiv.), aliphatic alkyne (0.75 mmol, 3.0 equiv.), PPh₃AuCl (0.025 mmol, 10 mol%), and Phen (0.125 mmol, 50 mol %) was added. The vial was placed on IKA Carousel and run under constant current at 5mA. The reaction is monitor by TLC for the completion. After the reaction was completed, the solvent was removed under reduced pressure and the residue was purified by flash chromatography on silica gel to give desired diyne product.

Handmade cell connection with IKA ElectraSyn



Scheme 6.2 General procedures for the ElectraSyn Setup.

6.2.4 General Procedure for Phenylacetylene Oxidative Coupling

A mixture of 2 mM Au(I) compound and 2 mM phenylacetylene in acetonitrile solution containing 0.1 mM of lithium perchlorate (LiClO_4) as the electrolyte was added into a glass vial (Scheme 6.3). A magnetic stirrer was added and stirred vigorously during the reaction. A piece of reticulated vitreous carbon (RVC) material (dimension $1.0 \times 0.5 \times 0.6 \text{ cm}^3$, 100 psi, ERG Materials and Aerospace Corp) was used as the anode and was connected with the DC power supply via a platinum wire (0.3 mm diameter, 99.99% purity, Goodfellow Corporation). A platinum metal piece (dimension $1.0 \times 0.5 \times 0.02 \text{ cm}^3$) was used as the cathode in the reaction. The applied potential was +5 V for the reaction, employing a Tekpower TP3005T DC power supply (Montclair, CA). The reaction solution was

collected and monitored with time using mass spectrometry (MS). The same setups and materials were adopted when different substrates such as phenylacetylene-d and 4-ethynyltoluene, and 1-ethynyl-4-fluorobenzene were used for electrolysis.

The nESI-MS spectra were collected by using a Thermo Fisher Orbitrap Q-Exactive Plus (Waltham, MA) in the positive ion mode. A borosilicate glass capillary (Sutter Instrument Co., Novato, CA) was used to make a spray emitter. The emitter tip opening size was pulled to 2 μm by a laser puller (Sutter Instrument Co., Model P-2000). After electrolysis reaction was finished, the solution was loaded into the pulled spray emitter. A platinum wire (0.025 mm diameter, 99.99% purity) was inserted into the emitter for conductivity and ionization, and the applied potential was + 2.5 kV. High resolution MS data was obtained and collision-induced dissociation (CID) was carried out by using nitrogen gas as the collision gas.

6.3 Results and Discussion

We initiated our investigation with oxidative coupling of terminal alkynes for the synthesis of conjugated 1,4-diynes (Figure 6.1A). The intrinsic reactivity of C-C triple bonds allows conjugated alkynes to occupy a privileged position in chemical, medicinal and material research.²⁶⁵ Recent publication reported the gold-catalyzed selective oxidative cross-coupling between aromatic and aliphatic terminal alkynes.²⁶⁶ This transformation is ideal for exploring electrochemical gold redox catalysis since the net reaction is the formation of diyne and H_2 , which are well-suited for both anode oxidation and cathode reduction.²⁶⁷ To testify whether the anode oxidation concept is viable, we first prepared Au(I) pyridine complex **1a** and charged it into typical electrochemical conditions (Figure 6.1B). To our

delight, with the presence of alkyne, the corresponding Au(III) complexes **2** were detected and monitored by MS within 30 minutes (see Figure 6.2). By comparing the observed MS spectrum with simulated result and collision-induced dissociation spectrum, the structural of m/z 672 and the existence of Au(III) in this intermediate has been confirmed (see Figure 6.3 and 6.4). Furthermore, electrochemical oxidation of gold acetylide complex **1b** yielded the desired diyne product **4a** together with alkyne **3a** within 30min. These promising results showed the feasibility of achieving gold redox chemistry under electrochemical conditions.

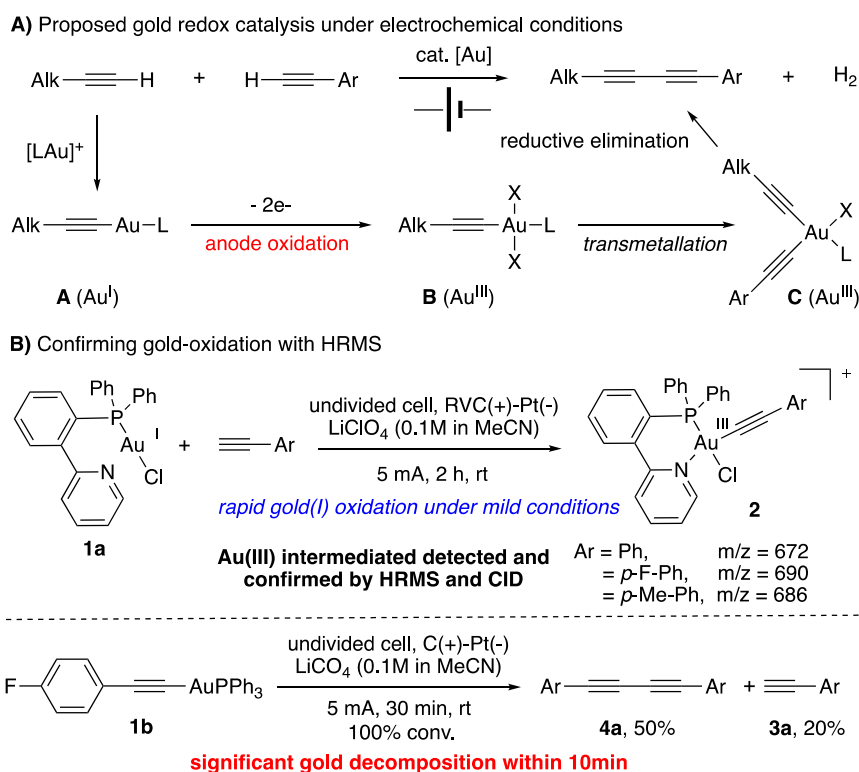


Figure 6.1 Exploring gold-catalyzed alkyne oxidation coupling.

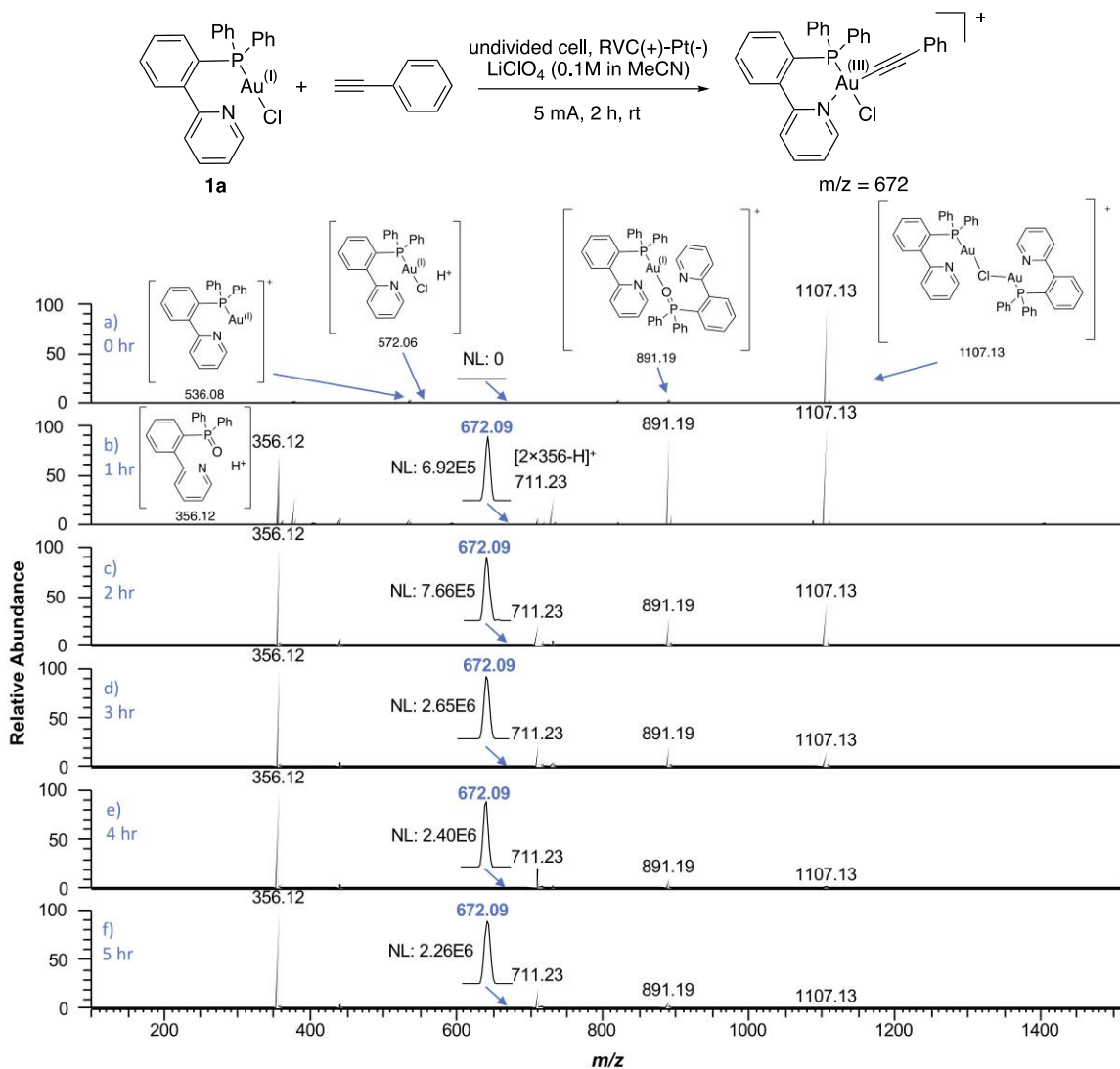


Figure 6.2 MS monitoring of gold-catalyzed phenylacetylene oxidative coupling.

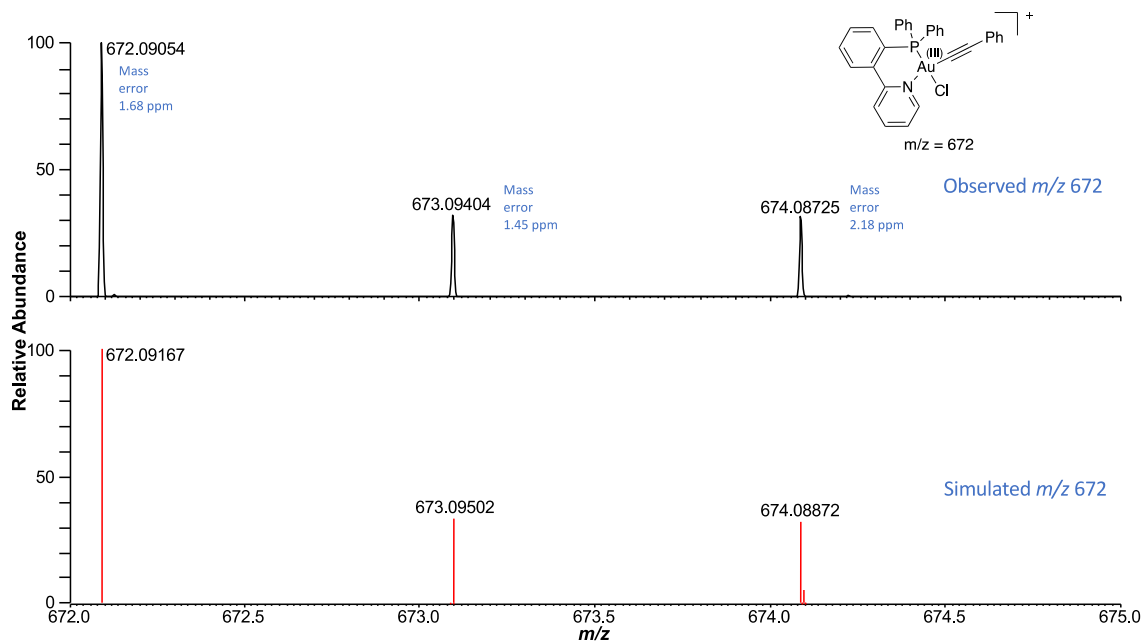


Figure 6.3 The observed Au(III) intermediate peaks compared with simulated results.

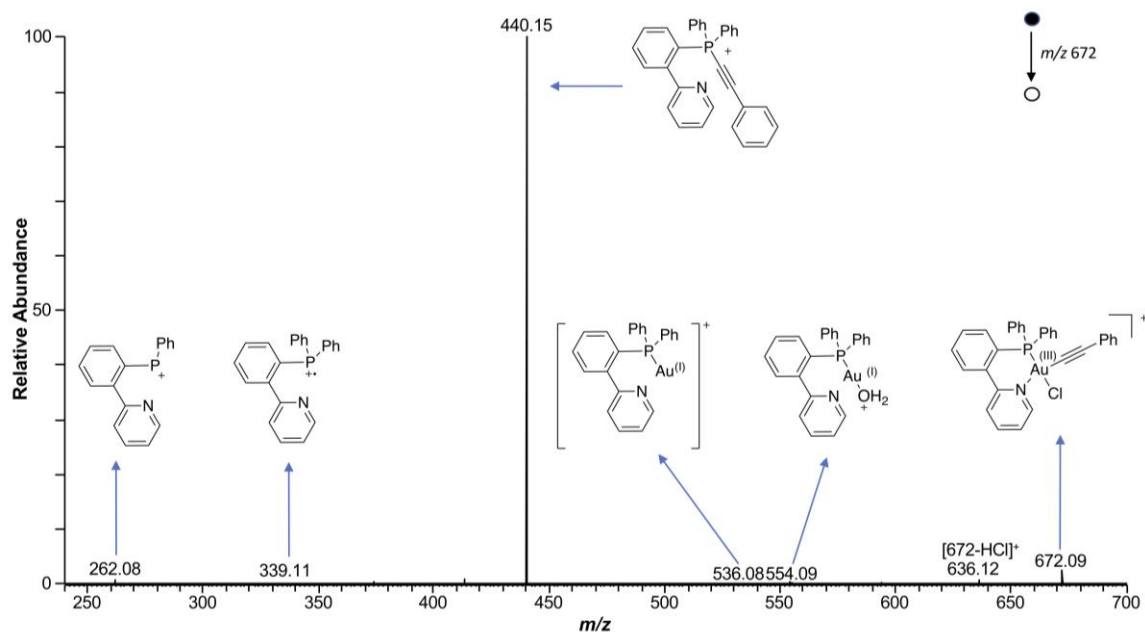


Figure 6.4 The collision-induced dissociation spectrum of Au(III) intermediate (m/z 672).

6.4 Conclusion

In summary, we herein reported the first example of electrochemical anodic oxidation of Au(I) to Au(III). Using this strategy, gold catalyzed oxidative coupling of terminal alkyne was successfully achieved with a broad substrate scope and excellent functional group tolerance under electrochemical condition. This protocol represents a new atom economy way to achieve the gold redox chemistry under mild condition, therefore, it is anticipated that this strategy will offer a new prospective to the community by probing the key elementary step for Au(I)/Au(III) oxidative.

CHAPTER 7

MICRODROPLET ULTRAFAST REACTIONS SPEED ANTIBODY CHARACTERIZATION

7.1 Introduction

Microdroplets have been recently found to be a unique reaction media in which reaction acceleration can occur.²⁶⁸ It has aroused much attention in the field of chemistry and has been extensively investigated.^{269,270,279–288,271,289,272–278} Various reactions of organic molecules are markedly promoted in sprayed micron-sized droplets (microdroplets) compared with the same reactions in bulk-phase solution.²⁹⁰ Numerous explanations have been offered for why reaction rate acceleration occurs in aqueous microdroplets. These explanations include evaporation, increased autoionization, partial desolvation, the presence of an intrinsic strong electric field at the interface, the enhanced concentration of solutes on the surface of the microdroplet, and restricted orientations.^{291–300} The factors that are dominant in any given situation still need to be identified. However, most previous work focused on one-step reactions of small molecules. Biochemical reactions involving proteins have been rarely investigated, except a recent report of trypsin digestion of proteins in microdroplets.³⁰¹

Therapeutic monoclonal antibodies (mAbs) are one of the fastest growing classes of drugs. More than one hundred mAbs for treatment of many pathologies such as cancer and autoimmune diseases have been approved or are in regulatory review in the US and EU.^{302,303} This ever-growing abundance has created a need for rapid technologies to characterize mAbs to secure drug product safety, quality, and efficacy.^{304–306} Traditional mass spectrometry (MS) mAb characterization methods include intact and subunit mass

analysis and peptide mapping.³⁰⁷⁻³¹¹ To characterize mAbs in a bottom-up or middle-down proteomics approach, mAbs must be subjected to enzymatic digestion into peptides or polypeptides before peptide mapping analysis by MS. However, digestion is usually a time-consuming step that can take from 30 min to overnight incubation.^{312,313} In addition, commonly used digestion methods often include additional steps of protein denaturation, reduction, and alkylation to unfold mAb structure and facilitate digestion; these additional steps may also lengthen process time and reduce analysis speed and throughput.³¹⁴ To accelerate digestion of mAb (or other proteins), a variety of methods have been investigated, including increasing the digestion temperature, adding organic solvents, applying microwave energy, using high intensity focused ultrasound or employing microchip reactor.³¹⁵⁻³²² Nevertheless, an alternative method that is very fast for mAb digestion would be highly valuable.

In this study, we present unprecedented and fast microdroplet reactions involving a large protein substrate (i.e., an antibody), which would have high impact in proteomics for rapid characterization of antibodies. In this work, ultrafast digestion of the NIST IgG1 antibody in 250 microseconds in microdroplets was achieved. The IgG1 was selectively cleaved by IdeS protease into antigen-binding fragment F(ab')₂ and single-chain, crystallizable fragment scFc (Figure 7.1a). When we included the reductant tris(2-carboxyethyl)phosphine (TCEP) in the spray solution, simultaneous disulfide bond reduction occurred, leading to digested and reduced IgG1 fragments that included light chain LC, *N*-terminal half of heavy chain Fd' and scFc subunits (Figure 7.2a). These fragments could be either collected for further analysis or detected online by MS. In addition, we achieved ultrafast deglycosylation of IgG1 by including PNGase F

glycosylase in the microdroplets (Figure 7.7a), which constituted an alternative method to rapidly remove glycans from antibodies. In addition, following incubation with glucose, we successfully digested and characterized glycosylated IgG1 fragments in microdroplets, which suggested a fast way to detect antibody modifications in general.

7.2 Experiments

7.2.1 Chemicals

NIST monoclonal antibody reference material 8671 (NIST mAb, humanized IgG1 κ monoclonal antibody) was obtained from the National Institute of Standards and Technology (Gaithersburg, MD). The IdeS enzyme was purchased from Genovis Inc (Cambridge, MA). Tris(2-carboxyethyl)phosphine hydrochloride (TCEP, bioultra grade), ammonium bicarbonate (bioultra grade), sodium phosphate dibasic (bioultra grade), and sodium phosphate monobasic (bioultra grade) were purchased from Sigma Aldrich (St. Louis, MO). D-(+)-Glucose (98% purity) was obtained from TCI America (Montgomeryville, PA). Acetonitrile (HPLC grade), formic acid (FA, LCMS grade) and trifluoroacetic acid (TFA, LCMS grade) were purchased from Fisher Scientific (Fair Lawn, NJ). A Millipore Direct-Q5 purification system (Burlington, MA) was used to obtain purified water for sample preparation.

7.2.2 Microdroplet Generation

Microdroplets were generated by spraying an aqueous sample solution (NIST IgG1 mixed with IdeS, TCEP, PNGase F, or all reagents together) at a flow rate of 10 μ L/min through a home-made sprayer with the assistance of nitrogen gas as nebulizer at 120 psi. The home-made sprayer was built exactly as a described for a sonic spray source.³²³ Briefly, the

aqueous sample solution was delivered through a fused-silica capillary (100 μm i.d. and 200 μm o.d., Polymicro Technologies, Phoenix, AZ). Another coaxial fused-silica capillary (250 μm i.d. and 300 μm o.d.) was used and the small size difference between two capillaries was capable of providing nebulizing gas at high velocity.²⁷¹ The sprayer did not need an applied voltage.

7.2.3 Microdroplet Digestion with nESI-MS Analysis

For the experiment shown in Figure 7.1b, 50 μL of 1 mg/mL IgG1 in 5 mM NH_4HCO_3 buffer (pH 8) was loaded in one syringe. Then 50 μL of 2 units/ μL IdeS enzyme in 5 mM NH_4HCO_3 buffer (pH 8) was loaded in the other syringe. The flow rate of both syringes were 5 $\mu\text{L}/\text{min}$ and the reactants were mixed by a Tee. The length of capillary between mixing Tee and sprayer was 2 cm. The microdroplets were generated through the sprayer and collected in a vial containing a quenching solvent of 50 μL of H_2O and 1% FA. The distance between the sprayer tip and the surface of quenching solution was 20 mm. After 5 min collection, desalting and reagent removal was performed with a C4 Ziptip (MilliporeSigma, Burlington, MA). The desalted sample was analyzed by nESI in front of a high-resolution QExactive Orbitrap mass spectrometer (Thermo Scientific, San Jose, CA). The injection flow rate was 2 $\mu\text{L}/\text{min}$ and +3 kV was applied for ionization. The temperature of the MS inlet was 250°C. All sample mixing and injecting steps were performed rapidly without delay time between each step to avoid any reaction occurring in the bulk solution under ambient temperature. For the experiment in the Figure 7.2b, 50 μL of 1 mg/mL IgG1 in 5 mM NH_4HCO_3 buffer containing 5 mM TCEP (pH 8) was loaded in one syringe. Then 50 μL of 2 units/ μL IdeS enzyme in 5 mM NH_4HCO_3 buffer (pH 8)

was loaded in the other syringe. The remaining steps were the same as the steps in the aforesaid Figure 7.1b experiment.

7.2.4 Microdroplet Digestion with Online EESI-MS Analysis

In the online workflow, the EESI-MS method reported by Chen and coworkers³²⁴ was adopted with minor modifications. The schematic drawing is shown in Figure 7.2e. Briefly, one sprayer was used to generate microdroplets from a one-pot mixture of NIST IgG1, IdeS and TCEP solution without applying any voltage. The mixed sample solution consisted of 5 μ L of 10 mg/mL NIST IgG1, 2 μ L of 50 units/ μ L IdeS enzyme and 93 μ L of 5 mM NH_4HCO_3 buffer containing 5 mM TCEP. The other sprayer emitted ACN/ H_2O /FA solvent (50:50:0.5%), and +3 kV voltage was applied to the solvent liquid through a metal alligator clip attached to the stainless-steel tip of the syringe used for solvent infusion. The flow rates of both sprayers were 10 μ L/min. The pressure of nitrogen gas for both sprayers was 120 psi. The distance between the tip of solvent sprayer to the MS inlet was 15 mm, and the distance between the tip of mixed sample sprayer to the MS inlet was 20 mm. The EESI source was aligned carefully to the MS inlet to achieve the highest sensitivity. The temperature of MS inlet was 250°C.

7.2.5 Glycated IgG1 Characterization

Twenty microliters of 10 mg/mL NIST IgG1 was added to 180 μ L of 200 mM NH_4HCO_3 buffer containing 200 mM glucose (pH 8). The final concentration of IgG1 was 1 mg/mL. Then, sample solution was incubated at 37°C for 0, 2 and 5 days. After incubation, 10 μ L of 1 mg/mL glycated IgG1 was drawn out and mixed with 2 μ L of 50 units/ μ L IdeS in 88 μ L of 5 mM NH_4HCO_3 buffer containing 5 mM TCEP (pH 8). The final concentration of glycated IgG1 was 0.1 mg/mL in the resulting mixture which was sprayed to trigger

microdroplet reactions as a flow rate of 10 $\mu\text{L}/\text{min}$ for 5 min. Then 50 μL of H_2O containing 0.1% TFA was added to reconstitute the collected microdroplets and terminate enzymatic reaction. Desalting and reagent removal was performed with a C4 Ziptip. The desalted sample was analyzed by nano-electrospray ionization (nESI) using the QExactive Orbitrap mass spectrometer. The injection flow rate was 2 $\mu\text{L}/\text{min}$ and +3 kV was applied for ionization. The temperature of the MS inlet was 250°C.

7.2.6 Deglycosylation of IgG1 by PNGase F

Fifty micrograms of NIST IgG1 in 5 mM NH_4HCO_3 buffer (pH 8) was loaded in one syringe. The final concentration of IgG1 was 1 mg/mL. Then 100 μL of 1 unit/ μL mM PNGase F in 5 mM NH_4HCO_3 buffer (pH 8) was loaded in the other syringe. The remaining steps were the same as the steps in the aforesaid Figure 7.1b experiment.

7.3 Results and Discussion

We first investigated the direct microdroplet digestion of IgG1 by IdeS enzyme. The IdeS enzyme, cloned from *Streptococcus pyogenes* and expressed in *Escherichia coli*, specifically digests IgG1 below the hinge region and generates $\text{F(ab}')_2$ and scFc fragments (Figure 7.1a). In our experiment, IgG1 and IdeS were pre-loaded in two syringes, respectively (Figure 7.1b). Both syringes were pumped at a flow rate of 5 $\mu\text{L}/\text{min}$ and reactants were brought together in a mixing Tee connected to a sprayer via a piece of 2 cm fused silica capillary. The mixed sample was sprayed for 5 min and the microdroplets were collected into a vial containing 1% formic acid in water as a quenching solvent (IdeS is inactivated at $\text{pH}<5$). The distance between sprayer and the quenching solution in the vial was 2 cm, and the speed of the sprayed microdroplets was 84 ± 18 m/s as previously

measured²⁷¹. Thus, the flight time of microdroplet between sprayer and quenching solution was only 250 μ s [$2 \text{ cm}/(84 \text{ m/s}) \cong 250 \mu\text{s}$]. Even in such a short spray time, we achieved optimal digestion efficiency of antibody in microdroplets. The collected sample was desalted and analyzed by nano-electrospray ionization mass spectrometry (nESI-MS, see the workflow shown in Figure 7.1b). Figure 7.1c shows that all the IdeS-cleaved subunits (i.e., F(ab')₂ and scFc) were clearly observed in the MS spectra. In addition, we efficiently detected and resolved different glycoforms (G0F, G1F, and G2F) of scFc fragments. Furthermore, we did not observe any remaining intact IgG1 after microdroplet digestion, which indicated 100% digestion efficiency in microdroplets. The time of 250 μ s in microdroplets for completely digesting an intact antibody at 25°C represented a 7.5 million-fold speed improvement, in comparison with traditional digestion in bulk solution that requires at least 30 minutes to 1 hour at 37°C.³¹² To prove that IgG1 was truly digested in microdroplets during the spray process (Figure 7.1b), we also conducted a control experiment in which IgG1 was incubated with IdeS in solution for digestion at 37°C for 5 min and no notable digestion was observed (Figure 7.1d). Clearly, the microdroplets did markedly accelerate enzymatic digestion of the intact antibody. Note that, in Figure 7.1b of the microdroplet experiment, the residual time of the IgG1 and IdeS in the 2-cm connection capillary after Tee mixing was only 4.4 seconds, which we did not expect to lead to noticeable digestion inside the capillary.

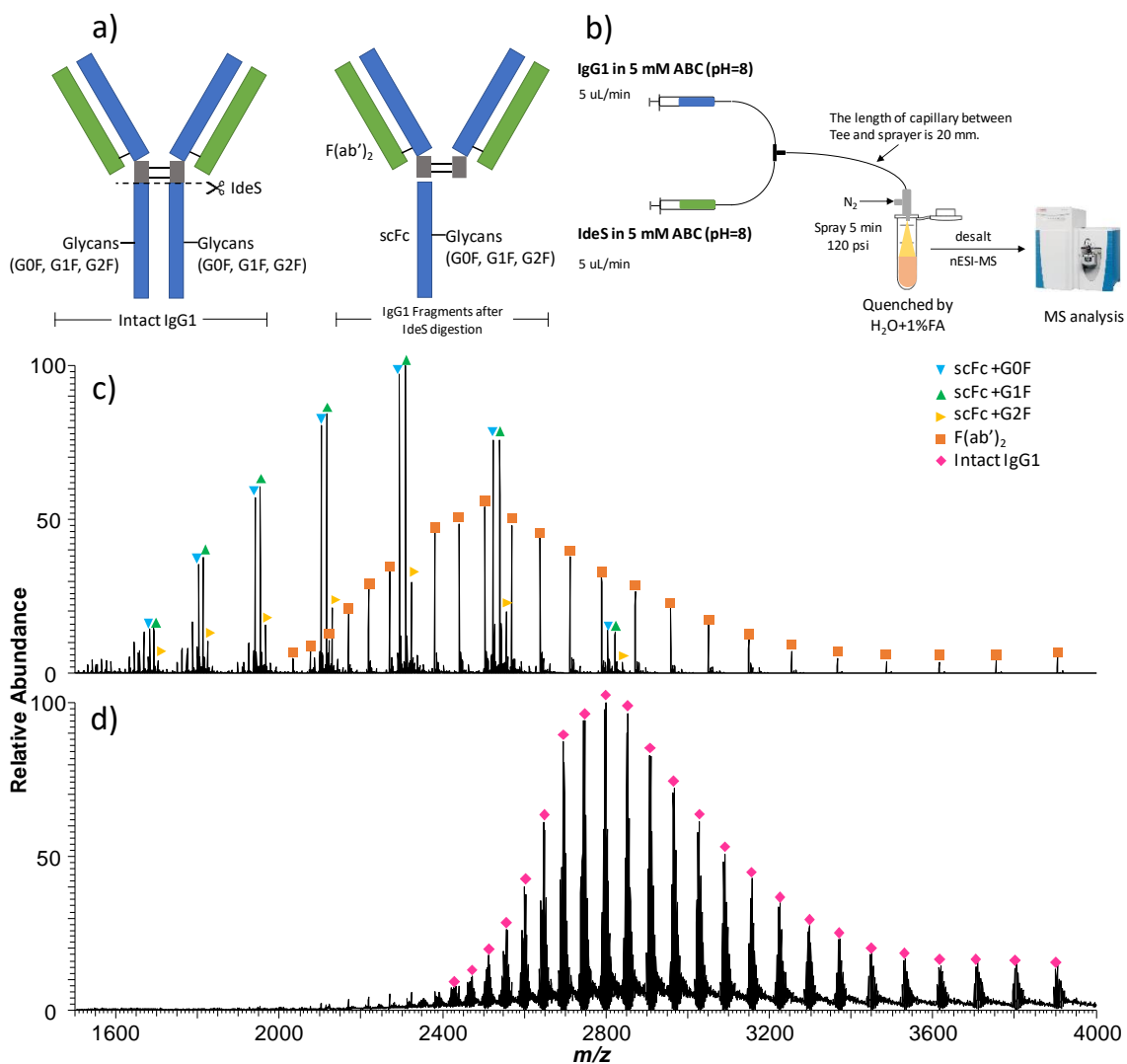


Figure 7.1 Microdroplet digestion of IgG1 (the NIST IgG1 monoclonal antibody reference material 8671) by IdeS enzyme: (a) Schematic drawing of intact IgG1 and IdeS-cleaved IgG1 fragments; The light chain, heavy chain, and hinge region are highlighted in green, blue, and grey, respectively. Black solid lines indicate disulfide bonds connecting heavy and light chains. The IdeS cleavage site is indicated with scissors and dash line. (b) Workflow of microdroplet digestion of IgG1 by IdeS; nESI-MS spectra of (c) antibody fragments obtained from microdroplet digestion of IgG1 by IdeS at room temperature and (d) In-solution digested IgG1 by IdeS for 5 min at 37°C.

Strikingly, we found that adding another reagent into the spray solvent enabled another ultrafast reaction step. For example, addition of the reducing reagent tris(2-carboxyethyl)phosphine (TCEP) in the spray solution containing IdeS and IgG1 accelerated disulfide bond reduction of antibody, leading to simultaneous digestion and

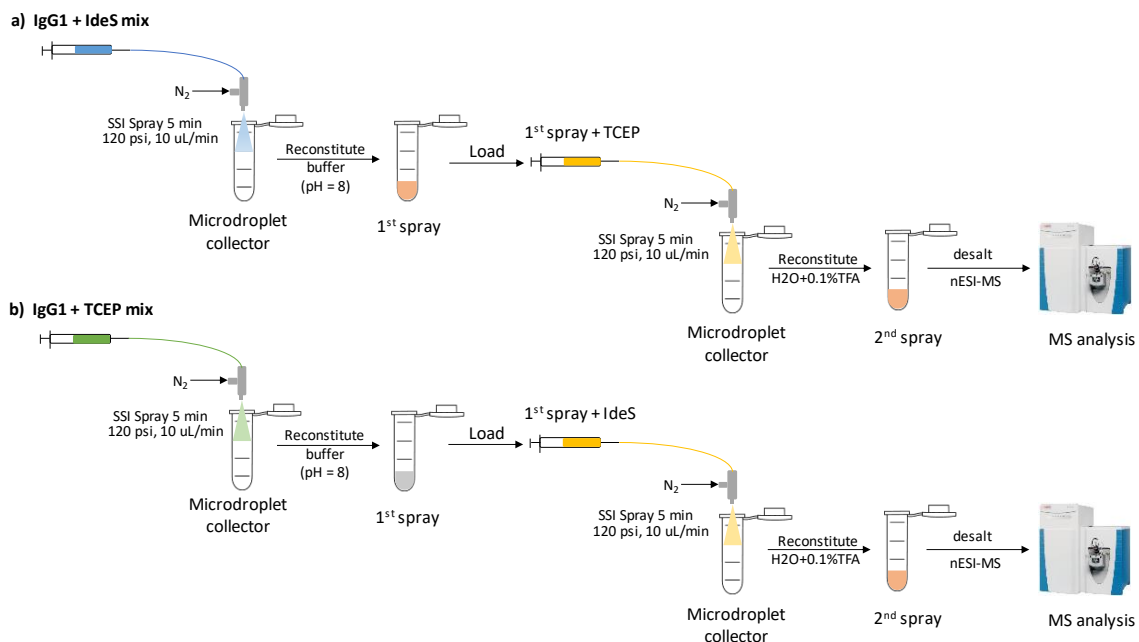
reduction of antibody in the microdroplets, which is illustrated in Figure 7.2a. Following the workflow shown in Figure 7.2b, IgG1 and TCEP were pre-mixed in one syringe, and the IdeS was pre-loaded in the other syringe. Both syringes were pumped at a flow rate of 5 μ L/min. Reactants were mixed via a Tee and transferred to the sprayer for generating microdroplets, which were again directed to a collection vial containing an acidic quenching solution (Figure 7.2b). After digestion in the microdroplets, we clearly observed in the MS spectrum all the digested and reduced fragments, LC, Fd', and glycosylated scFc including scFc+G0F, scFc+G1F, and scFc+G2F (Figure 7.2c) and the deconvoluted MS spectrum (Figure 7.2d), with mass of each fragment within the measurement accuracy (Table 7.1). In antibody characterization, reduced fragments are valuable because they are amenable to MS/MS techniques that provide high-sequence coverage and localization of structural modifications.

Table 7.1 Comparison Between Measured Mass for IgG1 Fragments in Figure 7.2c by Microdroplet Digestion and Previously Published Data

Fragment	Measured Mass ⁱ (Da)	Theoretical Mass ⁱⁱ (Da)	Mass Error (Da)
LC	23123	23113	10
scFc+G0F	25232	25220	12
scFc+G1F	25394	25383	11
scFc+G2F	25556	25545	11
Fd'	25685	25673	12

- i. Measured mass by using microdroplet digestion method (see Figure 7.2b)
- ii. Measured mass by using conventional LC-MS method³²⁵

Besides conducting the microdroplet reaction in an “one-pot reaction” manner as described above, the dual reaction of digestion and reduction could be performed stepwise. According to the stepwise workflow shown in Scheme 7.1a, we mixed IgG1 and IdeS via a Tee mixer and sprayed the mix as microdroplets to digest IgG1. The collected microdroplets were then mixed with TCEP in a vial and sprayed again to accelerate reduction in microdroplets. The F(ab')₂ fragment was further reduced to light chain (LC) and Fd' fragment. The collected microdroplets were reconstituted and desalted for nESI-MS analysis. Figure 7.3 shows that all the IdeS-cleaved and TCEP-reduced subunits (i.e., LC, Fd', and scFc_s) were clearly observed in the MS spectra. Different glycoforms (G0F, G1F, and G2F) of scFc fragments were also detected and resolved efficiently. In addition, this workflow successfully digested and reduced IgG1 in phosphate buffer (see Figure 7.4), which indicated that microdroplet digestion could be performed in a nonvolatile buffer solution. Likewise, for the stepwise workflow, we could mix IgG1 and TCEP first for microdroplet reduction and then further mixed with IdeS for digestion (Scheme 7.1b). All the IdeS-cleaved and TCEP-reduced fragments (LC, Fd' and scFc_s) were also observed (Figure 7.5), suggesting that the reduction and digestion reaction order can be switched.



Scheme 7.1 Schematics showing two microdroplet digestion workflows: a) microdroplet IdeS digestion followed with microdroplet TCEP reduction and b) microdroplet TCEP reduction followed with microdroplet IdeS digestion.

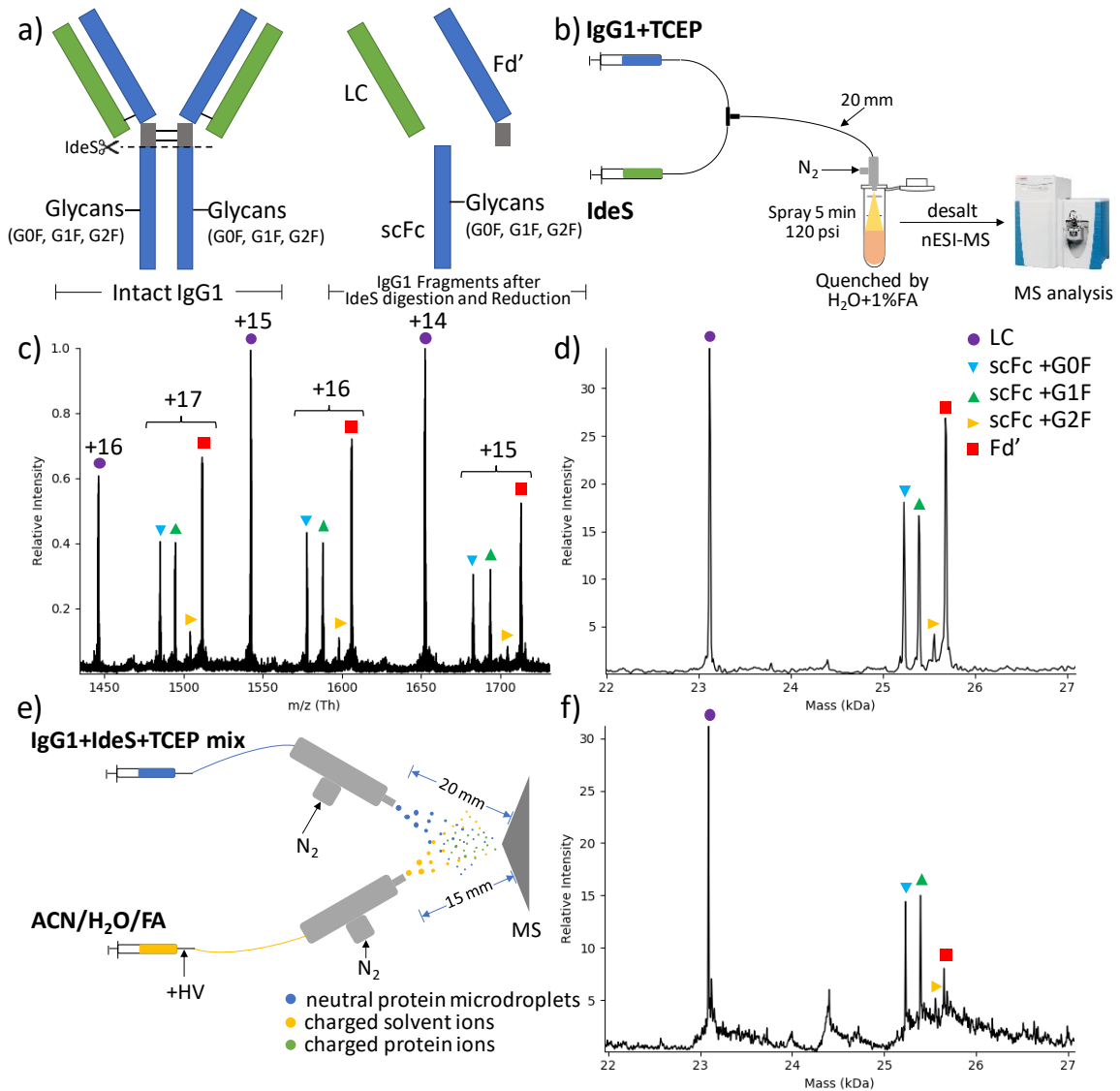


Figure 7.2 Simultaneous microdroplet digestion and reduction of IgG1. (a) Schematic representation of intact IgG1 and fragment structures of IgG1 after IdeS digestion and TCEP reduction. (b) Schematic drawing of the microdroplet digestion and reduction workflow. (c) The expanded MS spectrum with LC, Fd' and glycosylated scFc fragments detected and annotated. (d) The corresponding deconvoluted MS spectrum of (c). (e) Schematic drawing of simultaneous microdroplet digestion and reduction coupled with online EESI-MS detection. (f) Deconvoluted MS spectrum of digested and reduced IgG1 from online EESI-MS detection.

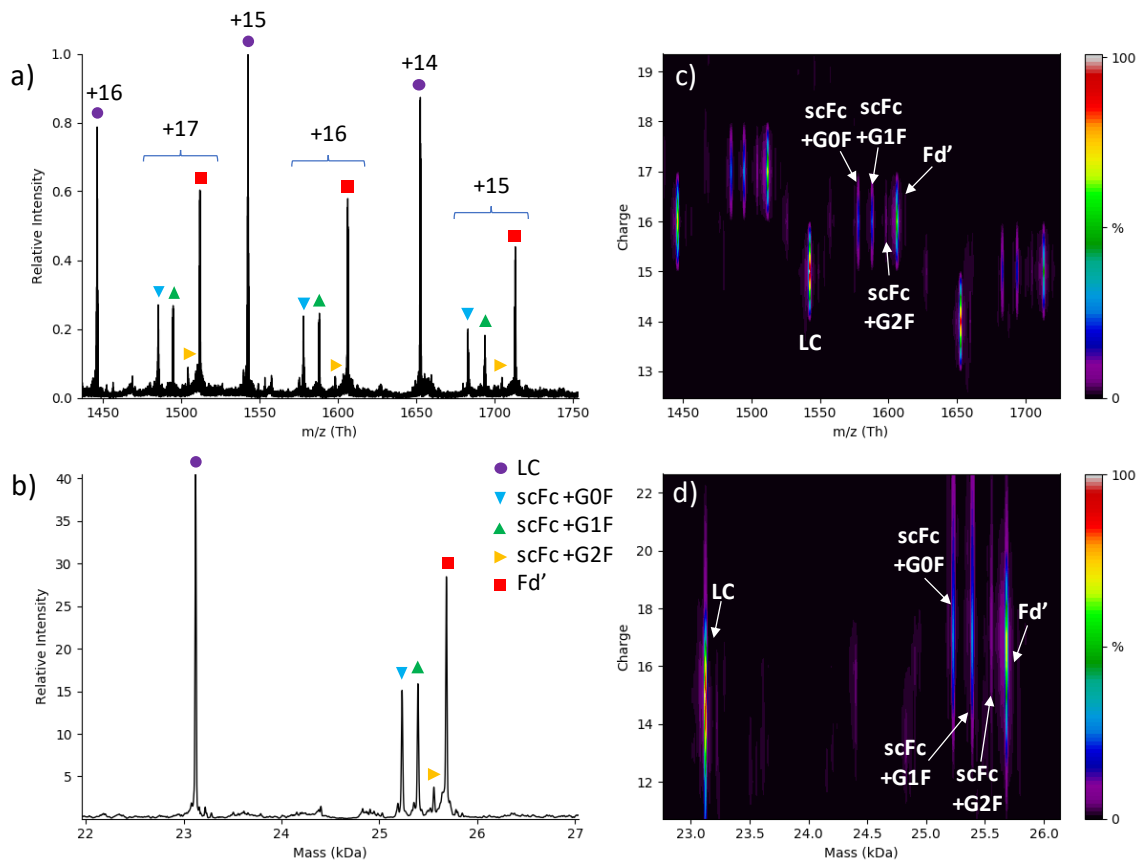


Figure 7.3 Stepwise microdroplet digestion and reduction of IgG1 in 5 mM NH_4HCO_3 buffer (pH 8). In this approach, IgG1 was first cleaved by IdeS into $\text{F}(\text{ab}')_2$ and scFc fragments, then TCEP was added to reduce $\text{F}(\text{ab}')_2$ into LC and Fd'. a) The expanded view of MS spectrum; b) The corresponding deconvoluted MS spectrum; c) 2D spectrum with m/z along the x-axis and charge number along the y-axis; and d) 2D spectrum with mass served along the x-axis and charge number along the y-axis.

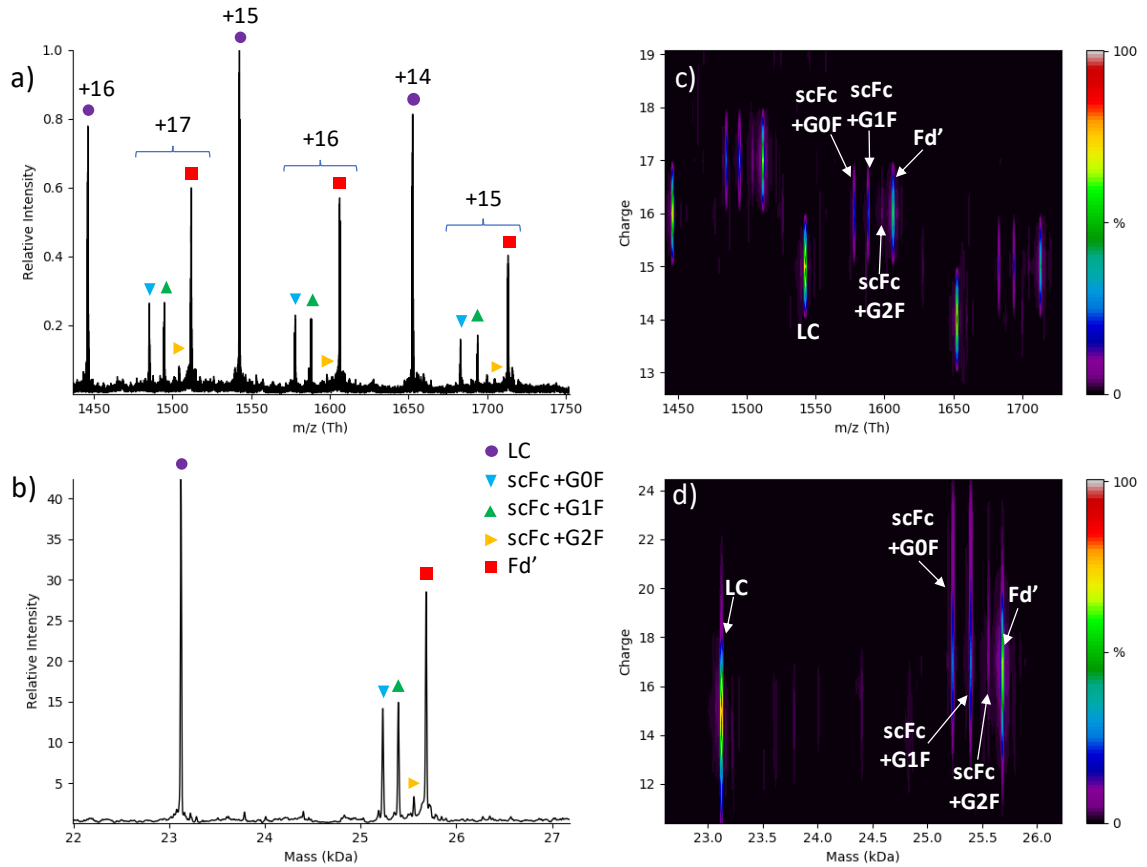


Figure 7.4 Stepwise microdroplet digestion and reduction of IgG1 in 5 mM phosphate buffer (pH 8). In this approach, IgG1 was first cleaved by IdeS into $F(ab')_2$ and scFc fragments, then TCEP was added to reduce $F(ab')_2$ into LC and Fd'. a) The expanded view of MS spectrum; b) The corresponding deconvoluted MS spectrum; c) 2D spectrum with m/z along the x-axis and charge number along the y-axis; and d) 2D spectrum with mass served along the x-axis and charge number along the y-axis.

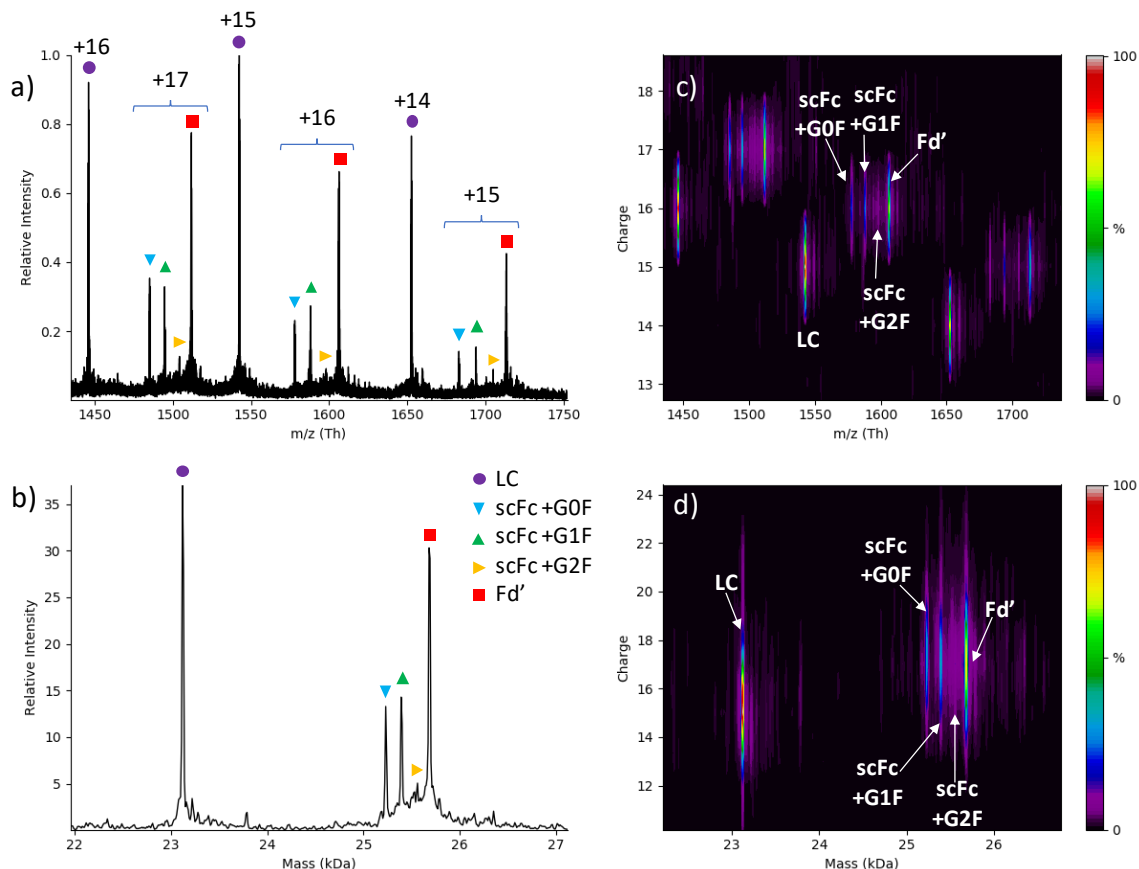


Figure 7.5 Stepwise microdroplet reduction and digestion of IgG1 in 5 mM NH_4HCO_3 buffer (pH 8). In this approach, IgG1 was first reduced into LC and HC fragments by TCEP, then IdeS was added to cleave HC into Fd' and scFc. a) The expanded view of MS spectrum; b) The corresponding deconvoluted MS spectrum; c) 2D spectrum with m/z along the x-axis and charge number along the y-axis; and d) 2D spectrum with mass served along the x-axis and charge number along the y-axis.

To accelerate further the analysis process, one can use online MS detection in combination with simultaneous microdroplet digestion and reduction. It would be worthwhile to conduct microdroplet digestion and MS detection simultaneously as a real-time analysis because simultaneous operation would condense the digestion and reduction time to a minimum.²⁷¹ For the online workflow, extractive electrospray ionization mass spectrometry (EESI-MS)^{324,326–328} was used, in which two sprayers were aligned and used together in the front of the MS inlet (Figure 7.2e). One sprayer served as the sample sprayer to generate microdroplets containing a mix of IgG1, IdeS and TCEP without applying any

voltage. The other sprayer worked as a solvent sprayer to generate microdroplets of ACN/H₂O/FA (50:50:0.5%) with +3 kV voltage applied to produce charged solvent microdroplets to assist the ionization of resulting fragments contained in the sample spray microdroplets. The IgG1 was cleaved with IdeS and reduced with TCEP into smaller fragments at the same time in the sample microdroplets in air at room temperature. Charged microdroplets of solvent mixed with and contacted the sample microdroplets and enabled sample ionization; the LC, Fd', scFc+G0F, scFc+G1F, and scFc+G2F fragments were all detected by online mass spectrometric analysis (Figure 7.2f). This approach allowed us to online detect digested and reduced IgG1 fragments directly online from the sprayed microdroplets, without any sample pretreatment or preparation.

Glycation is a nonenzymatic protein modification that occurs between reducing sugars (e.g., glucose, fructose, and galactose) and proteins.³²⁹ The primary amine groups of lysine residues and the N-termini of proteins react with aldehyde groups from reducing sugars to form Schiff base intermediates, which are further converted via Amadori rearrangement into more stable ketoamines. Glycation has been commonly observed in therapeutic antibodies during manufacturing and storage, and glycation could affect drug product stability, safety, and efficacy.³³⁰ Thus, it is of major importance to characterize and determine the effect of glycation on mAb structure. However, conventional methods, such as boronate affinity chromatography, capillary isoelectric focusing (cIEF), and liquid chromatography-mass spectrometry, suffer from low throughput because of the long separation times required. Fit-for-purpose assays are still lagging to meet the high-throughput demands of the pharmaceutical industry. It has been stated that a top priority of

the US Food and Drug Administration is development of new tools for high-throughput therapeutic protein characterization.³³¹

Consequently, we were motivated to attempt a rapid characterization method for glycosylated IgG1 using microdroplet digestion and reduction. After incubation with glucose, the glycosylated NIST IgG1 underwent microdroplet digestion and reduction in the “one-pot reaction” workflow (i.e., mixing with both IdeS and TCEP) and Figure 7.6a-c presents the MS spectra of IgG1 obtained after 0, 2 and 5 days of incubation with glucose. Figure 7.6a shows the digested and reduced IgG1 fragments from IgG1 sample without incubation with glucose. After 2-days incubation, mono-glycosylated LC and mono-glycosylated Fd' fragments were seen (Figure 7.6b). With 5-days continued incubation, di-glycosylated LC and di-glycosylated Fd' fragments were also detected and resolved in the MS spectra (Figure 7.6c). In addition, after 5-days incubation, both mono-glycosylated LC and Fd' fragments appeared to be more abundant (Figure 7.6c), in comparison to the sample after 2-days incubation (Figure 7.6b). With a longer incubation time, more glycosylated fragments were produced and detected (data not shown). All the antibody fragments including mono- and di-glycosylated LC and Fd' fragments were detected and resolved in the deconvoluted MS spectrum (Figure 7.6d) and 2D spectrum (Figure 7.6e). The microdroplet-based digestion facilitates rapid glycosylation analysis of mAb subunits subjected to glycosylation stress. Microdroplet digestion of glycosylated IgG constitutes a proof-of-concept of a method to analyze other modifications of mAbs, such as oxidation, small molecule or peptide conjugation, and sequence variations, truncations, and extensions. Thus, the mAb subunits generated via microdroplets add to the toolbox of methods available for antibody characterization and product quality assessment during development and manufacturing.

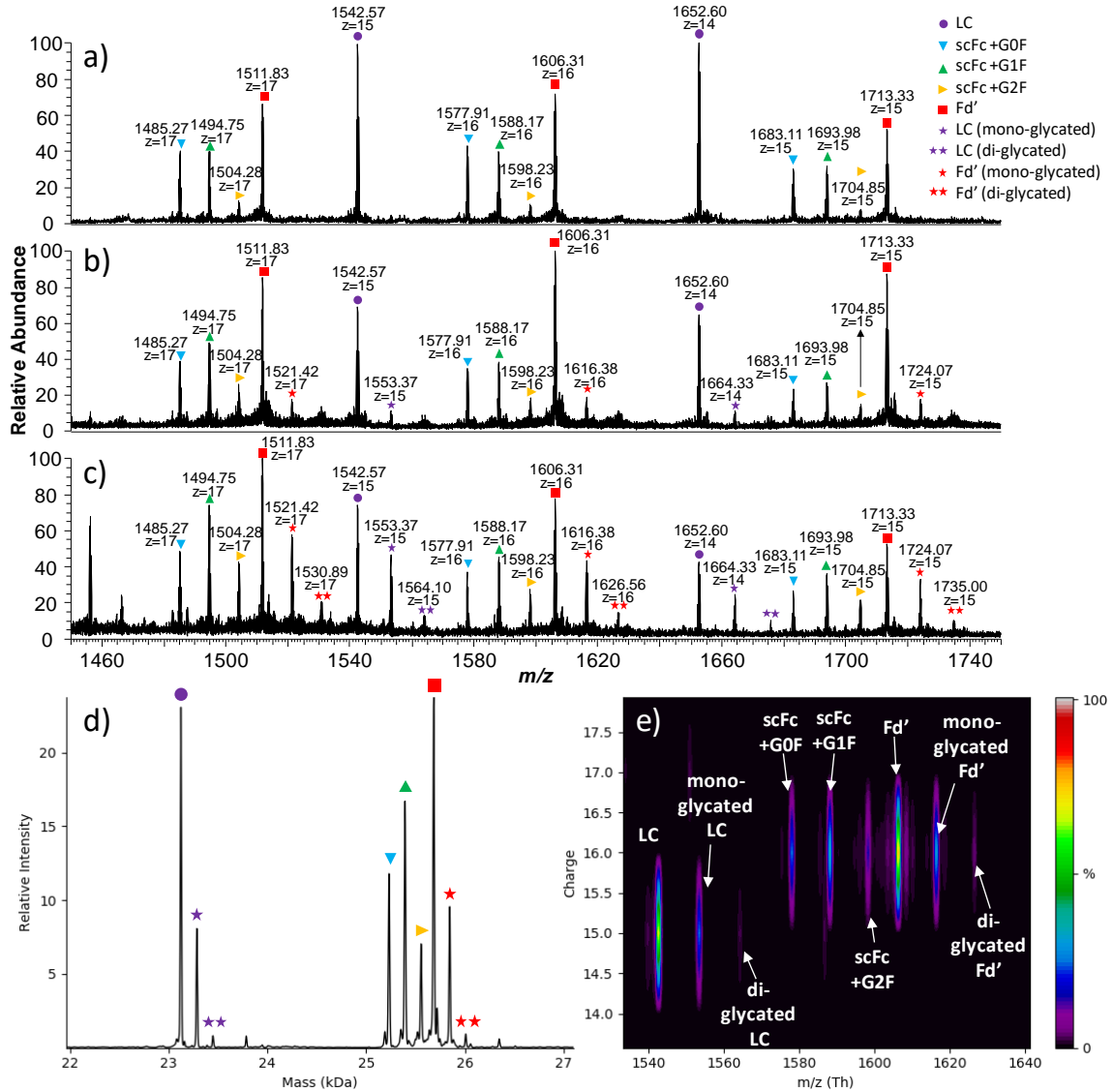


Figure 7.6 Microdroplet digestion of glycosylated IgG1. In this approach, glycosylated IgG1, IdeS and TCEP were mixed and reacted together in one-pot. The subunits of LC (and glycosylated-LC), Fd' (and glycosylated-Fd') and scFc fragments were produced simultaneously. (a) The expanded view of MS spectrum of non-glycosylated IgG1 (at day 0); (b) The MS spectrum of glycosylated IgG1 (incubated 2 days); (c) The MS spectrum of glycosylated IgG1 (incubated 5 days); (d) The deconvoluted MS spectrum of glycosylated IgG1 after 5 days incubation; and (e) 2D spectrum of glycosylated IgG1 after 5 days incubation with m/z along the x-axis and charge number along the y-axis.

Antibody glycosylation is heterogeneous, and variables in cell culture can increase glycan diversity. A conserved N-glycan at Asn297 of the scFc region of IgG1 is critical for

stability, conformation, aggregation, and effector function of therapeutic antibodies.³³² Removing glycosylation during pharmaceutical production analysis would be beneficial to ease the characterization of antibodies and to obtain the correct N-linked oligosaccharide (N-glycan) profile. N-Glycosidase F (PNGase F), a recombinant glycosidase from *Elizabethkingia miricola*, is one of the most effective enzymes to cleave N-glycans from proteins (illustrated in Figure 7.7a). In our experiment, first we pre-loaded IgG1 and PNGase F in two syringes, respectively (see the workflow in Figure 7.8). Both syringes were pumped at a flow rate of 5 $\mu\text{L}/\text{min}$ and reactants were mixed by a Tee and then sprayed to generate microdroplets. The microdroplets were quenched with H_2O containing 1% formic acid in the collection vial and collected for 5 min. The distance between sprayer and quenching solution was kept as 2 cm. The collected sample was desalted and analyzed by nESI-MS. Figure 7.8 shows the MS spectrum of deglycosylation of IgG1 by PNGase F in microdroplets at ambient temperature. In comparison to the intact IgG1 MS spectrum (Figure 7.8d), new antibody peaks appeared (Figure 7.8c). The deconvoluted MS spectrum (Figure 7.8b) clearly presents deglycosylated IgG1 peaks and a small amount of IgG1 with one glycan attached. This analysis indicated a high microdroplet reaction efficiency (the deglycosylation yield for IgG1 was estimated to be 90 %, based on the relative peak intensities of deglycosylated IgG1 and remaining glycosylated IgG1 in Figure 7.8b).

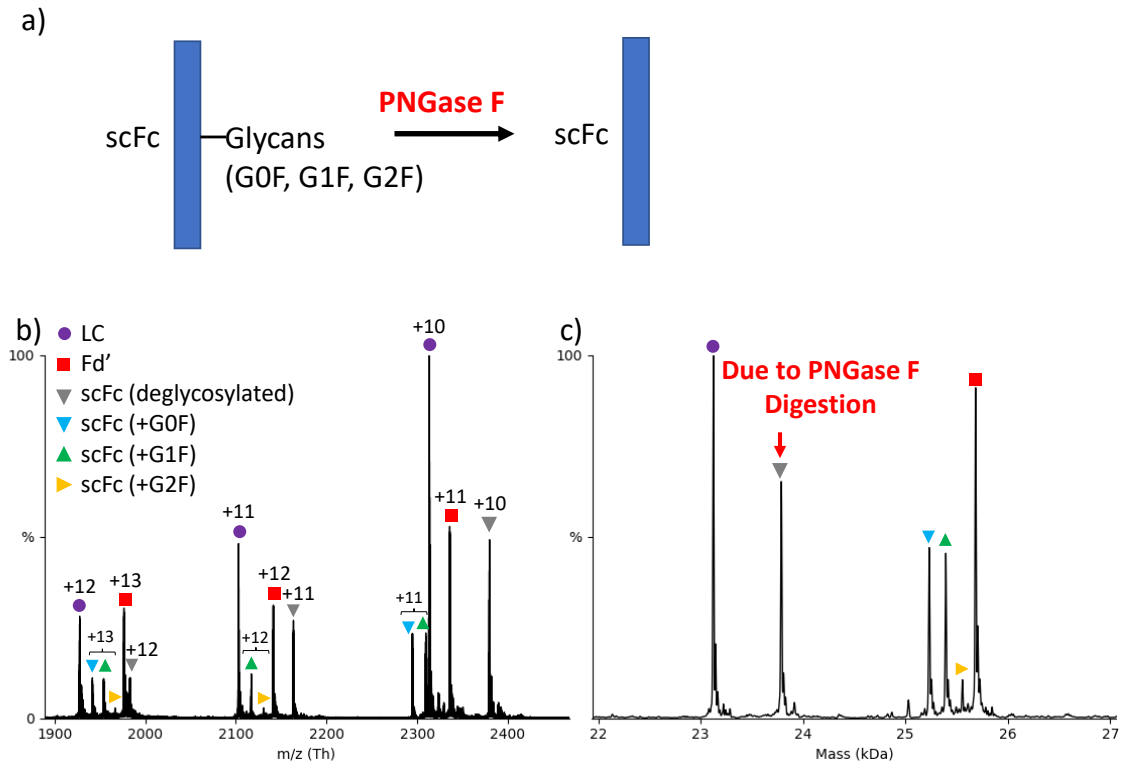


Figure 7.7 “One-pot” microdroplet reactions with IgG1, PNGase F, IdeS, and TCEP. (a) Schematic illustrating the PNGase F deglycosylation; (b) The expanded MS spectrum with LC, Fd’ and scFc (both deglycosylated and glycosylated) fragments detected and annotated; (c) The deconvoluted MS spectrum of (b).

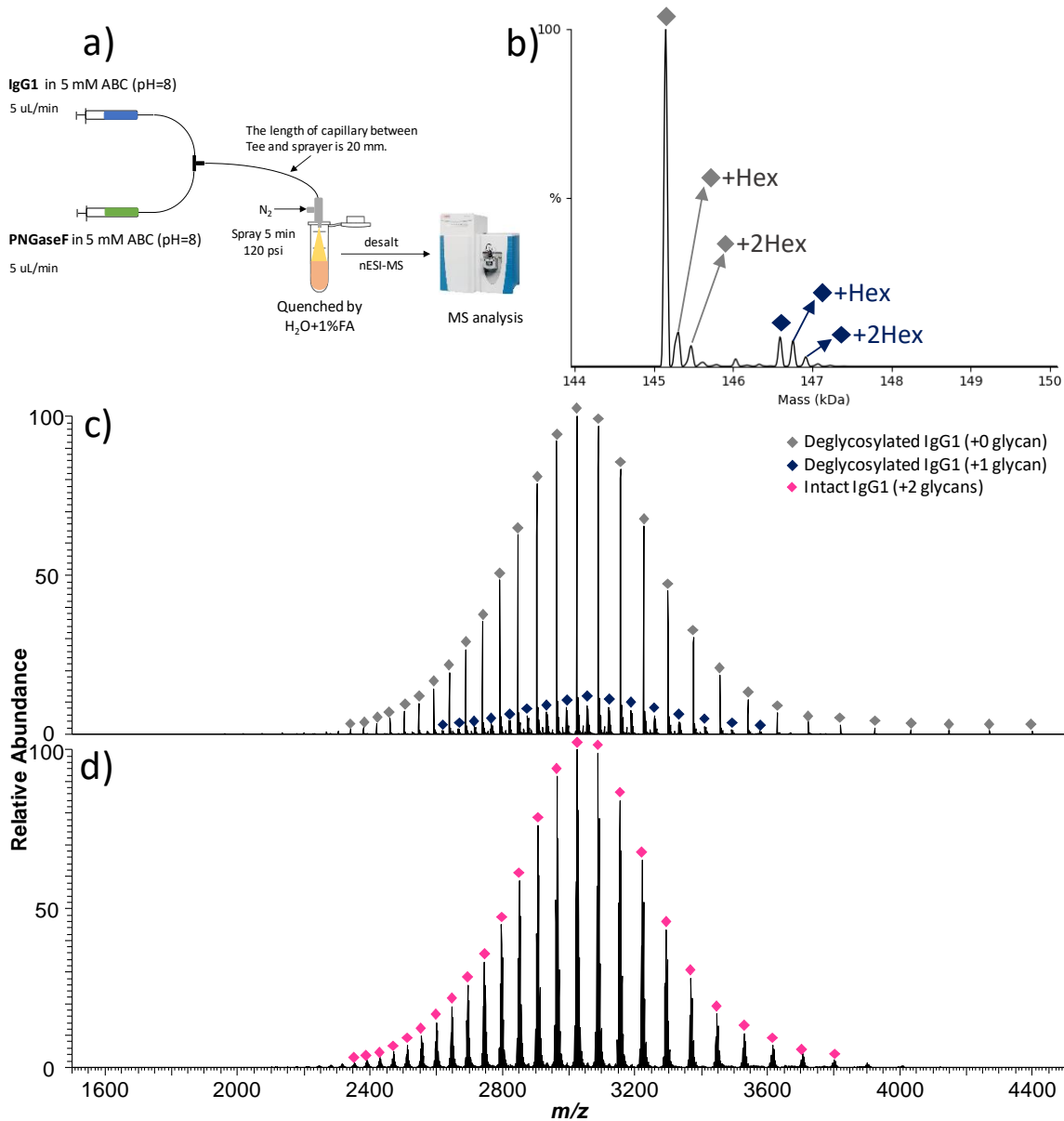


Figure 7.8 a) Schematic of microdroplet deglycosylation workflow; b) Deconvoluted MS spectrum of deglycosylated IgG1 by microdroplet reaction; c) MS spectrum of deglycosylated IgG1 by PNGase F in microdroplets at room temperature; d) MS spectrum of intact IgG1 as a comparison.

We further tested a stepwise workflow in which the IgG1 was first deglycosylated by PNGase F and then reduced and digested by addition of IdeS and TCEP at a second step (Figure 7.9a). In this workflow, the IgG1 and PNGase F were mixed via a Tee and sprayed as microdroplets to remove N-glycans from IgG1. Then, the collected microdroplets were

mixed with IdeS and TCEP and sprayed again to accelerate reduction and digestion in the microdroplets. The deglycosylated IgG1 was reduced and digested into LC, Fd', and deglycosylated scFc fragments. The collected microdroplets were reconstituted and desalted for nESI-MS analysis. Figure 7.9b shows that all the fragments were observed clearly in the MS spectra. In addition, we did not observe any glycosylated (G0F, G1F, and G2F) scFc fragments; thus, deglycosylation in the microdroplets appeared to be 100% efficient, a fact that was confirmed in the deconvoluted MS spectrum (Figure 7.9c). Therefore, by conducting deglycosylation in the microdroplets, non-glycosylated antibody fragments can be obtained for rapid structure characterization, thereby avoiding the influence of the complex profiles of the N-glycans.

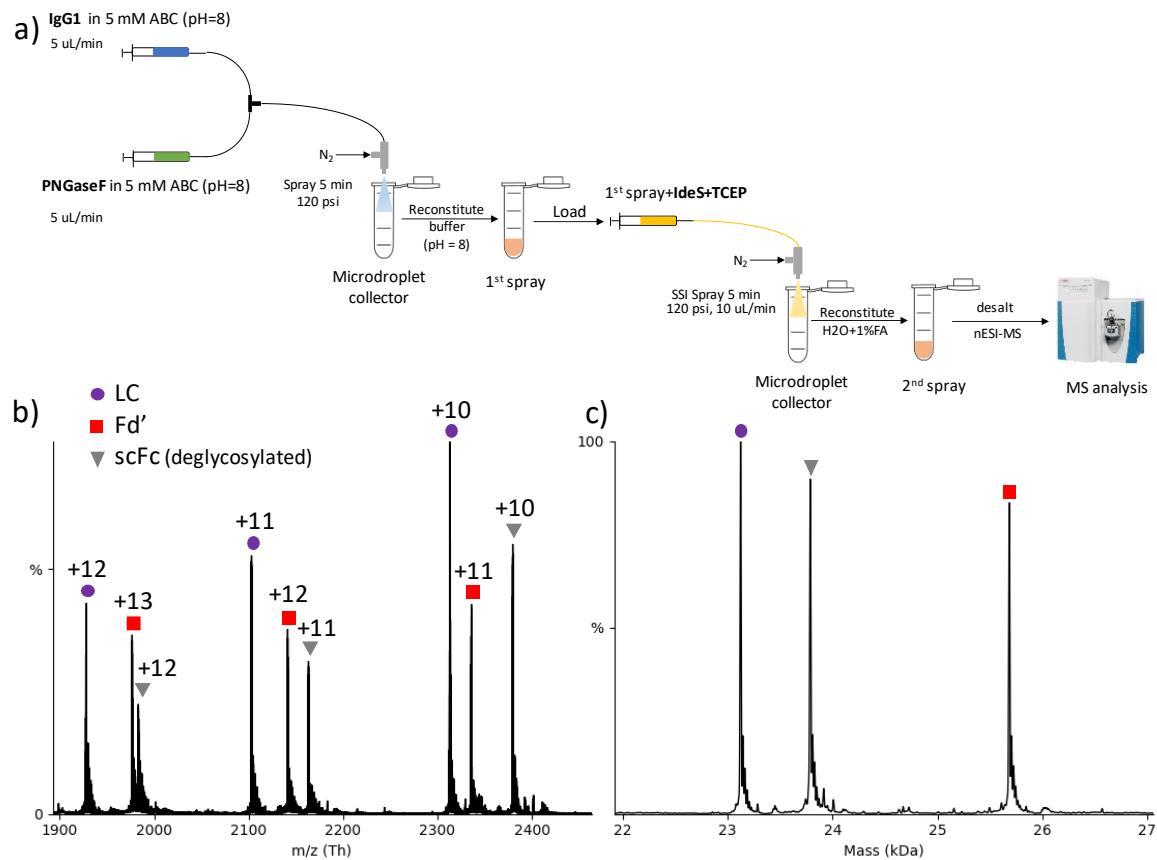


Figure 7.9 Microdroplet deglycosylation and subsequent digestion/reduction of IgG1. (a) Schematic of the deglycosylation of IgG1 in the microdroplet followed with microdroplet IdeS cleavage and TCEP reduction. (b) The expanded MS spectrum with LC, Fd', and deglycosylated scFc fragments detected and annotated. (c) The deconvoluted MS spectrum of b).

We went on to perform an “one-pot reaction” test, in which IgG1, PNGase F, IdeS and TCEP were mixed and sprayed for triggering simultaneously deglycosylation, digestion, and reduction in microdroplets. We observed the LC, Fd', and scFc (both deglycosylated and glycosylated) fragments by nESI-MS analysis after microdroplet reaction and sample collection (Figures 7.7b and 7.7c). Although deglycosylation of scFc was not complete (approximately 40% deglycosylation efficiency) in this trial, the results indicated that antibody digestion, deglycosylation, and reduction can occur simultaneously in the microdroplets in a short amount of time (250 μ s).

7.4 Conclusion

Currently, microdroplet reactions have been applied to many small molecule substrates, for various purposes including 1) synthesis of organic products and nanoparticles^{273,333}, 2) kinetic measurements²⁷¹, 3) rapid derivatization^{268,334} or degradation³³⁵, and 4) chemical behavior and fundamental studies²⁷⁴. Typically, only one-step reaction was involved in these reported microdroplet reactions. Biochemical reactions in microdroplets were rarely reported so far, with exception of the syntheses of sugar phosphates and uridine ribonucleoside via condensation²⁷⁵ and trypsin digestion of peptides and small proteins in microdroplets.³⁰¹ Our work represents the first report of multiple-step reactions involving a large protein of intact antibody in microdroplets.

In summary, we demonstrated ultrafast IdeS digestion of intact antibody in microdroplets. We achieved and detected digestion in 250 microseconds, a vastly improved efficiency compared with conventional in-solution digestion. Further ultrafast reduction is feasible by doping the spray solvent with TCEP, leading to the IdeS-cleaved and TCEP-reduced fragments (LC, Fd' and scFc with different glycoforms). Moreover, we have shown that microdroplet digestion can be achieved in both volatile and nonvolatile aqueous buffers; thus, other biochemical reactions are likely to occur in microdroplets. In addition, glycosylated IgG1 after incubation with glucose was digested successfully in microdroplets and analyzed by MS. Furthermore, microdroplet reaction coupled with online EESI-MS analysis would be an alternative approach having the least time for digestion, reduction and detection without sample pre-treatment. We also achieved rapid deglycosylation of IgG1 by PNGase F enzyme in the microdroplets. Although only NIST IgG1 was selected

as a test sample, we believe that all these workflows and approaches are general and will greatly aid efforts to reduce analysis time and improve throughput of mAb characterization.

CHAPTER 8

SUMMARY AND FUTURE WORK

In summary, this dissertation presents several mass spectrometric-based designs and setups have been applied to biomolecule quantitation analysis and structural elucidation. Three projects are absolute quantitation of various biomolecules by coulometric mass spectrometry (CMS). And one project focuses on structural elucidation by using atmospheric pressure thermal dissociation and mass spectrometry (APTD-MS).

To absolute quantify various biomolecules, a novel quantitation method has been developed by using coulometric mass spectrometry (CMS). The strength of this method is that no reference standard or isotope-labeled compound is required for absolute quantitation. The method relies on electrochemical oxidation of an electrochemically active target compound to determine the amount of the oxidized compound using Faraday's Law. On the other hand, the oxidation reaction yield can be determined based on the MS signal change following electrolysis. Therefore, the absolute amount of the analyte can be calculated. In the project for quantifying the mixture of dopamine and serotonin, this method is optimized and proved to quantify the compounds in a mixture after the chromatographic separation. Gradient elution is used for separation and each compound can be quantified using the electrochemical mass spectrometry method.

To apply the CMS method for quantifying peptides, the tyrosine-containing peptides are targeted and are electrochemically oxidized to generate current, which according to the Faraday's Law, provides the numbers of moles of oxidized analyte peptides. The ion intensity ratio of the target peptide before and after oxidation provides an excellent estimate of the fraction of the peptide that has been oxidized, from which the

total amount of peptide is calculated. This method is also applicable to quantify phosphopeptides and could be useful to the investigation of post-translational modifications on the peptides and proteins.

Furthermore, the CMS method has been further applied to absolute quantify proteins, based on the electrochemical oxidation of a surrogate tyrosine-containing peptide combined with mass spectrometric measurement of the oxidation yield. Several proteins were quantified such as model proteins β -casein and apomyoglobin as well as circadian clock protein KaiB isolated from *E. coli*. Our data showed that the results for surrogate peptide quantity measured by our method and by traditional isotope dilution method are in excellent agreement, with the discrepancy of 0.3-3%, validating our CMS method for absolute quantitation. Besides, therapeutic monoclonal antibody (mAb) could be quantified by CMS as well. Due to the high specificity and sensitivity of MS and no need to use isotope-labeled peptide standards, the CMS method would be of high value for the absolute proteomic quantification. For the future of CMS project, absolute quantitation of other intact proteins or protein complexes could be explored in the next steps. Besides, it would be also useful and important to develop a CMS method for relative quantitation of intact proteins.

In the APTD-MS project, it is of importance to elucidate ion dissociation patterns for structural analysis by mass spectrometry (MS). However, typically, only the charged fragments from an ion dissociation event are detected in tandem MS experiments; neutrals are not identified. Herein, we have presented an atmospheric pressure thermal dissociation (APTD) technique that can be applied to dissociate ions at atmosphere pressure and thus provide one way to characterize neutral fragments. By using this technique, we focus on

the detection of neutral CO resulting from amino acid and peptide ion dissociation. In the future, more meaningful analytes could be investigated by APTD-MS in order to study dissociation mechanisms at the ambient environment. For the future of APTD-MS project, it would be valuable to explore more fragmentation mechanisms of other biomolecules under ambient environment.

In the project for detecting intermediates in gold-catalyzed reactions, due to high oxidation potential between Au(I) and Au(III), gold redox catalysis requires at least stoichiometric amount of strong oxidants. We herein report the first example of electrochemical approach in promoting gold-catalyzed oxidative coupling of terminal alkynes. Oxidation of Au(I) to Au(III) was successfully achieved through anode oxidation, which enabled facile access to either symmetrical or unsymmetrical conjugated diynes via homo-coupling or cross-coupling. This study not only extends reaction scope with substrates that are not compatible with strong chemical oxidants, but also opens the possibility to conduct versatile gold redox chemistry under more efficient electro-chemical conditions.

In the microdroplet project, structural characterization of monoclonal antibodies is essential to assess its quality as a therapeutic drug, which often requires a time-consuming digestion process (>30 min). Herein we present a means to dramatically shorten the intact antibody digestion time. We digested IgG1 with IdeS protease in aqueous microdroplets. The time required was 0.25 milliseconds, a 7.5 million-fold improvement in speed. Strikingly, inclusion of the reductant tris(2-carboxyethyl)phosphine in the spray solution caused simultaneous antibody digestion and disulfide bond reduction. Digested and reduced antibody fragments were either collected or online analyzed by mass spectrometry

(MS). Further addition of PNGase F glycosylase into the spray solution led to antibody deglycosylation, thereby producing reduced and deglycosylated fragments of analytical importance. In addition, glycated fragments of IgG1 derived from glucose modification were identified quickly with this ultrafast digestion technique. We suggest that ultrafast microdroplet digestion can be used to advantage in high-throughput analysis of intact antibodies.

REFERENCES

- (1) McLafferty, F. W. A Century of Progress in Molecular Mass Spectrometry. *Annu. Rev. Anal. Chem.* **2011**, *4* (1), 1–22.
- (2) McLafferty, F. W. Tandem Mass Spectrometry: From Infancy to Maturity in Twenty-Five Years. *Org. Mass Spectrom.* **1993**, *28* (12), 1403–1406.
- (3) McLafferty, F. W. Analytical Information from Mass Spectrometry, Past and Future. *J. Am. Soc. Mass Spectrom.* **1990**, *1* (1), 1–5.
- (4) McLafferty, F. W. Mass Spectrometry across the Sciences. *Proc. Natl. Acad. Sci.* **2008**, 18088–18089.
- (5) Baghel, U. S.; Singh, A.; Singh, D.; Sinha, M. Application of Mass Spectroscopy in Pharmaceutical and Biomedical Analysis. *Spectroscopic Analyses - Developments and Applications*. London, United Kingdom: InTech, 2017.
- (6) McNaught, A. D.; Wilkinson, A. *IUPAC Compendium of Chemical Terminology*, 2nd ed.; Oxford, United Kingdom: Blackwell Scientific Publications, 1997.
- (7) Griffiths, J. A Brief History of Mass Spectrometry. *Anal Chem.* **2008**, 5678–5683.
- (8) Dass, C. *Fundamentals of Contemporary Mass Spectrometry*. Hoboken, NJ: John Wiley & Sons, Inc., 2007.
- (9) Głuch, K.; Cytawa, J.; Michalak, L. Electron Impact Ionization of Acrylonitrile. *Int. J. Mass Spectrom.* **2008**, *278* (1), 10–14.
- (10) Yamashita, M.; Fenn, J. B. Electrospray Ion Source. Another Variation on the Free-Jet Theme. *J. Phys. Chem.* **1984**, *88* (20), 4451–4459.
- (11) Zeleny, J. The Electrical Discharge from Liquid Points, and a Hydrostatic Method of Measuring the Electric Intensity at Their Surfaces. *Phys. Rev.* **1914**, *3* (2), 69–91.
- (12) Munson, M. S. B.; Field, F. H. Chemical Ionization Mass Spectrometry. I. General Introduction. *J. Am. Chem. Soc.* **1966**, *88* (12), 2621–2630.
- (13) Dole, M.; Mack, L. L.; Hines, R. L.; Chemistry, D. O.; Mobley, R. C.; Ferguson, L. D.; Alice, M. B. Molecular Beams of Macroions. *J. Chem. Phys.* **1968**, *49* (5), 2240–2249.
- (14) Iribarne, J. V.; Thomson, B. A. On the Evaporation of Small Ions from Charged Droplets. *J. Chem. Phys.* **1976**, *64* (6), 2287–2294.

- (15) Bottrill, A. R. High-Energy Collision-Induced Dissociation of Macromolecules Using Tandem Double-Focusing/Time-of-Flight Mass Spectrometry, University of Warwick, 2000.
- (16) Cech, N. B.; Enke, C. G. Practical Implications of Some Recent Studies in Electrospray Ionization Fundamentals. *Mass Spectrom. Rev.* **2001**, *20* (6), 362–387.
- (17) Wilm, M.; Mann, M. Analytical Properties of the Nanoelectrospray Ion Source. *Anal. Chem.* **1996**, *68* (1), 1–8.
- (18) Takáts, Z.; Wiseman, J. M.; Gologan, B.; Cooks, R. G. Electrosonic Spray Ionization. A Gentle Technique for Generating Folded Proteins and Protein Complexes in the Gas Phase and for Studying Ion-Molecule Reactions at Atmospheric Pressure. *Anal. Chem.* **2004**, *76* (14), 4050–4058.
- (19) Wang, R.; Allmendinger, P.; Zhu, L.; Gröhn, A. J.; Wegner, K.; Frankevich, V.; Zenobi, R. The Role of Nebulizer Gas Flow in Electrosonic Spray Ionization (ESSI). *J. Am. Soc. Mass Spectrom.* **2011**, *22*, 1234–1241.
- (20) Takáts, Z.; Wiseman, J. M.; Gologan, B.; Cooks, R. G. Mass Spectrometry Sampling under Ambient Conditions with Desorption Electrospray Ionization. *Science.* **2004**, *306* (5695), 471–473.
- (21) Liu, J.; Wang, H.; Manicke, N. E.; Lin, J. M.; Cooks, R. G.; Ouyang, Z. Development, Characterization, and Application of Paper Spray Ionization. *Anal. Chem.* **2010**, *82* (6), 2463–2471.
- (22) Takáts, Z.; Wiseman, J. M.; Cooks, R. G. Ambient Mass Spectrometry Using Desorption Electrospray Ionization (DESI): Instrumentation, Mechanisms and Applications in Forensics, Chemistry, and Biology. *J. Mass Spectrom.* **2005**, 1261–1275.
- (23) Wiseman, J. M.; Puolitaival, S. M.; Takáts, Z.; Cooks, R. G.; Caprioli, R. M. Mass Spectrometric Profiling of Intact Biological Tissue by Using Desorption Electrospray Ionization. *Angew. Chemie - Int. Ed.* **2005**, *44* (43), 7094–7097.
- (24) Dénes, J.; Katona, M.; Hosszú, Á.; Czuczy, N.; Takáts, Z. Analysis of Biological Fluids by Direct Combination of Solid Phase Extraction and Desorption Electrospray Ionization Mass Spectrometry. *Anal. Chem.* **2009**, *81* (4), 1669–1675.
- (25) Cooks, R. G.; Ouyang, Z.; Takats, Z.; Wiseman, J. M. Ambient Mass Spectrometry. *Science.* **2006**, 1566–1570.
- (26) Libarondi, M.; Binkley, J. Comparing the Capabilities of Time-of-Flight and Quadrupole Mass Spectrometers. *LCGC.* **2010**, *8* (3), 28–33.

- (27) Kaklamanos, G.; Aprea, E.; Theodoridis, G. Mass Spectrometry: Principles and Instrumentation. *Encyclo. Food. Health.* **2015**, 661–668.
- (28) Santoiemma, G. Recent Methodologies for Studying the Soil Organic Matter. *Appl. Soil Ecol.* **2018**, *123*, 546–550.
- (29) Tong, Q.; Yu, Q.; Jin, X.; He, J.; Hang, W.; Huang, B. Semi-Quantitative Analysis of Geological Samples Using Laser Plasma Time-of-Flight Mass Spectrometry. *J. Anal. At. Spectrom.* **2009**, *24* (2), 228–231.
- (30) Douglas, D. J.; Frank, A. J.; Mao, D. Linear Ion Traps in Mass Spectrometry. *Mass Spectrom. Rev.* **2005**, *24* (1), 1–29.
- (31) Schwartz, J. C.; Senko, M. W.; Syka, J. E. P. A Two-Dimensional Quadrupole Ion Trap Mass Spectrometer. *J. Am. Soc. Mass Spectrom.* **2002**, *13* (6), 659–669.
- (32) Scigelova, M.; Makarov, A. Orbitrap Mass Analyzer - Overview and Applications in Proteomics. In *Proteomics*; John Wiley & Sons, Ltd, 2006; Vol. 1, pp 16–21.
- (33) Savaryn, J. P.; Toby, T. K.; Kelleher, N. L. A Researcher's Guide to Mass Spectrometry-Based Proteomics. *Proteomics* **2016**, *16* (18), 2435–2443.
- (34) Atkins, P.; Paula, J. de. *Physical Chemistry for the Life Sciences*. Oxford, United Kingdom: Oxford University Press, 2015.
- (35) Oberacher; Pitterl, F.; Erb, R.; Plattner, S. Mass Spectrometric Methods for Monitoring Redox Processes in Electrochemical Cells. *Mass Spectrom. Rev.* **2015**, *34* (1), 64–92.
- (36) Hodnik, N.; Dehm, G.; Mayrhofer, K. J. J. Importance and Challenges of Electrochemical in Situ Liquid Cell Electron Microscopy for Energy Conversion Research. *Acc. Chem. Res.* **2016**, *49* (9), 2015–2022.
- (37) Fernández-Blanco, C.; Colina, Á.; Heras, A. UV/Vis Spectroelectrochemistry as a Tool for Monitoring the Fabrication of Sensors Based on Silver Nanoparticle Modified Electrodes. *Sensors* **2013**, *13* (5), 5700–5711.
- (38) You, L. X.; Rao, L.; Tian, X. C.; Wu, R. R.; Wu, X.; Zhao, F.; Jiang, Y. X.; Sun, S. G. Electrochemical in Situ FTIR Spectroscopy Studies Directly Extracellular Electron Transfer of *Shewanella Oneidensis* MR-1. *Electrochim. Acta* **2015**, *170*, 131–139.
- (39) Potęga, A.; Żelaszczyk, D.; Mazerska, Z. Electrochemical Simulation of Metabolism for Antitumor-Active Imidazoacridinone C-1311 and in Silico Prediction of Drug Metabolic Reactions. *J. Pharm. Biomed. Anal.* **2019**, *169*, 269–278.

- (40) Szultka-Młyńska, M.; Bajkacz, S.; Baranowska, I.; Buszewski, B. Structural Characterization of Electrochemically and in Vivo Generated Potential Metabolites of Selected Cardiovascular Drugs by EC-UHPLC/ESI-MS Using an Experimental Design Approach. *Talanta*. **2018**, *176*, 262–276.
- (41) Mao, F.; Yu, K.; He, J.; Zhou, Q.; Zhang, G.; Wang, W.; Li, N.; Zhang, H.; Jiang, J. Real-Time Monitoring of Electroreduction and Labelling of Disulfide-Bonded Peptides and Proteins by Mass Spectrometry. *Analyst*. **2019**, *144* (23), 6898–6904.
- (42) Cui, L.; Ma, Y.; Li, M.; Wei, Z.; Fei, Q.; Huan, Y.; Li, H.; Zheng, L. Disulfide Linkage Assignment Based on Reducing Electrochemistry and Mass Spectrometry Using a Lead Electrode. *Talanta*. **2019**, *199*, 643–651.
- (43) Zheng, Q.; Chen, H. Development and Applications of Liquid Sample Desorption Electrospray Ionization Mass Spectrometry. *Annu. Rev. Anal. Chem.* **2016**, *9* (1), 411–448.
- (44) Zheng, Q.; Zhang, H.; Wu, S.; Chen, H. Probing Protein 3D Structures and Conformational Changes Using Electrochemistry-Assisted Isotope Labeling Cross-Linking Mass Spectrometry. *J. Am. Soc. Mass Spectrom.* **2016**, *27* (5), 864–875.
- (45) Cai, Y.; Wang, J.; Zhang, Y.; Li, Z.; Hu, D.; Zheng, N.; Chen, H. Detection of Fleeting Amine Radical Cations and Elucidation of Chain Processes in Visible-Light-Mediated [3 + 2] Annulation by Online Mass Spectrometric Techniques. *J. Am. Chem. Soc.* **2017**, *139* (35), 12259–12266.
- (46) Brown, T. A.; Hosseini-Nassab, N.; Chen, H.; Zare, R. N. Observation of Electrochemically Generated Nitrenium Ions by Desorption Electrospray Ionization Mass Spectrometry. *Chem. Sci.* **2016**, *7* (1), 329–332.
- (47) Brown, T. A.; Chen, H.; Zare, R. N. Detection of the Short-Lived Radical Cation Intermediate in the Electrooxidation of *N,N*-Dimethylaniline by Mass Spectrometry. *Angew. Chemie Int. Ed.* **2015**, *54* (38), 11183–11185.
- (48) Brown, T. A.; Chen, H.; Zare, R. N. Identification of Fleeting Electrochemical Reaction Intermediates Using Desorption Electrospray Ionization Mass Spectrometry. *J. Am. Chem. Soc.* **2015**, *137* (23), 7274–7277.
- (49) Van Berkel, G. J.; McLuckey, S. A.; Glish, G. L. Electrochemical Origin of Radical Cations Observed in Electrospray Ionization Mass Spectra. *Anal. Chem.* **1992**, *64* (14), 1586–1593.
- (50) Charbonnier, F.; Rolando, C.; Saru, F.; Hapiot, P.; Pinson, J. Short Time-Scale Observation of an Electrospray Current. *Rapid Commun. Mass Spectrom.* **1993**, *7* (8), 707–710.

- (51) Blades, A. T.; Ikonou, M. G.; Kebarle, P. Mechanism of Electrospray Mass Spectrometry. Electrospray as an Electrolysis Cell. *Anal. Chem.* **1991**, *63* (19), 2109–2114.
- (52) Van Baikal, G. J.; Zhou, F. Characterization of an Electrospray Ion Source as a Controlled-Current Electrolytic Cell. *Anal. Chem.* **1995**, *67* (17), 2916–2923.
- (53) Van Berkel, G. J.; Zhou, F. Electrospray as a Controlled-Current Electrolytic Cell: Electrochemical Ionization of Neutral Analytes for Detection by Electrospray Mass Spectrometry. *Anal. Chem.* **1995**, *67* (21), 3958–3964.
- (54) Dupont, A.; Gisselbrecht, J. P.; Leize, E.; Wagner, L.; Dorsselaer, A. Van. Electrospray Mass Spectrometry of Electrochemically Ionized Molecules: Application to the Study of Fullerenes. *Tetrahedron Lett.* **1994**, *35* (33), 6083–6086.
- (55) Van Baikal, G. J.; Zhou, F. Electrochemistry Combined Online with Electrospray Mass Spectrometry. *Anal. Chem.* **1995**, *67* (20), 3643–3649.
- (56) Diehl, G.; Liesener, A.; Karst, U. Liquid Chromatography with Post-Column Electrochemical Treatment and Mass Spectrometric Detection of Non-Polar Compounds. *Analyst.* **2001**, *126* (3), 288–290.
- (57) Frensemeier, L. M.; Büter, L.; Vogel, M.; Karst, U. Investigation of the Oxidative Transformation of Roxarsone by Electrochemistry Coupled to Hydrophilic Interaction Liquid Chromatography/Mass Spectrometry. *J. Anal. At. Spectrom.* **2017**, *32* (1), 153–161.
- (58) Mekonnen, T. F.; Panne, U.; Koch, M. Electrochemistry Coupled Online to Liquid Chromatography-Mass Spectrometry for Fast Simulation of Biotransformation Reactions of the Insecticide Chlorpyrifos. *Anal. Bioanal. Chem.* **2017**, *409* (13), 3359–3368.
- (59) Mekonnen, T. F.; Panne, U.; Koch, M. Prediction of Biotransformation Products of the Fungicide Fluopyram by Electrochemistry Coupled Online to Liquid Chromatography-Mass Spectrometry and Comparison with in Vitro Microsomal Assays. *Anal. Bioanal. Chem.* **2018**, *410* (10), 2607–2617.
- (60) Zhang, T.; De Vries, M. P.; Permentier, H. P.; Bischoff, R. Specific Affinity Enrichment of Electrochemically Cleaved Peptides Based on Cu(II)-Mediated Spirolactone Tagging. *Anal. Chem.* **2017**, *89* (13), 7123–7129.
- (61) Xu, C.; Zheng, Q.; Zhao, P.; Paterson, J.; Chen, H. A New Quantification Method Using Electrochemical Mass Spectrometry. *J. Am. Soc. Mass Spectrom.* **2019**, *30* (4), 685–693.

- (62) Cooks, R. G.; Yan, X. Mass Spectrometry for Synthesis and Analysis. *Annu. Rev. Anal. Chem.* **2018**, *11* (1), 1–28.
- (63) Loo, J. A. Studying Noncovalent Protein Complexes by Electrospray Ionization Mass Spectrometry. *Mass Spectrom. Rev.* **1997**, *16* (1), 1–23.
- (64) Cui, W.; Rohrs, H. W.; Gross, M. L. Top-down Mass Spectrometry: Recent Developments, Applications and Perspectives. *Analyst* **2011**, *136* (19), 3854.
- (65) Zhang, H.; Cui, W.; Gross, M. L.; Blankenship, R. E. Native Mass Spectrometry of Photosynthetic Pigment-Protein Complexes. *FEBS Lett.* **2013**, *587* (8), 1012–1020.
- (66) Brodbelt, J. S. Photodissociation Mass Spectrometry: New Tools for Characterization of Biological Molecules. *Chem. Soc. Rev.* **2014**, *43* (8), 2757–2783.
- (67) Aebersold, R.; Mann, M. Mass Spectrometry-Based Proteomics. *Nature*. **2003**, *422* (6928), 198–207.
- (68) Clough, T.; Key, M.; Ott, I.; Ragg, S.; Schadow, G.; Vitek, O. Protein Quantification in Label-Free LC-MS Experiments. *J. Proteome Res.* **2009**, *8* (11), 5275–5284.
- (69) Sohn, C. H.; Lee, J. E.; Sweredoski, M. J.; Graham, R. L. J.; Smith, G. T.; Hess, S.; Czerwiec, G.; Loo, J. A.; Deshaies, R. J.; Beauchamp, J. L. Click Chemistry Facilitates Formation of Reporter Ions and Simplified Synthesis of Amine-Reactive Multiplexed Isobaric Tags for Protein Quantification. *J. Am. Chem. Soc.* **2012**, *134* (5), 2672–2680.
- (70) Hopfgartner, G.; Tonoli, D.; Varesio, E. High-Resolution Mass Spectrometry for Integrated Qualitative and Quantitative Analysis of Pharmaceuticals in Biological Matrices. *Anal. Bioanal. Chem.* **2012**, *402* (8), 2587–2596.
- (71) Verplaetse, R.; Henion, J. Quantitative Determination of Opioids in Whole Blood Using Fully Automated Dried Blood Spot Desorption Coupled to On-Line SPE-LC-MS/MS. *Drug Test. Anal.* **2016**, *8* (1), 30–38.
- (72) Heck, A. J.; Krijgsveld, J. Mass Spectrometry-Based Quantitative Proteomics. *Expert Rev. Proteomics.* **2004**, *1* (3), 317–326.
- (73) Sechi, S.; Oda, Y. Quantitative Proteomics Using Mass Spectrometry. *Curr. Opin. Chem. Biol.* **2003**, *7* (1), 70–77.
- (74) Righetti, P. G.; Campostrini, N.; Pascali, J.; Hamdan, M.; Astner, H. Quantitative Proteomics: A Review of Different Methodologies. *Eur. J. Mass Spectrom.* **2004**, *10* (3), 335–348.

- (75) Gygi, S. P.; Rist, B.; Gerber, S. A.; Turecek, F.; Gelb, M. H.; Aebersold, R. Quantitative Analysis of Complex Protein Mixtures Using Isotope-Coded Affinity Tags. *Nat. Biotechnol.* **1999**, *17* (10), 994–999.
- (76) Ong, S.-E.; Foster, L. J.; Mann, M. Mass Spectrometric-Based Approaches in Quantitative Proteomics. *Methods* **2003**, *29* (2), 124–130.
- (77) Tao, W. A.; Aebersold, R. Advances in Quantitative Proteomics via Stable Isotope Tagging and Mass Spectrometry. *Curr. Opin. Biotechnol.* **2003**, *14* (1), 110–118.
- (78) Ong, S.-E.; Mann, M. Mass Spectrometry–Based Proteomics Turns Quantitative. *Nat. Chem. Biol.* **2005**, *1* (5), 252–262.
- (79) Ong, S.-E.; Blagoev, B.; Kratchmarova, I.; Kristensen, D. B.; Steen, H.; Pandey, A.; Mann, M. Stable Isotope Labeling by Amino Acids in Cell Culture, SILAC, as a Simple and Accurate Approach to Expression Proteomics. *Mol. Cell. Proteomics* **2002**, *1* (5), 376–386.
- (80) Krijgsveld, J.; Ketting, R. F.; Mahmoudi, T.; Johansen, J.; Artal-Sanz, M.; Verrijzer, C. P.; Plasterk, R. H. A.; Heck, A. J. R. Metabolic Labeling of *C. Elegans* and *D. Melanogaster* for Quantitative Proteomics. *Nat. Biotechnol.* **2003**, *21* (8), 927–931.
- (81) Wu, C. C.; MacCoss, M. J.; Howell, K. E.; Dwight E. Matthews, A.; Yates, J. R. Metabolic Labeling of Mammalian Organisms with Stable Isotopes for Quantitative Proteomic Analysis. *Anal. Chem.* **2004**, *76* (17), 4951–4959.
- (82) Gruhler, A.; Schulze, W. X.; Matthiesen, R.; Mann, M.; Jensen, O. N. Stable Isotope Labeling of *Arabidopsis Thaliana* Cells and Quantitative Proteomics by Mass Spectrometry. *Mol. Cell. Proteomics* **2005**, *4* (11), 1697–1709.
- (83) Sturm, R. M.; Lietz, C. B.; Li, L. Improved Isobaric Tandem Mass Tag Quantification by Ion Mobility Mass Spectrometry. *Rapid Commun. Mass Spectrom.* **2014**, *28* (9), 1051–1060.
- (84) Thompson, A.; Schäfer, J.; Kuhn, K.; Kienle, S.; Schwarz, J.; Schmidt, G.; Neumann, T.; Hamon, C. Tandem Mass Tags: A Novel Quantification Strategy for Comparative Analysis of Complex Protein Mixtures by MS/MS. *Anal Chem* **2003**, *75* (8), 1895–1904.
- (85) Zhang, H.; Li, X.; Martin, D. B.; Aebersold, R. Identification and Quantification of N-Linked Glycoproteins Using Hydrazide Chemistry, Stable Isotope Labeling and Mass Spectrometry. *Nat. Biotechnol.* **2003**, *21* (6), 660–666.

- (86) Ross, P. L.; Huang, Y. N.; Marchese, J. N.; Williamson, B.; Parker, K.; Hattan, S.; Khainovski, N.; Pillai, S.; Dey, S.; Daniels, S.; Purkayastha, S.; Juhasz, P.; Martin, S.; Bartlet-Jones, M.; He, F.; Jacobson, A.; Pappin, D. J. Multiplexed Protein Quantitation in *Saccharomyces Cerevisiae* Using Amine-Reactive Isobaric Tagging Reagents. *Mol. Cell. Proteomics* **2004**, *3* (12), 1154–1169.
- (87) Liu, H.; Zhang, Y.; Wang, J.; Wang, D.; Zhou, C.; Cai, Y.; Qian, X. Method for Quantitative Proteomics Research by Using Metal Element Chelated Tags Coupled with Mass Spectrometry. *Anal. Chem.* **2006**, *78* (18), 6614–6621.
- (88) Schmidt, A.; Kellermann, J.; Lottspeich, F. A Novel Strategy for Quantitative Proteomics Using Isotope-Coded Protein Labels. *Proteomics*. **2005**, *5* (1), 4–15.
- (89) Bantscheff, M.; Schirle, M.; Sweetman, G.; Rick, J.; Kuster, B. Quantitative Mass Spectrometry in Proteomics: A Critical Review. *Anal. Bioanal. Chem.* **2007**, *389* (4), 1017–1031.
- (90) Bantscheff, M.; Lemeer, S.; Savitski, M. M.; Kuster, B. Quantitative Mass Spectrometry in Proteomics: Critical Review Update from 2007 to the Present. *Anal. Bioanal. Chem.* **2012**, *404* (4), 939–965.
- (91) Boyd, R. K.; Basic, C.; Bethem, R. A. *Trace Quantitative Analysis by Mass Spectrometry*. Hoboken, NJ: John Wiley & Sons, Inc., 2008.
- (92) Korfmacher, W. A. *Mass Spectrometry for Drug Discovery and Drug Development*. Hoboken, NJ: John Wiley & Sons, Inc., 2013.
- (93) Xu, C.; Zheng, Q.; Zhao, P.; Paterson, J.; Chen, H. A New Quantification Method Using Electrochemical Mass Spectrometry. *J. Am. Soc. Mass Spectrom.* **2019**, *30* (4), 685–693.
- (94) Guo, Y.; Bhalodia, N.; Fattal, B.; Serris, I.; Guo, Y.; Bhalodia, N.; Fattal, B.; Serris, I. Evaluating the Adsorbed Water Layer on Polar Stationary Phases for Hydrophilic Interaction Chromatography (HILIC). *Separations*. **2019**, *6* (2), 19.
- (95) B. V. Sarada; Tata N. Rao; D. A. Tryk, A.; Fujishima, A. Electrochemical Oxidation of Histamine and Serotonin at Highly Boron-Doped Diamond Electrodes. *Anal. Chem.* **2000**, *72* (7), 1632–1638.
- (96) Ong, S.-E.; Mann, M. Mass Spectrometry–Based Proteomics Turns Quantitative. *Nat. Chem. Biol.* **2005**, *1* (5), 252–262.
- (97) Bantscheff, M.; Lemeer, S.; Savitski, M. M.; Kuster, B. Quantitative Mass Spectrometry in Proteomics: Critical Review Update from 2007 to the Present. *Anal. Bioanal. Chem.* **2012**, *404* (4), 939–965.

- (98) Schubert, O. T.; Röst, H. L.; Collins, B. C.; Rosenberger, G.; Aebersold, R. Quantitative Proteomics: Challenges and Opportunities in Basic and Applied Research. *Nat. Protoc.* **2017**, *12* (7), 1289–1294.
- (99) Li, H.; Han, J.; Pan, J.; Liu, T.; Parker, C. E.; Borchers, C. H. Current Trends in Quantitative Proteomics - an Update. *J. Mass Spectrom.* **2017**, *52* (5), 319–341.
- (100) Gallien, S.; Duriez, E.; Crone, C.; Kellmann, M.; Moehring, T.; Domon, B. Targeted Proteomic Quantification on Quadrupole-Orbitrap Mass Spectrometer. *Mol. Cell. Proteomics.* **2012**, *11* (12), 1709–1723.
- (101) Li, Q.; Zubieta, J.-K.; Kennedy, R. T. Practical Aspects of in Vivo Detection of Neuropeptides by Microdialysis Coupled Off-Line to Capillary LC with Multistage MS. *Anal. Chem.* **2009**, *81* (6), 2242–2250.
- (102) Zhang, F.; Xiao, Y.; Wang, Y. SILAC-Based Quantitative Proteomic Analysis Unveils Arsenite-Induced Perturbation of Multiple Pathways in Human Skin Fibroblast Cells. *Chem. Res. Toxicol.* **2017**, *30* (4), 1006–1014.
- (103) Serrano, M. A. C.; He, H.; Zhao, B.; Ramireddy, R. R.; Vachet, R. W.; Thayumanavan, S. Polymer-Mediated Ternary Supramolecular Interactions for Sensitive Detection of Peptides. *Analyst.* **2016**, *142* (1), 118–122.
- (104) Patti, G. J.; Chen, J.; Gross, M. L. Method Revealing Bacterial Cell-Wall Architecture by Time-Dependent Isotope Labeling and Quantitative Liquid Chromatography/Mass Spectrometry. *Anal. Chem.* **2009**, *81* (7), 2437–2445.
- (105) Jiang, W.; Wysocki, V. H.; Dodds, E. D.; Miesfeld, R. L.; Scaraffia, P. Y. Differentiation and Quantification of C1 and C2 ¹³C-Labeled Glucose by Tandem Mass Spectrometry. *Anal. Biochem.* **2010**, *404* (1), 40–44.
- (106) Lindemann, C.; Thomanek, N.; Hundt, F.; Lerari, T.; Meyer, H. E.; Wolters, D.; Marcus, K. Strategies in Relative and Absolute Quantitative Mass Spectrometry Based Proteomics. *Biol. Chem.* **2017**, *398* (5–6), 687–699.
- (107) Neilson, K. A.; Ali, N. A.; Muralidharan, S.; Mirzaei, M.; Mariani, M.; Assadourian, G.; Lee, A.; van Sluyter, S. C.; Haynes, P. A. Less Label, More Free: Approaches in Label-Free Quantitative Mass Spectrometry. *Proteomics.* **2011**, *11* (4), 535–553.
- (108) Wang, W.; Zhou, H.; Lin, H.; Roy, S.; Shaler, T. A.; Hill, L. R.; Norton, S.; Kumar, P.; Anderle, M.; Becker, C. H. Quantification of Proteins and Metabolites by Mass Spectrometry without Isotopic Labeling or Spiked Standards. *Anal. Chem.* **2003**, *75* (18), 4818–4826.
- (109) Sechi, S.; Oda, Y. Quantitative Proteomics Using Mass Spectrometry. *Curr. Opin. Chem. Biol.* **2003**, *7* (1), 70–77.

- (110) Righetti, P. G.; Campostrini, N.; Pascali, J.; Hamdan, M.; Astner, H. Quantitative Proteomics: A Review of Different Methodologies. *Eur. J. Mass Spectrom.* **2004**, *10* (3), 335–348.
- (111) Ong, S.-E.; Foster, L. J.; Mann, M. Mass Spectrometric-Based Approaches in Quantitative Proteomics. *Methods.* **2003**, *29* (2), 124–130.
- (112) Wu, C. C.; MacCoss, M. J.; Howell, K. E.; Matthews, D. E.; Yates, J. R. Metabolic Labeling of Mammalian Organisms with Stable Isotopes for Quantitative Proteomic Analysis. *Anal. Chem.* **2004**, *76* (17), 4951–4959.
- (113) Gruhler, A.; Schulze, W. X.; Matthiesen, R.; Mann, M.; Jensen, O. N. Stable Isotope Labeling of *Arabidopsis Thaliana* Cells and Quantitative Proteomics by Mass Spectrometry. *Mol. Cell. Proteomics* **2005**, *4* (11), 1697–1709.
- (114) Wiese, S.; Reidegeld, K. A.; Meyer, H. E.; Warscheid, B. Protein Labeling by ITRAQ: A New Tool for Quantitative Mass Spectrometry in Proteome Research. *Proteomics.* **2007**, *7* (3), 340–350.
- (115) Thompson, A.; Schäfer, J.; Kuhn, K.; Kienle, S.; Schwarz, J.; Schmidt, G.; Neumann, T.; Johnstone, R.; Mohammed, A. K. A.; Hamon, C. Tandem Mass Tags: A Novel Quantification Strategy for Comparative Analysis of Complex Protein Mixtures by MS/MS. *Anal. Chem.* **2003**, *75* (8), 1895–1904.
- (116) Han, H.; Pappin, D. J.; Ross, P. L.; McLuckey, S. A. Electron Transfer Dissociation of ITRAQ Labeled Peptide Ions. *J. Proteome Res.* **2008**, *7* (9), 3643–3648.
- (117) Schmidt, A.; Kellermann, J.; Lottspeich, F. A Novel Strategy for Quantitative Proteomics Using Isotope-Coded Protein Labels. *Proteomics.* **2005**, *5* (1), 4–15.
- (118) Xiang, F.; Ye, H.; Chen, R.; Fu, Q.; Li, L. *N, N*-Dimethyl Leucines as Novel Isobaric Tandem Mass Tags for Quantitative Proteomics and Peptidomics. *Anal. Chem.* **2010**, *82* (7), 2817–2825.
- (119) Frost, D. C.; Greer, T.; Li, L. High-Resolution Enabled 12-Plex DiLeu Isobaric Tags for Quantitative Proteomics. *Anal. Chem.* **2015**, *87* (3), 1646–1654.
- (120) Frost, D. C.; Buchberger, A. R.; Li, L. Mass Defect-Based Dimethyl Pyrimidinyl Ornithine (DiPyrO) Tags for Multiplex Quantitative Proteomics. *Anal. Chem.* **2017**, *89* (20), 10798–10805.
- (121) Frost, D. C.; Rust, C. J.; Robinson, R. A. S.; Li, L. Increased *N, N*-Dimethyl Leucine Isobaric Tag Multiplexing by a Combined Precursor Isotopic Labeling and Isobaric Tagging Approach. *Anal. Chem.* **2018**, *90* (18), 10664–10669.

- (122) Narumi, R.; Shimizu, Y.; Ukai-Tadenuma, M.; Ode, K. L.; Kanda, G. N.; Shinohara, Y.; Sato, A.; Matsumoto, K.; Ueda, H. R. Mass Spectrometry-Based Absolute Quantification Reveals Rhythmic Variation of Mouse Circadian Clock Proteins. *Proc. Natl. Acad. Sci.* **2016**, *113* (24), E3461-7.
- (123) Lange, V.; Picotti, P.; Domon, B.; Aebersold, R. Selected Reaction Monitoring for Quantitative Proteomics: A Tutorial. *Mol. Syst. Biol.* **2008**, *4*, 222.
- (124) Boyd, B.; Basic, C.; Bethem, R. *Trace Quantitative Analysis by Mass Spectrometry*. Hoboken, NJ: John Wiley & Sons, Inc., 2008.
- (125) Harriman, A. Further Comments on the Redox Potentials of Tryptophan and Tyrosine. *J. Phys. Chem.* **1987**, *91* (24), 6102–6104.
- (126) Kozłowski, L. P. Proteome-PI: Proteome Isoelectric Point Database. *Nucleic Acids Res.* **2017**, *45* (D1), D1112–D1116.
- (127) Poole, L. B. The Basics of Thiols and Cysteines in Redox Biology and Chemistry. *Free Radic. Biol. Med.* **2015**, *80*, 148–157.
- (128) Scuderi, D.; Bergès, J.; de Oliveira, P.; Houée-Levin, C. Methionine One-Electron Oxidation: Coherent Contributions from Radiolysis, IRMPD Spectroscopy, DFT Calculations and Electrochemistry. *Radiat. Phys. Chem.* **2016**, *128*, 103–111.
- (129) Permentier, H. P.; Bruins, A. P.; Bischoff, R. Electrochemistry-Mass Spectrometry in Drug Metabolism and Protein Research. *Mini Rev. Med. Chem.* **2008**, *8* (1), 46–56.
- (130) Diehl, G.; Karst, U. On-Line Electrochemistry – MS and Related Techniques. *Anal. Bioanal. Chem.* **2002**, *373* (6), 390–398.
- (131) Gun, J.; Bharathi, S.; Gutkin, V.; Rizkov, D.; Voloshenko, A.; Shelkov, R.; Sladkevich, S.; Kyi, N.; Rona, M.; Wolanov, Y.; Rizkov, D.; Koch, M.; Mizrahi, S.; Pridkhochenko, P. V.; Modestov, A.; Lev, O. Highlights in Coupled Electrochemical Flow Cell-Mass Spectrometry, EC/MS. *Isr. J. Chem.* **2010**, *50* (3), 360–373.
- (132) Zhou, F.; Van Berkel, G. J. Electrochemistry Combined Online with Electrospray Mass Spectrometry. *Anal. Chem.* **1995**, *67* (20), 3643–3649.
- (133) Liu, Y.-M.; Perry, R. H. Paper-Based Electrochemical Cell Coupled to Mass Spectrometry. *J. Am. Soc. Mass Spectrom.* **2015**, *26* (10), 1702–1712.
- (134) Liu, Y.-M.; Nicolau, B.; Esbenshade, J. L.; Gewirth, A. A. Characterization of the Cathode Electrolyte Interface in Lithium Ion Batteries by Desorption Electrospray Ionization Mass Spectrometry. *Anal. Chem.* **2016**, *88* (14), 7171–7177.

- (135) Qiu, R.; Zhang, X.; Luo, H.; Shao, Y. Mass Spectrometric Snapshots for Electrochemical Reactions. *Chem. Sci.* **2016**, *7* (11), 6684–6688.
- (136) Cheng, H.; Yan, X.; Zare, R. N. Two New Devices for Identifying Electrochemical Reaction Intermediates with Desorption Electrospray Ionization Mass Spectrometry. *Anal. Chem.* **2017**, *89* (5), 3191–3198.
- (137) Lu, J.; Hua, X.; Long, Y.-T. Recent Advances in Real-Time and in Situ Analysis of an Electrode–Electrolyte Interface by Mass Spectrometry. *Analyst.* **2017**, *142* (5), 691–699.
- (138) van den Brink, F. T. G.; Büter, L.; Odijk, M.; Olthuis, W.; Karst, U.; van den Berg, A. Mass Spectrometric Detection of Short-Lived Drug Metabolites Generated in an Electrochemical Microfluidic Chip. *Anal. Chem.* **2015**, *87* (3), 1527–1535.
- (139) Brown, T. A.; Chen, H.; Zare, R. N. Identification of Fleeting Electrochemical Reaction Intermediates Using Desorption Electrospray Ionization Mass Spectrometry. *J. Am. Chem. Soc.* **2015**, *137* (23), 7274–7277.
- (140) Brown, T. A.; Chen, H.; Zare, R. N. Detection of the Short-Lived Radical Cation Intermediate in the Electrooxidation of *N,N*-Dimethylaniline by Mass Spectrometry. *Angew. Chemie Int. Ed.* **2015**, *54* (38), 11183–11185.
- (141) Brown, T. A.; Hosseini-Nassab, N.; Chen, H.; Zare, R. N. Observation of Electrochemically Generated Nitrenium Ions by Desorption Electrospray Ionization Mass Spectrometry. *Chem. Sci.* **2016**, *7* (1), 329–332.
- (142) Cai, Y.; Wang, J.; Zhang, Y.; Li, Z.; Hu, D.; Zheng, N.; Chen, H. Detection of Fleeting Amine Radical Cations and Elucidation of Chain Processes in Visible-Light-Mediated [3 + 2] Annulation by Online Mass Spectrometric Techniques. *J. Am. Chem. Soc.* **2017**, *139* (35), 12259–12266.
- (143) Miao, Z.; Chen, H. Direct Analysis of Liquid Samples by Desorption Electrospray Ionization-Mass Spectrometry (DESI-MS). *J. Am. Soc. Mass Spectrom.* **2009**, *20* (1), 10–19.
- (144) Li, J.; Dewald, H. D.; Chen, H. Online Coupling of Electrochemical Reactions with Liquid Sample Desorption Electrospray Ionization-Mass Spectrometry. *Anal. Chem.* **2009**, *81* (23), 9716–9722.
- (145) Zhang, Y.; Dewald, H. D.; Chen, H. Online Mass Spectrometric Analysis of Proteins/Peptides Following Electrolytic Cleavage of Disulfide Bonds. *J. Proteome Res.* **2011**, *10* (3), 1293–1304.

- (146) Zhang, Y.; Yuan, Z.; Dewald, H. D.; Chen, H. Coupling of Liquid Chromatography with Mass Spectrometry by Desorption Electrospray Ionization (DESI). *Chem. Commun.* **2011**, 47 (14), 4171–4173.
- (147) Lu, M.; Wolff, C.; Cui, W.; Chen, H. Investigation of Some Biologically Relevant Redox Reactions Using Electrochemical Mass Spectrometry Interfaced by Desorption Electrospray Ionization. *Anal. Bioanal. Chem.* **2012**, 403 (2), 355–365.
- (148) Liu, P.; Lu, M.; Zheng, Q.; Zhang, Y.; Dewald, H. D.; Chen, H. Recent Advances of Electrochemical Mass Spectrometry. *Analyst.* **2013**, 138 (19), 5519.
- (149) Zheng, Q.; Chen, H. Development and Applications of Liquid Sample Desorption Electrospray Ionization Mass Spectrometry. *Annu. Rev. Anal. Chem.* **2016**, 9 (1), 411–448.
- (150) Roeser, J.; Permentier, H. P.; Bruins, A. P.; Bischoff, R. Electrochemical Oxidation and Cleavage of Tyrosine- and Tryptophan-Containing Tripeptides. *Anal. Chem.* **2010**, 82 (18), 7556–7565.
- (151) Permentier, H. P.; Jurva, U.; Barroso, B.; Bruins, A. P. Electrochemical Oxidation and Cleavage of Peptides Analyzed with On-Line Mass Spectrometric Detection. *Rapid Commun. Mass Spectrom.* **2003**, 17 (14), 1585–1592.
- (152) Permentier, H. P.; Bruins, A. P. Electrochemical Oxidation and Cleavage of Proteins with On-Line Mass Spectrometric Detection: Development of an Instrumental Alternative to Enzymatic Protein Digestion. *J. Am. Soc. Mass Spectrom.* **2004**, 15 (12), 1707–1716.
- (153) Kageyama, R.; Ohkubo, H.; Nakanishi, S. Primary Structure of Human Preangiotensinogen Deduced from the Cloned CDNA Sequence. *Biochemistry* **1984**, 23 (16), 3603–3609.
- (154) Qu, N.; Wan, B.; Guo, L.-H. Label-Free Electrochemical Differentiation of Phosphorylated and Non-Phosphorylated Peptide by Electro-Catalyzed Tyrosine Oxidation. *Analyst.* **2008**, 133 (9), 1246–1249.
- (155) Kerman, K.; Vestergaard, M.; Chikae, M.; Yamamura, S.; Tamiya, E. Label-Free Electrochemical Detection of the Phosphorylated and Non-Phosphorylated Forms of Peptides Based on Tyrosine Oxidation. *Electrochem. commun.* **2007**, 9 (5), 976–980.
- (156) Robinson, M. R.; Moore, K. L.; Brodbelt, J. S. Direct Identification of Tyrosine Sulfation by Using Ultraviolet Photodissociation Mass Spectrometry. *J. Am. Soc. Mass Spectrom.* **2014**, 25 (8), 1461–1471.

- (157) McLachlin, D. T.; Chait, B. T. Analysis of Phosphorylated Proteins and Peptides by Mass Spectrometry. *Curr. Opin. Chem. Biol.* **2001**, *5* (5), 591–602.
- (158) Gerber, S. A.; Rush, J.; Stemman, O.; Kirschner, M. W.; Gygi, S. P. Absolute Quantification of Proteins and Phosphoproteins from Cell Lysates by Tandem MS. *Proc. Natl. Acad. Sci.* **2003**, *100* (12), 6940–6945.
- (159) Yasuda, I.; Kishimoto, A.; Tanaka, S.; Tominaga, M.; Sakurai, A.; Nishizuka, Y. A Synthetic Peptide Substrate for Selective Assay of Protein Kinase C. *Biochem. Biophys. Res. Commun.* **1990**, *166* (3), 1220–1227.
- (160) Tamvakopoulos, C. Mass Spectrometry for the Quantification of Bioactive Peptides in Biological Fluids. *Mass Spectrom. Rev.* **2007**, *26* (3), 389–402.
- (161) Dallas, D. C.; Guerrero, A.; Parker, E. A.; Robinson, R. C.; Gan, J.; German, J. B.; Barile, D.; Lebrilla, C. B. Current Peptidomics: Applications, Purification, Identification, Quantification, and Functional Analysis. *Proteomics.* **2015**, *15* (5–6), 1026–1038.
- (162) Lee, J. E. Neuropeptidomics: Mass Spectrometry-Based Identification and Quantitation of Neuropeptides. *Genomics Inform.* **2016**, *14* (1), 12–19.
- (163) Johnson, M. Protein Quantitation. *Mater. Methods* **2012**, *2*, 115.
- (164) Yuan, L.; Zhu, M. Quantitative Bioanalysis of Proteins by Mass Spectrometry. *Mater. Methods* **2015**, *5*, 1332.
- (165) Brun, V.; Masselon, C.; Garin, J.; Dupuis, A. Isotope Dilution Strategies for Absolute Quantitative Proteomics. *J. of Proteomics.* **2009**, *72* (5), 740–749.
- (166) Narumi, R.; Shimizu, Y.; Ukai-Tadenuma, M.; Ode, K. L.; Kanda, G. N.; Shinohara, Y.; Sato, A.; Matsumoto, K.; Ueda, H. R. Mass Spectrometry-Based Absolute Quantification Reveals Rhythmic Variation of Mouse Circadian Clock Proteins. *Proc. Natl. Acad. Sci.* **2016**, *113* (24), E3461–E3467.
- (167) Hober, A.; Edfors, F.; Ryaboshapkina, M.; Malmqvist, J.; Rosengren, L.; Percy, A. J.; Lind, L.; Forsström, B.; Uhlén, M.; Oscarsson, J.; Miliotis, T. Absolute Quantification of Apolipoproteins Following Treatment with Omega-3 Carboxylic Acids and Fenofibrate Using a High Precision Stable Isotope-Labeled Recombinant Protein Fragments Based SRM Assay. *Mol. Cell. Proteomics* **2019**, *18* (12), 2433–2446.
- (168) Calderón-Celis, F.; Encinar, J. R.; Sanz-Medel, A. Standardization Approaches in Absolute Quantitative Proteomics with Mass Spectrometry. *Mass Spectrom. Rev.* **2018**, *37* (6), 715–737.

- (169) Yang, Z.; Li, N. Absolute Quantitation of Protein Posttranslational Modification Isoform. *Methods Mol. Biol.* **2015**, *1306*, 105–119.
- (170) Bigeleisen, J. The Relative Reaction Velocities of Isotopic Molecules. *J. Chem. Phys.* **1949**, *17* (8), 675–678.
- (171) Carpenter, B. K. Unearthing the Unconventional. *Nat. Chem.* **2010**, *2* (2), 80–82.
- (172) Zhang, R.; Sioma, C. S.; Wang, S.; Regnier, F. E. Fractionation of Isotopically Labeled Peptides in Quantitative Proteomics. *Anal. Chem.* **2001**, *73* (21), 5142–5149.
- (173) Ow, S. Y.; Salim, M.; Noirel, J.; Evans, C.; Rehman, I.; Wright, P. C. ITRAQ Underestimation in Simple and Complex Mixtures: “The Good, the Bad and the Ugly.” *J. Proteome Res.* **2009**, *8* (11), 5347–5355.
- (174) Karp, N. A.; Huber, W.; Sadowski, P. G.; Charles, P. D.; Hester, S. V.; Lilley, K. S. Addressing Accuracy and Precision Issues in ITRAQ Quantitation. *Mol. Cell. Proteomics.* **2010**, *9* (9), 1885–1897.
- (175) Zhao, P.; Guo, Y.; Dewald, H. D.; Chen, H. Improvements for Absolute Quantitation Using Electrochemical Mass Spectrometry. *Int. J. Mass Spectrom.* **2019**, *443*, 41–45.
- (176) Chen, H. A NEW METHOD AND DEVICE FOR CHEMICAL QUANTIFICATION USING ELECTROCHEMICAL MASS SPECTROMETRY WITHOUT THE USE OF STANDARD TARGET COMPOUNDS. WO/2018/081228, May 3, 2018.
- (177) Zhao, P.; Zare, R. N.; Chen, H. Absolute Quantitation of Oxidizable Peptides by Coulometric Mass Spectrometry. *J. Am. Soc. Mass Spectrom.* **2019**, *30* (11), 2398–2407.
- (178) Kim, Y.-I.; Boyd, J. S.; Espinosa, J.; Golden, S. S. Detecting KaiC Phosphorylation Rhythms of the Cyanobacterial Circadian Oscillator In Vitro and In Vivo. *Methods Enzymol.* **2015**, *551*, 153–173.
- (179) Kaur, M.; Ng, A.; Kim, P.; Diekman, C.; Kim, Y.-I. CikA Modulates the Effect of KaiA on the Period of the Circadian Oscillation in KaiC Phosphorylation. *J. Biol. Rhythms.* **2019**, *34* (2), 218–223.
- (180) Duan, X.; Young, R.; Straubinger, R. M.; Page, B.; Cao, J.; Wang, H.; Yu, H.; Canty, J. M.; Qu, J. A Straightforward and Highly Efficient Precipitation/on-Pellet Digestion Procedure Coupled with a Long Gradient Nano-LC Separation and Orbitrap Mass Spectrometry for Label-Free Expression Profiling of the Swine Heart Mitochondrial Proteome. *J. Proteome Res.* **2009**, *8* (6), 2838–2850.

- (181) Duan, X.; Abuqayyas, L.; Dai, L.; Balthasar, J. P.; Qu, J. High-Throughput Method Development for Sensitive, Accurate, and Reproducible Quantification of Therapeutic Monoclonal Antibodies in Tissues Using Orthogonal Array Optimization and Nano Liquid Chromatography/Selected Reaction Monitoring Mass Spectrometry. *Anal. Chem.* **2012**, *84* (10), 4373–4382.
- (182) Lowenthal, M. S.; Liang, Y.; Phinney, K. W.; Stein, S. E. Quantitative Bottom-Up Proteomics Depends on Digestion Conditions. *Anal. Chem.* **2014**, *86* (1), 551–558.
- (183) Jennifer A. Siepen; Emma-Jayne Keevil; David Knight, A.; Hubbard*, S. J. Prediction of Missed Cleavage Sites in Tryptic Peptides Aids Protein Identification in Proteomics. *J Proteome Res.* **2007**, *6* (1), 399–408.
- (184) Alabadi, D.; Oyama, T.; Yanovsky, M. J.; Harmon, F. G.; Más, P.; Kay, S. A.; Hibberd, J. M.; Millar, A. J.; Webb, A. A. R. Reciprocal Regulation Between TOC1 and LHY/CCA1 Within the Arabidopsis Circadian Clock. *Science.* **2001**, *293* (5531), 880–883.
- (185) Dunlap, J. C.; Loros, J. J.; DeCoursey, P. J. *Chronobiology : Biological Timekeeping*. Sunderland, MA: Sinauer Associates, Inc., 2004.
- (186) Bell-Pedersen, D.; Cassone, V. M.; Earnest, D. J.; Golden, S. S.; Hardin, P. E.; Thomas, T. L.; Zoran, M. J. Circadian Rhythms from Multiple Oscillators: Lessons from Diverse Organisms. *Nat. Rev. Genet.* **2005**, *6* (7), 544–556.
- (187) Sahar, S.; Sassone-Corsi, P. Metabolism and Cancer: The Circadian Clock Connection. *Nat. Rev. Cancer.* **2009**, *9* (12), 886–896.
- (188) Takeda, N.; Maemura, K. Circadian Clock and Cardiovascular Disease. *J. Cardiol.* **2011**, *57* (3), 249–256.
- (189) Young, C. R.; Jones, G. E.; Figueiro, M. G.; Soutière, S. E.; Keller, M. W.; Richardson, A. M.; Lehmann, B. J.; Rea, M. S. At-Sea Trial of 24-h-Based Submarine Watchstanding Schedules with High and Low Correlated Color Temperature Light Sources. *J. Biol. Rhythms.* **2015**, *30* (2), 144–154.
- (190) Albrecht, U. Circadian Clocks in Mood-Related Behaviors. *Ann. Med.* **2010**, *42* (4), 241–251.
- (191) Zee, P. C.; Attarian, H.; Videnovic, A. Circadian Rhythm Abnormalities. *Continuum Minneap. Minn.* **2013**, *19*, 132–147.
- (192) Ito, H.; Mutsuda, M.; Murayama, Y.; Tomita, J.; Hosokawa, N.; Terauchi, K.; Sugita, C.; Sugita, M.; Kondo, T.; Iwasaki, H. Cyanobacterial Daily Life with Kai-Based Circadian and Diurnal Genome-Wide Transcriptional Control in *Synechococcus Elongatus*. *Proc. Natl. Acad. Sci.* **2009**, *106* (33), 14168–14173.

- (193) Markson, J. S.; Piechura, J. R.; Puszynska, A. M.; O'Shea, E. K. Circadian Control of Global Gene Expression by the Cyanobacterial Master Regulator RpaA. *Cell*. **2013**, *155* (6), 1396–1408.
- (194) Heudi, O.; Barteau, S.; Zimmer, D.; Schmidt, J.; Bill, K.; Lehmann, N.; Bauer, C.; Kretz, O. Towards Absolute Quantification of Therapeutic Monoclonal Antibody in Serum by LC-MS/MS Using Isotope-Labeled Antibody Standard and Protein Cleavage Isotope Dilution Mass Spectrometry. *Anal. Chem.* **2008**, *80* (11), 4200–4207.
- (195) Hao, P.; Aday, S. S.; Gallart-Palau, X.; Sze, S. K. Recent Advances in Mass Spectrometric Analysis of Protein Deamidation. *Mass Spectrometry Reviews*. Hoboken, NJ: John Wiley and Sons Inc., 2017, 677–692.
- (196) Gaza-Bulsecó, G.; Li, B.; Bulsecó, A.; Liu, H. Method to Differentiate Asn Deamidation That Occurred Prior to and during Sample Preparation of a Monoclonal Antibody. *Anal. Chem.* **2008**, *80* (24), 9491–9498.
- (197) Zhang, L.; English, A. M.; Bai, D. L.; Ugrin, S. A.; Shabanowitz, J.; Ross, M. M.; Hunt, D. F.; Wang, W. H. Analysis of Monoclonal Antibody Sequence and Post-Translational Modifications by Time-Controlled Proteolysis and Tandem Mass Spectrometry. *Mol. Cell. Proteomics* **2016**, *15* (4), 1479–1488.
- (198) Beranová, S.; Cai, J.; Wesdemiotis, C. Unimolecular Chemistry of Protonated Glycine and Its Neutralized Form in the Gas Phase. *J. Am. Chem. Soc.* **1995**, *117* (37), 9492–9501.
- (199) Steen, H.; Mann, M. The Abc's (and Xyz's) of Peptide Sequencing. *Nat. Rev. Mol. Cell Biol.* **2004**, *5* (9), 699–711.
- (200) Medzihradszky, K. F.; Chalkley, R. J. Lessons in de Novo Peptide Sequencing by Tandem Mass Spectrometry. *Mass Spectrom. Rev.* **2015**, *34* (1), 43–63.
- (201) Seidler, J.; Zinn, N.; Boehm, M. E.; Lehmann, W. D. De Novo Sequencing of Peptides by MS/MS. *Proteomics*. **2010**, *10* (4), 634–649.
- (202) Marzluff, E. M.; Campbell, S.; Rodgers, M. T.; Beauchamp, J. L. Low-Energy Dissociation Pathways of Small Deprotonated Peptides in the Gas Phase. *J. Am. Chem. Soc.* **1994**, *116* (17), 7787–7796.
- (203) Ly, T.; Julian, R. R. Ultraviolet Photodissociation: Developments towards Applications for Mass-Spectrometry-Based Proteomics. *Angew. Chemie Int. Ed.* **2009**, *48* (39), 7130–7137.

- (204) Butcher, D. J.; Asano, K. G.; Goeringer, D. E.; McLuckey, S. A. Thermal Dissociation of Gaseous Bradykinin Ions. *J. Phys. Chem. A* **1999**, *103* (43), 8664–8671.
- (205) Roman A. Zubarev; Neil L. Kelleher, A.; McLafferty, F. W. Electron Capture Dissociation of Multiply Charged Protein Cations. A Nonergodic Process. *J Am Chem Soc* **1998**, *120* (13), 3265–3266.
- (206) Wesdemiotis, C.; McLafferty, F. W. Neutralization-Reionization Mass Spectrometry (NRMS). *Chem. Rev.* **1987**, *87* (3), 485–500.
- (207) Goldberg, N.; Schwarz, H. Neutralization-Reionization Mass Spectrometry: A Powerful “Laboratory” to Generate and Probe Elusive Neutral Molecules. *Acc. Chem. Res.* **1994**, *27* (11), 347–352.
- (208) Zagorevskii, D. V.; Holmes, J. L.; Zverev, D. V.; Orlova, T. Y.; Nekrasov, Y. S. The Structure of C₅H₅RFe⁺ (R = F, Cl, Br, I, O, OH, OCH₃, C₆H₅, H) Ions in the Gas Phase and the Generation of Their Neutral Counterparts by Neutralization-Reionization Mass Spectrometry. *J. Am. Soc. Mass Spectrom.* **1995**, *6* (12), 1143–1153.
- (209) Polce, M. J.; Nold, M. J.; Wesdemiotis, C. Characterization of Neutral Fragments in Tandem Mass Spectrometry: A Unique Route to Mechanistic and Structural Information. *J. Mass Spectrom.* **1996**, *31*, 1073–1085.
- (210) Chen, H.; Eberlin, L. S.; Nefliu, M.; Augusti, R.; Cooks, R. G. Organic Reactions of Ionic Intermediates Promoted by Atmospheric-Pressure Thermal Activation. *Angew. Chemie Int. Ed.* **2008**, *47* (18), 3422–3425.
- (211) Eberlin, L. S.; Xia, Y.; Chen, H.; Cooks, R. G. Atmospheric Pressure Thermal Dissociation of Phospho- and Sulfopeptides. *J. Am. Soc. Mass Spectrom.* **2008**, *19* (12), 1897–1905.
- (212) Chen, H.; Eberlin, L. S.; Cooks, R. G. Neutral Fragment Mass Spectra via Ambient Thermal Dissociation of Peptide and Protein Ions. *J. Am. Chem. Soc.* **2007**, *129* (18), 5880–5886.
- (213) Liu, P.; Cooks, R. G.; Chen, H. Nuclear Magnetic Resonance Structure Elucidation of Peptide B₂ Ions. *Angew. Chemie - Int. Ed.* **2015**, *54* (5), 1547–1550.
- (214) Liu, P.; Zhao, P.; Cooks, R. G.; Chen, H. Atmospheric Pressure Neutral Reionization Mass Spectrometry for Structural Analysis. *Chem. Sci.* **2017**, *8* (9), 6499–6507.
- (215) Thomas, D. A.; Sohn, C. H.; Gao, J.; Beauchamp, J. L. Hydrogen Bonding Constrains Free Radical Reaction Dynamics at Serine and Threonine Residues in Peptides. *J. Phys. Chem. A* **2014**, *118* (37), 8380–8392.

- (216) Sohn, C. H.; Gao, J.; Thomas, D. A.; Kim, T.-Y.; Goddard III, W. A.; Beauchamp, J. L. Mechanisms and Energetics of Free Radical Initiated Disulfide Bond Cleavage in Model Peptides and Insulin by Mass Spectrometry. *Chem. Sci.* **2015**, *6* (8), 4550–4560.
- (217) Tureček, F.; Julian, R. R. Peptide Radicals and Cation Radicals in the Gas Phase. *Chem. Rev.* **2013**, *113* (8), 6691–6733.
- (218) Ly, T.; Julian, R. R. Residue-Specific Radical-Directed Dissociation of Whole Proteins in the Gas Phase. *J. Am. Chem. Soc.* **2007**, *130* (1), 351–358.
- (219) Yang, L.; Mazyar, O. A.; Lourderaj, U.; Wang, J.; Rodgers, M. T.; Martínez-Núñez, E.; Addepalli, S. V.; Hase, W. L. Chemical Dynamics Simulations of Energy Transfer in Collisions of Protonated Peptide–Ions with a Perfluorinated Alkylthiol Self-Assembled Monolayer Surface. *J. Phys. Chem. C* **2008**, *112* (25), 9377–9386.
- (220) Benninghoven, A.; Sichtermann, W. K. Detection, Identification, and Structural Investigation of Biologically Important Compounds by Secondary Ion Mass Spectrometry. *Anal. Chem.* **1978**, *50* (8), 1180–1184.
- (221) Milne, G. W. A.; Axenrod, T.; Fales, H. M. Chemical Ionization Mass Spectrometry of Complex Molecules. IV. Amino Acids. *J. Am. Chem. Soc.* **1970**, *92* (17), 5170–5175.
- (222) Bouchonnet, S.; Denhez, J. P.; Hoppilliard, Y.; Mauriac, C. Is Plasma Desorption Mass Spectrometry Useful for Small-Molecule Analysis? Fragmentations of the Natural .Alpha.-Amino Acids. *Anal. Chem.* **1992**, *64* (7), 743–754.
- (223) Leclercq, P. A.; Desiderio, D. M. Chemical Ionization Mass Spectra of Amino Acids and Derivatives. Occurrence and Fragmentation of Ion-Molecule Reaction Products. *Org. Mass Spectrom.* **1973**, *7* (5), 515–533.
- (224) Tsang, C. W.; Harrison, A. G. Chemical Ionization of Amino Acids. *J Am Chem Soc.* **1975**, *98*, 1301–1308.
- (225) Ambihapathy, K.; Yalcin, T.; Leung, H.-W.; Harrison, A. G. Pathways to Immonium Ions in the Fragmentation of Protonated Peptides. *J. Mass Spectrom.* **1997**, *32* (2), 209–215.
- (226) Pingitore, F.; Polce, M. J.; Wang, P.; Wesdemiotis, C.; Paizs, B. Intramolecular Condensation Reactions in Protonated Dipeptides: Carbon Monoxide, Water, and Ammonia Losses in Competition. *J. Am. Soc. Mass Spectrom.* **2004**, *15* (7), 1025–1038.

- (227) Reid, G. E.; Simpson, R. J.; O'Hair, R. A. J. A Mass Spectrometric and Ab Initio Study of the Pathways for Dehydration of Simple Glycine and Cysteine-Containing Peptide [M+H]⁺ Ions. *J. Am. Soc. Mass Spectrom.* **1998**, *9* (9), 945–956.
- (228) O'Hair, R. A. J.; Broughton, P. S.; Styles, M. L.; Frink, B. T.; Hadad, C. M. The Fragmentation Pathways of Protonated Glycine: A Computational Study. *J. Am. Soc. Mass Spectrom.* **2000**, *11* (8), 687–696.
- (229) Kulik, W.; Heerma, W. Fast Atom Bombardment Tandem Mass Spectrometry for Amino Acid Sequence Determination in Tripeptides. *Biol. Mass Spectrom.* **1989**, *18* (10), 910–917.
- (230) Meot-Ner, M.; Field, F. H. Chemical Ionization Mass Spectrometry. XX. Energy Effects and Virtual Ion Temperature in the Decomposition Kinetics of Amino Acids and Amino Acid Derivatives. *J. Am. Chem. Soc.* **1973**, *95* (22), 7207–7211.
- (231) Zoltán Takáts; Justin M. Wiseman; Bogdan Gologan, and; Cooks, R. G. Electrosonic Spray Ionization. A Gentle Technique for Generating Folded Proteins and Protein Complexes in the Gas Phase and for Studying Ion–Molecule Reactions at Atmospheric Pressure. *Anal. Chem.* **2004**, *76* (14), 4050–4058.
- (232) Clipston, N. L.; Jai-nhuknan, J.; Cassady, C. J. A Comparison of Negative and Positive Ion Time-of-Flight Post-Source Decay Mass Spectrometry for Peptides Containing Basic Residues. *Int. J. Mass Spectrom.* **2003**, *222* (1–3), 363–381.
- (233) Harrison, A. G. Sequence-Specific Fragmentation of Deprotonated Peptides Containing H or Alkyl Side Chains. *J. Am. Soc. Mass Spectrom.* **2001**, *12* (1), 1–13.
- (234) Johnson, R. S.; Martin, S. A.; Biemann, K.; Stults, J. T.; Watson, J. T. Novel Fragmentation Process of Peptides by Collision-Induced Decomposition in a Tandem Mass Spectrometer: Differentiation of Leucine and Isoleucine. *Anal. Chem.* **1987**, *59* (21), 2621–2625.
- (235) Roepstorff, P.; Fohlman, J. Letter to the Editors. *Biol. Mass Spectrom.* **1984**, *11* (11), 601–601.
- (236) Verkerk, U. H.; Siu, C.-K.; Steill, J. D.; El Aribi, H.; Zhao, J.; Rodriguez, C. F.; Oomens, J.; Hopkinson, A. C.; Siu, K. W. M. A₂ Ion Derived from Triglycine: An N₁-Protonated 4-Imidazolidinone. *J. Phys. Chem. Lett.* **2010**, *1* (5), 868–872.
- (237) Bythell, B. J.; Maître, P.; Paizs, B. Cyclization and Rearrangement Reactions of a_n Fragment Ions of Protonated Peptides. *J. Am. Chem. Soc.* **2010**, *132* (42), 14766–14779.
- (238) Paizs, B.; Suhai, S. Fragmentation Pathways of Protonated Peptides. *Mass Spectrom. Rev.* **2005**, *24* (4), 508–548.

- (239) Polfer, N. C.; Oomens, J.; Suhai, S.; Paizs, B. Infrared Spectroscopy and Theoretical Studies on Gas-Phase Protonated Leu-Enkephalin and Its Fragments: Direct Experimental Evidence for the Mobile Proton. *J Am Chem Soc.* **2007**, *129* (18), 5887–5897.
- (240) Chakravarty, A. R.; Cotton, F. A.; Tocher, D. A.; Tocher, J. H. Structural and Electrochemical Characterization of the Novel Ortho-Metalated Dirhodium(II) Compounds $\text{Rh}_2(\text{O}_2\text{CMe})_2[\text{Ph}_2\text{P}(\text{C}_6\text{H}_4)]_2$. *Organometallics* **1985**, *4* (1), 8–13.
- (241) Marks, G. S.; Vreman, H. J.; McLaughlin, B. E.; Brien, J. F.; Nakatsu, K. Measurement of Endogenous Carbon Monoxide Formation in Biological Systems. *Antioxid. Redox Signal.* **2002**, *4* (2), 271–277.
- (242) McLean, S.; Mann, B. E.; Poole, R. K. Sulfite Species Enhance Carbon Monoxide Release from CO-Releasing Molecules: Implications for the Deoxymyoglobin Assay of Activity. *Anal. Biochem.* **2012**, *427* (1), 36–40.
- (243) Atkin, A. J.; Lynam, J. M.; Moulton, B. E.; Sawle, P.; Motterlini, R.; Boyle, N. M.; Pryce, M. T.; Fairlamb, I. J. S. Modification of the Deoxy-Myoglobin/Carbonmonoxy-Myoglobin UV-Vis Assay for Reliable Determination of CO-Release Rates from Organometallic Carbonyl Complexes. *Dalt. Trans.* **2011**, *40* (21), 5755.
- (244) Park, S. S.; Kim, J.; Lee, Y. Improved Electrochemical Microsensor for the Real-Time Simultaneous Analysis of Endogenous Nitric Oxide and Carbon Monoxide Generation. *Anal. Chem.* **2012**, *84* (3), 1792–1796.
- (245) Hasegawa, U.; van der Vlies, A. J.; Simeoni, E.; Wandrey, C.; Hubbell, J. A. Carbon Monoxide-Releasing Micelles for Immunotherapy. *J. Am. Chem. Soc.* **2010**, *132* (51), 18273–18280.
- (246) Esteban, J.; Ros-Lis, J. V.; Martínez-Máñez, R.; Marcos, M. D.; Moragues, M.; Soto, J.; Sancenón, F. Sensitive and Selective Chromogenic Sensing of Carbon Monoxide by Using Binuclear Rhodium Complexes. *Angew. Chemie Int. Ed.* **2010**, *49* (29), 4934–4937.
- (247) Moragues, M. E.; Esteban, J.; Ros-Lis, J. V.; Martínez-Máñez, R.; Marcos, M. D.; Martínez, M.; Soto, J.; Sancenón, F. Sensitive and Selective Chromogenic Sensing of Carbon Monoxide via Reversible Axial CO Coordination in Binuclear Rhodium Complexes. *J. Am. Chem. Soc.* **2011**, *133* (39), 15762–15772.
- (248) Morimoto, Y.; Durante, W.; Lancaster, D. G.; Klattenhoff, J.; Tittel, F. K. Real-Time Measurements of Endogenous CO Production from Vascular Cells Using an Ultrasensitive Laser Sensor. *Am. J. Physiol. Heart Circ. Physiol.* **2001**, *280* (1), H483-8.

- (249) Wang, J. *Electroanalytical Techniques in Clinical Chemistry and Laboratory Medicine*. Hoboken, NJ: John Wiley & Sons, Inc., 1988.
- (250) Woermann, D. J. Janata: Principles of Chemical Sensors. Plenum Press, New York and London 1989. 317 Seiten, Preis in Europa: US \$ 47.40. *Berichte der Bunsengesellschaft für Phys. Chemie* **1990**, 94 (4), 543–543.
- (251) Wang, J. *Analytical Electrochemistry*. Hoboken, NJ: John Wiley & Sons, Inc., 2006.
- (252) Brinker, U. H. *Advances in Carbene Chemistry*. Greenwich, CT: JAI Press, 1994.
- (253) Yoshiro Yasaka; Ken Yoshida; Chihiro Wakai; Nobuyuki Matubayasi, A.; Nakahara, M. Kinetic and Equilibrium Study on Formic Acid Decomposition in Relation to the Water-Gas-Shift Reaction. *J. Phys. Chem. A* **2006**, 110 (38), 11082–11090.
- (254) Bythell, B. J.; Barofsky, D. F.; Pingitore, F.; Polce, M. J.; Wang, P.; Wesdemiotis, C.; Paizs, B. Backbone Cleavages and Sequential Loss of Carbon Monoxide and Ammonia from Protonated AGG: A Combined Tandem Mass Spectrometry, Isotope Labeling, and Theoretical Study. *J. Am. Soc. Mass Spectrom.* **2007**, 18 (7), 1291–1303.
- (255) Paizs, B.; Suhai, S. Theoretical Study of the Main Fragmentation Pathways for Protonated Glycylglycine. *Rapid Commun. Mass Spectrom.* **2001**, 15 (8), 651–663.
- (256) Hashmi, A. S. K.; Hutchings, G. J. Gold Catalysis. *Angew. Chem. Int. Ed.* **2006**, 45 (47), 7896–7936.
- (257) Gorin, D. J.; Toste, F. D. Relativistic Effects in Homogeneous Gold Catalysis. *Nature*. **2007**, 446, 395–403.
- (258) Garcia, P.; Malacria, M.; Aubert, C.; Gandon, V.; Fensterbank, L. Gold-Catalyzed Cross-Couplings: New Opportunities for C-C Bond Formation. *ChemCatChem* **2010**, 2 (5), 493–497.
- (259) Bratsch, S. G. Standard Electrode Potentials and Temperature Coefficients in Water at 298.15 K. *J. Phys. Chem. Ref. Data*. **1989**, 18, 1–21.
- (260) Kar, A.; Mangu, N.; Kaiser, H. M.; Tse, M. K. Gold-Catalyzed Direct Oxidative Coupling Reactions of Non-Activated Arenes. *J. Organomet. Chem.* **2009**, 694, 524–537.
- (261) Hopkinson, M. N.; Tlahuext-Aca, A.; Glorius, F. Merging Visible Light Photoredox and Gold Catalysis. *Acc. Chem. Res.* **2016**, 49, 2261–2272.
- (262) Horn, E. J.; Rosen, B. R.; Baran, P. S. Synthetic Organic Electrochemistry: An Enabling and Innately Sustainable Method. *ACS Cent. Sci.* **2016**, 2 (302–308).

- (263) Moeller, K. D. Synthetic Applications of Anodic Electrochemistry. *Tetrahedron* **2000**, *56*, 9527–9554.
- (264) Sauermann, N.; Meyer, T. H.; Qiu, Y.; Ackermann, L. Electrocatalytic C–H Activation. *ACS Catal.* **2018**, *8*, 7086–7103.
- (265) Bunz, U. H. F. Poly(Aryleneethynylene)s: Syntheses, Properties, Structures, and Applications. *Chem. Rev.* **2000**, *100*, 1605–1644.
- (266) Peng, H.; Xi, Y.; Ronaghi, N.; Dong, B.; Akhmedov, N. G.; Shi, X. Gold-Catalyzed Oxidative Cross-Coupling of Terminal Al-Kynes: Selective Synthesis of Unsymmetrical 1,3-Diynes. *J. Am. Chem. Soc.* **2014**, *136*, 13174–13177.
- (267) Tang, S.; Liu, Y.; Lei, A. Electrochemical Oxidative Cross-Coupling with Hydrogen Evo-Lution: A Green and Sustainable Way for Bond Formation. *Chem.* **2018**, *4*, 27–45.
- (268) Girod, M.; Moyano, E.; Campbell, D. I.; Cooks, R. G. Accelerated Bimolecular Reactions in Microdroplets Studied by Desorption Electrospray Ionization Mass Spectrometry. *Chem. Sci.* **2011**, *2* (3), 501–510.
- (269) Lee, J. K.; Walker, K. L.; Han, H. S.; Kang, J.; Prinz, F. B.; Waymouth, R. M.; Nam, H. G.; Zare, R. N. Spontaneous Generation of Hydrogen Peroxide from Aqueous Microdroplets. *Proc. Natl. Acad. Sci.* **2019**, *116* (39), 19294–19298.
- (270) Lee, J. K.; Samanta, D.; Nam, H. G.; Zare, R. N. Micrometer-Sized Water Droplets Induce Spontaneous Reduction. *J. Am. Chem. Soc.* **2019**, *141* (27), 10585–10589.
- (271) Lee, J. K.; Kim, S.; Nam, H. G.; Zare, R. N. Microdroplet Fusion Mass Spectrometry for Fast Reaction Kinetics. *Proc. Natl. Acad. Sci.* **2015**, *112* (13), 3898–3903.
- (272) Bain, R. M.; Sathyamoorthi, S.; Zare, R. N. “On-Droplet” Chemistry: The Cycloaddition of Diethyl Azodicarboxylate and Quadricyclane. *Angew. Chemie* **2017**, *129* (47), 15279–15283.
- (273) Lee, J. K.; Samanta, D.; Nam, H. G.; Zare, R. N. Spontaneous Formation of Gold Nanostructures in Aqueous Microdroplets. *Nat. Commun.* **2018**, *9*, 1562.
- (274) Gnanamani, E.; Yan, X.; Zare, R. N. Chemoselective N-Alkylation of Indoles in Aqueous Microdroplets. *Angew. Chemie Int. Ed.* **2020**, *59* (8), 3069–3072.
- (275) Nam, I.; Lee, J. K.; Nam, H. G.; Zare, R. N. Abiotic Production of Sugar Phosphates and Uridine Ribonucleoside in Aqueous Microdroplets. *Proc. Natl. Acad. Sci.* **2017**, *114* (47), 12396–12400.

- (276) Banerjee, S.; Zare, R. N. Syntheses of Isoquinoline and Substituted Quinolines in Charged Microdroplets. *Angew. Chemie - Int. Ed.* **2015**, *54* (49), 14795–14799.
- (277) Gao, D.; Jin, F.; Lee, J. K.; Zare, R. N. Aqueous Microdroplets Containing Only Ketones or Aldehydes Undergo Dakin and Baeyer-Villiger Reactions. *Chem. Sci.* **2019**, *10* (48), 10974–10978.
- (278) Luo, K.; Li, J.; Cao, Y.; Liu, C.; Ge, J.; Chen, H.; Zare, R. N. Reaction of Chloroauric Acid with Histidine in Microdroplets Yields a Catalytic Au-(His)₂ Complex. *Chem. Sci.* **2020**, *11* (9), 2558–2565.
- (279) Wei, Z.; Li, Y.; Cooks, R. G.; Yan, X. Accelerated Reaction Kinetics in Microdroplets: Overview and Recent Developments. *Annu. Rev. Phys. Chem.* **2020**, *71*, 31–51.
- (280) Yan, X.; Bain, R. M.; Cooks, R. G. Organic Reactions in Microdroplets: Reaction Acceleration Revealed by Mass Spectrometry. *Angew. Chem. Int. Ed.* **2016**, *55* (42), 12960–12972.
- (281) Nie, H.; Wei, Z.; Qiu, L.; Chen, X.; Holden, D. T.; Cooks, R. G. High-Yield Gram-Scale Organic Synthesis Using Accelerated Microdroplet/Thin Film Reactions with Solvent Recycling. *Chem. Sci.* **2020**, *11* (9), 2356–2361.
- (282) Basuri, P.; Gonzalez, L. E.; Morato, N. M.; Pradeep, T.; Cooks, R. G. Accelerated Microdroplet Synthesis of Benzimidazoles by Nucleophilic Addition to Protonated Carboxylic Acids. *Chem. Sci.* **2020**.
- (283) Li, Y.; Mehari, T. F.; Wei, Z.; Liu, Y.; Cooks, R. G. Reaction Acceleration at Air-Solution Interfaces: Anisotropic Rate Constants for Katritzky Transamination. *J. Mass Spectrom.* **2020**, e4585.
- (284) Li, Y.; Yan, X.; Cooks, R. G. The Role of the Interface in Thin Film and Droplet Accelerated Reactions Studied by Competitive Substituent Effects. *Angew. Chemie Int. Ed.* **2016**, *55* (10), 3433–3437.
- (285) Sahraeian, T.; Kulyk, D. S.; Badu-Tawiah, A. K. Droplet Imbibition Enables Nonequilibrium Interfacial Reactions in Charged Microdroplets. *Langmuir* **2019**, *35* (45), 14451–14457.
- (286) Tang, S.; Cheng, H.; Yan, X. On-Demand Electrochemical Epoxidation in Nano-Electrospray Ionization Mass Spectrometry to Locate Carbon–Carbon Double Bonds. *Angew. Chemie Int. Ed.* **2020**, *59* (1), 209–214.
- (287) Vaitheeswaran, S.; Thirumalai, D. Hydrophobic and Ionic Interactions in Nanosized Water Droplets. *J. Am. Chem. Soc.* **2006**, *128* (41), 13490–13496.

- (288) Sahota, N.; Abusalim, D. I.; Wang, M. L.; Brown, C. J.; Zhang, Z.; El-Baba, T. J.; Cook, S. P.; Clemmer, D. E. A Microdroplet-Accelerated Biginelli Reaction: Mechanisms and Separation of Isomers Using IMS-MS. *Chem. Sci.* **2019**, *10* (18), 4822–4827.
- (289) Cheng, H.; Tang, S.; Yang, T.; Xu, S.; Yan, X. Accelerating Electrochemical Reactions in a Voltage-Controlled Interfacial Microreactor. *Angew. Chemie Int. Ed.* **2020**, *59* (45), 19862–19867.
- (290) Banerjee, S.; Gnanamani, E.; Yan, X.; Zare, R. N. Can All Bulk-Phase Reactions Be Accelerated in Microdroplets? *Analyst.* **2017**, *142*, 1399–1402.
- (291) Marsh, B. M.; Iyer, K.; Cooks, R. G. Reaction Acceleration in Electrospray Droplets: Size, Distance, and Surfactant Effects. *J. Am. Soc. Mass Spectrom.* **2019**, *30* (10), 2022–2030.
- (292) Mondal, S.; Acharya, S.; Biswas, R.; Bagchi, B.; Zare, R. N. Enhancement of Reaction Rate in Small-Sized Droplets: A Combined Analytical and Simulation Study. *J. Chem. Phys.* **2018**, *148* (24), 244704.
- (293) Xiong, H.; Lee, J. K.; Zare, R. N.; Min, W. Strong Electric Field Observed at the Interface of Aqueous Microdroplets. *J. Phys. Chem. Lett.* **2020**, *11*, 7423–7428.
- (294) Chamberlayne, C. F.; Zare, R. N. Simple Model for the Electric Field and Spatial Distribution of Ions in a Microdroplet. *J. Chem. Phys.* **2020**, *152* (18), 184702.
- (295) Tuck, A. F. Gibbs Free Energy and Reaction Rate Acceleration in and on Microdroplets. *Entropy.* **2019**, *21* (11), 1044.
- (296) Xiong, H.; Lee, J. K.; Zare, R. N.; Min, W. Strong Concentration Enhancement of Molecules at the Interface of Aqueous Microdroplets. *J. Phys. Chem. B* **2020**, *124* (44), 9938–9944.
- (297) Chamberlayne, C. F.; Zare, R. N.; Santiago, J. G. Effects of Weak Electrolytes on Electric Double Layer Ion Distributions. *J. Phys. Chem. Lett.* **2020**, *11* (19), 8302–8306.
- (298) Narendra, N.; Chen, X.; Wang, J.; Charles, J.; Cooks, R. G.; Kubis, T. Quantum Mechanical Modeling of Reaction Rate Acceleration in Microdroplets. *J. Phys. Chem. A* **2020**, *124* (24), 4984–4989.
- (299) Zhou, Z.; Yan, X.; Lai, Y. H.; Zare, R. N. Fluorescence Polarization Anisotropy in Microdroplets. *J. Phys. Chem. Lett.* **2018**, *9* (11), 2928–2932.

- (300) Rovelli, G.; Jacobs, M. I.; Willis, M. D.; Rapf, R. J.; Prophet, A. M.; Wilson, K. R. A Critical Analysis of Electrospray Techniques for the Determination of Accelerated Rates and Mechanisms of Chemical Reactions in Droplets. *Chem. Sci.* **2020**.
- (301) Zhong, X.; Chen, H.; Zare, R. N. Ultrafast Enzymatic Digestion of Proteins by Microdroplet Mass Spectrometry. *Nat. Commun.* **2020**, *11*, 1049.
- (302) Tsumoto, K.; Isozaki, Y.; Yagami, H.; Tomita, M. Future Perspectives of Therapeutic Monoclonal Antibodies. *Immunotherapy.* **2019**, *11* (2), 119–127.
- (303) Kaplon, H.; Muralidharan, M.; Schneider, Z.; Reichert, J. M. Antibodies to Watch in 2020. *MAbs.* **2020**, *12* (1), 1703531.
- (304) Carter, P. J.; Lazar, G. A. Next Generation Antibody Drugs: Pursuit of the “High-Hanging Fruit.” *Nat. Rev. Drug Discov.* **2018**, *17*, 197–223.
- (305) Fisher, A. C.; Lee, S. L.; Harris, D. P.; Buhse, L.; Kozlowski, S.; Yu, L.; Kopcha, M.; Woodcock, J. Advancing Pharmaceutical Quality: An Overview of Science and Research in the U.S. FDA’s Office of Pharmaceutical Quality. *Int. J. Pharm.* **2016**, *515* (1–2), 390–402.
- (306) Nagy, G.; Attah, I. K.; Conant, C. R.; Liu, W.; Garimella, S. V. B.; Gunawardena, H. P.; Shaw, J. B.; Smith, R. D.; Ibrahim, Y. M. Rapid and Simultaneous Characterization of Drug Conjugation in Heavy and Light Chains of a Monoclonal Antibody Revealed by High-Resolution Ion Mobility Separations in SLIM. *Anal. Chem.* **2020**, *92* (7), 5004–5012.
- (307) Beck, A.; Wagner-Rousset, E.; Ayoub, D.; Van Dorsselaer, A.; Sanglier-Cianféroni, S. Characterization of Therapeutic Antibodies and Related Products. *Anal. Chem.* **2013**, *85* (2), 715–736.
- (308) Kang, L.; Weng, N.; Jian, W. LC–MS Bioanalysis of Intact Proteins and Peptides. *Biomed. Chromatogr.* **2020**, *34* (1), e4633.
- (309) Jin, Y.; Lin, Z.; Xu, Q.; Fu, C.; Zhang, Z.; Zhang, Q.; Pritts, W. A.; Ge, Y. Comprehensive Characterization of Monoclonal Antibody by Fourier Transform Ion Cyclotron Resonance Mass Spectrometry. *MAbs.* **2019**, *11* (1), 106–115.
- (310) Donnelly, D. P.; Rawlins, C. M.; DeHart, C. J.; Fornelli, L.; Schachner, L. F.; Lin, Z.; Lippens, J. L.; Aluri, K. C.; Sarin, R.; Chen, B.; Lantz, C.; Jung, W.; Johnson, K. R.; Koller, A.; Wolff, J. J.; Campuzano, I. D. G.; Auclair, J. R.; Ivanov, A. R.; Whitelegge, J. P.; Paša-Tolić, L.; Chamot-Rooke, J.; Danis, P. O.; Smith, L. M.; Tsybin, Y. O.; Loo, J. A.; Ge, Y.; Kelleher, N. L.; Agar, J. N. Best Practices and Benchmarks for Intact Protein Analysis for Top-down Mass Spectrometry. *Nat. Methods* **2019**, *16* (7), 587–594.

- (311) Lodge, J. M.; Schauer, K. L.; Brademan, D. R.; Riley, N. M.; Shishkova, E.; Westphall, M. S.; Coon, J. J. Top-Down Characterization of an Intact Monoclonal Antibody Using Activated Ion Electron Transfer Dissociation. *Anal. Chem.* **2020**, *92* (15), 10246–10251.
- (312) An, Y.; Zhang, Y.; Mueller, H.-M.; Shameem, M.; Chen, X. A New Tool for Monoclonal Antibody Analysis. *MAbs.* **2014**, *6* (4), 879–893.
- (313) Huang, L.; Wang, N.; Mitchell, C. E.; Brownlee, T.; Maple, S. R.; De Felippis, M. R. A Novel Sample Preparation for Shotgun Proteomics Characterization of HCPs in Antibodies. *Anal. Chem.* **2017**, *89* (10), 5436–5444.
- (314) Fekete, S.; Guillarme, D.; Sandra, P.; Sandra, K. Chromatographic, Electrophoretic, and Mass Spectrometric Methods for the Analytical Characterization of Protein Biopharmaceuticals. *Anal. Chem.* **2016**, *88* (1), 480–507.
- (315) Mouchahoir, T.; Schiel, J. E. Development of an LC-MS/MS Peptide Mapping Protocol for the NISTmAb. *Anal. Bioanal. Chem.* **2018**, *410* (8), 2111–2126.
- (316) Carvalho, L. B.; Capelo-Martínez, J.-L.; Lodeiro, C.; Wiśniewski, J. R.; Santos, H. M. Ultrasonic-Based Filter Aided Sample Preparation as the General Method to Sample Preparation in Proteomics. *Anal. Chem.* **2020**, *92* (13), 9164–9171.
- (317) Rivera-Albarran, M. E.; Ray, S. J. A Novel Combined Microstrip Resonator/Nanospray Ionization Source for Microwave-Assisted Trypsin Digestion of Proteins. *J. Am. Soc. Mass Spectrom.* **2020**, *31* (8), 1684–1696.
- (318) Basile, F.; Hauser, N. Rapid Online Nonenzymatic Protein Digestion Combining Microwave Heating Acid Hydrolysis and Electrochemical Oxidation. *Anal. Chem.* **2011**, *83* (1), 359–367.
- (319) López-Ferrer, D.; Capelo, J. L.; Vázquez, J. Ultra Fast Trypsin Digestion of Proteins by High Intensity Focused Ultrasound. *J. Proteome Res.* **2005**, *4* (5), 1569–1574.
- (320) Russell, W. K.; Park, Z. Y.; Russell, D. H. Proteolysis in Mixed Organic-Aqueous Solvent Systems: Applications for Peptide Mass Mapping Using Mass Spectrometry. *Anal. Chem.* **2001**, *73* (11), 2682–2685.
- (321) Ji, J.; Zhang, Y.; Zhou, X.; Kong, J.; Tang, Y.; Liu, B. Enhanced Protein Digestion through the Confinement of Nanozeolite-Assembled Microchip Reactors. *Anal. Chem.* **2008**, *80* (7), 2457–2463.
- (322) Bark, S. J.; Muster, N.; Yates, J. R.; Siuzdak, G. High-Temperature Protein Mass Mapping Using a Thermophilic Protease. *J. Am. Chem. Soc.* **2001**, *123* (8), 1774–1775.

- (323) Takáts, Z.; Wiseman, J. M.; Gologan, B.; Cooks, R. G. Electrosonic Spray Ionization. A Gentle Technique for Generating Folded Proteins and Protein Complexes in the Gas Phase and for Studying Ion-Molecule Reactions at Atmospheric Pressure. *Anal. Chem.* **2004**, *76* (14), 4050–4058.
- (324) Chen, H.; Yang, S.; Li, M.; Hu, B.; Li, J.; Wang, J. Sensitive Detection of Native Proteins Using Extractive Electrospray Ionization Mass Spectrometry. *Angew. Chemie Int. Ed.* **2010**, *49* (17), 3053–3056.
- (325) Formolo, T.; Ly, M.; Levy, M.; Kilpatrick, L.; Lute, S.; Phinney, K.; Marzilli, L.; Brorson, K.; Boyne, M.; Davis, D.; Schiel, J. Determination of the NISTmAb Primary Structure. In *State-of-the-Art and Emerging Technologies for Therapeutic Monoclonal Antibody Characterization Volume 2. Biopharmaceutical Characterization: The NISTmAb Case Study*; UTC, 2015; Vol. 24, pp 1–62.
- (326) Chen, H.; Venter, A.; Cooks, R. G. Extractive Electrospray Ionization for Direct Analysis of Undiluted Urine, Milk and Other Complex Mixtures without Sample Preparation. *Chem. Commun.* **2006**, No. 19, 2042–2044.
- (327) Chen, H.; Gamez, G.; Zenobi, R. What Can We Learn from Ambient Ionization Techniques? *J. Am. Soc. Mass Spectrom.* **2009**, *20* (11), 1947–1963.
- (328) Chen, H.; Yang, S.; Wortmann, A.; Zenobi, R. Neutral Desorption Sampling of Living Objects for Rapid Analysis by Extractive Electrospray Ionization Mass Spectrometry. *Angew. Chemie - Int. Ed.* **2007**, *46* (40), 7591–7594.
- (329) Quan, C.; Alcalá, E.; Petkovska, I.; Matthews, D.; Canova-Davis, E.; Taticek, R.; Ma, S. A Study in Glycation of a Therapeutic Recombinant Humanized Monoclonal Antibody: Where It Is, How It Got There, and How It Affects Charge-Based Behavior. *Anal. Biochem.* **2008**, *373* (2), 179–191.
- (330) Wei, B.; Berning, K.; Quan, C.; Zhang, Y. T. Glycation of Antibodies: Modification, Methods and Potential Effects on Biological Functions. *mAbs.* **2017**, *9* (4), 586–594.
- (331) Woodcock, J.; Woosley, R. The FDA Critical Path Initiative and Its Influence on New Drug Development. *Annu. Rev. Med.* **2008**, *59* (1), 1–12.
- (332) Jefferis, R. Glycosylation as a Strategy to Improve Antibody-Based Therapeutics. *Nat Rev Drug Discov.* **2009**, *8*, 226–234.
- (333) Espy, R. D.; Wleklinski, M.; Yan, X.; Cooks, R. G. Beyond the Flask: Reactions on the Fly in Ambient Mass Spectrometry. *TrAC.* **2014**, *57*, 135–146.
- (334) Chen, H.; Cotte-Rodríguez, I.; Cooks, R. G. Cis-Diol Functional Group Recognition by Reactive Desorption Electrospray Ionization (DESI). *Chem. Commun.* **2006**, *6* (6), 597–599.

- (335) Li, Y.; Hu, Y.; Logsdon, D. L.; Liu, Y.; Zhao, Y.; Cooks, R. G. Accelerated Forced Degradation of Therapeutic Peptides in Levitated Microdroplets. *Pharm. Res.* **2020**, *37* (7), 138.